

# **Study of Conophylline and Its Inspired Analogues as Potent Pancreatic Lipase Inhibitors for Obesity Treatment**

## **THESIS**

Submitted in partial fulfilment  
of the requirements for the degree of  
**DOCTOR OF PHILOSOPHY**

by

**S N C SRIDHAR**  
**ID. No. 2013PHXF0006P**

Under the Supervision of  
**Dr. Paul Atish Tulshiram**



**BITS Pilani**  
Pilani | Dubai | Goa | Hyderabad

**BIRLA INSTITUTE OF TECHNOLOGY & SCIENCE, PILANI**

**2019**

***Dedicated to God and  
My Family!!***

**BIRLA INSTITUTE OF TECHNOLOGY AND SCIENCE, PILANI**

**CERTIFICATE**

This is to certify that the thesis titled “**Study of Conophylline and Its Inspired Analogues as Potent Pancreatic Lipase Inhibitors for Obesity Treatment**” submitted by **S N C Sridhar** ID No **2013PHXF0006P** for the award of Ph.D. of the Institute embodies original work done by him under my supervision.

**Signature of the Supervisor:**

**Name in capital letters:** Dr. PAUL ATISH TULSHIRAM

**Designation:** Assistant Professor & Head,

Department of Pharmacy,

Birla Institute of Technology and Science, Pilani (BITS Pilani)

Pilani campus, Rajasthan

**Date:**

## ACKNOWLEDGEMENTS

I take this opportunity to put my gratitude and thanks to many people who were responsible in one or the other way for supporting me to reach this point of my life. I shall begin with the **Almighty** who decided this righteous path for me that has ultimately resulted in unleashing my true potential. I would like to express my gratitude and love for **my family** for their continuous support and motivation during the course of my thesis.

I take this opportunity to express my gratitude to my research supervisor, **Dr. Paul Atish Tulshiram**. I feel privileged to work under his supervision for the doctoral degree. I am extremely thankful for his understanding during my tough times by providing consistent encouragement. His guidance has helped me in establishing a potential research environment through freedom of thought. I thank him for providing academic assistance, emotional guidance and moral support throughout my PhD journey.

I would like to thank **Prof. Souvik Bhattacharyya** (Vice Chancellor, BITS Pilani), **Prof. B. N. Jain** (Ex-Vice Chancellor, BITS Pilani), **Prof. A. K. Sarkar** (Director, BITS Pilani, Pilani Campus) and **Prof. G. Raghurama** (Ex-Director, BITS Pilani, Pilani Campus) for allowing me to pursue my doctoral thesis. I would like to express my gratitude to **Prof. Srinivas Krishnaswamy** (Dean, Academic - Graduate Studies and Research Division, BITS Pilani, Pilani Campus), **Prof. Jitendra Panwar** (Associate Dean, Academic Graduate Studies and Research Division, BITS Pilani, Pilani Campus) and **Prof. S. K. Verma** (Former Dean, Academic Research Division) for their kind support.

My whole-hearted gratitude to **Dr. Deepak Chitkara**, (Convener, Departmental Research Committee, Department of Pharmacy, BITS Pilani, Pilani Campus), **Prof. Hemant R. Jadhav** and **Dr. S Murugesan** (Doctoral Advisory Committee members) and **Prof. Dalip Kumar** (Department of Chemistry, BITS Pilani, Pilani Campus) for their official support and encouragement. I would like to acknowledge the **Council of Scientific and Industrial Research (CSIR)** for providing the **Senior Research Fellowship (SRF)** during 2018-2019 (File No: 09/719(0088)/2018-EMR-I).

My special thanks to all the **faculty members, seniors, colleagues and juniors** (Department of Pharmacy, BITS Pilani, Pilani Campus) who enriched my life at BITS Pilani. My special thanks to **Mr. Ginson George, Ms. Pracheta Sengupta, Mrs. Priyadeep Manchanda, Ms. Nisha Yadav** (PhD scholars), **Mr. Saksham Palawat** and **Mr. Dileep P S** (M. Pharm students) in our group for their extended support during the final phase of my thesis. I would

like to thank the **Central Animal facility staff**, and **Dr. Sushil K Yadav**, (Senior Vet. In charge) for their support during my work. I wish to extend my appreciation for the **non-teaching staff** (Department of Pharmacy, BITS Pilani, Pilani Campus) for their support in conducting labs. Thank you all.

I would like to acknowledge **Birla Institute of Technology and Science, Pilani (BITS Pilani)**, Pilani Campus, Pilani, Rajasthan, India for providing necessary laboratory facilities. I would like to acknowledge **Department of Science and Technology (DST)**, New Delhi, India for sponsoring HR-MS facility at BITS Pilani under **FIST** program.

**S N C Sridhar**

## ABSTRACT

Obesity is defined as an excessive fat accumulation that presents a risk to health. Worldwide, obesity has tripled since 1975 with recent reports from the World Health Organization indicating a rapid upsurge in obese population. Amongst the several targets that have been explored to treat obesity, pancreatic lipase (PL) inhibition is considered a validated strategy due to its tolerable side effects. Orlistat, a potent PL inhibitor, is widely prescribed for long term obesity treatment. However, a chronic exposure to this drug resulted in severe adverse events like hepatotoxicity, highlighting the urge to develop safer and effective anti-obesity drugs.

Natural products (NPs) represent an effective source for the treatment of various ailments, while maintaining tolerable side effects. NPs provided significant share of new clinical drugs, despite the severe competition from other drug discovery methods. Further, the use of detailed molecular modelling studies can potentiate NP-based drug discovery in more scientific manner. In the past two decades, at least 377 NP based drugs have been approved, including 54 unmodified NPs, 268 NP derivatives and 55 synthetic drugs with NP pharmacophore. Considering these advantages of NP-based drug discovery, a detailed literature search was performed to identify NP-based PL inhibitors. The search highlighted around 750 NP based PL inhibitors, apart from 300 synthetic compounds. Nevertheless, these compounds exhibited enormous chemical diversity, while a majority of these compounds did not possess potent PL inhibitory activity comparable to that of orlistat. Hence, the present thesis aims at “the study of NP lead(s) and its inspired analogues as potent PL inhibitors for obesity treatment”. Accordingly, the present thesis is sub-divided into two parts with the first part focussed into identification of the NP lead(s), while the second part deals with molecular modelling-based lead optimization of the NP lead that would result in potent PL inhibitor(s).

A preliminary structural analysis of the reported PL inhibitors highlighted various pharmacophoric features that resulted in potent PL inhibition. These features along with the hints from traditional medicines were utilised to select a pool of plants, that were evaluated for their PL inhibitory activity. The screening highlighted *Tabernaemontana divaricata* leaves as a source of potential PL inhibitory leads. Further experiments that involved bioassay guided fractionation resulted in the isolation and identification of conophylline as a potent PL inhibitory lead ( $IC_{50} = 3.31 \mu M$ ). Nevertheless, conophylline exhibited lower potency compared to orlistat ( $IC_{50} = 0.99 \mu M$ ). An *in silico* analysis of conophylline in the active site of Human PL highlighted a high degree of unfavourable steric interactions.

Further, conophylline lacked a highly reactive carbonyl group, in contrary to orlistat, that would interact with the Ser152 of the active site of PL. Previous literature reports suggested  $\alpha$ -ketoamides to possess a reactive carbonyl functionality that can act as an ester mimicking group for potential PL inhibition. Hence, we hypothesized the carbazolyl oxoacetamide analogues to possess potent PL inhibitory activity. These carbazolyl oxoacetamide analogues can be considered a pharmacophore hybrid of the carbazole scaffold (present in conophylline) linked to an  $\alpha$ -ketoamide functionality, that can interact with the lid domain and Ser152 of PL, respectively.

In total, 24 carbazolyl oxoacetamide analogues (**DK-1** to **DK-24**) were evaluated for their PL inhibitory activity. The most potential analogue from the series, **DK-5**, exhibited an  $IC_{50}$  of 6.31  $\mu$ M. Further, **DK-5** was devoid of unfavourable steric bumps that were observed with conophylline. **DK-5** exhibited a stable binding conformation during first 4ns in the active site of PL during the MD simulation (RMSD < 2 Å). Nevertheless, **DK-5** exhibited lower potency compared to conophylline, and was attributed to three drawbacks; i) A greater interaction distance between the reactive carbonyl group of the ketoamide and Ser152; ii) A lesser intensity of hydrophobic interactions exhibited by **DK-5** in comparison to conophylline and orlistat, and iii) the strength of the  $\pi$ -cation interaction with Arg 256. The replacement of carbazole scaffold with an indole scaffold resulted in the reduction of the interaction distance between carbonyl group and Ser152 as confirmed by preliminary docking study.

Accordingly, the first series of indolyl oxoacetamide analogues were designed to understand the variability in replacing the carbazole scaffold with an indole scaffold. In total, 39 indolyl oxoacetamide analogues (**AP-1** to **AP-39**) were synthesized and evaluated for PL inhibition assay, and a potent activity was obtained with analogues **AP-37** and **AP-21** ( $IC_{50}$  4.53 and 4.92  $\mu$ M). Molecular modelling studies were in agreement to the PL inhibitory activity, wherein **AP-37** exhibited a stable binding conformation in the active site of PL during the MD simulation (RMSD < 2 Å). Nevertheless, the PL inhibitory activities of these analogues were still significantly lower compared to that of orlistat. Hence, the indolyl oxoacetamide series was further optimized with inclusion of dense hydrophobic moieties ( $R_1$ =benzyloxy,  $R_2$ =benzyl/prenyl/geranyl) on the indole scaffold, and various other substitutions (Ar = 3,4,5-trimethoxyphenyl/3,4,5-trimethoxybenzyl/2-(indol-3-yl) ethyl) that favoured better  $\pi$ -cation interaction with Arg 256. In total, 41 analogues (**SS-1** to **SS-41**) were synthesized and evaluated for PL inhibitory activity. Analogue **SS-39** exhibited potent activity ( $IC_{50}$  = 1.68  $\mu$ M) comparable to orlistat ( $IC_{50}$  = 0.99  $\mu$ M). Apart from, 10

other analogues (**SS-7**, **SS-10**, **SS-11**, **SS-16**, **SS-24**, **SS-25**, **SS-26**, **SS-30**, **SS-38**, **SS-40**) exhibited potent activity compared to the NP lead, conophylline ( $IC_{50} = 3.31 \mu M$ ).

The potent PL inhibitory conophylline inspired analogues were further investigated for their *in vivo* efficacy. Prior to the *in vivo* experiments, the most potent analogues from various series of carbazolyl and indolyl oxoacetamide analogues, alongside conophylline and orlistat, were evaluated for their ADMET properties using various *in silico* tools, that in turn decided the suitable candidate for *in vivo* experiments. The prediction highlighted **SS-39** to possess low GI absorption similar to orlistat and was devoid of any form of toxicity in contrary to orlistat. Hence **SS-39** was selected for further *in vivo* experiments, that was further divided into two parts; i) oral triglyceride tolerance test and ii) High Fat Diet (HFD) fed mice model (4-week treatment). For the OTTT, three doses of **SS-39** were considered (5, 10 and 20 mg/kg) and compared with orlistat (10 mg/kg). **SS-39** at 10 and 20 mg/kg dose exhibited profiles comparable to the standard drug orlistat. Consequently, two doses of **SS-39** (10 and 20 mg/kg) were selected for the 4-week treatment in HFD fed mice model. **SS-39** at 20 mg/kg dose exhibited a comparable activity with orlistat (10 mg/kg) for various biochemical parameters *viz.*, triglycerides and cholesterol etc. Further, the quantification of faecal triglycerides of mice clearly indicated that **SS-39** acted through PL inhibition.

In conclusion, the thesis work resulted in a potent indolyl oxoacetamide analogue, **SS-39** identified through a series of structural modifications (using molecular modelling followed by synthesis) of the lead molecule, conophylline. The anti-obesity efficacy of this analogue was significantly similar to orlistat. Further, **SS-39** did not possess any toxicity in contrary to orlistat, as observed with preliminary ADMET prediction.

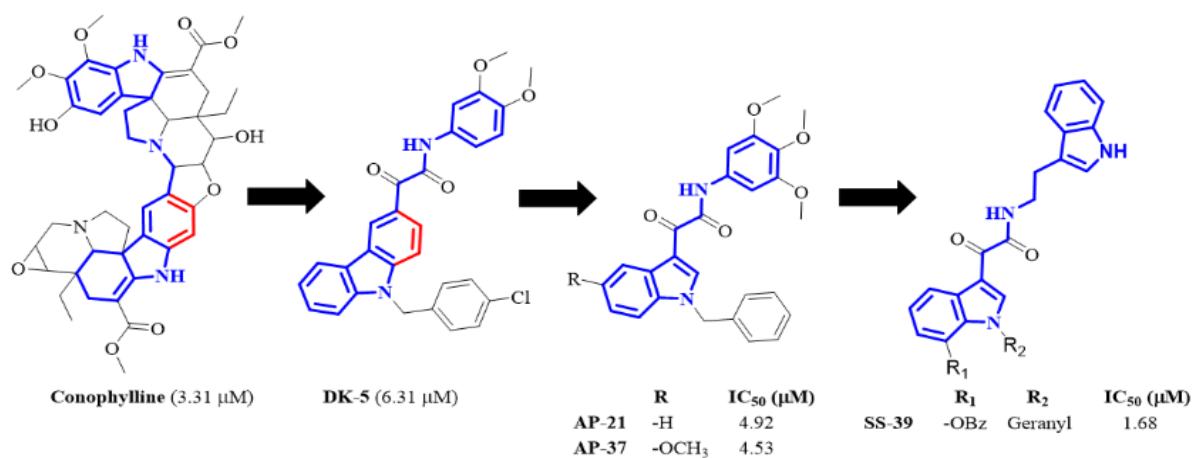




## Table of Contents

<b>Content</b>	<b>Title</b>	<b>Page No.</b>
	<i>Certificate page</i>	<i>i</i>
	<i>Acknowledgements</i>	<i>ii</i>
	<i>Abstract</i>	<i>iv</i>
	<i>List of Tables</i>	<i>vii</i>
	<i>List of Figures</i>	<i>ix</i>
	<i>List of Schemes and Formulae</i>	<i>xiv</i>
	<i>List of Abbreviations and Symbols</i>	<i>xv</i>
Chapter 1	Introduction	1
Chapter 2	Literature Review	17
Chapter 3	Aim and Objectives	44
Chapter 4	Materials and Methods	45
Chapter 5	Identification of NP Lead from <i>T. divaricata</i> and Its Validation	50
Chapter 6	Synthesis - Series I - Carbazolyl Oxoacetamide Analogues	74
Chapter 7	Synthesis - Series II - Indolyl Oxoacetamide Analogues (Part 1)	91
Chapter 8	Synthesis - Series III - Indolyl Oxoacetamide Analogues (Part 2)	113
Chapter 9	ADMET Prediction and <i>In Vivo</i> Experiments	138
Chapter 10	Conclusion and Future Perspectives	148
	<i>Publications</i>	<i>A1</i>
	<i>Conferences</i>	<i>A2</i>
<i>Appendices</i>	<i>Brief Biography of the Candidate</i>	<i>A3</i>
	<i>Brief Biography of the Supervisor</i>	<i>A3</i>

## List of Tables

#	Title	Page
<b>Table 1.1</b>	Summary of BMI based classification for overweight and obesity in different age groups	2
<b>Table 1.2</b>	List of withdrawn anti-obesity drugs	5
<b>Table 1.3</b>	List of currently available anti-obesity drugs	5
<b>Table 2.1</b>	PL inhibitory activity of flavanol gallates reported from <i>C. sinensis</i>	22
<b>Table 2.2</b>	A summary of various saponins and their PL inhibitory activity	27-28
<b>Table 5.1</b>	Plants and parts selected for preliminary screening in PL inhibition assay	50
<b>Table 5.2</b>	PL inhibitory activity of 120 plant extracts obtained from 20 plants/parts	51
<b>Table 5.3</b>	Summary of various alkaloids and their pharmacological properties reported from <i>T. divaricata</i> leaves	53
<b>Table 5.4</b>	Column dimensions and other parameters used in column chromatography	56
<b>Table 5.5</b>	Summary of docking scores and interactions exhibited by top four scoring molecules	59
<b>Table 5.6</b>	Summary of hydrophobic interactions exhibited by top four scoring molecules during MD simulations	60
<b>Table 5.7</b>	Summary of the validated HPTLC parameters for conophylline.	64
<b>Table 5.8</b>	Mean areas and their % RSD at various concentrations of conophylline	65
<b>Table 5.9</b>	Summary of intra- and inter-day precision studies	66
<b>Table 5.10</b>	Accuracy study of the developed method summarizing the % recovery values	66-67
<b>Table 5.11</b>	Summary of robustness results of the developed method	67
<b>Table 6.1</b>	<i>In vitro</i> PL inhibitory activities of carbazolyl oxoacetamide analogues <b>DK-1</b> to <b>DK-24</b>	83-84
<b>Table 6.2</b>	$V_{max}$ , $K_m$ and $K_i$ values calculated from Lineweaver-Burk plots at different inhibitory concentrations [I] of <b>DK-5</b> , <b>DK-6</b> and <b>DK-16</b>	84
<b>Table 6.3</b>	MolDock scores and interaction summary of carbazolyl oxoacetamide analogues <b>DK-1</b> to <b>DK-24</b> with the active site of PL	86

<b>Table 6.4</b>	Interaction chart of <b>DK-5</b> with the active site of PL at different time frames during MD simulation.	89
<b>Table 7.1</b>	<i>In vitro</i> PL inhibitory activities of indolyl oxoacetamides analogues <b>AP-1</b> to <b>AP-39</b>	104
<b>Table 7.2</b>	$V_{max}$ , $K_m$ and $K_i$ values calculated from Lineweaver-Burk plots at different inhibitory concentrations [I] of <b>AP-21</b> , <b>AP-36</b> and <b>AP-37</b>	105
<b>Table 7.3</b>	MolDock scores and interaction summary of indolyl oxoacetamide analogues <b>AP-1</b> to <b>AP-39</b> with the active site of PL	107-108
<b>Table 7.4</b>	Interaction chart of <b>AP-21</b> with PL at different time frames during MD simulation	110
<b>Table 7.5</b>	Interaction chart of <b>AP-36</b> with PL at different time frames during MD simulation	111
<b>Table 7.6</b>	Interaction chart of <b>AP-37</b> with PL at different time frames during MD simulation	111
<b>Table 8.1</b>	<i>In vitro</i> PL inhibitory activities of indolyl oxoacetamide analogues <b>SS-1</b> to <b>SS-41</b>	130
<b>Table 8.2</b>	MolDock scores and interaction summary of indolyl oxoacetamide analogues <b>SS-1</b> to <b>SS-41</b> with the active site of PL	133-134
<b>Table 8.3</b>	Interaction chart of <b>SS-39</b> with PL at different time frames during MD simulation	137
<b>Table 9.1</b>	Composition of the HFD used in the <i>in vivo</i> experiments	139
<b>Table 9.2</b>	Summary of various groups and drugs administered during the 4-week treatment study	140
<b>Table 9.3</b>	Summary of ADMET parameters predicted for the potent analogues from each series along with conophylline and orlistat	142

## List of Figures

#	Title	Page
<b>Fig. 1.1</b>	Structures of withdrawn anti-obesity drugs	4
<b>Fig. 1.2</b>	Structures of drugs approved for obesity treatment	4
<b>Fig. 1.3</b>	A schematic representation of various targets being explored for the treatment of obesity	6
<b>Fig. 1.4</b>	Schematic representation of the lipid digestion in the gastrointestinal tract	7
<b>Fig. 1.5</b>	Secondary structure of the human PL-colipase complex co-crystallised with methoxyundecyl phosphinic acid (MUP) at the active site	8
<b>Fig. 1.6</b>	Representation of closed (A, B) and open (C, D) lid forms of human PL	9
<b>Fig. 1.7</b>	Schematic flow representing series of biochemical reactions at the catalytic triad of PL during ester hydrolysis	10
<b>Fig. 2.1</b>	Structures of various NPs ( <b>1-3</b> ), NP derivatives ( <b>4-5</b> ) and synthetic drugs with NP pharmacophore ( <b>6-9</b> ) used as drugs	18
<b>Fig. 2.2</b>	Structures of various NPs from <i>Ayurveda</i> used as drugs	18
<b>Fig. 2.3</b>	Distribution of PL inhibitory NPs among various chemical classes	20
<b>Fig. 2.4</b>	A general representation of flavonoid backbone and its various classes	21
<b>Fig. 2.5</b>	Representation of various flavanols and their gallates from <i>C. sinensis</i> and <i>B. crassifolia</i>	21
<b>Fig. 2.6</b>	Various flavan oligomers with potential PL inhibitory activity	22
<b>Fig. 2.7</b>	PL inhibitory potential of theaflavin and its galloyl esters	23
<b>Fig. 2.8</b>	Luteolin and its <i>C</i> -glycosides from <i>E. ophiuroides</i>	23
<b>Fig. 2.9</b>	Prenylated flavones from <i>Artocarpus sps</i> with potent PL inhibitory activity	24
<b>Fig. 2.10</b>	Chemical structures of quercetin ( <b>48</b> ), kaempferol ( <b>49</b> ) and morachalcone A ( <b>50</b> )	24
<b>Fig. 2.11</b>	Prenylated flavanones from <i>C. tricuspidata</i> and <i>M. alba</i> and their PL inhibitory activity	25
<b>Fig. 2.12</b>	Chemical structures of various flavans and their PL inhibitory activity	26
<b>Fig. 2.13</b>	Resveratrol and its derivatives ( <b>61-63</b> ) from <i>V. vinifera</i> and morusibene A ( <b>64</b> ) from <i>M. alba</i> with their PL inhibitory activity	26

<b>Fig. 2.14</b>	Chemical structures of various saponins ( <b>65-87</b> ) evaluated for their PL inhibitory activity	29
<b>Fig. 2.15</b>	Alkaloids from <i>N. nucifera</i> , <i>Berberis sps.</i> and <i>M. koenigii</i>	30
<b>Fig. 2.16</b>	Prenylated benzofurans from <i>M. alba</i> and their PL inhibitory activity	31
<b>Fig. 2.17</b>	Benzofurans from <i>S. roxburghii</i> and <i>V. vinifera</i>	32
<b>Fig. 2.18</b>	Various monascus pigments and their PL inhibitory activity	33
<b>Fig. 2.19</b>	PL inhibitory activities of ebelactones and esterastin from MG7-G1 strain of actinomycetes	33
<b>Fig. 2.20</b>	Panclicins and their PL inhibitory activities from <i>Streptomyces sp.</i> NR 0619	34
<b>Fig. 2.21</b>	Vibrallactone ( <b>114</b> ), its oxime derivative ( <b>115</b> ) from <i>B. vibrans</i> and synthetic analogue of vibrallactone ( <b>116</b> ) with their PL inhibitory activity	34
<b>Fig. 2.22</b>	Boronic acids ( <b>117, 118</b> ), alkyl phosphonates ( <b>119, 120</b> ) and bis 2-oxoamides ( <b>121, 122</b> ) with their PL inhibitory activity	35
<b>Fig. 2.23</b>	Summary of PL inhibitory activity of various synthetic molecules	36
<b>Fig. 4.1</b>	Screenshots retrieved from the Molegro Virtual Docker 6.0, summarizing various parameters and their values used in the molecular docking studies.	47
<b>Fig. 4.2</b>	Superimposition of re-docked pose of MUP (Brown) with the co-crystallised pose (Grey).	47
<b>Fig. 5.1</b>	Taxonomical classification of <i>T. divaricata</i>	52
<b>Fig. 5.2</b>	Structures of various alkaloids reported from the leaves of <i>T. divaricata</i>	53
<b>Fig. 5.3</b>	Schematic flow representing processing and extraction of <i>T. divaricata</i> leaves	54
<b>Fig. 5.4</b>	Schematic flow representing the weights of various fractions obtained through liquid-liquid partition and their PL inhibitory activities	55
<b>Fig. 5.5</b>	A schematic flow summarising the yields and the PL inhibitory activities of various fractions obtained through the column chromatography of the dichloromethane fraction	56
<b>Fig. 5.6</b>	Linear regression curves obtained from PL inhibition assay for orlistat and conophylline	57

<b>Fig. 5.7</b>	Lineweaver-Burk plots of orlistat and conophylline representing reversible competitive inhibition	57
<b>Fig. 5.8</b>	Structures of conophylline, conophyllinine, conophyllidine and taberhanine	58
<b>Fig. 5.9</b>	Backbone RMSD (in red) and Ligand RMSD (in black) of conophylline, conophyllinine, conophyllidine and taberhanine	59
<b>Fig. 5.10</b>	TLC of conophylline in different mobile phases	63
<b>Fig. 5.11</b>	(A) Unresolved chromatogram with 10 cm length TLC plate (Solvent run length - 8 cm); (B) Resolved chromatogram with 15 cm length TLC plate (Solvent run length - 13 cm)	63
<b>Fig. 5.12</b>	HPTLC chromatograms of standard conophylline and ARFs from August samples of <i>T. divaricata</i> leaves	64
<b>Fig. 5.13</b>	Regression plot representing the linearity of the validated HPTLC method	65
<b>Fig. 5.14</b>	Representation of extractive yields of conophylline (mg/g) in different ARF Samples	69
<b>Fig. 5.15</b>	Representation of PL inhibitory activity of different ARF samples	70
<b>Fig. 6.1</b>	2D pose of conophylline highlighting the unfavourable steric interactions (in red)	74
<b>Fig. 6.2</b>	Rationale for selecting carbazolyl oxoacetamide analogues as PL inhibitors	75
<b>Fig. 6.3</b>	Double reciprocal Lineweaver-Burk plots of analogues <b>DK-5</b> , <b>DK-6</b> and <b>DK-16</b>	84
<b>Fig. 6.4</b>	Structure-activity relationship for carbazolyl oxoacetamide analogues <b>DK-1</b> to <b>DK-24</b>	85
<b>Fig. 6.5</b>	(A) Representation of <b>DK-5</b> in the binding pocket of PL (brown region indicates hydrophobic lid domain); (B) 2D interaction diagram of <b>DK-5</b> with PL	87
<b>Fig. 6.6</b>	3D pose of <b>DK-5</b> in the active site of PL highlighting the distance of the reactive carbonyl group from Ser152.	87
<b>Fig. 6.7</b>	(A) RMSD of the backbone; (B) Radius of gyration of the protein and (C) RMSD of the ligand ( <b>DK-5</b> ) retrieved through 10 ns MD trajectory.	88

<b>Fig. 7.1</b>	(A) 3D poses of orlistat, conophylline and <b>DK-5</b> highlighting the distance of reactive carbonyl from Ser152; (B) 2D interactions highlighting no unfavourable steric bumps and low degree of hydrophobic interactions in <b>DK-5</b>	91
<b>Fig. 7.2</b>	Rationale for designing indolyl oxoacetamide analogues as PL inhibitors	92
<b>Fig. 7.3</b>	Double reciprocal Lineweaver-Burk plots of analogues <b>AP-21</b> , <b>AP-36</b> and <b>AP-37</b> indicating reversible competitive inhibition	103
<b>Fig. 7.4</b>	Structure-activity relationship for indolyl oxoacetamide analogues <b>AP-1</b> to <b>AP-39</b>	105
<b>Fig. 7.5</b>	(A) 2D interaction diagrams (B) 3D interaction diagrams (highlighting the lid domain interactions (in pink) and reactive carbonyl position with reference to Ser152 (in green)) and (C) Binding conformations in the active site of PL of <b>AP-21</b> (I) and <b>AP-27</b> (II) respectively	109
<b>Fig. 7.6</b>	RMSD of the ligands <b>AP-21</b> , <b>AP-36</b> and <b>AP-37</b> retrieved through 10 ns MD trajectory	110
<b>Fig. 8.1</b>	2D interaction poses <b>AP-21</b> (I) and its N-geranyl counterpart (II) highlighting dense hydrophobic interactions with the lid domain amino acids (in light pink)	113
<b>Fig. 8.2</b>	2D interaction pose of <b>AP-37</b> (I) and its 5-benzyloxy-N-geranyl substituted counterpart (II) highlighting an increase in $\pi$ - $\pi$ stacking density (in dark pink)	114
<b>Fig. 8.3</b>	General representation of indolyl oxoacetamide analogues highlighting various positions for substitution	114
<b>Fig. 8.4</b>	Lineweaver-Burk plot for <b>SS-39</b> representing reversible competitive inhibition	129
<b>Fig. 8.5</b>	Structure-activity relationship for indolyl oxoacetamide analogues <b>SS-1</b> to <b>SS-41</b>	131
<b>Fig. 8.6</b>	2D docking poses of <b>SS-41</b> (A), <b>SS-35</b> (B), <b>SS-40</b> (C) and <b>SS-39</b> (D) highlighting the distance of the reactive carbonyl from Ser 152	135
<b>Fig. 8.7</b>	2D docking poses of <b>SS-33</b> (A), <b>SS-36</b> (B), <b>SS-34</b> (C) and <b>SS-35</b> (D) highlighting the distance of the reactive carbonyl from Ser 152	136
<b>Fig. 8.8</b>	RMSD of <b>SS-39</b> retrieved through 10 ns MD trajectory	136

---

<b>Fig. 9.1</b>	Graphical representation of results from the OTTT summarising the serum triglyceride levels at various time points	143
<b>Fig. 9.2</b>	(A) Increment in body weights of various groups during the four-week treatment protocol; (B) Serum glucose levels determined from various groups at the end of the four-week treatment period	144
<b>Fig. 9.3</b>	(A) Serum triglyceride (B) Serum total cholesterol (C) Serum HDL-cholesterol (D) Serum LDL-cholesterol	145
<b>Fig. 9.4</b>	Faecal triglyceride levels determined from various groups.	146
<b>Fig. 10.1</b>	Schematic flow representing the structural modifications of conophylline to identify potent PL inhibitory bis(indolyl)oxoacetamide analogues	149

---



## List of Schemes and Formulae

#	Title	Page
<b>Scheme 6.1</b>	Reagents and conditions: <b>(a)</b> KOH, CH <sub>3</sub> I/C <sub>2</sub> H <sub>5</sub> I/4-ClC <sub>6</sub> H <sub>4</sub> CH <sub>2</sub> Cl, DMF, RT, 13 h; <b>(b)</b> Cl(CO) <sub>2</sub> OEt, AlCl <sub>3</sub> , DCM, 0 °C to RT, 3 h; <b>(c)</b> LiOH, THF:H <sub>2</sub> O (1:1), RT, 2 h; <b>(d)</b> ArNH <sub>2</sub> , HATU, DIPEA, DMF, 70 °C, 45 min, MW (100 watt).	76
<b>Scheme 7.1</b>	Reagents and conditions: <b>(i)</b> Benzyl chloride/Ethyl bromide, KOH, DMF, RT, 12 h; <b>(ii)</b> (COCl) <sub>2</sub> , Et <sub>2</sub> O, 0 °C, 30 min; <b>(iii)</b> Ar-NH <sub>2</sub> , TEA, THF, RT, 2 h.	93
<b>Scheme 8.1</b>	Reagents and conditions: <b>(i)</b> Ethyl bromide/Benzyl chloride/Prenyl bromide/Geranyl bromide, KOH, DMF, RT, 12-16 h; <b>(ii)</b> (COCl) <sub>2</sub> , THF, 0 °C, 30-180 min; <b>(iii)</b> Ar-NH <sub>2</sub> , TEA, THF, RT, 2 h.	115
<b>Formula 1.1</b>		2
<b>Formula 4.1</b>		45
<b>Formula 9.1</b>		140

## List of Abbreviations and Symbols

4-NPB	4-nitrophenyl butyrate
5-HT <sub>2C</sub>	5-Hydroxytryptamine type 2C receptor
ADMET	Absorption, Distribution, Metabolism, Excretion and Toxicity
AHA/ACC/TOS	American Heart Association/American College of Cardiology/The Obesity Society
ANOVA	Analysis of variance
API	<i>Ayurvedic</i> Pharmacopoeia of India
ARF	Alkaloid rich fractions
AU	Absorbance Unit
BBB	Blood Brain Barrier
BMI	Body Mass Index
CB <sub>1</sub>	Cannabinoid type 1 receptor
CHARMM	Chemistry at Harvard Macromolecular Mechanics
CDCl <sub>3</sub>	Deuteriated chloroform
CM	Cold Maceration
CNS	Central Nervous System
CYP	Cytochrome P
DCM	Dichloromethane
DG	Diglyceride
DIPEA	N,N-Diisopropylethylamine
DMF	Dimethyl formamide
DMSO	Dimethyl sulfoxide
DMSO- <i>d</i> <sub>6</sub>	Deuteriated dimethyl sulfoxide
ESI	Electrospray ionization
FA	Fatty acid
FDA	Food Drug Administration
Fig.	Figure
FTIR	Fourier Transform Infrared
G	Galloyl
GABA	Gamma-aminobutyric acid
GI	Gastro-Intestinal
GLP-1	Glucagon like peptide type 1 receptor

GROMACS	GRoningen Machine for Chemical Simulations
HATU	1-[Bis(dimethylamino)methylene]-1H-1,2,3-triazolo[4,5-b]pyridinium 3-oxide hexafluorophosphate
HDL	High-density lipoproteins
HFD	High Fat Diet
HP	Hot Percolation
HPLC	High Performance Liquid Chromatography
HPTLC	High Performance Thin Layer Chromatography
HRMS	High Resolution Mass Spectrometry
IC <sub>50</sub>	Half maximal inhibitory concentration
ICH	International Conference on Harmonization
KBr	Potassium bromide
KOH	Potassium hydroxide
LCMS	Liquid Chromatography Mass Spectrometry
LD <sub>50</sub>	Half maximal lethal dose
LDL	Low-density lipoprotein
LINCS	Linear Constraint Solver
LiOH	Lithium hydroxide
LOD	Limit of Detection
LOQ	Limit of Quantification
MD	Molecular Dynamics
MeOH	Methanol
MG	Monoglyceride
M	Molar
Min	Minute
MM2	Molecular Mechanics 2
m.p.	Melting point
MUP	Methoxyundecyl phosphinic acid
<i>n</i>	Number of replicates
ND	Not determined
nM	Nanomolar
nm	Nanometre
NMR	Nuclear Magnetic Resonance

NPs	Natural Products
NPD	Normal Pellet Diet
NPT	Number of particles, Pressure and Temperature
Ns	not significant
NVT	Number of particles, Volume and Temperature
OTTT	Oral Triglyceride Tolerance Test
PDB	Protein Data Bank
Pen	Pencillamine
Pgp	P-glycoprotein
Phe	Phenyl alanine
PL	Pancreatic lipase
R <sub>f</sub>	Retardation factor
RMSD	Root Mean Square Deviation
rpm	Rotation per minute
RSD	Relative Standard Deviation
RT	Room Temperature
SD	Standard Deviation
SEM	Standard error of mean
Sps.	Species
STEPS	STEPwise Approach to Surveillance
TC	Total cholesterol
TCM	Traditional Chinese Medicine
TEA	Triethylamine
TG	Triglycerides
THF	Tetrahydrofuran
TLC	Thin Layer Chromatography
Tyr	Tyrosine
UE	Ultrasonic Extraction
UK	United Kingdom
US	United States
WHO	World Health Organization
WHR	Waist-Hip Ratio
kg	kilogram

%	percentage
°C	Degree Celsius
g	Gram
mg	Milligram
µg	Microgram
ng	Nanogram
µL	Microliter
µM	Micromolar
mL	Millilitre
kcal/mol	Kilocalorie per mole
Å	Angstrom
h	Hour
ns	Nanosecond
ps	Picosecond

## 1 | Introduction

### 1.1 | Obesity

#### *1.1.1 / Definition, etymology and statistics*

Overweight and obesity are defined as abnormal or excessive fat accumulation that may impair health [1]. The word “obesity” originated from the Latin word ‘*Obesitas* (*Ob* - over; *Esus* - Eating)’ which means “fat, stout, or plump”. The first usage of the word was observed in 1611 by Randle Cotgrave in ‘The Oxford English Dictionary’. While obesity was earlier considered a metabolic disorder, the World Obesity Federation in 2017, declared obesity as a chronic, relapsing progressive disease process [2].

Worldwide, obesity has tripled since 1975 with recent reports from the World Health Organization (WHO) indicating a rapid upsurge in obese population. As of 2016, over 1.9 billion adults (accounting to 39% of the global population) were found overweight, of which 650 million adults were found obese (13% of global population). While obesity has been prevalent in adults, recent decades has seen a phenomenal rise in adolescent and childhood obesity with 340 million adolescents (aged below 18) and 41 million children (aged under 5) being found overweight or obese [3]. Once identified a problem with the developed countries, obesity now is observed with the developing nations. For instance, a survey conducted by the Ministry of Health and Family Welfare (India) during 2015-2016, indicated that around 40.5% of the total Indian population are either overweight or obese [4].

#### *1.1.2 / Types of obesity*

Obesity is classified under two major classes, based on the fat distribution, as Central (android) and Peripheral (gynoid). Central obesity is characterized by fat depots around the abdomen, and hence is also named as the abdominal obesity or the apple-shaped obesity, while peripheral obesity is characterized by fat depots around hips and thighs (pear-shaped obesity). Central obesity can also be observed in the upper chest, neck and shoulders [5].

A different classification indicated by the National Health Service (UK), classified obese individuals under six categories, and is based on a study conducted by University of Sheffield in the UK and the Harvard School of Public Health in the US. The study included data from 4000 obese adults and reported six clusters. These were: (i) young healthy females; (ii) heavy-drinking males; (iii) unhappy and anxious middle-aged; (iv) affluent and healthy elderly; (v) physically sick but happy elderly and (vi) poorest health [6,7].

# Chapter 1

## 1.1.3 / Causes and comorbidities

At least 10 factors have been identified that contribute to obesity, and include (i) the food environment; (ii) decrease in physical activity; (iii) sleep debt; (iv) drug-induced weight gain; (v) decline in cigarette smoking; (vi) endocrine disruptors; (vii) infections; (viii) ethnicity (ix) age and (x) intrauterine effects [8,9]. However, *a vast majority of the obesity has been observed with the food environment and reduced physical activity*, while other factors share a minor role in the global obesity epidemic [10].

While obesity is preventable and does not itself impose any risk to the health, a chronic condition might lead to severe comorbid risks including insulin resistance, diabetes mellitus (Type II), hypertension, dyslipidaemia, coronary heart disease, sleep apnea, gall bladder disease, gout, osteoarthritis, and certain cancers [11]. In particular, these comorbid risks are known to be observed in people with central obesity, while the peripheral obesity was found to be protective [12,13].

## 1.1.4 / Classification

Overweight and obesity are preliminarily classified using the Body Mass Index (BMI) and is calculated using the formula

$$\text{BMI} = \frac{\text{weight of the individual (in kg)}}{\text{square of the height of the individual (in m}^2\text{)}} \quad \text{-----} \quad \boxed{\text{Formula 1.1}}$$

As represented in Table 1.1, an individual with BMI ranging between 25-29.9 kg/m<sup>2</sup> is considered overweight, while a BMI greater than 30 kg/m<sup>2</sup> is obese. Similarly, for children aged between 5 - 19 years or under 5 years, overweight and obesity are determined using the respective WHO Growth Reference Medians [14–16].

**Table 1.1.** Summary of BMI based classification for overweight and obesity in different age groups

	Adults (>19 years)	Children (5-19 years)	Children (< 5 years)
<b>Overweight</b>	25 - 29.9 kg/m <sup>2</sup>	BMI-for-age > 1 standard deviation above WHO Growth Reference Median	BMI-for-age > 2 standard deviations above WHO Growth Reference Median
<b>Obesity</b>	30 - 34.9 kg/m <sup>2</sup> (Class I) 35 – 39.9 kg/m <sup>2</sup> (Class II) ≥ 40 kg/m <sup>2</sup> (Class III)	BMI-for-age > 2 standard deviations above WHO Growth Reference Median	BMI-for-age > 3 standard deviations above WHO Growth Reference Median

While consistent evidences have indicated BMI to be highly specific it has also been reported to have low to moderate sensitivity in determining an individual as overweight or obese. For instance, literature reports suggest that around half of all adults with excess body

## Chapter 1

---

fat have been defined as non-obese according to BMI. Similarly, at least 25-50 % of children and adolescents with excess body fat have been defined as having a healthy BMI-for-age [17–19].

Waist-Hip Ratio (WHR) is the other parameter used to determine obesity and is considered more accurate in comparison to BMI. The WHO STEPwise Approach to Surveillance (STEPS) provides a simple standardized protocol for measuring the waist and hip circumference, which states that:

- The measurement of waist circumference must be made at the approximate midpoint between the lower margin of the last palpable rib and the top of the iliac crest
- The measurement of hip circumference must be made at the widest portion of the buttocks

Further, the tightness of the tape and the subject posture are to be maintained as suggested in the STEPS protocol. A WHR greater than 0.85 (for women) and 1.00 (for men) are considered obese [20].

### ***1.1.5 / Treatment***

The current guidelines suggested by the “American Heart Association/American College of Cardiology/The Obesity Society (AHA/ACC/TOS)” recommends a minimum loss of 500 kcal per day, through physical activity and diet modification to achieve significant weight loss [21]. However, a negative response to life style modification alone, might necessitate either bariatric surgery and/or anti-obesity pharmacotherapy as adjunctive strategies to achieve significant weight loss [22]. Of these two adjuncts, bariatric surgery is recommended only to patients with BMI  $\geq 40$  kg/m<sup>2</sup> or BMI  $\geq 35$  kg/m<sup>2</sup> with comorbidities, while anti-obesity pharmacotherapy is recommended to the other classes of obese patients who do not qualify for surgery [23].

Since 1930s, many drugs have been approved for the treatment of obesity, however, most of these drugs were withdrawn due to their severe adverse effects during post marketing surveillance. A concise list of the approved and withdrawn drugs used in the treatment of obesity are summarized in Fig. 1.1 and 1.2, Tables 1.2 and 1.3. The approved drugs are further classified under two main classes based on the duration of administration, namely short-term and long-term anti-obesity pharmacotherapy [24–27].



## Chapter 1

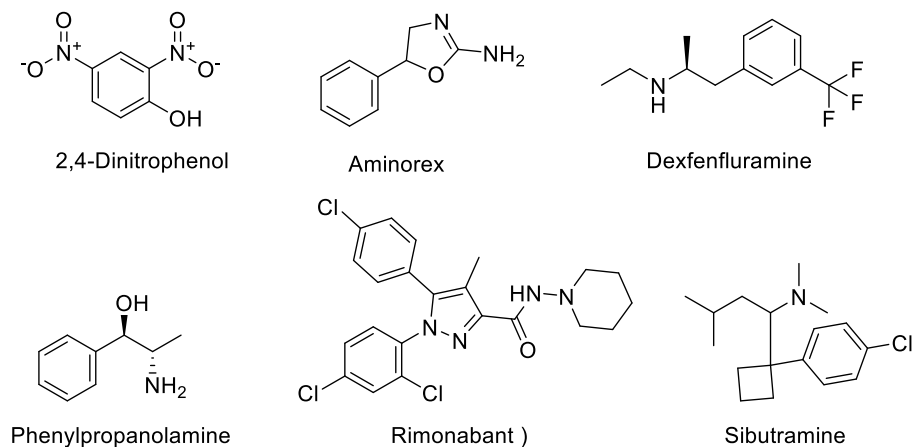
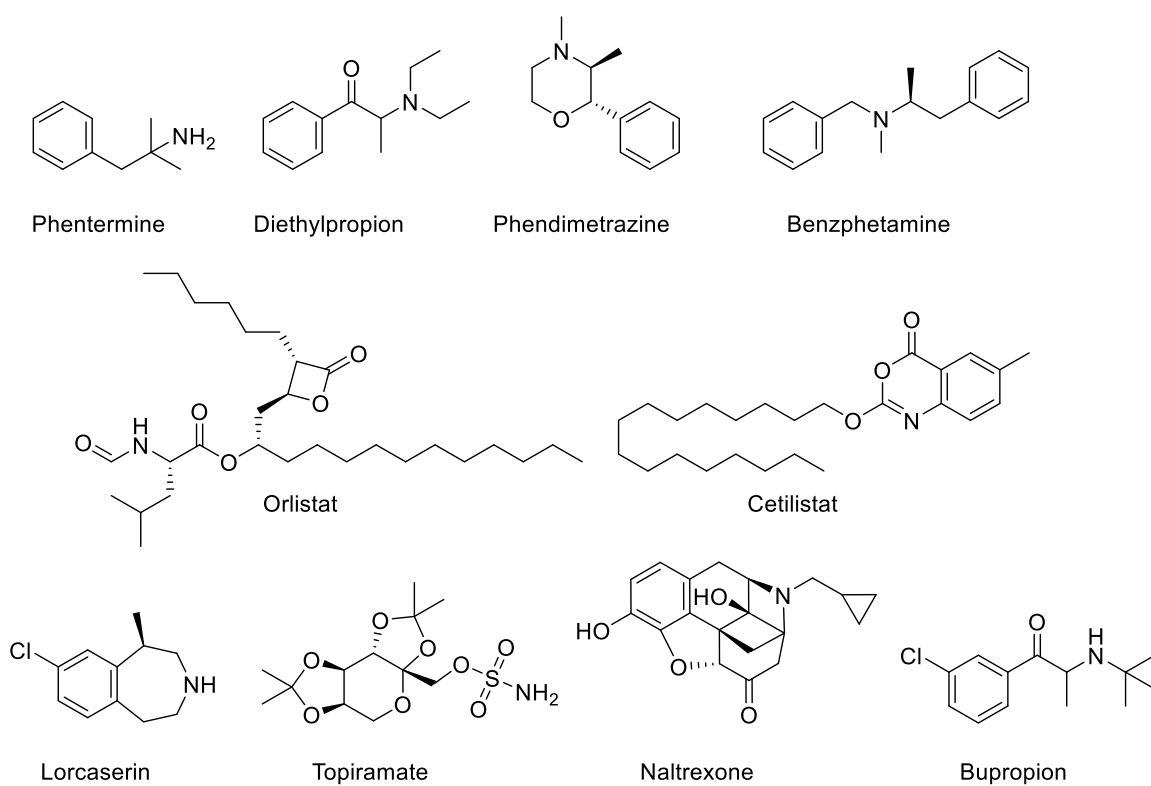


**Fig. 1.1.** Structures of withdrawn anti-obesity drugs



H-His-Ala-Glu-Gly-Thr-Phe-Thr-Ser-Asp-Val-Ser-Ser-Tyr-Leu-Glu-Gly-Gln-Ala-Ala-Lys( $\gamma$ -Glu-palmitoyl)-Glu-Phe-Ile-Ala-Trp-Leu-Val-Arg-Gly-Arg-Gly-OH

Liraglutide

**Fig. 1.2.** Structures of drugs approved for obesity treatment

## Chapter 1

**Table 1.2.** List of withdrawn anti-obesity drugs

Drug	Mechanism of action	Approved	Withdrawn	Reasons for Withdrawal
2,4-Dinitrophenol	Uncoupler of oxidative phosphorylation in phospholipid bilayer	1933	1938	Dermatitis, Agranulocytosis, Visual impairment, and death
Aminorex	Anorectic stimulant	1965	1968	Pulmonary hypertension
Amphetamines (Schedule II)	Stimulates CNS through norepinephrine release, increases resting energy expenditure and suppresses appetite	1945 - 1962	1971	Addiction, hypertension, myocardial toxicity
Fenfluramine & dexfenfluramine	Serotonergic agent; suppresses appetite	1973/1996	1997	Valvular heart disease
Phenylpropanolamine	Norepinephrine release inducer; suppresses appetite	1982	2000	Haemorrhagic stroke
Rimonabant	Cannabinoid (CB <sub>1</sub> ) receptor antagonist	2006	2009	Mood disorders
Sibutramine	Monoamine reuptake inhibitor; suppresses appetite	1997	2010	Cardiovascular risks and stroke

**Table 1.3.** List of currently available anti-obesity drugs

Drug	Approved	Mechanism of action
<i>Short-term</i>		
Phentermine	1959	
Diethylpropion	2011	Norepinephrine release inducers and appetite suppressors
Phendimetrazine	2010	
Benzphetamine	2010	
<i>Long-term</i>		
Orlistat, Cetilistat	1999, 2013	Pancreatic lipase inhibitors; inhibits dietary lipid digestion
Lorcaserin	2012	5-HT <sub>2C</sub> receptor agonist
Phentermine/topiramate extended release (ER)	2012	Sympathomimetic / increases GABA activity and modulates voltage-gated ion channels
Naltrexone/Bupropion	2014	Opioid receptor antagonist/aminoketone antidepressant
Liraglutide	2014	GLP-1 receptor agonist

### 1.1.6 Emerging targets for obesity treatment

Several targets are being explored for the treatment of obesity and can be sub-divided into three categories, as represented in Fig. 1.3, as; **a)** Central targets and hormones, the regulation of which suppresses the appetite; **b)** the peripheral hormones of the gastrointestinal (GI) tract, pancreas, and adipose tissue, that aid in satiety or appetite suppression, and **c)** the metabolic modifiers through which lipid metabolism is altered [27-42].

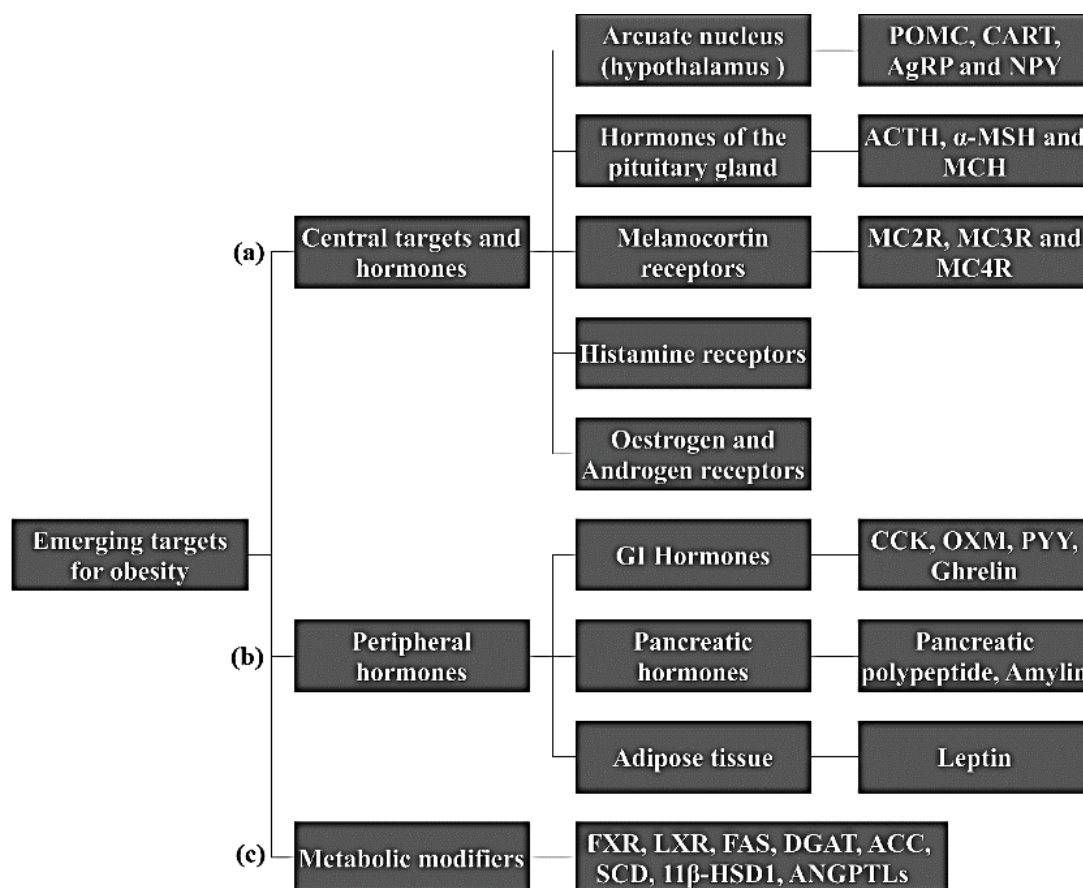


**Fig. 1.3.** A schematic representation of various targets being explored for the treatment of obesity

*However, a majority of these targets are directed towards reducing the appetite, that would result in an overall inhibition of nutrition intake, and hence cannot be considered a rightful approach.*

Thus, based on overall facts it is clear that **(i)** a vast majority of the global obesity epidemic is observed with the food environment that contained higher percentage of dietary fats; and **(ii)** a majority of the targets under research for the treatment of obesity are focussed on suppressing the appetite and are associated with severe adverse effects. Hence, it can be concluded that pancreatic lipase is a validated target for the treatment of obesity, wherein its

inhibition would result in prevention of dietary fat digestion and subsequent absorption, and the inhibitor does not require any systemic absorption ruling out the possible adverse effects.

### 1.2 | Pancreatic lipase

Also known as the pancreatic triacylglycerol lipase (hereafter abbreviated as PL), it is a primary enzyme involved in the digestion of dietary lipids and is classified under the family of serine hydrolases (EC 3.1.1.3) along with the lingual lipase and gastric lipase. In humans, the lingual lipase possesses a negligible role in the lipid digestion while a major part occurs in the stomach and duodenum. As represented in Fig. 1.4, the dietary triglycerides are first hydrolysed to diglycerides in the presence of gastric lipase in the stomach, releasing one free fatty acid. The diglyceride is further hydrolyzed to monoglyceride and a free fatty acid in the presence of PL. Of these two lipases, gastric lipase is primarily involved in the hydrolysis of short chain esters and does not exhibit prominent role in adult humans, while 60-70% of the lipid digestion occurs in the presence of PL. However, the fatty acids generated during the gastric lipolysis act as emulsifiers alongside the bile salts, for the digestion of long chain fatty esters in duodenum [43,44].

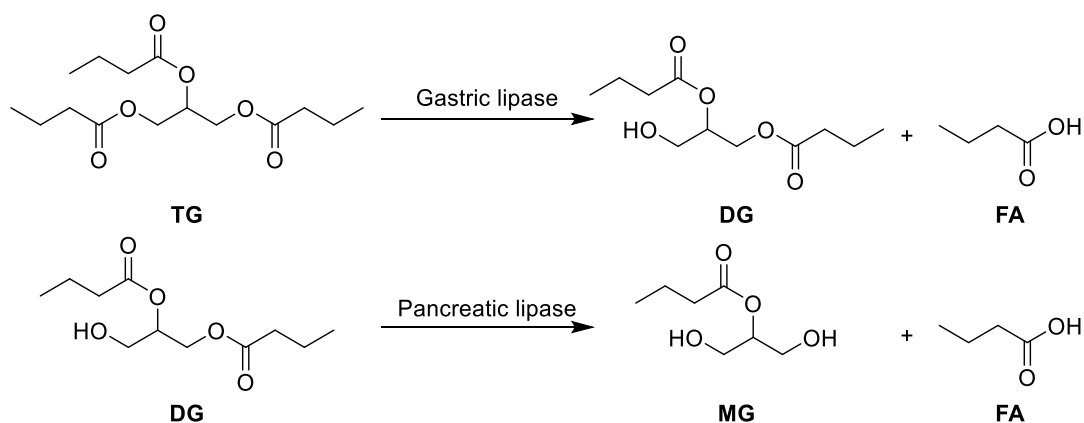


**Fig. 1.4.** Schematic representation of the lipid digestion in the gastrointestinal tract (TG: Triglyceride; DG: Diglyceride; MG: Monoglyceride; FA: Fatty acid)

#### 1.2.1 | PL and its crystal structure

The human PL is encoded by the *PNLIP* gene located at 10q25.3 region of the chromosome and is secreted from the pancreatic exocrine, along with the other pancreatic enzymes [45,46]. The crystal structure of the human PL is composed of 449 amino acids. As represented in Fig. 1.5, the larger protein chain constitutes the PL, while the smaller chain constitutes the pancreatic colipase, a small protein (with 85 amino acids) bound to the C-terminal of PL, and is involved in the activation of the PL. The active site of the human PL comprises of a catalytic triad of the amino acids, Ser152 - Asp176 - His263 [47]. This triad

## Chapter 1

is highly restricted and is surrounded by the hydrophobic lid domain which consists of the amino acids Gly76-Lys80 and Leu213-Met217 [48].

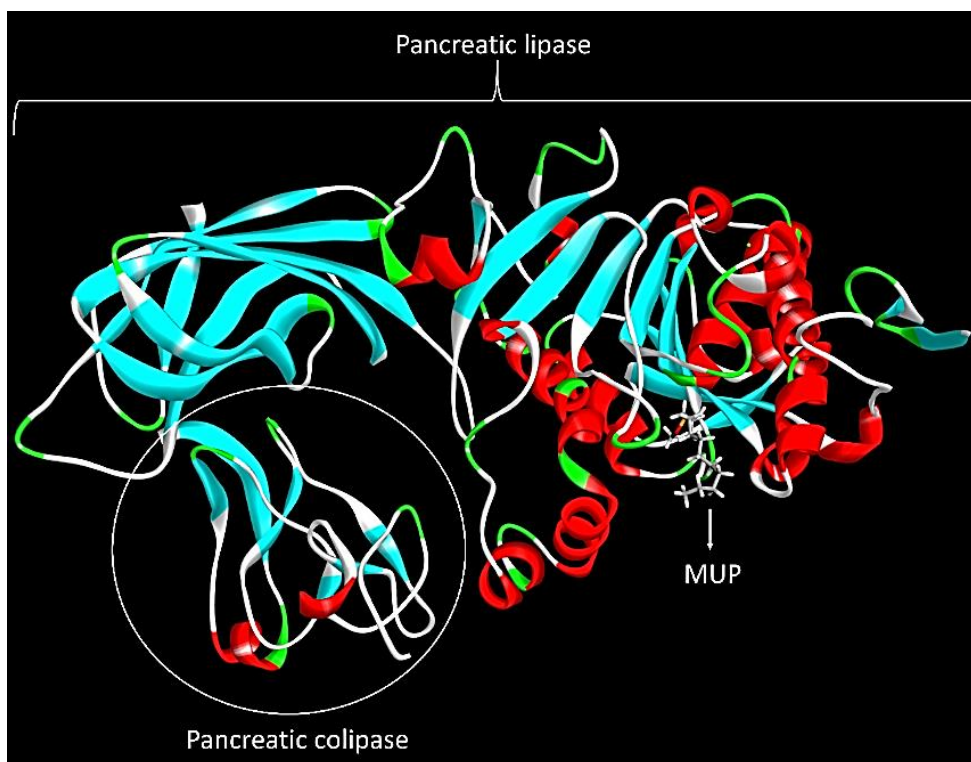


**Fig. 1.5.** Secondary structure of the human PL-colipase complex co-crystallised with methoxyundecyl phosphinic acid (MUP) at the active site

During the inactivated phase, the triad is inaccessible and enclosed within the lid domain. However, the activation of the PL leads to conformational change in the lid domain, resulting in the opening of the active site. Accordingly, the human PL exists in two conformations; the closed lid (inactivated) and the open lid (activated) conformations as represented in Fig. 1.6. The crystal structures of these two conformations were revealed through X-ray diffractions and are designated by the PDB codes, 1N8S and 1LPB, respectively [47,49].

## Chapter I

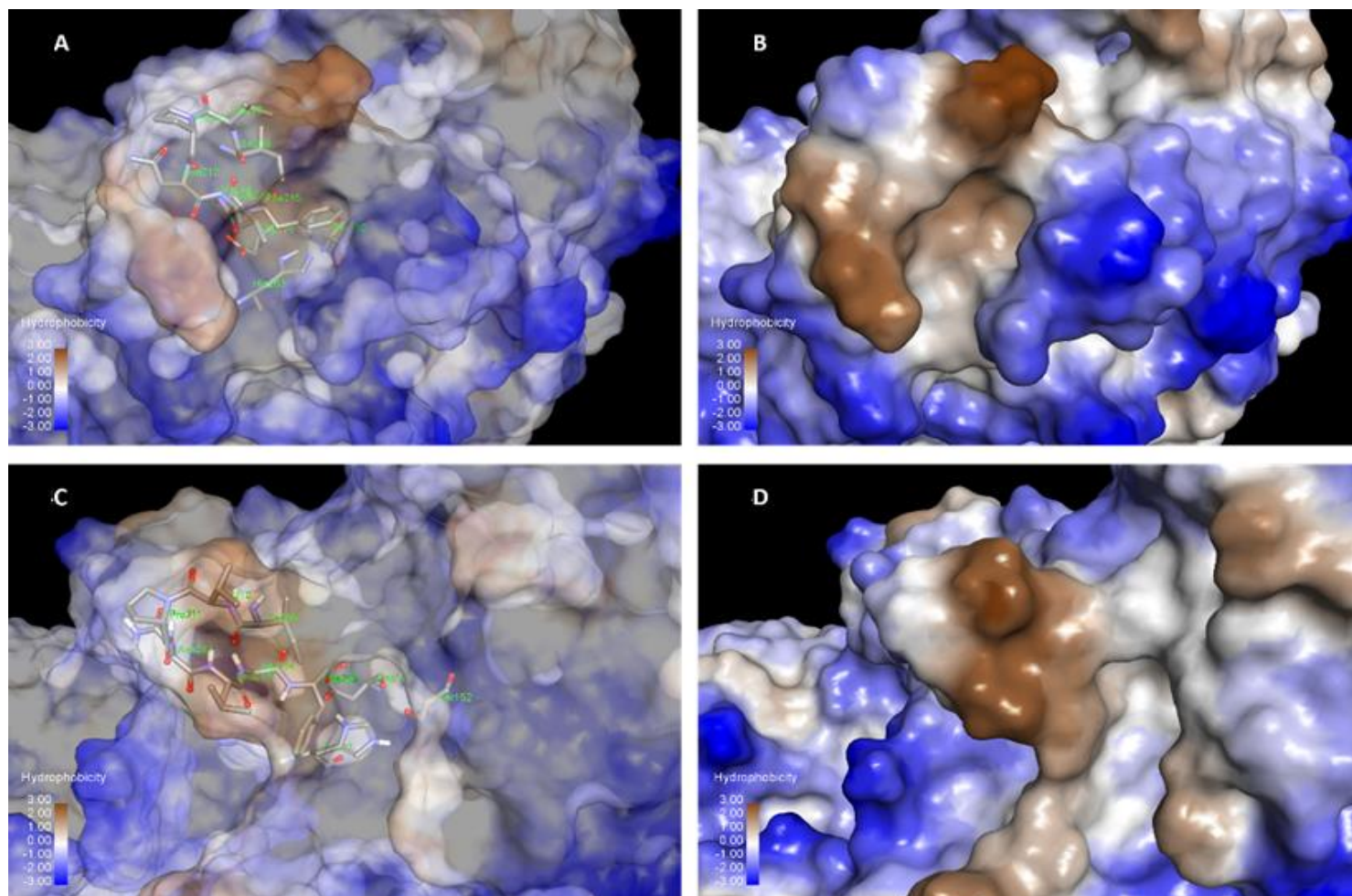


**Fig. 1.6.** Representation of closed (A, B) and open (C, D) lid forms of human PL. A & C represents transparent hydrophobic surface with active site amino acids; B & D includes only hydrophobic surface clearly representing the closed and open lid conformations (in brown), respectively

## 1.2.2 / Activation of PL and digestion of lipids

The physiology of lipid digestion involves a series of events, starting with the formation of lipid micelles in the duodenum, in the presence of bile salts and the free fatty acids (released from the gastric lipolysis). This micelle formation allows the interfacial activation of PL [50], facilitating hydrophobic interactions of the long alkyl chains of the lipids with the hydrophobic lid domain of the PL. This phenomenon results in conformational change of PL from the closed lid to the open lid form [51]. The conformational change is further facilitated through a salt bridge formation by Arg256-Asp257 with Tyr267-Lys268 [52]. The subsequent steps involve various biochemical reactions between the ester linkage of the triglyceride and the catalytic triad (Fig. 1.7), that results in the ester hydrolysis of the triglyceride [53].

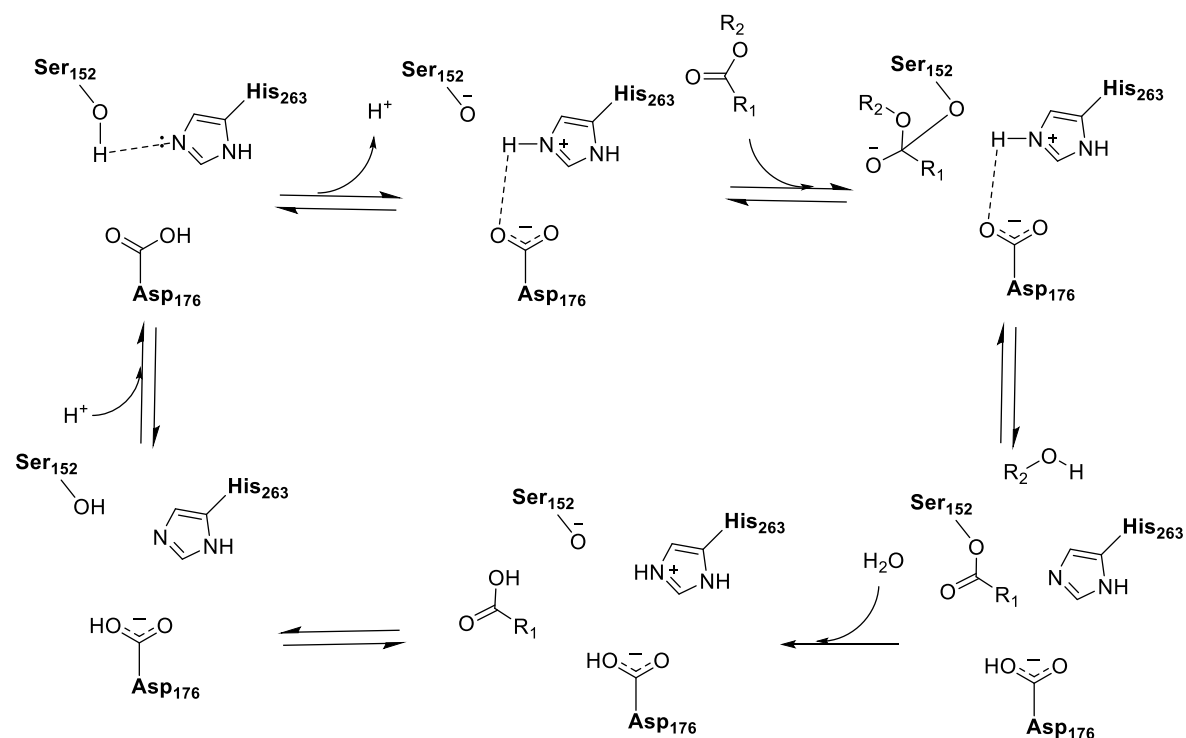


**Fig. 1.7.** Schematic flow representing series of biochemical reactions at the catalytic triad of PL during ester hydrolysis

### 1.3 | Problem Statement

Orlistat, is one among the few drugs (Fig 1.1 and Table 1.3), clinically approved for long term treatment of obesity. Since its approval in 1998 by the Food and Drug Administration (FDA), orlistat remains to be the most widely prescribed anti-obesity medication marketed under the trade names Xenical (Roche Pharmaceuticals Inc.) and Alli (GlaxoSmithKline Inc.) [54]. Further, orlistat was considered an effective medication with tolerable side effects *viz.*, steatorrhea, oily stools, frequent or urgent bowel movements [55]. However, recent decade has seen considerable reports on the severe adverse effects produced by chronic administration of orlistat. In 2010, FDA has approved a revised label for orlistat that included safety information about cases of severe liver injury [56]. Further, in April 2011, the consumer advocacy group and drug safety watchdog “Public Citizen” sent a letter to the FDA requesting the ban of orlistat, citing liver toxicity as well as the evidences from the FDA adverse-reaction files that included 47 cases of acute pancreatitis and 73 cases of kidney stones [57]. Further, the FDA Center for Drug Evaluation and Research, in 2015, approved safety labelling changes for orlistat, that included various adverse effects and possible risks *viz.*, kidney stones, gall stones, liver injury and pancreatitis [58]. Cetilistat, on the other hand, has successfully completed its phase III clinical trial, and has been approved for the treatment of obesity with complications, by the Japanese Ministry of Health, Family and Welfare on September 20, 2013 [59]. However, the drug has not been approved by the FDA to date. The scenario clearly highlights the urgent need for safer and effective PL inhibitors for obesity treatment.



## Chapter 1

---

### References

- [1] <http://www.who.int/topics/obesity/en/> (last accessed May 23, 2019).
- [2] G.A. Bray, K.K. Kim, J.P.H. Wilding, Obesity: A chronic relapsing progressive disease process. A position statement of the World Obesity Federation, *Obes. Rev.* 18 (2017) 715–723.
- [3] <http://www.who.int/mediacentre/factsheets/fs311/en/> (last accessed May 23, 2019).
- [4] <http://rchiips.org/nfhs/pdf/NFHS4/India.pdf> (last accessed May 23, 2019).
- [5] S. Aras, S. Üstünsoy, F. Armutçu, Indices of central and peripheral obesity; Anthropometric measurements and laboratory parameters of metabolic syndrome and thyroid function, *Balkan Med. J.* 32 (2015) 414–420.
- [6] <https://www.nhs.uk/news/obesity/there-are-six-different-types-of-obesity-study-argues/> (last accessed May 23, 2019).
- [7] M.A. Green, M. Strong, F. Razak, S. V Subramanian, C. Relton, P. Bissell, Who are the obese? A cluster analysis exploring subgroups of the obese, *J. Public Health (Bangkok)*. 38 (2016) 258–264.
- [8] S.M. Wright, L.J. Aronne, Causes of obesity, *Abdom. Radiol.* 37 (2012) 730–732.
- [9] S.M. Grundy, Multifactorial causation of obesity: Implications for prevention, *Am. J. Clin. Nutr.* 67 (1998) 563S–572S.
- [10] E.J. McAllister, N. V Dhurandhar, S.W. Keith, L.J. Aronne, J. Barger, M. Baskin, R.M. Benca, J. Biggio, M.M. Boggiano, J.C. Eisenmann, Ten putative contributors to the obesity epidemic, *Crit. Rev. Food Sci. Nutr.* 49 (2009) 868–913.
- [11] L. Khaodhjar, K.C. McCowen, G.L. Blackburn, Obesity and its comorbid conditions, *Clin. Cornerstone*. 2 (1999) 17–31.
- [12] S.H. Chang, T.S. Beason, J.M. Hunleth, G.A. Colditz, A systematic review of body fat distribution and mortality in older people, *Maturitas*. 72 (2012) 175–191.
- [13] M.J. Lee, Y. Wu, S.K. Fried, Adipose tissue heterogeneity: Implication of depot differences in adipose tissue for obesity complications, *Mol. Aspects Med.* 34 (2013) 1–11.
- [14] <http://www.who.int/mediacentre/factsheets/fs311/en/> (last accessed May 23, 2019).
- [15] [http://www.who.int/childgrowth/standards/weight\\_for\\_height/en/](http://www.who.int/childgrowth/standards/weight_for_height/en/) (last accessed May 23, 2019).
- [16] [http://www.who.int/growthref/who2007\\_bmi\\_for\\_age/en/](http://www.who.int/growthref/who2007_bmi_for_age/en/) (last accessed May 23, 2019).
- [17] D.O. Okorodudu, M.F. Jumean, V.M. Montori, A. Romero-Corral, V.K. Somers, P.J.

## Chapter 1

---

- Erwin, F. Lopez-Jimenez, Diagnostic performance of body mass index to identify obesity as defined by body adiposity: A systematic review and meta-analysis, *Int. J. Obes.* 34 (2010) 791–799.
- [18] J.J. Reilly, J. Kelly, D.C. Wilson, Accuracy of simple clinical and epidemiological definitions of childhood obesity: Systematic review and evidence appraisal, *Obes. Rev.* 11 (2010) 645–655.
- [19] A. Javed, M. Jumean, M.H. Murad, D. Okorodudu, S. Kumar, V.K. Somers, O. Sochor, F. Lopez-Jimenez, Diagnostic performance of body mass index to identify obesity as defined by body adiposity in children and adolescents: A systematic review and meta-analysis, *Pediatr. Obes.* 10 (2015) 234–244.
- [20] Waist circumference and waist-hip ratio: Report of a WHO expert consultation, Geneva, 8-11 December 2008, ISBN 978 92 4 150149 1.
- [21] M.D. Jensen, D.H. Ryan, C.M. Apovian, J.D. Ard, A.G. Comuzzie, K.A. Donato, F.B. Hu, V.S. Hubbard, J.M. Jakicic, R.F. Kushner, 2013 AHA/ACC/TOS guideline for the management of overweight and obesity in adults: A report of the American College of Cardiology/American Heart Association Task Force on Practice Guidelines and The Obesity Society, *J. Am. Coll. Cardiol.* 63 (2014) 2985–3023.
- [22] D. Patel, Pharmacotherapy for the management of obesity, *Metab. Exp.* 64 (2015) 1376–1385.
- [23] <https://asmbs.org/patients/who-is-a-candidate-for-bariatric-surgery> (last accessed May 23, 2019).
- [24] D. Haslam, Weight management in obesity-Past and present, *Int. J. Clin. Pract.* 70 (2016) 206–217.
- [25] S. Manning, A. Pucci, N. Finer, Pharmacotherapy for obesity: Novel agents and paradigms, *Ther. Adv. Chronic Dis.* 5 (2014) 135–148.
- [26] I.J. Onakpoya, C.J. Heneghan, J.K. Aronson, Post-marketing withdrawal of anti-obesity medicinal products because of adverse drug reactions: A systematic review, *BMC Med.* 14 (2016) 191.
- [27] G.W. Kim, J.E. Lin, E.S. Blomain, S.A. Waldman, Antiobesity pharmacotherapy: New drugs and emerging targets, *Clin. Pharmacol. Ther.* 95 (2014) 53–66.
- [28] G.W.M. Millington, The role of proopiomelanocortin (POMC) neurones in feeding behaviour, *Nutr. Metab. (Lond)*. 4 (2007) 1.
- [29] M.L. Raffin-Sanson, Y. De Keyzer, X. Bertagna, Proopiomelanocortin, a polypeptide precursor with multiple functions: From physiology to pathological conditions, *Eur.*

- J. Endocrinol. 149 (2003) 79–90.
- [30] A. Vicentic, D.C. Jones, The CART (cocaine-and amphetamine-regulated transcript) system in appetite and drug addiction, *J. Pharmacol. Exp. Ther.* 320 (2007) 499–506.
- [31] L. Verret, R. Goutagny, P. Fort, L. Cagnon, D. Salvert, L. Léger, R. Boissard, P. Salin, C. Peyron, P.H. Luppi, A role of melanin-concentrating hormone producing neurons in the central regulation of paradoxical sleep, *BMC Neurosci.* 4 (2003) 19.
- [32] H. Shimizu, H. Arima, M. Watanabe, M. Goto, R. Banno, I. Sato, N. Ozaki, H. Nagasaki, Y. Oiso, Glucocorticoids increase neuropeptide Y and agouti-related peptide gene expression via adenosine monophosphate-activated protein kinase signaling in the arcuate nucleus of rats, *Endocrinology.* 149 (2008) 4544–4553.
- [33] C. Xu, J. He, H. Jiang, L. Zu, W. Zhai, S. Pu, G. Xu, Direct effect of glucocorticoids on lipolysis in adipocytes, *Mol. Endocrinol.* 23 (2009) 1161–1170.
- [34] P. Holzer, F. Reichmann, A. Farzi, Neuropeptide Y, peptide YY and pancreatic polypeptide in the gut-brain axis, *Neuropeptides.* 46 (2012) 261–274.
- [35] T. Masaki, S. Chiba, G. Yoshimichi, T. Yasuda, H. Noguchi, T. Kakuma, T. Sakata, H. Yoshimatsu, Neuronal histamine regulates food intake, adiposity, and uncoupling protein expression in Agouti yellow (A y/a) obese mice, *Endocrinology.* 144 (2003) 2741–2748.
- [36] R.L. Batterham, C.W. Le Roux, M.A. Cohen, A.J. Park, S.M. Ellis, M. Patterson, G.S. Frost, M.A. Ghatei, S.R. Bloom, Pancreatic polypeptide reduces appetite and food intake in humans, *J. Clin. Endocrinol. Metab.* 88 (2003) 3989–3992.
- [37] M.D. Klok, S. Jakobsdottir, M.L. Drent, The role of leptin and ghrelin in the regulation of food intake and body weight in humans: A review, *Obes. Rev.* 8 (2007) 21–34.
- [38] M.A. Cowley, J.L. Smart, M. Rubinstein, M.G. Cerdán, S. Diano, T.L. Horvath, R.D. Cone, M.J. Low, Leptin activates anorexigenic POMC neurons through a neural network in the arcuate nucleus, *Nature.* 411 (2001) 480–484.
- [39] R.S. Ahima, Revisiting leptin’s role in obesity and weight loss, *J. Clin. Invest.* 118 (2008) 2380–2383.
- [40] J.Y.L. Chiang, R. Kimmel, C. Weinberger, D. Stroup, Farnesoid X receptor responds to bile acids and represses cholesterol 7 $\alpha$ -hydroxylase gene (CYP7A1) transcription, *J. Biol. Chem.* 275 (2000) 10918–10924.
- [41] D.J. Peet, S.D. Turley, W. Ma, B.A. Janowski, J.M.A. Lobaccaro, R.E. Hammer, D.J. Mangelsdorf, Cholesterol and bile acid metabolism are impaired in mice lacking the

- nuclear oxysterol receptor LXR $\alpha$ , *Cell*. 93 (1998) 693–704.
- [42] S.B. Joseph, B.A. Laffitte, P.H. Patel, M.A. Watson, K.E. Matsukuma, R. Walczak, J.L. Collins, T.F. Osborne, P. Tontonoz, Direct and indirect mechanisms for regulation of fatty acid synthase gene expression by liver X receptors, *J. Biol. Chem.* 277 (2002) 11019–11025.
- [43] E. Bauer, S. Jakob, R. Mosenthin, Principles of physiology of lipid digestion, *Asian-Australasian J. Anim. Sci.* 18 (2005) 282–295.
- [44] M.C. Carey, D.M. Small, C.M. Bliss, Lipid digestion and absorption, *Annu. Rev. Physiol.* 45 (1983) 651–677.
- [45] R.C. Davis, A. Diep, W. Hunziker, I. Klisak, T. Mohandas, M.C. Schotz, R.S. Sparkes, A.J. Lusic, Assignment of human pancreatic lipase gene (*PNLIP*) to chromosome 10q24--q26, *Genomics*. 11 (1991) 1164–1166.
- [46] G.E. Palade, P. Siekevitz, L.G. Caro, Structure, chemistry and function of the pancreatic exocrine cell, in: A. de Reuck, M. Cameron (Eds.), *Ciba Found. Symp. Exocrine Pancreas Norm. Abnorm. Funct.*, John Wiley & Sons Ltd, Chichester, UK, 2008: pp. 23–55.
- [47] M.P. Egloff, F. Marguet, G. Buono, R. Verger, C. Cambillau, H. van Tilbeurgh, The 2.46 Å resolution structure of the pancreatic lipase-colipase complex inhibited by a C11 alkyl phosphonate, *Biochemistry*. 34 (1995) 2751–2762.
- [48] F.K. Winkler, A. D’Arcy, W. Hunziker, Structure of human pancreatic lipase, *Nature*. 343 (1990) 771–774.
- [49] H. van Tilbeurgh, L. Sarda, R. Verger, C. Cambillau, Structure of the pancreatic lipase-procolipase complex. *Nature*. 359 (1992) 159–162.
- [50] C. Chapus, M. Semeriva, C. Bovier-Lapierre, P. Desnuelle, Mechanism of pancreatic lipase action. 1. Interfacial activation of pancreatic lipase, *Biochemistry*. 15 (1976) 4980–4987.
- [51] H. van Tilbeurgh, M.P. Egloff, C. Martinez, N. Rugani, R. Verger, C. Cambillau, Interfacial activation of the lipase-procolipase complex by mixed micelles revealed by X-ray crystallography, 362 (1993) 814–820.
- [52] M.E. Lowe, The triglyceride lipases of the pancreas, *J. Lipid Res.* 43 (2002) 2007–2016.
- [53] M. Kokkinou, L.G. Theodorou, E.M. Papamichael, Aspects on the catalysis of lipase from porcine pancreas (type VI-s) in aqueous media: Development of ion-pairs, *Braz. Arch. Biol. Tech.* 55 (2012) 231–236.

## Chapter 1

---

- [54] <https://www.fda.gov/Drugs/DrugSafety/PostmarketDrugSafetyInformationforPatientsandProviders/ucm180076.htm> (last accessed May 23, 2019).
- [55] A.M. Heck, J.A. Yanovski, K.A. Calis, Orlistat, a new lipase inhibitor for the management of obesity, *Pharmacother. J. Hum. Pharmacol. Drug Ther.* 20 (2000) 270–279.
- [56] <http://www.fda.gov/Drugs/DrugSafety/PostmarketDrugSafetyInformationforPatientsandProviders/ucm213038.htm> (last accessed May 23, 2019).
- [57] <http://citizen.org/petition-to-fda-to-ban-orlistat-alli-xenical-2011> (last accessed May 23, 2018).
- [58] <https://wayback.archive-it.org/7993/20170112172652/http://www.fda.gov/Safety/MedWatch/SafetyInformation/ucm215504.htm> (last accessed May 23, 2019).
- [59] [https://www.norgine.com/press\\_release/norgine-and-takeda-announce-the-new-drug-application-approval-of-oblean-cetilistat-tablets-120mg-in-japan/](https://www.norgine.com/press_release/norgine-and-takeda-announce-the-new-drug-application-approval-of-oblean-cetilistat-tablets-120mg-in-japan/) (last accessed May 23, 2019).

### 2 | Literature Review

#### 2.1 | Natural products and their role in drug discovery

Natural products (NPs) are secondary metabolites, produced by any living organism in response to external stimuli such as nutritional changes, infection and competition. Higher plants, fungi, bacteria, protozoans, insects and animals provide a large untapped reservoir of such NPs that can be studied for their chemistry and bioactivity prospective. NPs from these reservoirs have always been an important source for the treatment of various human diseases and disorders [1], and have a tremendous potential as lead compounds, for the development of new drugs. Moreover, NPs provide significant share of new clinical candidates and drugs, despite the severe competition from other drug discovery methods. As per an extensive analysis provided by Cragg and Newman [2] on the various sources of new drugs covered over a period of 1980-2014, at least 377 NP based drugs have been approved during this period, that included 54 unmodified NPs, 268 NP derivatives and 55 synthetic drugs with a NP pharmacophore. Notable examples include fidaxomicin (**1**), ingenol mebutate (**2**), voglibose (**3**), laninamivir octanoate (**4**), vinflunine (**5**), brodimoprim (**6**), sofosbuvir (**7**), tipiracil (**8**) and nateglinide (**9**) (Fig. 2.1).

Success in NP based drug discovery is dependent on various factors like careful plant selection, which in turn can be decided based on the *information from traditional medicine*. The use of NPs in various systems of medicine dates back to 7000 BC, with *Ayurveda* and the Traditional Chinese Medicine (TCM) representing the two famous systems of traditional medicine from India and China, respectively [3]. The word “*Ayurveda*” is derived from the two Sanskrit words; *Ayur* (life) and *Veda* (science), which literally means “the science of life”. It remains one of the most ancient medical system, widely practiced in the Indian subcontinent and has both philosophical and experimental basis. *Charaka Samhita* and *Sushruta Samhita* (100–500 BC) are the two main classical texts of *Ayurveda*, that described over 700 plants along with their classification, pharmacological and therapeutic properties [4]. *Ayurveda* has its significant contribution to the drug development program, and has provided numerous lead molecules such as vasicine (**10**) [bronchodilator], psoralen (**11**) [anti-vitiligo], curcumin (**12**) [anti-inflammatory], andrographolide (**13**) [hepatoprotective], withanolide D (**14**) [immunomodulator] and reserpine (**15**) [anti-hypertension] from its rich plethora of knowledge (Fig. 2.2).

## Chapter 2

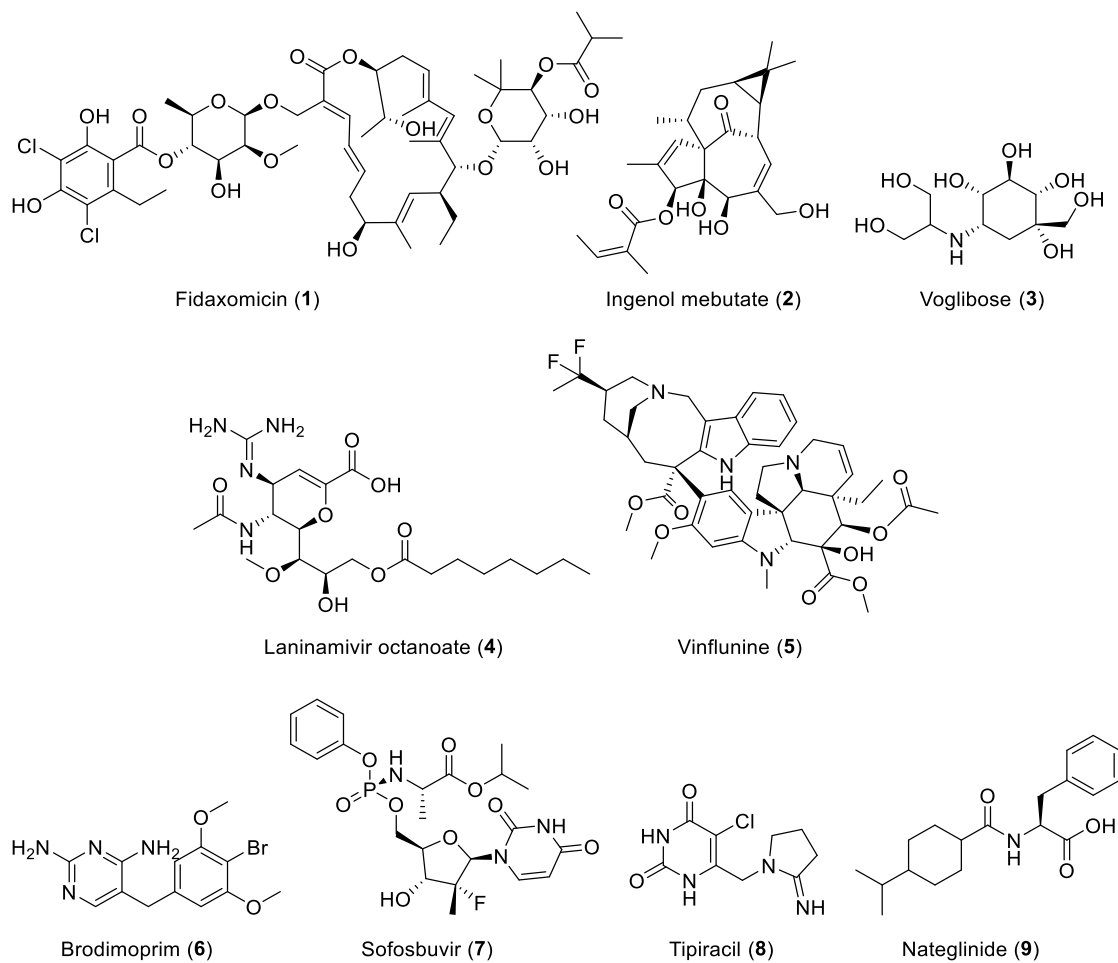


**Fig. 2.1.** Structures of various NPs (1-3), NP derivatives (4-5) and synthetic drugs with NP pharmacophore (6-9) used as drugs

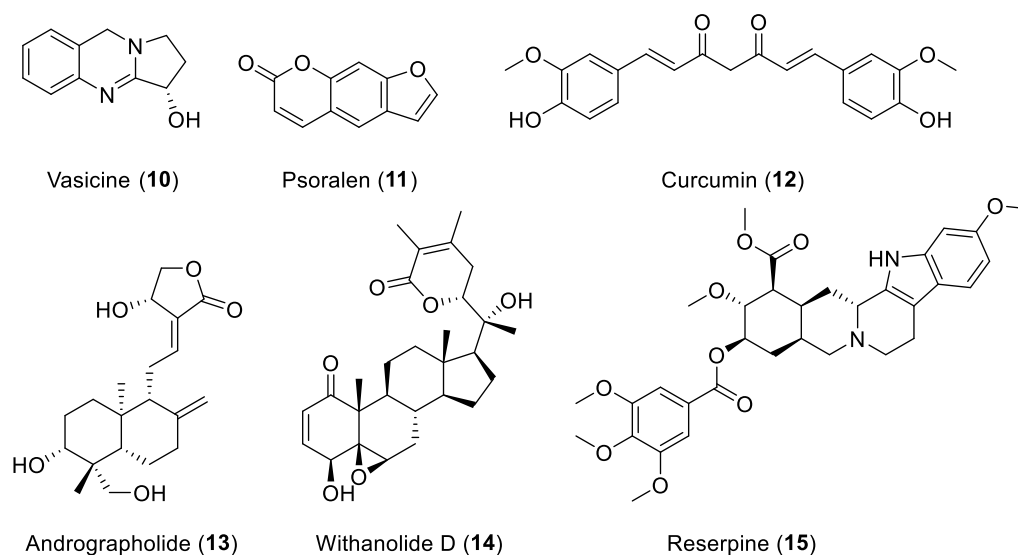


**Fig. 2.2.** Structures of various NPs from *Ayurveda* used as drugs

In addition, successful clinical trials of few *Ayurvedic* preparations exhibited promising results that included preparations for treatment of bronchial asthma, rheumatoid arthritis and ischemic heart disease etc. ***Further, the use of detailed molecular level studies to prove the effectiveness of ayurvedic drugs can potentiate the role of Ayurveda in drug discovery in more sound and scientific manner*** [5]. The *Ayurvedic* Pharmacopoeia of India (API) provides monographs for 258 different *Ayurvedic* drugs that contribute significantly to the drug discovery program [6].

### **2.2 | Natural products in PL inhibition**

Recent decades have seen a wide exploration of NPs for their PL inhibitory potential. At least 300 species, that include plants, marine algae and fungi, have been evaluated for their PL inhibitory activity [7–10].

Considering the advantages of NP-based drug discovery, a detailed literature search was performed to identify NP-based PL inhibitors that in turn would provide structural features required for potential PL inhibition. The search highlighted around 750 NPs that have been found to possess PL inhibitory activity. The literature review detailed in here discusses notable examples of these NPs, classified under diverse chemical classes (Fig. 2.3). Further, various structural features that resulted in potential PL inhibition have been identified and discussed. Since, the PL inhibitory activity of these NPs have been determined using different assay procedures, the activity profile of these NPs could not be compared. However, the PL inhibitory potential of these NPs were defined either as potent, potential, moderate or poor, by comparing their IC<sub>50</sub> (or % inhibition) with that of the orlistat (standard) reported using similar assay procedure.

#### **2.2.1 | Polyphenols**

Polyphenols represent a wide range of phytochemicals found largely in fruits, leaves, vegetables etc., and are generally involved in defence mechanism against ultraviolet radiation or aggression by pathogens. These compounds are well known for their multifaceted biological activities and are widely explored for their potential as anti-carcinogenic, anti-inflammatory, and anti-obesity agents etc [11,12].



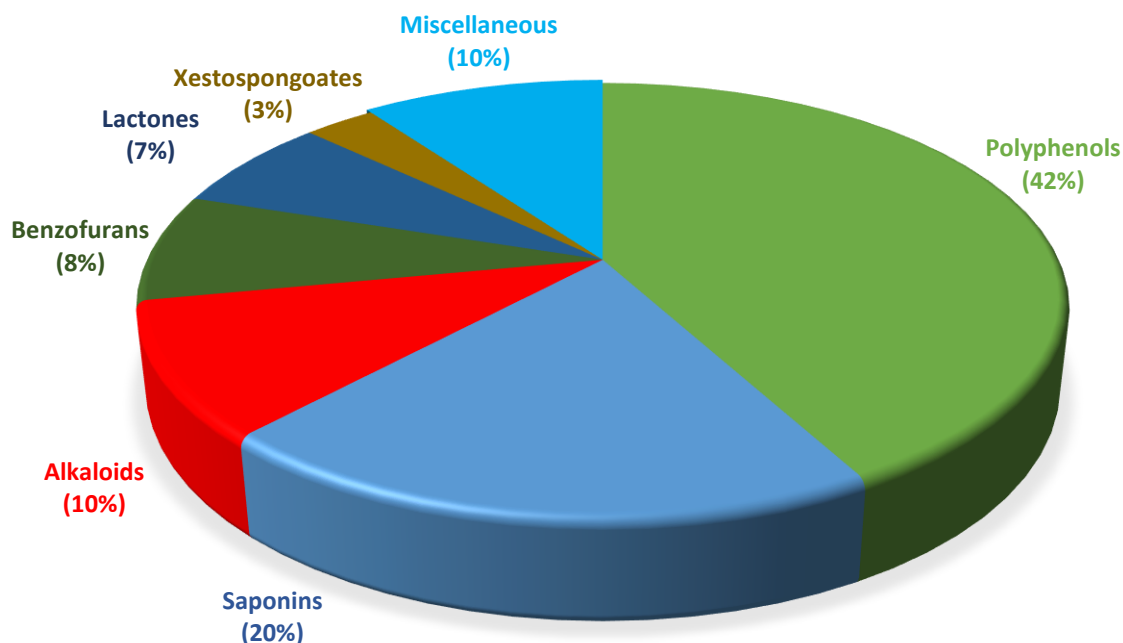


**Fig. 2.3.** Distribution of PL inhibitory NPs among various chemical classes

Within the area PL inhibitors, polyphenols contribute to the most explored class with over 200 compounds reported to date [13]. These polyphenols can be further classified into two major classes; flavonoids and stilbenes.

### 2.2.1.1 / Flavonoids

Flavonoids consist a C<sub>6</sub>-C<sub>3</sub>-C<sub>6</sub> structural backbone, in which the two C<sub>6</sub> units (Ring A and Ring B) are phenolic in nature and are linked to a chromane ring (Ring C). These flavonoids are further divided into various classes depending on the hydroxylation pattern and variations in the chromane ring [14]. A general representation of the structural backbones of various flavonoid classes is provided in Fig. 2.4.

#### *Flavanols and its oligomers*

Flavanols and its oligomers constitute the major class of PL inhibitory polyphenols, with a majority of flavanols identified from *Camellia sinensis* (Theaceae). In a study conducted by Nakai *et. al.*, around 50 flavanol derivatives have been isolated from the leaves of *C. sinensis* and screened for PL inhibitory activity [15]. These derivatives included the unsubstituted flavanols, their galloylated esters, and various flavanol based dimers. The unsubstituted flavanols *viz.*, (+)-catechin (**16**), (-)-epicatechin (**17**), (+)-gallocatechin (**18**) and (-)-epigallocatechin (**19**), did not exhibit potential PL inhibitory activity (IC<sub>50</sub> > 20 μM), with an exception for the 8-C-ascorbyl (-)-epigallocatechin (**20**) that exhibited a potent IC<sub>50</sub> of 0.646 μM.

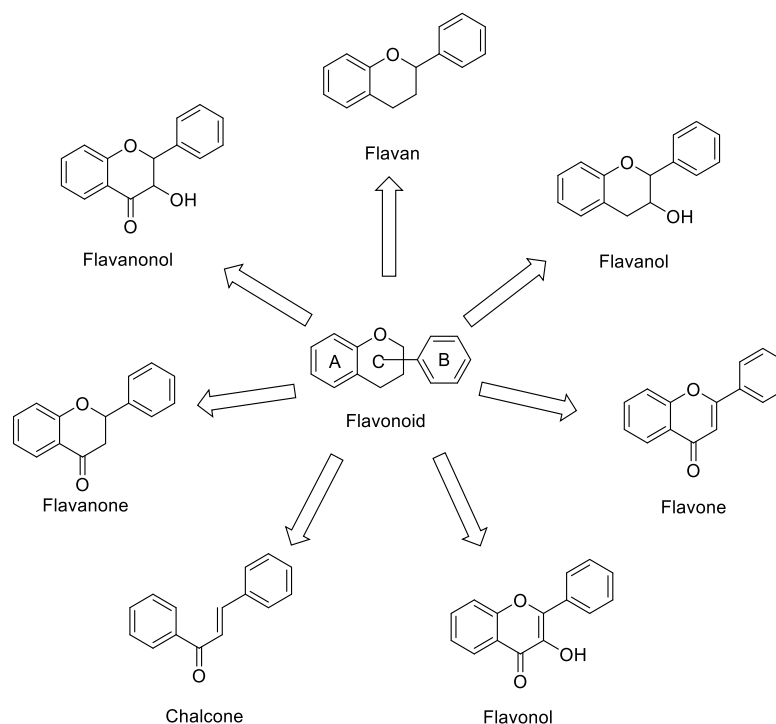


**Fig. 2.4.** A general representation of flavonoid backbone and its various classes

However, *the galloylated esters of these flavanols (21-27) exhibited a potent PL inhibitory activity* with  $IC_{50}$  values less than 1  $\mu M$ , highlighting the importance of gallate substitution (Fig. 2.5 and Table 2.1). Similar reports have been identified by Ivanov *et. al.*, wherein (+)-catechin 3-*O*-gallate (**28**) and (+)-catechin 3,5-di-*O*-gallate (**29**), isolated from the aqueous ethanol extract of *Bergenia crassifolia* rhizomes (Saxifragaceae) exhibited potent inhibitory activity towards PL with  $IC_{50}$  of 4.52 and 0.706  $\mu M$ , respectively [16].

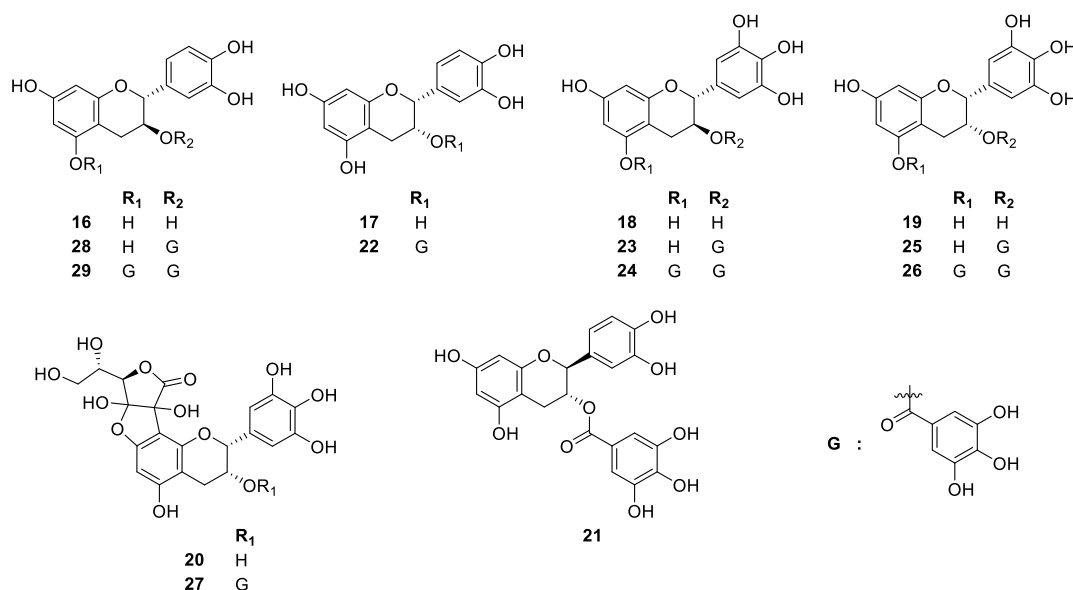


**Fig. 2.5.** Representation of various flavanols and their gallates from *C. sinensis* and *B. crassifolia* (G: Galloyl)

## Chapter 2

The study conducted by Nakai *et. al.*, also reported several flavan based dimers, listed under various sub-classes (Fig. 2.6). Oolonghomobisflavan A (**30**) was the most active compound in the study with an  $IC_{50}$  of 0.048  $\mu\text{M}$ , and the *potent activity of this analogue over other dimers was explained due to the presence of the methylene bridge* linking the 8,8'-positions of the two flavan units [15]

**Table 2.1.** PL inhibitory activity of flavanol gallates reported from *C. sinensis*

Compound	$IC_{50}$ ( $\mu\text{M}$ )
(-)-Catechin 3- <i>O</i> -gallate ( <b>21</b> )	0.543
(-)-Epicatechin 3- <i>O</i> -gallate ( <b>22</b> )	0.452
(-)-Gallocatechin 3- <i>O</i> -gallate ( <b>23</b> )	0.437
(-)-Gallocatechin 3,5-di- <i>O</i> -gallate ( <b>24</b> )	0.213
(-)-Epigallocatechin 3- <i>O</i> -gallate ( <b>25</b> )	0.349
(-)-Epigallocatechin 3,5-di- <i>O</i> -gallate ( <b>26</b> )	0.098
8- <i>C</i> -ascorbyl (-)-epigallocatechin 3- <i>O</i> -gallate ( <b>27</b> )	0.791

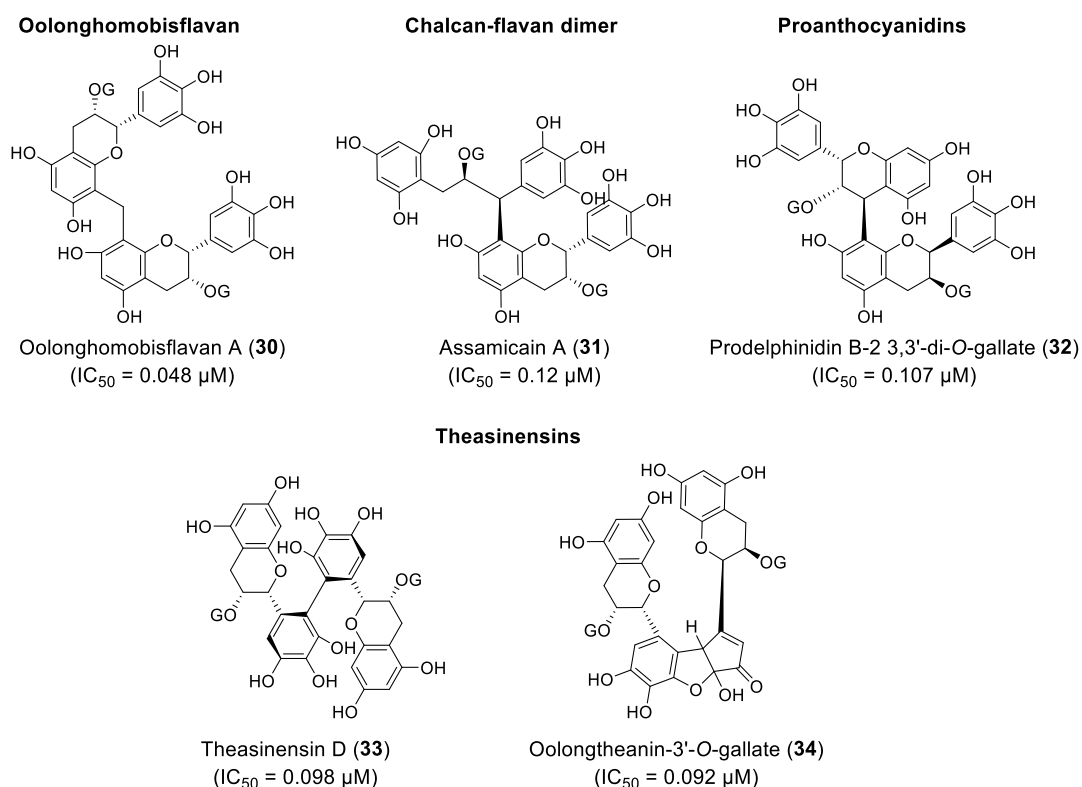
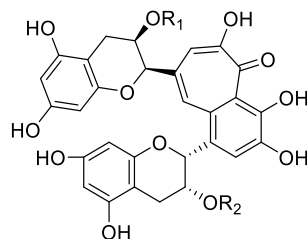


**Fig. 2.6.** Various flavan oligomers with potential PL inhibitory activity (G: Galloyl)

In another study conducted by Shannon *et. al* [17], the PL inhibitory potential of theaflavin (**35**) and its galloyl esters was determined (Fig. 2.7). *The study highlighted the prominent role of the galloyl ester and its location for greater potential of the galloylated esters (36-38) over their unsubstituted counterpart, theaflavin (35).*

## Chapter 2



	R <sub>1</sub>	R <sub>2</sub>	IC <sub>50</sub> (μM)
Theaflavin ( <b>35</b> )	H	H	>10
Theaflavin-3-O-gallate ( <b>36</b> )	H	G	3.0
Theaflavin-3'-O-gallate ( <b>37</b> )	G	H	4.2
Theaflavin-3,3'-di-O-gallate ( <b>38</b> )	G	G	1.9

**Fig. 2.7.** PL inhibitory potential of theaflavin and its galloyl esters (G: Galloyl)

### Flavones, flavonols and chalcones

Flavones and their hydroxy derivatives (flavonols) contribute to the second most explored PL inhibitory class of polyphenols. In a study conducted by Lee *et. al.*, luteolin (**39**) and its *C*-glycoside derivatives (**40-44**), isolated from the leaves of *Eremochloa ophiuroides* (Poaceae) have been screened for PL inhibition assay (Fig. 2.8), wherein neither the glycosides, nor the aglycone exhibited potential activity [18]. Similar results have been identified by Rahim *et. al.* where apigenin and its glycosides were found to possess moderate to poor PL inhibitory activity [19].

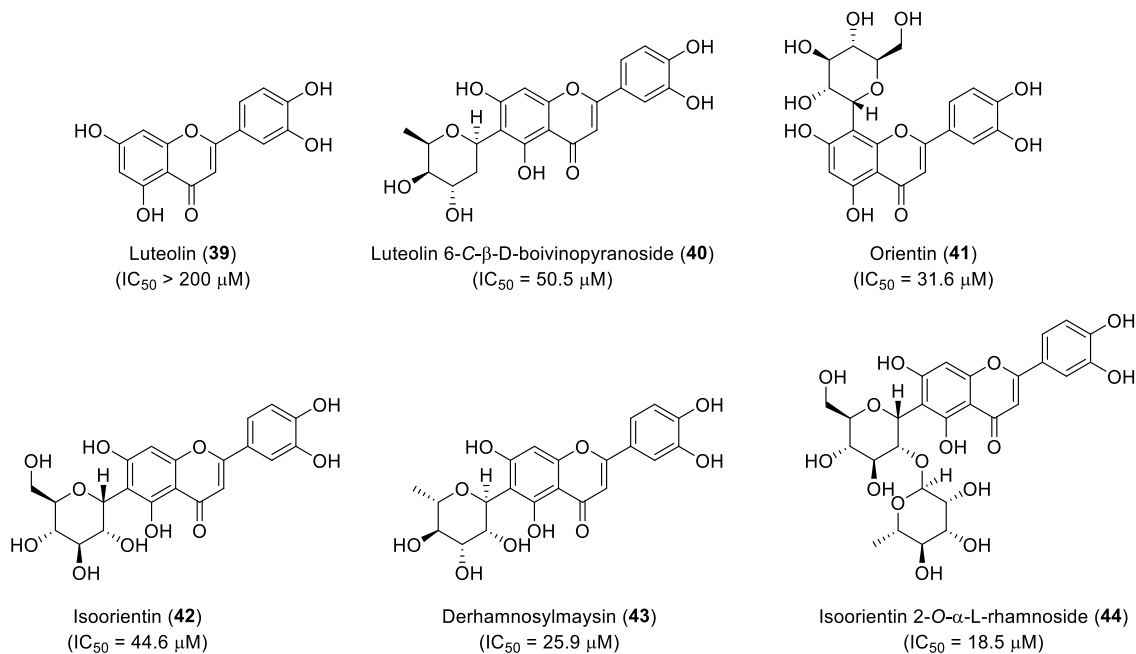


**Fig. 2.8.** Luteolin (**39**) and its *C*-glycosides from *E. ophiuroides*

Apart from, *prenylated derivatives constitute another sub-class of the flavones, that have been reported for potent PL inhibitory activity*. Examples include, norartocarpin (**45**), brosimone I (**46**) and hypargyflavone A (**47**) isolated from the stems of *Artocarpus nitidus*

## Chapter 2

and *Artocarpus hypargeus* (Moraceae) respectively [20,21], that possessed potent PL inhibitory activity (Fig. 2.9).

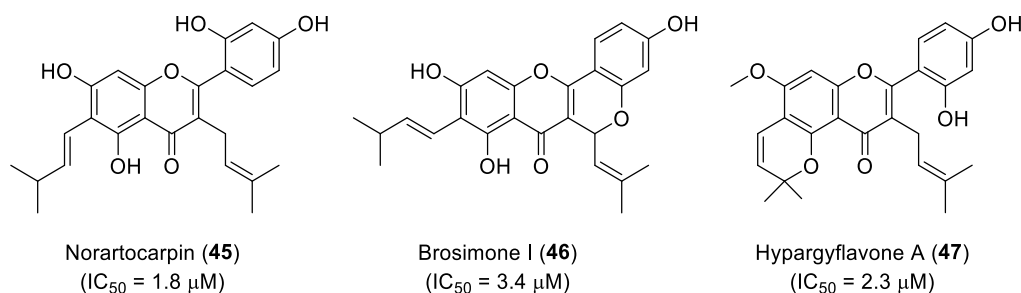


**Fig. 2.9.** Prenylated flavones from *Artocarpus* spp with potent PL inhibitory activity

Of the various flavonols, quercetin, kaempferol and their *O*-glycosides contribute to the majorly explored flavonol derivatives for PL inhibition. In a study conducted by Sergent *et. al.*, quercetin (48) and kaempferol (49) possessed potential PL inhibition, with IC<sub>50</sub> of 21.5 and 13.4 μM respectively (Fig. 2.10)[22]. However, ***the O-glycoside derivatives of these flavonols did not possess PL inhibitory activity***, similar to that of flavones [23,24].

Chalcones represent a special class of flavonoids that does not contain the chromane ring. Chalcones have been found to exhibit a similar pattern of activity as that of flavones, wherein morachalcone A (50), a ***prenylated chalcone*** from the leaves of *Morus alba* (Moraceae), ***possessed potent PL inhibitory activity*** with IC<sub>50</sub> of 6.2 μM (Fig. 2.10). The unsubstituted chalcones, however, possessed poor PL inhibition [25].

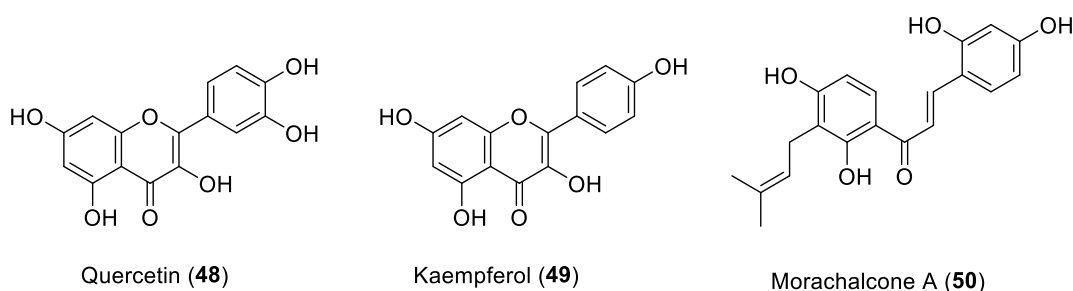


**Fig. 2.10.** Chemical structures of quercetin (48), kaempferol (49) and morachalcone A (50)

### Flavanones

A majority of the flavanones reported for PL inhibition have been isolated from the root barks of *Cudrania tricuspidata* (Moraceae), of which two prenylated flavanones, Cudraflavanones A and D (51 and 52) possessed potent activity. However, two other prenylated flavanones (53, 54) exhibited poor PL inhibition (Fig. 2.11). A structural analysis of these flavanones indicated that ***the prenyl substitution at C6 position resulted in potential***

## Chapter 2

**PL inhibition** (as seen in **51** and **52**), while **C8 position reduced the activity** (for **53** and **54**). Similar reports have been identified with morusalnol A (**55**), isolated from root barks of *M. alba* (Fig. 2.11), wherein a **geranyl substitution on C6 resulted in potent IC<sub>50</sub> value of 0.71 μM** [25].

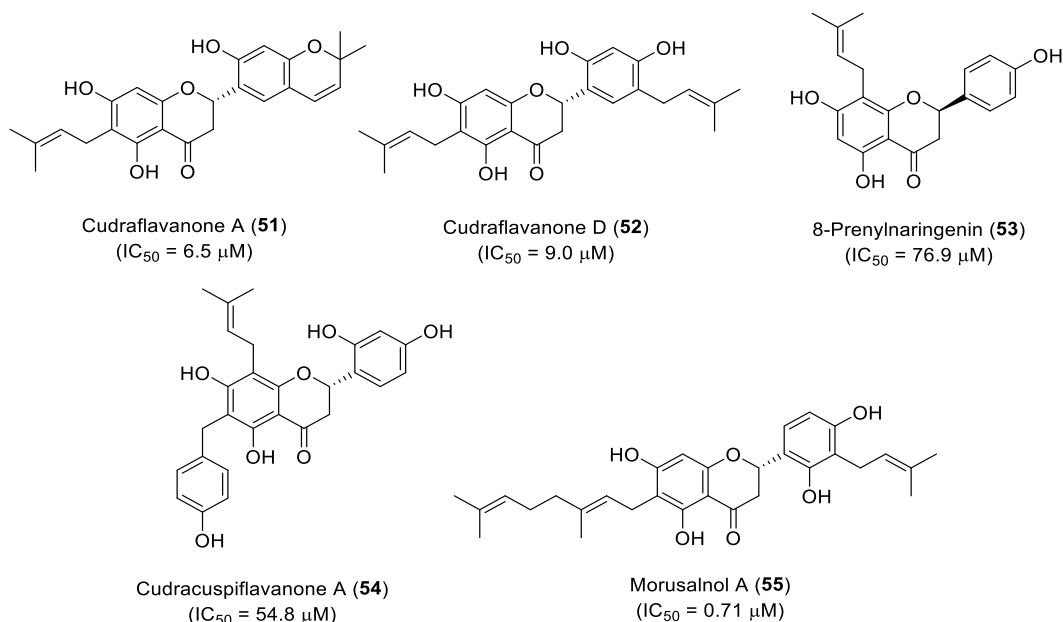


**Fig. 2.11.** Prenylated flavanones from *C. tricuspidata* and *M. alba*, and their PL inhibitory activity

### Flavans

Flavans are amongst the least explored flavonoid classes studied for PL inhibition. To date, only five flavans have been reported, and include 7,4'-dihydroxy flavan (**56**) and 3',7-dihydroxy-4'-methoxyflavan (**57**) from the stem barks of *Broussonetia kanzinoki* (Moraceae), and hispaglabridin A (**58**), glabridin (**59**) and its 4'-*O*-methoxy derivative (**60**), isolated from the roots of *Glycyrrhiza glabra* (Fabaceae) [26,27]. These flavans, however, exhibited poor PL inhibitory activity with the IC<sub>50</sub> values ranging from 85.1 to 485.6 μM (Fig. 2.12).

#### 2.2.1.2 / Stilbenes

Apart from flavonoids, few stilbene derivatives (Fig. 2.13) have also been evaluated for their PL inhibitory potential. Examples include resveratrol (**61**) and its *O*-glycosides *viz.*, *cis*- and *trans*-piceid (**62**, **63**) from *Vitis vinifera* (Vitaceae) and a prenylated stilbene, morusibene A (**64**), from the root barks of *M. alba* [28,29]. While the prenylated stilbene, morusibene A (**64**) exhibited a potent activity, resveratrol and its *O*-glycosides (**61-63**) possessed poor PL inhibitory activity.

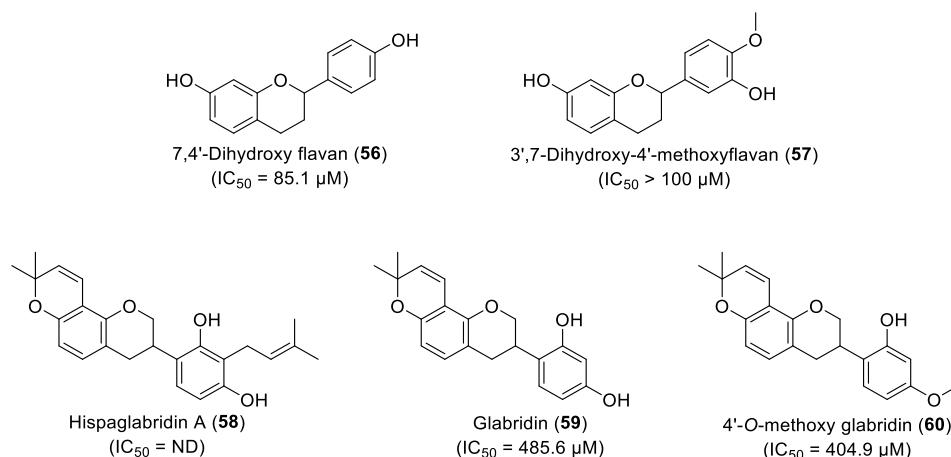


**Fig. 2.12.** Chemical structures of various flavans and their PL inhibitory activity (The  $IC_{50}$  of hispaglabridin A (**58**) was not determined (ND), but it exhibited 43.8% inhibition at 250  $\mu g/mL$ )

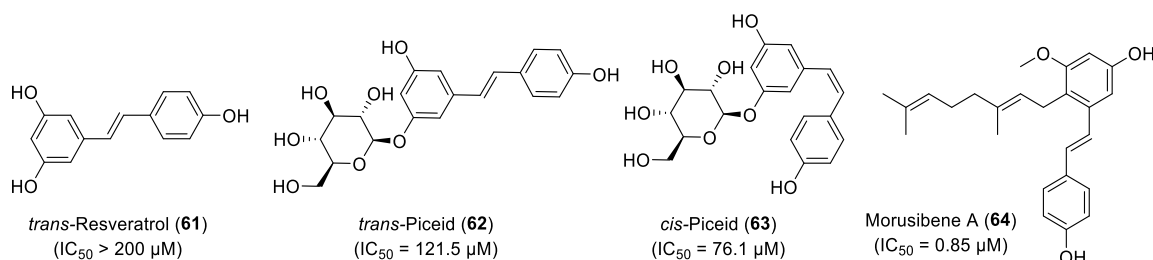


**Fig. 2.13.** Resveratrol and its derivatives (**61-63**) from *V. vinifera* and morusibene A (**64**) from *M. alba* with their PL inhibitory activity

In summary, polyphenols contributed to the most explored class of phytochemicals for PL inhibition. In particular, flavanols and its various derivatives, account to the majority of PL inhibitory polyphenols. A preliminary structure-activity relationship for the various classes of polyphenols highlighted three conclusive points;

- (i) **Presence of a reactive carbonyl group resulted in greater potential for PL inhibition.** For instance, flavans and stilbenes that did not possess any carbonyl group were the least active PL inhibitors, compared to the other classes of polyphenols. Similar phenomenon can be observed with the flavanols, wherein the galloylated flavanols were potent PL inhibitors in comparison to their unsubstituted counterparts
- (ii) **The dimers exhibited comparatively several folds greater activity than the monomers.** In particular, oolonghomobisflavan A that possessed **greater flexibility due to the methylene bridge** was the most active amongst the polyphenols with an  $IC_{50}$  of 0.048  $\mu M$
- (iii) **Prenyl or geranyl substitution resulted in enhanced PL inhibitory activity**

## Chapter 2

### 2.2.2 / Saponins

Saponins are a class of natural products, that are non-volatile, surface-active, structurally diverse, and are chemically referred to as glycosides of triterpenes and steroids. They have been widely explored for various biological activities, including anti-inflammatory, anti-parasitic and haemolytic effects [30]. Within the area of PL inhibition, saponins contribute to the second most explored class of NPs with over 200 saponins that have been evaluated for their PL inhibitory activity. However, a majority of the saponins have been found to exhibit moderate to poor PL inhibition. A summary of various saponins and their PL inhibitory activity are represented in Table 2.2 and Figure 2.14.

While an appropriate structure-activity relationship could not be constructed, a preliminary analysis indicated the role of glycosides to impart PL inhibitory potency to this class of phytochemicals. Moreover, the activity varied with the number of glycoside units and their location. A similar phenomenon could be observed with the acetyl substitution, as seen with the Perennisaponins (**84-87**). Nevertheless, an overall poor PL inhibitory activity observed with this phytochemical class, can be explained due to the *presence of structural rigidity that might result in steric hinderance to interact with the amino acids of the active site of PL*.

**Table 2.2.** A summary of various saponins and their PL inhibitory activity

Compound	Plant source	Activity (IC <sub>50</sub> or % inhibition)	Ref
Prosapogenin D ( <b>65</b> )		1.3 mM	
Platycodin A ( <b>66</b> )	<i>Platycodon grandiflorum</i>	*204 µM	[31,32]
Platycodin C ( <b>67</b> )	(Campanulaceae)	*208 µM	
Deapioplatycodin D ( <b>68</b> )		*259 µM	
Silphioside F ( <b>69</b> )	<i>Acanthopanax senticosus</i>	0.22 mM	
Copteroside B ( <b>70</b> )	(Araliaceae)	0.25 mM	[33]
Gypsogenin 3-O-β-D-glucuronide ( <b>71</b> )		0.29 mM	
Rarasaponin I ( <b>72</b> )		131 µM	
Rarasaponin II ( <b>73</b> )	<i>Sapindus rarak</i>	172 µM	[34]
Rarasaponin III ( <b>74</b> )	(Sapindaceae)	576 µM	
Raraoside A ( <b>75</b> )		151 µM	
Matesaponin I ( <b>76</b> )	<i>Ilex paraguariensis</i>	*53.2 µM	[24]
Nudicaucin C ( <b>77</b> )	(Aquifoliaceae)	*65 µM	
Gypsosaponin A ( <b>78</b> )	<i>Gypsophila oldhamiana</i>	*522 µM	[35]
Gypsosaponin B ( <b>79</b> )	(Caryophyllaceae)	*327 µM	



## Chapter 2

Gypsosaponin C ( <b>80</b> )		*876 $\mu$ M	
Alisol F 24-acetate ( <b>81</b> )	<i>Alisma orientale</i> (Alismataceae)	45.5 $\mu$ M	[36]
Prosapogenin A ( <b>82</b> )	<i>Dioscorea nipponica</i> (Dioscoreaceae)	2.48 $\mu$ M	[37]
3- <i>O</i> - <i>trans</i> - <i>p</i> -coumaroyl actinidic acid ( <b>83</b> )	<i>Actinidia arguta</i> (Actinidiaceae)	14.95 $\mu$ M	[38]
Perennisaponin H ( <b>84</b> )		137 $\mu$ M	
Perennisaponin I ( <b>85</b> )	<i>Bellis perennis</i>	147 $\mu$ M	[39]
Perennisaponin J ( <b>86</b> )	(Asteraceae)	148 $\mu$ M	
Perennisaponin L ( <b>87</b> )		81.4 $\mu$ M	

\*The IC<sub>50</sub> values were calculated as approximate from the % inhibition reported in the literature

## Chapter 2

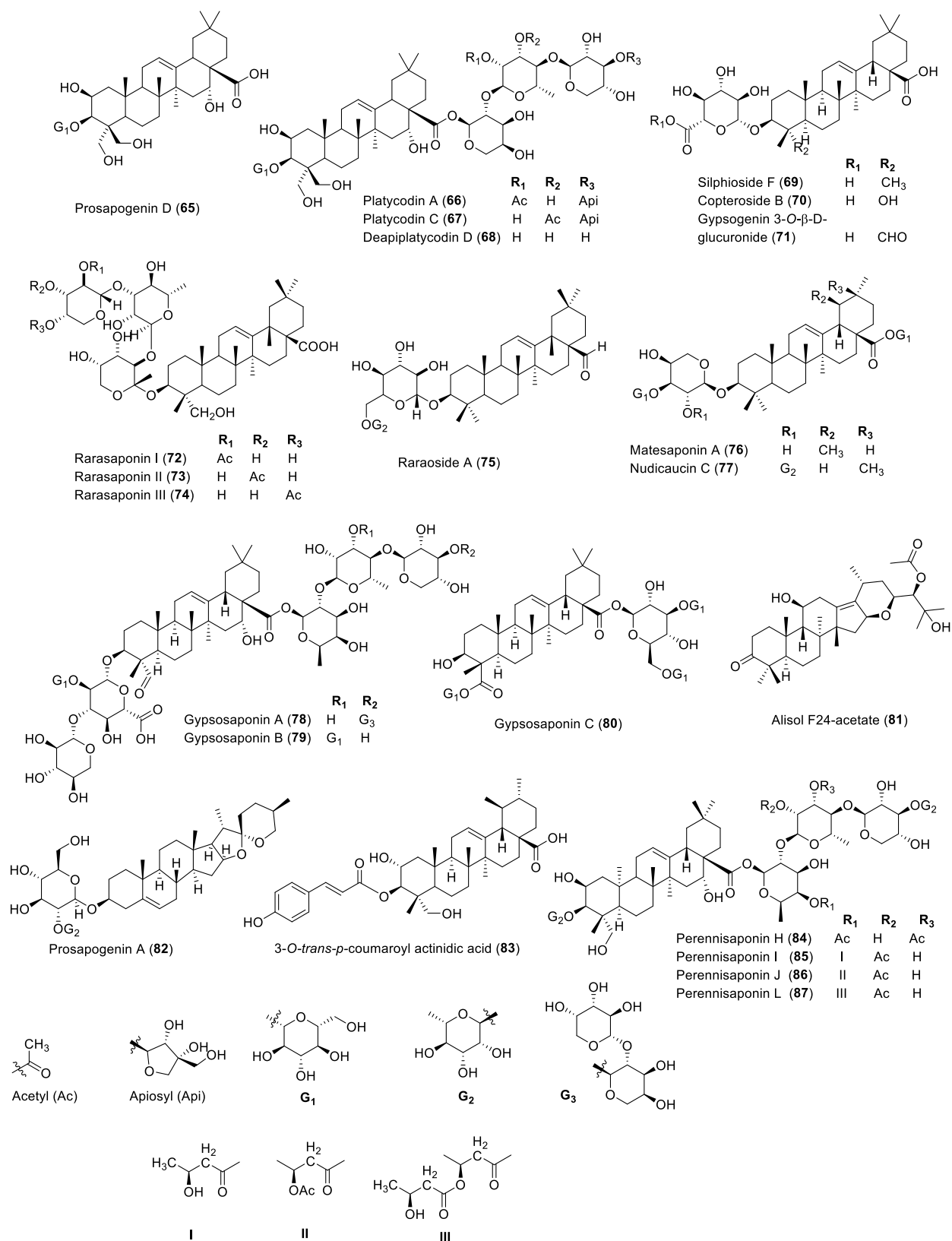


**Fig. 2.14.** Chemical structures of various saponins (65-87) evaluated for their PL inhibitory activity

## Chapter 2

### 2.2.3 / Alkaloids

The term “alkaloid” was first proposed and defined by Meissner as “*plant-derived substance that react like alkalis*”. However, the modern definition of alkaloid was proposed by Pelletier as “*a cyclic organic compound containing nitrogen in a negative oxidation state which is of limited distribution among living organisms*” [40]. Alkaloids are majorly known for their anti-carcinogenic property apart from various other biological activities. However, very few alkaloids have been explored in the area of PL inhibition, with 40 alkaloids reported to date. Notable examples include liriodenine (**88**) from *Nelumbo nucifera* (Nelumbonaceae) [41], dihydroberberine (**89**) and its unsaturated derivative, berberine (**90**) from *Berberis* *sps.* (Berberidaceae) [42], and mahanimbine (**91**) and koenimbine (**92**) from leaves of *Murraya koenigii* (Rutaceae) [43].

Mohammad *et. al.* reported that molecular docking studies of dihydroberberine (**89**) and berberine (**90**) in to the active site of PL indicated a similar binding pattern, exhibiting  $\pi$ -stacking with Phe 77 and Phe 215, as well as H-bond with Ser 152 and His 263. However, the potential activity of dihydroberberine (**89**) over berberine (**90**) was explained due to the absence of a permanent cationic centre on the nitrogen, leading to a higher binding affinity. A comparison of the structural features of mahanimbine (**91**) and koenimbine (**92**) highlighted a similar phenomenon as observed with various polyphenols, wherein the prenyl substitution on mahanimbine (**76**) resulted in potential activity (Fig. 2.15).

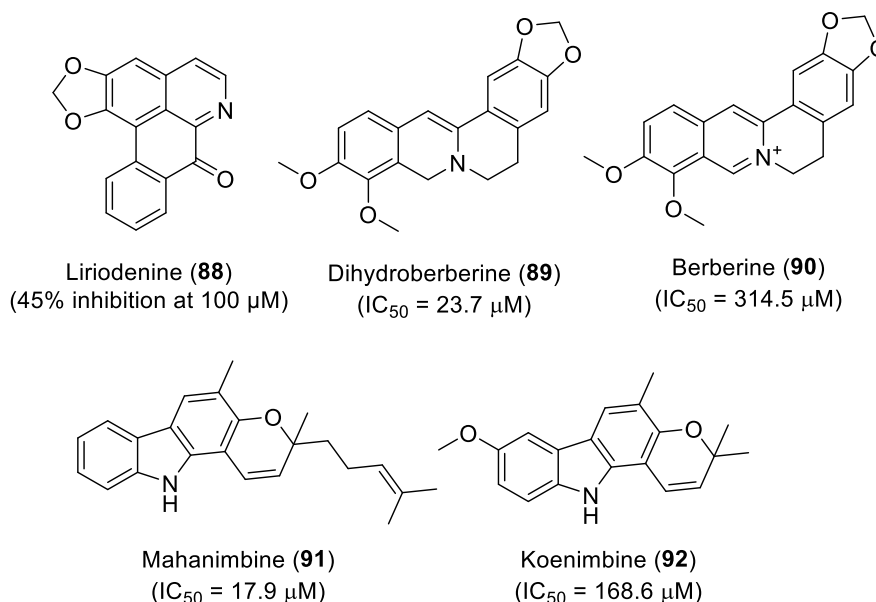


**Fig. 2.15.** Alkaloids from *N. nucifera*, *Berberis* *sps.* and *M. koenigii*

## 2.2.4 / Benzofurans

Benzofurans are among the major group of phytochemicals, that contain an oxygen heterocycle nucleus, and are widely explored for various biological activities *viz.*, anti-carcinogenic, anti-microbial, anti-viral, anti-inflammatory and anti-Alzheimer's etc [44]. However, they are less explored in the area of PL inhibition, similar to alkaloids. To date, around 40 benzofurans from various plants have been explored, with the major source being *M. alba* and *Shorea roxburghii* (Dipterocarpaceae). In two different studies conducted by Jeong *et. al.* and Ha *et. al.*, on the leaves and root bark of *M. alba* respectively, 15 benzofuran derivatives have been studied for their PL inhibitory activity [25,29]. The mono-prenylated benzofurans, moracin N (**93**) and moracin C (**94**) from the leaves, exhibited moderate PL inhibitory activity, while potent activity has been observed for morusalfuran B (**95**), morusalfuran C (**96**), morusalfuran E (**97**) from the root barks. This potent activity of benzofuran derivatives (**95-97**) may be due to the higher degree of prenylation (Fig. 2.16).

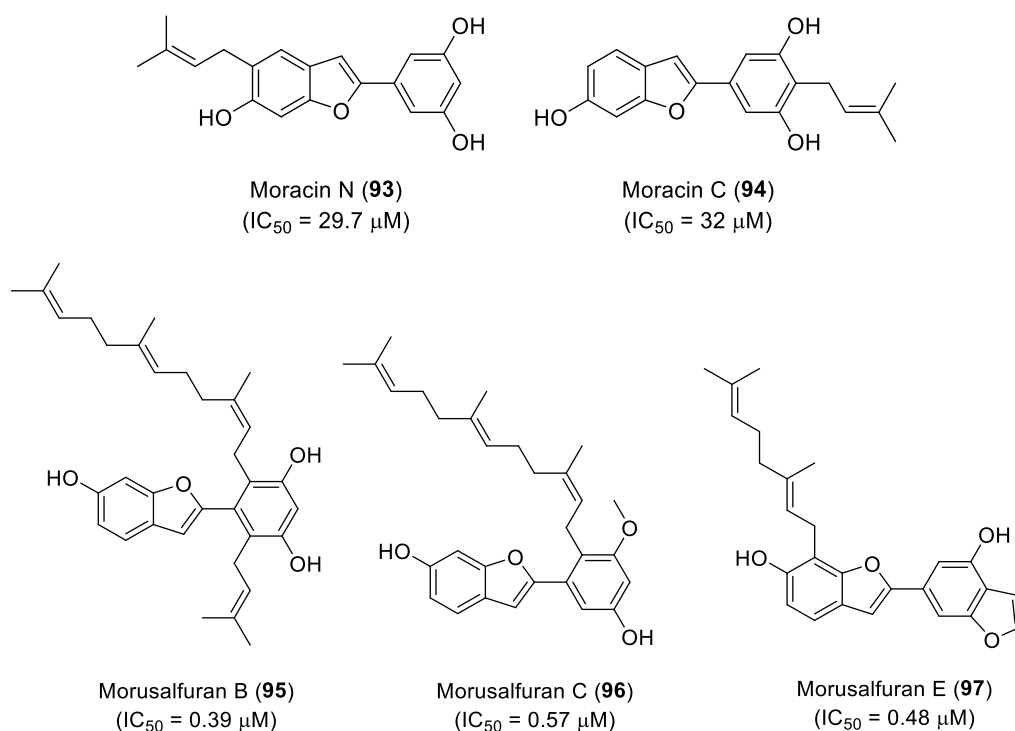


**Fig. 2.16.** Prenylated benzofurans from *M. alba* and their PL inhibitory activity

In a study conducted by Morikawa *et. al.*, various benzofuran derivatives from bark of *S. roxburghii* have been studied for their PL inhibitory potential [45]. While the dimeric benzofurans (**98-99**) exhibited comparatively potential activity, the monomeric derivatives (**100-101**) possessed moderate to poor PL inhibition (Fig. 2.17). Further, wilsonol C (**102**), a benzofuran trimer from the roots of *V. vinifera*, also exhibited potent PL inhibition [28].

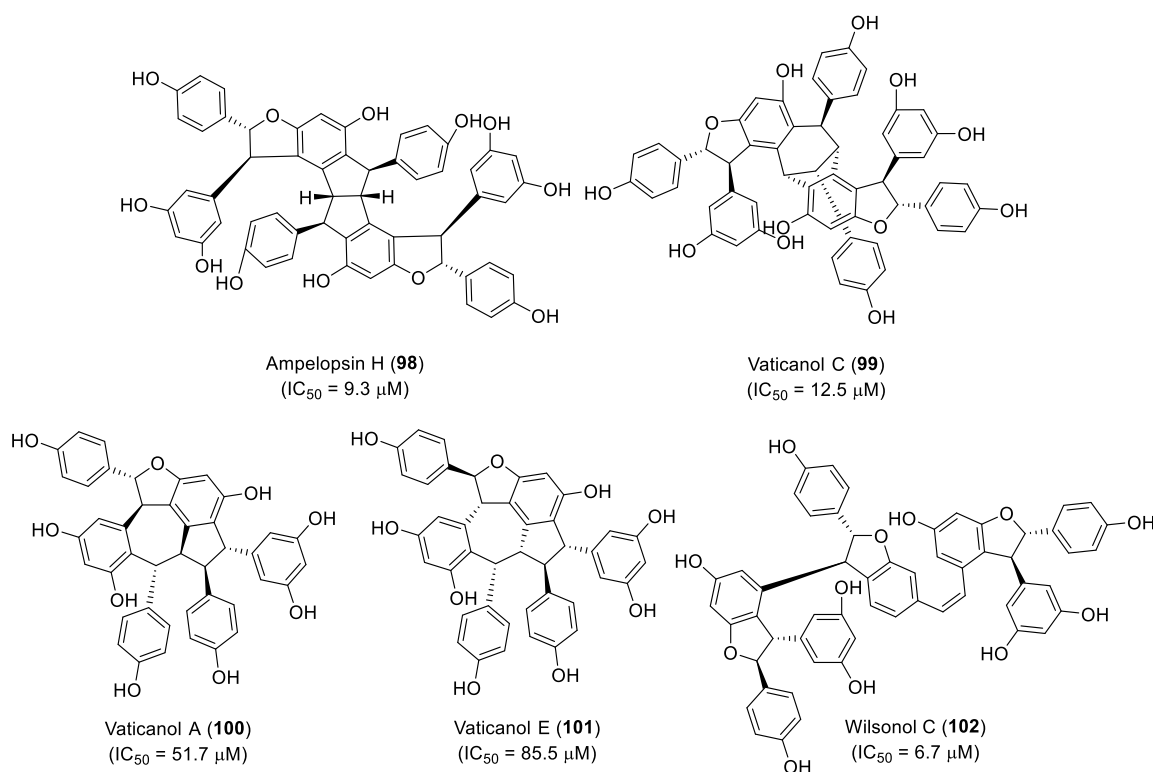


**Fig. 2.17.** Benzofurans from *S. roxburghii* and *V. vinifera*

Benzofurans exhibited a similar phenomenon as observed with the flavanols, wherein the dimers and the prenylated benzofurans exhibited comparatively greater PL inhibitory potential.

## 2.2.5 / PL inhibitors from non-plant sources

### 2.2.5.1 / *Monascus* pigments

*Monascus* pigments are a group of natural compounds produced by the molds of various *Monascus* *sps.* (Elaphomycetaceae). They are widely utilised as natural food colorants in East Asia, and possess a range of biological activities including anti-mutagenic, antimicrobial activities and potential anti-obesity characteristics. In two different studies conducted by Kim *et. al.*, over 50 *monascus* pigments, derived with various amino acids, have been extracted and evaluated for PL inhibitory activity [46,47]. The L-Tyr ethyl ester derivative (**103**) was found to be the most active in the series, with a potential IC<sub>50</sub> of 13.8 μM, alongside few other derivatives that exhibited potential PL inhibitory activity (Fig. 2.18).

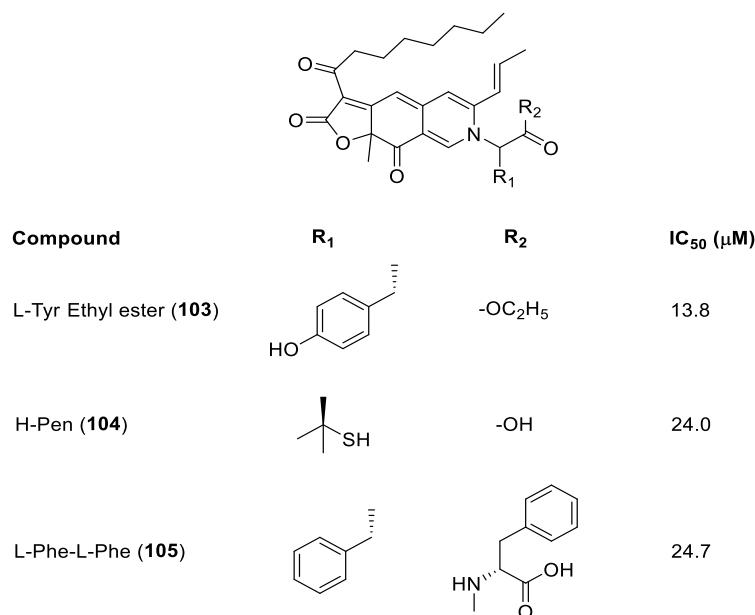


**Fig. 2.18.** Various monascus pigments and their PL inhibitory activity  
(*L-Tyr*: *L-Tyrosine*; *H-Pen*: *Pencillamine*; *L-Phe*: *L-Phenylalanine*)

### 2.2.5.2 | Lactones and their derivatives

Lactones from fungi are the earliest class of molecules explored for their potential towards PL inhibition. Apart from the clinically approved drug, orlistat, various other fungal derived lactones have been evaluated since 1980s. Amongst these, the major lactones include the ebelactones, panclicins and vibractones obtained from various species of *Streptomyces* and *Boreostereum* (Streptomycetaceae and Gloeophyllaceae, respectively). In a study conducted by Umezawa *et. al.*, two ebelactones, A (**106**) and B (**107**), have been isolated along with esterastin (**108**), from the MG7-G1 strain of actinomycetes (a strain closely related to *Streptomyces aburaviensis*). All the three lactones possessed a potent inhibitory activity against PL (Fig. 2.19). Esterastin (**108**), a closely related analogue of orlistat was the most active compound with an IC<sub>50</sub> of 0.4 nM [48].

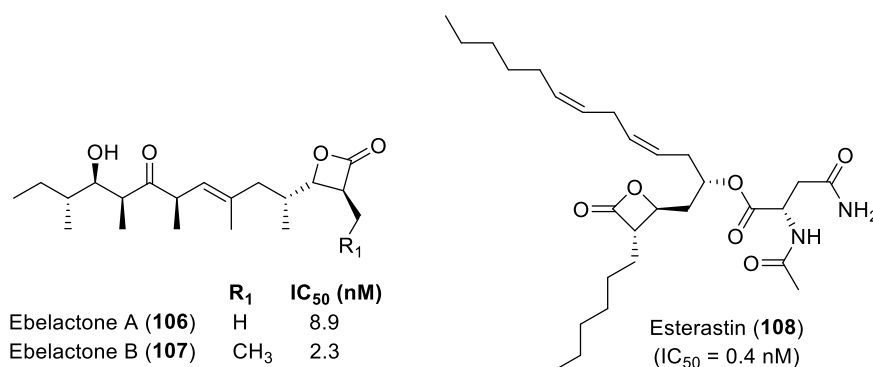


**Fig. 2.19.** PL inhibitory activities of ebelactones and esterastin from MG7-G1 strain of actinomycetes

## Chapter 2

In another study, Mutoh *et. al.* isolated five structural analogues of orlistat, panclicins A-E (**109-114**), from *Streptomyces sps.* NR 0619 and evaluated its PL inhibitory potential [49]. Panclicin C (**110**) was the most active in the series with an  $IC_{50}$  of 0.62  $\mu$ M, followed by panclicins D and E (Fig. 2.20).

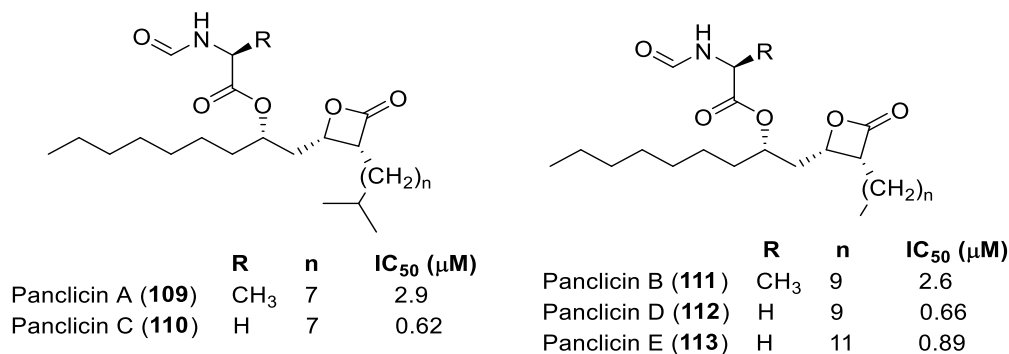


**Fig. 2.20.** Panclicins and their PL inhibitory activities from *Streptomyces sp.* NR 0619

In a study conducted by Chen *et. al.*, vibrallactone (**114**) and its oxime derivatives from *Boreostereum vibrans* (basidiomycete) have been evaluated for their PL inhibitory potential [50]. In general, the oximes exhibited a greater potential over vibrallactone (**114**), however, did not possess potential PL inhibitory activity comparable to that of orlistat. Vibrallactoxime K (**115**) was the most active oxime in the series with an  $IC_{50}$  of 11.1  $\mu$ M. Apart from natural vibrallactones, Wei *et. al.* have reported the PL inhibitory activity of 104 semi-synthetic vibrallactone analogues [51], wherein compound **116** with a dialkyl amide extension on the vibrallactone exhibited potent activity with an  $IC_{50}$  of 14 nM (Fig. 2.21).

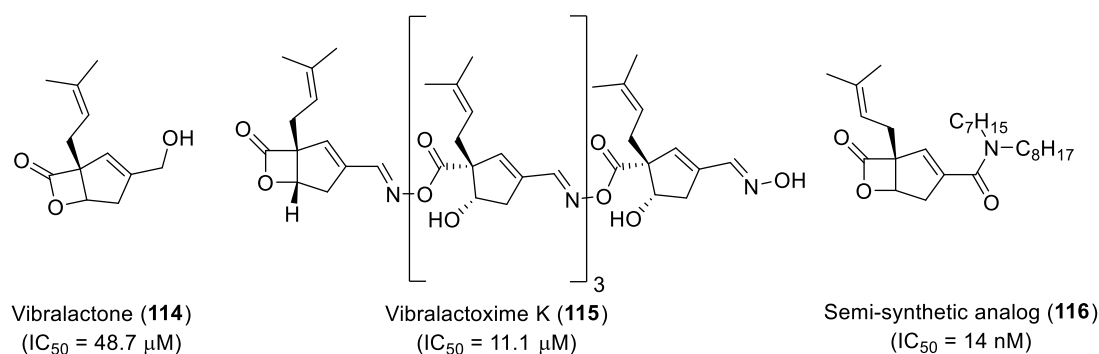


**Fig. 2.21.** Vibrallactone (**114**), its oxime derivative (**115**) from *B. vibrans* and synthetic analogue of vibrallactone (**116**) with their PL inhibitory activity

In summary, two features were observed in common with the non-plant based natural product PL inhibitors; i) *the presence of highly reactive and constrained lactone ring*; and b) *long alkyl chains similar to the natural triglycerides that resulted in potent PL*

*inhibition*. Further, the ebelactones and panclicins have been reported to exhibit covalent inhibition of PL similar to that of the orlistat.

### 2.3 | Synthetic PL inhibitors

Apart from the vast NP based PL inhibitors, few synthetic pharmacophores have also been reported for PL inhibition. Among these, the earliest class of molecules belonged to the boronic acids, wherein nine analogues have been evaluated by Garner [52]. The 3-nitro-4-bromobenzene and 4-bromobenzene analogues (**117** and **118**) derivatives possessed potent activity of 0.163 and 0.243  $\mu\text{M}$  (Fig. 2.22). Apart from, alkyl phosphonates and  $\alpha$ -ketoamides are the other earlier classes of synthetic PL inhibitors that have been evaluated by Cavalier *et. al* and Kotsovolou *et. al* respectively [53,54]. These pharmacophores have been designed by replacing the esters of the natural triglycerides with phosphonates and  $\alpha$ -ketoamides respectively.  $\text{R}_{11}\text{Y}_{16}$  and  $\text{R}_{16}\text{Y}_{11}$  analogues (**119** and **120**) from the phosphonates and compounds **121** and **122**, from the  $\alpha$ -ketoamides exhibited potential PL inhibitory activity among the respective series (Fig. 2.22). *The  $\alpha$ -ketoamide moiety have been reported to act as an ester mimicking group due to its reactive carbonyl functionality that could bind covalently to Ser152 of the PL.*

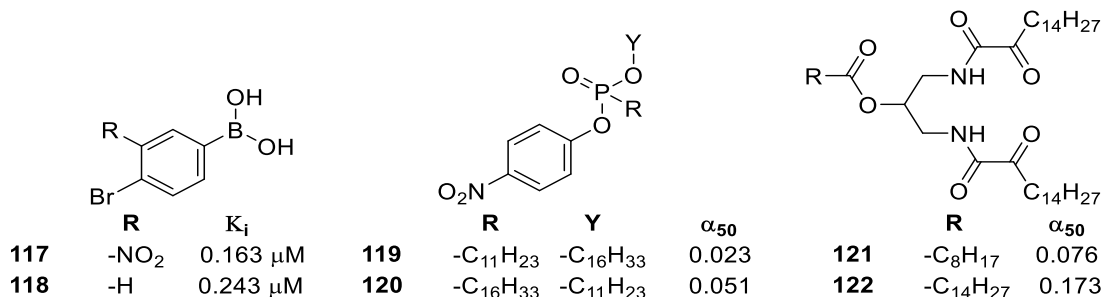


**Fig. 2.22.** Boronic acids (**117**, **118**), alkyl phosphonates (**119**, **120**) and bis 2-oxoamides (**121**, **122**) with their PL inhibitory activity ( $K_i$  - inhibitory constant;  $\alpha_{50}$  - molar fraction relative to PL that exhibited 50% inhibition)

A majority of the reports on synthetic PL inhibitors have been observed during the past decade, and included various pharmacophores *viz.*, squaric acid derivatives (**123**), oxadiazolones (**124**), chalcones (**125**), benzyloquinolines (**126**), bisbenzimidazoles (**127**), triazoles (**128**) and thiazolidinediones (**129**) etc. The most potential analogue from the respective series and their PL inhibitory activity are summarized in Fig. 2.23. Among these, the squaric acid derivative (**123**) and the thiazolidinedione (**129**) has exhibited a potent activity and can be attributed to the *presence of a highly reactive carbonyl functionality* [55,56]. *Both these scaffolds consisted diketo functionality*, either linked directly ( $\alpha$ -



## Chapter 2

ketoester as in squaric acid) or through a -NH linker (N-centred diamide as in thiazolidinedione) *which might have attributed to the highly reactive carbonyl functionality*. Compounds **125** to **128** exhibited potential PL inhibitory activity with a exception of compound **124** [57-61].

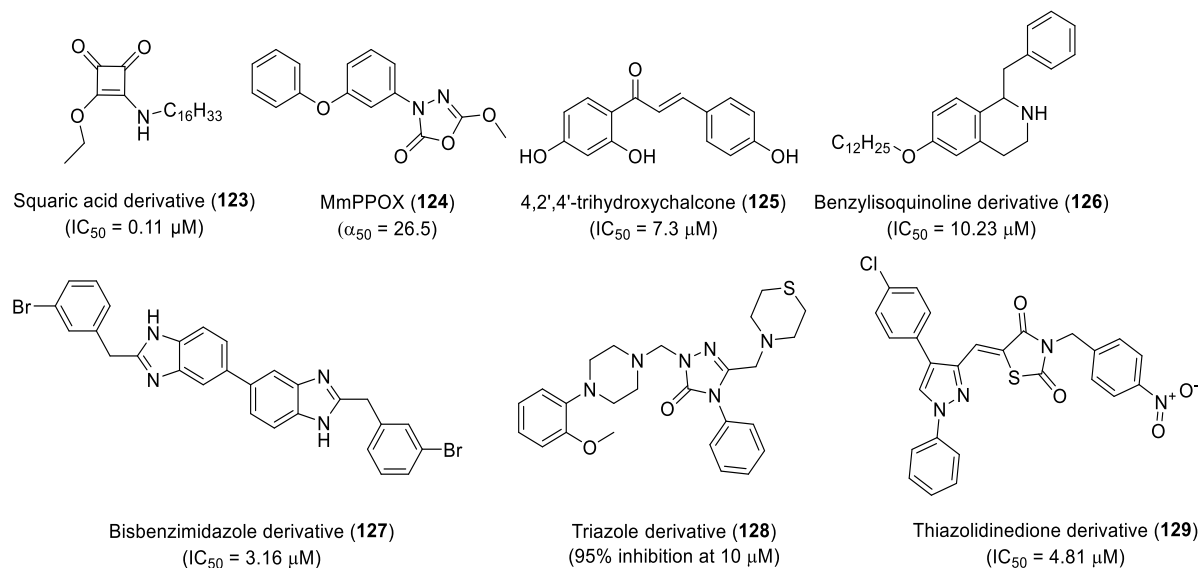


**Fig. 2.23.** Summary of PL inhibitory activity of various synthetic molecules ( $\alpha_{50}$  - molar fraction relative to PL that exhibited 50% inhibition)

### 2.4 | Gaps in existing research

The literature review has resulted in the identification of around 750 NP-based PL inhibitors in addition to 300 synthetic analogues. However, these compounds exhibited enormous chemical diversity, while a majority of these compounds did not possess potent PL inhibitory activity comparable to that of orlistat. Further, the existing research was focussed more into the isolation and evaluation of NPs for their PL inhibitory activity, while no systematic efforts have been made to understand the structural features from these molecules that would result in potent PL inhibition. Moreover, a negligible expanse of research used the advantage of the advanced *in silico* techniques in understanding the molecular interactions with the active site of PL. Also, no further in-depth studies have been made to identify and incorporate chemical modifications to these molecules that would enhance their PL inhibitory activity.

## Chapter 2

---

### References

- [1] G.M. Cragg, D.J. Newman, Natural products: A continuing source of novel drug leads, *Biochim. Biophys. Acta-General Subj.* 1830 (2013) 3670–3695.
- [2] D.J. Newman, G.M. Cragg, Natural products as sources of new drugs from 1981 to 2014, *J. Nat. Prod.* 79 (2016) 629–661.
- [3] B. Patwardhan, D. Warude, P. Pushpangadan, N. Bhatt, *Ayurveda* and Traditional Chinese Medicine: A comparative overview, *Evid. Based Complement. Altern. Med.* 2 (2005) 465–473.
- [4] B. Patwardhan, A.D.B. Vaidya, M. Chorghade, *Ayurveda* and natural products drug discovery, *Curr. Sci.* (2004) 789–799.
- [5] B. Patwardhan, R.A. Mashelkar, Traditional medicine-inspired approaches to drug discovery: Can *Ayurveda* show the way forward?, *Drug Discov. Today.* 14 (2009) 804–811.
- [6] V.K. Joshi, A. Joshi, K.S. Dhiman, The *Ayurvedic* Pharmacopoeia of India, development and perspectives, *J. Ethnopharmacol.* 197 (2017) 32–38.
- [7] A. Seyedan, M.A. Alshawsh, M.A. Alshagga, S. Koosha, Z. Mohamed, Medicinal plants and their inhibitory activities against pancreatic lipase: A review, *Evid. Based Complement. Altern. Med.* 2015 (2015).
- [8] A.L. de la Garza, F.I. Milagro, N. Boque, J. Campión, J.A. Martinez, Natural inhibitors of pancreatic lipase as new players in obesity treatment, *Planta Med.* 77 (2011) 773–785.
- [9] Y. Bustanji, M. Mohammad, M. Hudaib, K. Tawaha, I.M. Al-Masri, H.S. AlKhatib, A. Issa, F.Q. Alali, Screening of some medicinal plants for their pancreatic lipase inhibitory potential, *Jordan J. Pharm. Sci.* 4 (2011) 81–88.
- [10] A. Gholamhoseinian, B. Shahouzehi, F. Sharifi-Far, Inhibitory effect of some plant extracts on pancreatic lipase, *Int. J. Pharmacol.* 6 (2010) 18–24.
- [11] A.N. Li, S. Li, Y. J. Zhang, X.R. Xu, Y. M. Chen, H. B. Li, Resources and biological activities of natural polyphenols, *Nutrients.* 6 (2014) 6020–6047.
- [12] T. Srivastava, S. Kumar Mishra, Novel function of polyphenols in human health: A review, *Res. J. Phytochem.* 9 (2015) 116–126.
- [13] T. Buchholz, M.F. Melzig, Polyphenolic compounds as pancreatic lipase inhibitors, *Planta Med.* 81 (2015) 771–783.
- [14] R. Tsao, Chemistry and biochemistry of dietary polyphenols, *Nutrients.* 2 (2010) 1231–1246.

## Chapter 2

---

- [15] M. Nakai, Y. Fukui, S. Asami, Y. Toyoda-Ono, T. Iwashita, H. Shibata, T. Mitsunaga, F. Hashimoto, Y. Kiso, Inhibitory effects of oolong tea polyphenols on pancreatic lipase *in vitro*, *J. Agric. Food Chem.* 53 (2005) 4593–4598.
- [16] S.A. Ivanov, K. Nomura, I.L. Malfanov, I. V Sklyar, L.R. Ptitsyn, Isolation of a novel catechin from *Bergenia* rhizomes that has pronounced lipase-inhibiting and antioxidative properties, *Fitoterapia.* 82 (2011) 212–218.
- [17] S.L. Glisan, K.A. Grove, N.H. Yennawar, J.D. Lambert, Inhibition of pancreatic lipase by black tea theaflavins: Comparative enzymology and *in silico* modeling studies, *Food Chem.* 216 (2017) 296–300.
- [18] E.M. Lee, S.S. Lee, B.Y. Chung, J.Y. Cho, I.C. Lee, S.R. Ahn, S.J. Jang, T.H. Kim, Pancreatic lipase inhibition by C-glycosidic flavones isolated from *Eremochloa ophiuroides*, *Molecules.* 15 (2010) 8251–8259.
- [19] A.T.M.A. Rahim, Y. Takahashi, K. Yamaki, Mode of pancreatic lipase inhibition activity *in vitro* by some flavonoids and non-flavonoid polyphenols, *Food Res. Int.* 75 (2015) 289–294.
- [20] M.H. Yu, T. Zhao, G.R. Yan, H.X. Yang, H.Y. Wang, A.J. Hou, New isoprenylated flavones and stilbene derivative from *Artocarpus hypargyreus*, *Chem. Biodivers.* 9 (2012) 394–402.
- [21] T. Zhao, G.R. Yan, S.L. Pan, H.Y. Wang, A.J. Hou, New isoprenylated 2-arylbenzofurans and pancreatic lipase inhibitory constituents from *Artocarpus nitidus*, *Chem. Biodivers.* 6 (2009) 2209–2216.
- [22] T. Sergent, J. Vanderstraeten, J. Winand, P. Beguin, Y.J. Schneider, Phenolic compounds and plant extracts as potential natural anti-obesity substances, *Food Chem.* 135 (2012) 68–73.
- [23] N. Yuda, M. Tanaka, M. Suzuki, Y. Asano, H. Ochi, K. Iwatsuki, Polyphenols extracted from black tea (*Camellia sinensis*) residue by hot-compressed water and their inhibitory effect on pancreatic lipase *in vitro*, *J. Food Sci.* 77 (2012) H254–H261.
- [24] S. Sugimoto, S. Nakamura, S. Yamamoto, C. Yamashita, Y. Oda, H. Matsuda, M. Yoshikawa, Brazilian natural medicines. III. Structures of triterpene oligoglycosides and lipase inhibitors from Mate, leaves of *Ilex paraguariensis*, *Chem. Pharm. Bull.* 57 (2009) 257–261.
- [25] J.Y. Jeong, Y.H. Jo, S.B. Kim, Q. Liu, J.W. Lee, E.J. Mo, K.Y. Lee, B.Y. Hwang, M.K. Lee, Pancreatic lipase inhibitory constituents from *Morus alba* leaves and optimization for extraction conditions, *Bioorg. Med. Chem. Lett.* 25 (2015) 2269–

- 2274.
- [26] J.H. Ahn, Q. Liu, C. Lee, M.J. Ahn, H.S. Yoo, B.Y. Hwang, M.K. Lee, A new pancreatic lipase inhibitor from *Broussonetia kanzinoki*, *Bioorg. Med. Chem. Lett.* 22 (2012) 2760–2763.
- [27] R.B. Birari, S. Gupta, C.G. Mohan, K.K. Bhutani, Antiobesity and lipid lowering effects of *Glycyrrhiza* chalcones: Experimental and computational studies, *Phytomedicine*. 18 (2011) 795–801.
- [28] Y.M. Kim, E.W. Lee, S.H. Eom, T.H. Kim, Pancreatic lipase inhibitory stilbenoids from the roots of *Vitis vinifera*, *Int. J. Food Sci. Nutr.* 65 (2014) 97–100.
- [29] M.T. Ha, M.H. Tran, K.J. Ah, K.J. Jo, J. Kim, W.D. Kim, W.J. Cheon, M.H. Woo, S.H. Ryu, B.S. Min, Potential pancreatic lipase inhibitory activity of phenolic constituents from the root bark of *Morus alba* L., *Bioorg. Med. Chem. Lett.* 26 (2016) 2788–2794.
- [30] S. Sparg, M.E. Light, J. Van Staden, Biological activities and distribution of plant saponins, *J. Ethnopharmacol.* 94 (2004) 219–243.
- [31] B.J. Xu, L.K. Han, Y.N. Zheng, J.H. Lee, C.K. Sung, *In vitro* inhibitory effect of triterpenoidal saponins from *Platycodi Radix* on pancreatic lipase, *Arch. Pharm. Res.* 28 (2005) 180–185.
- [32] H.L. Zhao, J.S. Sim, S.H. Shim, Y.W. Ha, S.S. Kang, Y.S. Kim, Antiobese and hypolipidemic effects of platycodin saponins in diet-induced obese rats: Evidences for lipase inhibition and calorie intake restriction, *Int. J. Obes.* 29 (2005) 983–990.
- [33] F. Li, W. Li, H. Fu, Q. Zhang, K. Koike, Pancreatic lipase-inhibiting triterpenoid saponins from fruits of *Acanthopanax senticosus*, *Chem. Pharm. Bull.* 55 (2007) 1087–1089.
- [34] T. Morikawa, Y. Xie, Y. Asao, M. Okamoto, C. Yamashita, O. Muraoka, H. Matsuda, Y. Pongpiriyadacha, D. Yuan, M. Yoshikawa, Oleanane-type triterpene oligoglycosides with pancreatic lipase inhibitory activity from the pericarps of *Sapindus rarak*, *Phytochemistry*. 70 (2009) 1166–1172.
- [35] Q. Zheng, W. Li, L. Han, K. Koike, Pancreatic lipase-inhibiting triterpenoid saponins from *Gypsophila oldhamiana*, *Chem. Pharm. Bull.* 55 (2007) 646–650.
- [36] J. Cang, C. Wang, X.K. Huo, X.G. Tian, C.P. Sun, S. Deng, B.J. Zhang, H.L. Zhang, K.X. Liu, X.C. Ma, Sesquiterpenes and triterpenoids from the rhizomes of *Alisma orientalis* and their pancreatic lipase inhibitory activities, *Phytochem. Lett.* 19 (2017) 83–88.

- [37] C.S. Kwon, H.Y. Sohn, S.H. Kim, J.H. Kim, K.H. Son, J.S. Lee, J.K. Lim, J.S. Kim, Anti-obesity effect of *Dioscorea nipponica* Makino with lipase-inhibitory activity in rodents, *Biosci. Biotechnol. Biochem.* 67 (2003) 1451–1456.
- [38] D.S. Jang, G.Y. Lee, J. Kim, Y.M. Lee, J.M. Kim, Y.S. Kim, J.S. Kim, A new pancreatic lipase inhibitor isolated from the roots of *Actinidia arguta*, *Arch. Pharm. Res.* 31 (2008) 666–670.
- [39] T. Morikawa, X. Li, E. Nishida, S. Nakamura, K. Ninomiya, H. Matsuda, Y. Oda, O. Muraoka, M. Yoshikawa, Medicinal Flowers. Part 29. Acylated oleanane-type triterpene bisdesmosides: Perennisaponins G, H, I, J, K, L, and M with pancreatic lipase inhibitory activity from the flowers of *Bellis perennis*, *Helv. Chim. Acta.* 93 (2010) 573–586.
- [40] S.W. Pelletier, The nature and definition of an alkaloid, in: *Alkaloids Chem. Biol. Perspect.*, John Wiley & Sons New York, 1983: pp. 1–31.
- [41] J.H. Ahn, E.S. Kim, C. Lee, S. Kim, S.H. Cho, B.Y. Hwang, M.K. Lee, Chemical constituents from *Nelumbo nucifera* leaves and their anti-obesity effects, *Bioorg. Med. Chem. Lett.* 23 (2013) 3604–3608.
- [42] M. Mohammad, I.M. Al-Masri, A. Issa, A. Khdair, Y. Bustanji, Inhibition of pancreatic lipase by berberine and dihydroberberine: An investigation by docking simulation and experimental validation, *Med. Chem. Res.* 22 (2013) 2273–2278.
- [43] R. Birari, S.K. Roy, A. Singh, K.K. Bhutani, Pancreatic lipase inhibitory alkaloids of *Murraya koenigii* leaves., *Nat. Prod. Commun.* 4 (2009) 1089–1092.
- [44] H. Khanam, Shamsuzzaman, Bioactive benzofuran derivatives: A review, *Eur. J. Med. Chem.* 97 (2015) 483–504.
- [45] T. Morikawa, S. Chaipech, H. Matsuda, M. Hamao, Y. Umeda, H. Sato, H. Tamura, K. Ninomiya, M. Yoshikawa, Y. Pongpiriyadacha, Anti-hyperlipidemic constituents from the bark of *Shorea roxburghii*, *J. Nat. Med.* 66 (2012) 516–524.
- [46] J.H. Kim, H.J. Kim, C. Kim, H. Jung, Y.O. Kim, J.Y. Ju, C.S. Shin, Development of lipase inhibitors from various derivatives of *Monascus* pigment produced by *Monascus* fermentation, *Food Chem.* 101 (2007) 357–364.
- [47] J.H. Kim, H.J. Kim, H.W. Park, S.H. Youn, D.Y. Choi, C.S. Shin, Development of inhibitors against lipase and  $\alpha$ -glucosidase from derivatives of *Monascus* pigment, *FEMS Microbiol. Lett.* 276 (2007) 93–98.
- [48] H. Umezawa, T. Aoyagi, K. Uotani, M. Hamada, T. Takeuchi, S. Takahashi, Ebelactone, an inhibitor of esterase, produced by *Actinomycetes*, *J. Antibiot. (Tokyo)*.

- 33 (1980) 1594–1596.
- [49] M. Mutoh, N. Nakada, S. Matsukuma, S. Ohshima, K. Yoshinri, J. Watanabe, M. Arisawa, Panlicins, novel pancreatic lipase inhibitors, *J. Antibiot. (Tokyo)*. 47 (1994) 1369–1375.
- [50] H.P. Chen, Z.Z. Zhao, Z.H. Li, Z.J. Dong, K. Wei, X. Bai, L. Zhang, C.N. Wen, T. Feng, J.K. Liu, Novel natural oximes and oxime esters with a vibractone backbone from the basidiomycete *Boreostereum vibrans*, *ChemistryOpen*. 5 (2016) 142–149.
- [51] K. Wei, G.Q. Wang, X. Bai, Y.F. Niu, H.P. Chen, C.N. Wen, Z.H. Li, Z.J. Dong, Z.L. Zuo, W.Y. Xiong, others, Structure-based optimization and biological evaluation of pancreatic lipase inhibitors as novel potential antiobesity agents, *Nat. Products Bioprospect*. 5 (2015) 129–157.
- [52] C.W. Garner, Boronic acid inhibitors of porcine pancreatic lipase., *J. Biol. Chem.* 255 (1980) 5064–5068.
- [53] J.F. Cavalier, S. Ransac, R. Verger, G. Buono, Inhibition of human gastric and pancreatic lipases by chiral alkylphosphonates. A kinetic study with 1, 2-didecanoyl-sn-glycerol monolayer, *Chem. Phys. Lipids*. 100 (1999) 3–31.
- [54] S. Kotsovolou, A. Chiou, R. Verger, G. Kokotos, Bis-2-oxo amide triacylglycerol analogues: A novel class of potent human gastric lipase inhibitors, *J. Org. Chem.* 66 (2001) 962–967.
- [55] Z. Bobcheva, D. Zhiryakova, M. Guncheva, Evaluation of the inhibitory potential of five squaric acid derivatives against pancreatic lipase, *J. Enzyme Inhib. Med. Chem.* 26 (2011) 587–591.
- [56] S.N.C. Sridhar, D. Bhurta, D. Kantiwal, G. George, V. Monga, A.T. Paul, Design, synthesis, biological evaluation and molecular modelling studies of novel diaryl substituted pyrazolyl thiazolidinediones as potent pancreatic lipase inhibitors, *Bioorg. Med. Chem. Lett.* 27 (2017) 3749–3754.
- [57] V. Point, K.V.P.P. Kumar, S. Marc, V. Delorme, G. Parsieglia, S. Amara, F. Carrière, G. Buono, F. Fotiadu, S. Canaan, Analysis of the discriminative inhibition of mammalian digestive lipases by 3-phenyl substituted 1, 3, 4-oxadiazol-2 (3H)-ones, *Eur. J. Med. Chem.* 58 (2012) 452–463.
- [58] T.D. Tran, Design, synthesis and biological evaluation of some chalcone derivatives as potential pancreatic lipase inhibitors, in: 17<sup>th</sup> Int. Electron. Conf. Synth. Org. Chem., 2013.
- [59] S. Demirci, A. Mermer, G. Ak, F. Aksakal, N. Colak, A. Demirbas, F.A. Ayaz, N.

## Chapter 2

---

- Demirbas, conventional and microwave-assisted total synthesis, Antioxidant capacity, biological activity, and molecular docking studies of new hybrid compounds, *J. Heterocycl. Chem.* 54 (2017) 1785–1805.
- [60] T. Feng, H.Y. Lv, Z.O.U. Ji-Long, W. Yi, D. Meng-Jun, C.H.U. Xiao-Qin, L.I. Dan, Z.H.U. Liang, J.Q. Jiang, Synthesis and evaluation of benzyloquinoline derivatives for their inhibition on pancreatic lipase and preadipocyte proliferation, *Chin. J. Nat. Med.* 14 (2016) 382–390.
- [61] E. Mentеше, F. Yılmaz, N. Karaali, S. Ülker, B. Kahveci, Rapid synthesis and lipase inhibition activity of some new benzimidazole and perimidine derivatives, *Russ. J. Bioorganic Chem.* 40 (2014) 336–342.



### 3 | Aim and Objectives

#### 3.1 | Aim

Considering the potential gaps in the existing research, the present thesis aims at “*the study of NP lead(s) and its inspired analogues as potent PL inhibitors for obesity treatment*”.

#### 3.2 | Objectives

To achieve the above aim, following studies were set as objectives;

1. To prepare extracts from selected Indian medicinal plants and determine their *in vitro* PL inhibitory activity
2. To perform bioassay guided fractionation of the most potent extract followed by purification and characterization of the isolated NP lead(s)
3. To evaluate the NP lead(s) for *in vitro* PL inhibition and identify the structural features required for activity using *in silico* methods
4. To design, synthesise and evaluate various analogues of NPs lead for their PL inhibitory activity.
5. To evaluate the *in vivo* efficacy of the most potent synthetic analogue using High Fat Diet (HFD) fed mice model

### 4 | Materials and Methods

#### 4.1 | Plant material collection, procurement, processing and extraction

Plant materials were either collected from BITS Pilani (located at 28.36°N 75.58°E and 285 m above the sea level) or procured from commercial suppliers (at Nashik, Chandigarh and Dehradun). All the plants were authenticated by Dr. A. S. Sandhu, Department of Natural Products, NIPER (S.A.S. Nagar), and the specimens of the same were deposited at the Herbarium of the Natural Products (BITS/Pilani/NP01 – NP20), Laboratory of Natural Drugs, Department of Pharmacy, BITS Pilani (Pilani Campus). Each plant material was shade dried, powdered (using a pulveriser) and sieved (through BSS No. 10 mesh). Further, each plant material (30g x 3) was subjected to sequential extraction using hexane and methanol with the aid of three extraction techniques; cold maceration (CM - RT, 72 h), hot percolation (HP - 40°C and 60°C for hexane and methanol, respectively for 24 h) and ultrasonic extraction (UE -  $\approx$  25-30°C, 1 h); The respective extracts were then concentrated *in vacuo* to obtain six different extracts per plant material. Hot percolation was carried using Soxhlet apparatus (Perfit, India)

#### 4.2 | PL inhibition assay and enzyme kinetics

Orlistat, Porcine PL (Type II) and 4-nitrophenyl butyrate (4-NPB) were procured from Sigma-Aldrich, USA. Tris buffer and sodium chloride (Molecular Biology grade) were procured from Sisco Research Laboratories, India.

The procedure for PL inhibition assay was performed as per the previously reported literature with minor modifications [1]. Briefly, 50 mg of porcine pancreatic lipase was suspended in 10 mL of Tris-HCl buffer (containing 0.25 M of Tris and NaCl each, adjusted to pH 7.4 with HCl) and subjected to vigorous shaking for 15 min. The suspension was then centrifuged at 4000 rpm for 10 min, and the supernatant was used afresh as the enzyme solution. Stock solutions of the extracts and orlistat (standard) were prepared in DMSO at linear concentrations. The final reaction mixture comprised of 875  $\mu$ L of buffer, 100  $\mu$ L of enzyme and 20  $\mu$ L of the extracts/compounds/orlistat of various stock concentrations, pre-incubated for 5 min at 37°C, followed by addition of 10  $\mu$ L of the substrate (4-NPB, 10 mM in acetonitrile). The amount of DMSO in the final concentration did not exceed 2%. The absorbance of the final mixture was taken on EPOCH microplate spectrophotometer (BioTek, USA) after 5 min at 405 nm (absorbance maximum of 4-nitrophenol). The assay was performed in triplicate and the percentage inhibition was calculated using the formula

$$\% \text{ Inhibition} = [(A_E - A_T) / A_E] \times 100 \text{ ----- Formula 4.1}$$

where  $A_E$  is the absorbance of enzyme control (without inhibitor), and  $A_T$  is the difference between the absorbance of test sample, with and without substrate. The  $IC_{50}$  of the extracts and orlistat were calculated by plotting linear regression curve (% inhibition *Vs.* concentration).

For the inhibition kinetics, the assay protocol was repeated at four different concentrations of substrate (25, 50, 100 and 200  $\mu\text{M}$ ) using increasing concentrations of the inhibitor. The absorbance of the final reaction mixture was taken in kinetic mode (16 readings for 30 minutes) and the respective concentration of 4-nitrophenol was calculated from its calibration curve. The velocity of the reaction was then calculated as the slope of the graph for concentration *Vs.* time. A double reciprocal Lineweaver-Burk plot with reciprocals of velocity and substrate concentration (on y-axis and x-axis, respectively) was plotted to understand the nature of inhibition [2]. The inhibition constant,  $K_i$ , was calculated using Cheng-Prusoff equation [3].

### 4.3 | Molecular docking and molecular dynamics simulations

Molecular docking studies were performed with the aid of Molegro Virtual Docker 6.0 (CLC Bio, Denmark), and the crystal structure of the open lid conformation of the Human PL was retrieved from the RCSB Protein Data Bank (PDB Code: 1LPB) [4,5]. Prior to the docking, the structures of the ligands were drawn using Chemdraw 2D module and the energy minimised structures were obtained using Molecular Mechanics 2 (MM2) force field in Chemdraw 3D module of ChemBioOffice v12 and v16 (PerkinElmer, USA). The details of the validated grid parameters are detailed in Fig. 4.1. The validation was performed by redocking the co-crystallised ligand (subjected to energy minimization) into the active site of PL. The redocked pose was deviated from the co-crystallised pose by an RMSD of 0.692 Å (Fig. 4.2). The obtained docked poses of the ligands were analysed for their MolDock scores, while the various interactions exhibited by the ligands with the active site were visualised in Discovery Studio Visualizer (Dassault Systemes Biovia, USA).

Molecular dynamics (MD) represents a useful technique in understanding the ligand interactions and its binding stability in a dynamic environment. Hence, the MD simulations for the most potent ligands were performed using GRONingen Machine for Chemical Simulations (GROMACS 5.0.4), compiled on a CentOS 7 operating system equipped with Intel(R) Xeon(R) CPU W3565 and NVIDIA Quadro 4000 Quad-Core Processor. CHARMM27 (Chemistry at Harvard Macromolecular Mechanics 27) force field was applied during the MD run [6], and the topology of the ligands were generated using online tool provided by Swiss Institute of Bioinformatics [7]. Prior to the initiation of the MD, the

## Chapter 4

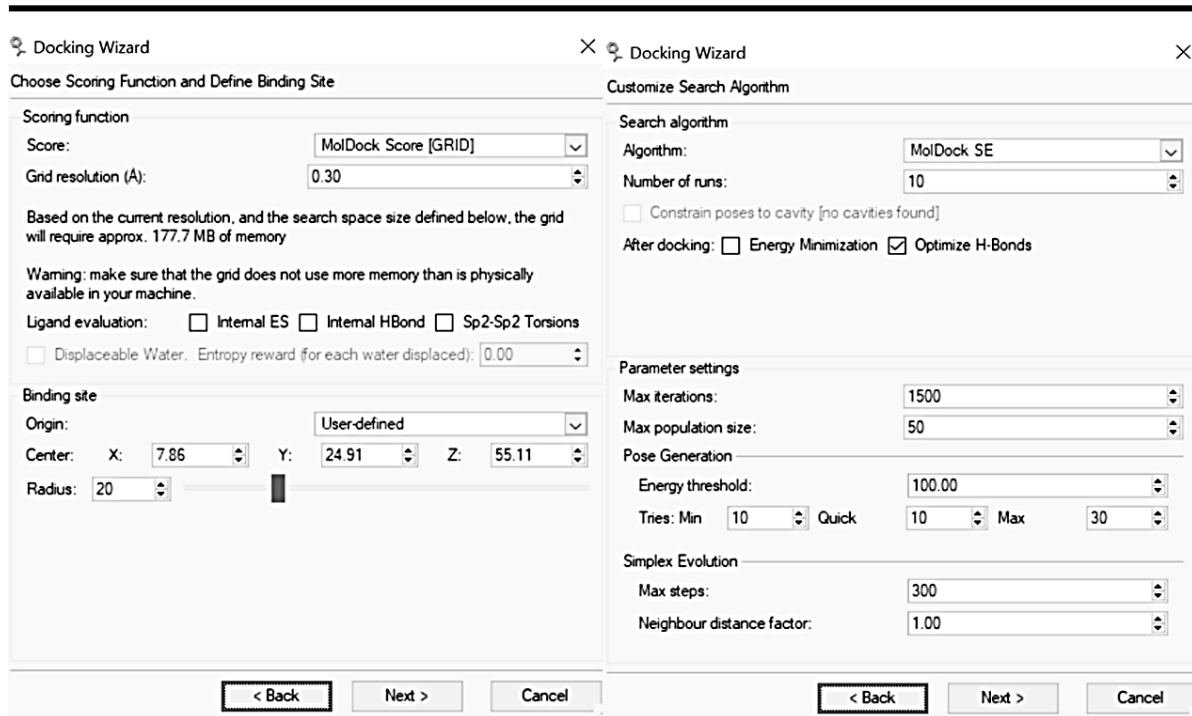


**Fig. 4.1.** Screenshots retrieved from the Molegro Virtual Docker 6.0, summarizing various parameters and their values used in the molecular docking studies

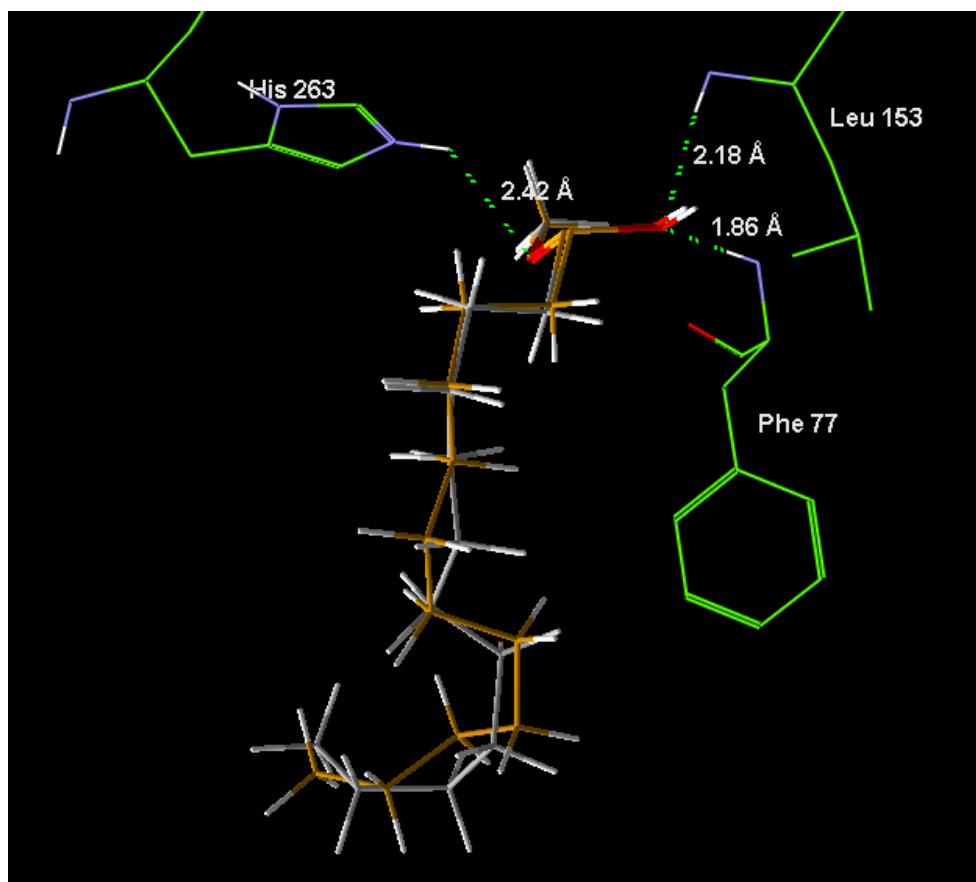


**Fig. 4.2.** Superimposition of re-docked pose of MUP (Brown) with the co-crystallised pose (Grey)

complex was minimized using Steepest Descent algorithm for 1000 steps, followed by stabilization of the system to 310 K and 1 atm pressure for 50 ps, using the canonical NVT and NPT ensembles. Parameters like Particle Mesh Ewald method for long-range electrostatics [8], and 14 Å cut-off for *van der Waals* and columbic interactions were set during the MD simulation. Linear Constraint Solver (LINCS) algorithm was applied for the calculation of bond length [9]. Discovery Studio visualizer was used to depict the graphical representations of the complex.

### 4.4 | Synthesis and characterization

The synthesis of various series of carbazolyl and indolyl oxoacetamides are detailed under corresponding chapters 6-8. Reactions were carried using Spinot (Tarson, India) magnetic hot plate. Progress of the reactions was followed by Thin Layer Chromatography (TLC) analysis (Silica gel G60 F<sub>254</sub>, Merck). The reactions were concentrated using rotary evaporator (Heidolph, Germany). The synthesised analogues were purified either by column chromatography or recrystallization. Melting points were determined with electro thermal capillary melting point apparatus (E-Z melting) and are uncorrected. IR spectra were recorded either on ABB Bomen MB 3000 FTIR machine (for carbazolyl oxoacetamide analogues) or Shimadzu Prestige21 machine (for indolyl oxoacetamide analogues) using KBr pellets. <sup>1</sup>H and <sup>13</sup>C NMR spectra were recorded on a Bruker Avance II 400 spectrometer (400 MHz and 100 MHz, respectively) using DMSO-*d*<sub>6</sub> and CDCl<sub>3</sub> as solvents. HR-MS analysis was performed on Bruker Compass Data Analysis 4.1 mass instrument. LC-MS analysis was done using WATERS ACQUITY UPLC<sup>®</sup> Instrument.

### References

- [1] Y. Bustanji, I.M. Al-Masri, M. Mohammad, M. Hudaib, K. Tawaha, H. Tarazi, H.S. AlKhatib, Pancreatic lipase inhibition activity of trilactone terpenes of *Ginkgo biloba*, *J. Enzyme Inhib. Med. Chem.* 26 (2011) 453–459.
- [2] H. Lineweaver, D. Burk, The determination of enzyme dissociation constants, *J. Am. Chem. Soc.* 56 (1934) 658–666.
- [3] B.T. Burlingham, T.S. Widlanski, An intuitive look at the relationship of  $K_i$  and  $IC_{50}$ : A more general use for the Dixon plot, *J. Chem. Educ.* 80 (2003) 214.
- [4] M.P. Egloff, F. Marguet, G. Buono, R. Verger, C. Cambillau, H. van Tilbeurgh, The 2.46 Å resolution structure of the pancreatic lipase-colipase complex inhibited by a  $C_{11}$  alkyl phosphonate, *Biochemistry.* 34 (1995) 2751–2762.
- [5] R. Thomsen, M.H. Christensen, MolDock: A new technique for high-accuracy molecular docking, *J. Med. Chem.* 49 (2006) 3315–3321.
- [6] A.D. MacKerell, N. Banavali, N. Foloppe, Development and current status of the CHARMM force field for nucleic acids, *Biopolymers.* 56 (2000) 257–265.
- [7] V. Zoete, M.A. Cuendet, A. Grosdidier, O. Michielin, SwissParam: A fast force field generation tool for small organic molecules, *J. Comput. Chem.* 32 (2011) 2359–2368.
- [8] T. Darden, D. York, L. Pedersen, Particle mesh Ewald: An  $N \cdot \log(N)$  method for Ewald sums in large systems, *J. Chem. Phys.* 98 (1993) 10089–10092.
- [9] B. Hess, H. Bekker, H.J.C. Berendsen, J.G.E.M. Fraaije, LINCS: A linear constraint solver for molecular simulations, *J. Comput. Chem.* 18 (1997) 1463–1472.

### 5 | Identification of NP Lead from *T. divaricata* and Its Validation

#### 5.1 | Preliminary Screening

A detailed literature review (chapter 2) resulted in the identification of structural features required for PL inhibitory activity. For the identification of PL inhibitory NPs leads, medicinal plants were selected based on two criteria given below.

- i. Their use in traditional and other folkloric systems of medicine for obesity treatment
- ii. The presence of chemical constituents with the following features; a) large molecular volume that can be able to interact with the active site as well as the hydrophobic lid domain; b) presence of an ester or ester mimicking group with a reactive carbonyl functionality that would interact with Ser152 of the active site

In total, a pool of 20 Indian medicinal plants/parts (Herbarium No: BITS/Pilani/NP01 – NP20) were selected (Table 5.1) and subjected to sequential extraction with three extraction techniques (See section 4.1) to obtain 120 plant extracts. The PL inhibitory potential of these extracts was evaluated using method described in section 4.2, and the results of PL inhibition are summarized in Table 5.2. The methanol extract of *T. divaricata* leaves obtained through ultrasonic extraction exhibited greater PL inhibitory potential ( $IC_{50} = 12.73 \mu\text{g/mL}$ ).

**Table 5.1.** Plants and parts selected for screening in PL inhibition assay [1,2]

#	Plant and part	#	Plant and part
1	<i>Atrocarpus heterophyllus</i> bark	11	<i>Plumbago zeylanica</i> root
2	<i>Azadirachta indica</i> fruit	12	<i>Semecarpus anacardium</i> fruit
3	<i>Clerodendrum serratum</i> leaf	13	<i>Sphaeranthus indicus</i> bark
4	<i>Embelia ribes</i> fruit	14	<i>Symplocos racemosa</i> bark
5	<i>Euphorbia nerifolia</i> leaf	15	<i>Tabernaemontana divaricata</i> leaf
6	<i>Mesua ferrea</i> leaf	16	<i>Tabernaemontana divaricata</i> stem
7	<i>Piper chaba</i> fruit	17	<i>Uraria picta</i> whole plant
8	<i>Piper cubeba</i> fruit	18	<i>Vitex negundo</i> leaf
9	<i>Piper nigrum</i> fruit	19	<i>Vitex negundo</i> seed
10	<i>Piper retrofractum</i> fruit	20	<i>Berberis aristata</i> leaf

## Chapter 5

**Table 5.2.** PL inhibitory activity of 120 plant extracts obtained from 20 plants/parts

#	Plant and part	IC <sub>50</sub> (µg/mL)*					
		Methanol			Hexane		
		UE	HP	CM	UE	HP	CM
1	<i>Atrocarpus heterophyllus</i> bark	16.63 ± 1.08	31.72 ± 2.20	64.02 ± 6.01	36.05 ± 1.87	62.77 ± 4.95	44.17 ± 2.88
2	<i>Azadirachta indica</i> fruit	49.97 ± 3.92	55.45 ± 5.24	64.77 ± 5.01	32.87 ± 3.21	49.91 ± 5.03	32.37 ± 3.37
3	<i>Clerodendrum serratum</i> leaf	18.59 ± 0.31	28.69 ± 1.65	49.86 ± 4.04	35.63 ± 1.22	35.48 ± 0.18	49.05 ± 5.20
4	<i>Embelia ribes</i> fruit	18.87 ± 1.68	24.89 ± 1.18	34.72 ± 5.71	19.02 ± 3.63	41.77 ± 0.11	22.72 ± 1.86
5	<i>Euphorbia nerifolia</i> leaf	59.93 ± 4.21	61.16 ± 3.44	56.71 ± 5.34	44.23 ± 1.48	36.10 ± 1.19	62.56 ± 4.10
6	<i>Mesua ferrea</i> leaf	38.98 ± 0.77	43.70 ± 4.92	39.93 ± 2.68	24.34 ± 1.91	40.10 ± 4.44	32.86 ± 4.19
7	<i>Piper chaba</i> fruit	25.85 ± 2.05	31.10 ± 1.94	45.12 ± 1.40	42.74 ± 0.69	33.11 ± 0.92	51.99 ± 6.03
8	<i>Piper cubeba</i> fruit	27.01 ± 0.76	30.85 ± 3.02	52.71 ± 5.57	38.53 ± 0.50	45.63 ± 3.56	37.59 ± 0.45
9	<i>Piper nigrum</i> fruit	20.23 ± 0.44	19.67 ± 0.49	23.75 ± 1.73	31.16 ± 2.40	38.76 ± 1.16	47.84 ± 2.64
10	<i>Piper retrofractum</i> fruit	21.64 ± 3.17	27.34 ± 3.22	54.17 ± 4.25	37.67 ± 3.24	36.77 ± 3.03	46.13 ± 1.43
11	<i>Plumbago zeylanica</i> root	40.65 ± 0.81	81.59 ± 4.65	61.66 ± 0.39	97.68 ± 6.93	98.46 ± 11.40	120.38 ± 13.67
12	<i>Semecarpus anacardium</i> fruit	15.12 ± 1.27	18.18 ± 1.50	36.20 ± 1.58	28.99 ± 1.96	66.53 ± 0.86	104.96 ± 6.90
13	<i>Sphaeranthus indicus</i> bark	23.99 ± 0.60	21.40 ± 0.98	31.78 ± 0.45	31.43 ± 1.54	34.09 ± 0.56	39.07 ± 0.97
14	<i>Symplocos racemosa</i> bark	28.37 ± 0.35	34.75 ± 1.64	39.06 ± 0.56	34.66 ± 0.07	32.12 ± 0.43	48.09 ± 1.87
15	<b><i>Tabernaemontana divaricata</i> leaf</b>	<b>12.73 ± 1.57</b>	28.91 ± 4.31	55.40 ± 2.88	27.42 ± 0.30	32.04 ± 2.03	43.81 ± 3.03
16	<i>Tabernaemontana divaricata</i> stem	18.62 ± 1.24	23.63 ± 1.28	36.18 ± 2.11	27.38 ± 1.40	32.66 ± 0.96	35.84 ± 1.43
17	<i>Uraria picta</i> whole plant	17.15 ± 1.30	38.55 ± 4.10	47.18 ± 1.63	39.06 ± 4.22	77.25 ± 1.22	59.10 ± 1.23
18	<i>Vitex negundo</i> leaf	18.95 ± 2.31	37.68 ± 0.99	38.04 ± 2.96	19.11 ± 1.36	44.80 ± 2.05	88.30 ± 4.80
19	<i>Vitex negundo</i> seed	64.48 ± 3.53	47.36 ± 0.84	50.66 ± 2.67	16.67 ± 0.18	16.68 ± 2.13	30.78 ± 2.79
20	<i>Berberis aristata</i> leaf	22.76 ± 2.11	36.15 ± 3.95	54.00 ± 5.44	45.04 ± 2.96	44.78 ± 4.89	47.17 ± 1.45

\* All experiments were performed in triplicate and the values are expressed as mean ± SEM.



### 5.2 | Literature Review of *T. divaricata*

Preliminary screening identified the methanol extract of *T. divaricata* leaves obtained through ultrasonic extraction to possess better PL inhibitory potential ( $IC_{50}=12.73 \mu\text{g/mL}$ ). *T. divaricata* is a tropical evergreen shrub native to India, and widely grown in many other Southeast Asian countries including Sri Lanka, Malaysia and Thailand. The plant exists in two distinct varieties, the singleflower variety and the double flower variety. A detailed taxonomical classification of *T. divaricata* is summarised in Fig. 5.1. The leaves of *T. divaricata* are widely reported for its use in various systems of traditional medicine for the treatment of fever, pain and dysentery [3]. Further, previous literature has highlighted the potential of *T. divaricata* leaves against metabolic disorders viz., diabetes mellitus and obesity. The hot aqueous decoction of the leaves is reported to be consumed by the tribal communities of Assam for the treatment of diabetes mellitus [4]. Moreover, the methanol extract of the aerial parts of *T. divaricata* has been investigated for its pre-clinical anti-obesity effect [5].



<b>Kingdom:</b>	Plantae
<b>Subkingdom:</b>	Tracheobionta
<b>Superdivision:</b>	Spermatophyta
<b>Division:</b>	Magnoliophyta
<b>Class:</b>	Magnoliopsida
<b>Subclass:</b>	Asteridae
<b>Order:</b>	Gentianales
<b>Family:</b>	Apocynaceae
<b>Genus:</b>	<i>Tabernaemontana</i> L.
<b>Species:</b>	<i>T. divaricata</i> (L.) R. Br. ex Roem. & Schult.

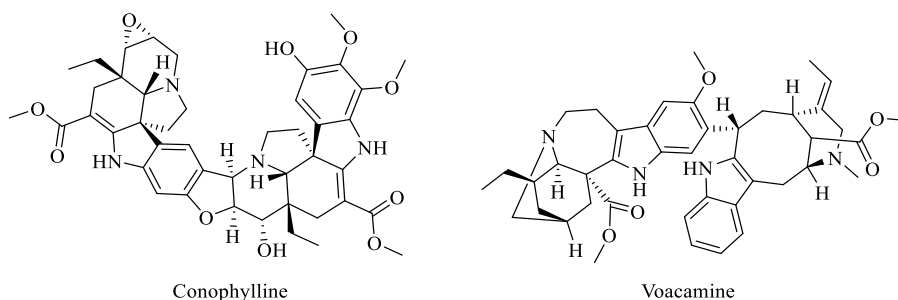
**Fig. 5.1.** Taxonomical classification of *T. divaricata*

Phytochemically, the leaves of *T. divaricata* are a rich source of indole alkaloids apart from various other classes of minor chemical constituents. To date, around 40 alkaloids have been identified from the leaves and reported for a wide array of pharmacological properties (Fig. 5.2 and Table 5.3).

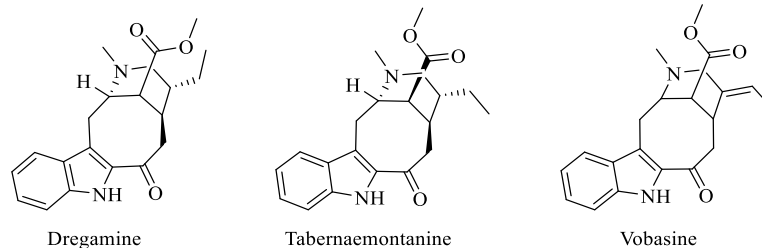
The present chapter discusses the various techniques and strategies employed to identify NP lead from the leaves of *T. divaricata* and validate its potential.

## Chapter 5

### Bis-indole alkaloids



### Corynanthean alkaloids



### Ibogan alkaloids

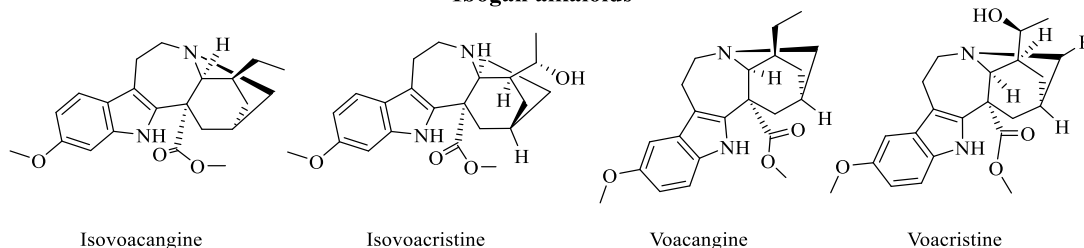


**Fig. 5.2.** Structures of various alkaloids reported from the leaves of *T. divaricata*

**Table 5.3.** Summary of various alkaloids and their pharmacological properties reported from *T. divaricata* leaves

Alkaloids	Class	Reported pharmacological activity	References
Conophylline	Bis-indole	Induces differentiation of pancreatic precursor cells and $\beta$ -cells, ameliorates blood glucose levels and cytotoxicity	[6–11]
Voacamine	Bis-indole	Cardiotonic, mild analgesic and anti-microbial	[12,13]
Dregamine	Corynanthean	CNS stimulant and analeptic effect	[13]
Tabernaemontanine	Corynanthean	Vasodilator	[13]
Vobasine	Corynanthean	Mild CNS depressant	[14]
Isovoacangine	Ibogan	Negative chronotropic and inotropic activity	[15]
Isovoacristine	Ibogan	Bradycardia, anticholinergic, antihistaminic, and skeletal muscle relaxant	[16,17]
Voacangine	Ibogan	Mild CNS stimulant, negative chronotropic activity and acetylcholine esterase inhibitor	[15,18,19]
Voacristine	Ibogan	Mild CNS stimulant and negative chronotropic activity	[13,15]

### 5.3 | Seasonal variations Vs. PL inhibitory profile

The effect of seasons on the metabolic profile of plants can be understood from the fact that some seasons produce high extractive yields of chemical constituents while some do not [20,21]. These variations in the yields of chemical constituents might result in varied pharmacological activity. Hence, the leaves of *T. divaricata* (var. *I*) were collected every trimester over a period of one year *i.e.*, during the 15<sup>th</sup> day of November 2013, February 2014, May 2014 and August 2014, processed and subjected to ultrasonic extraction (See section 4.1). The methanol extracts of these samples were then subjected to PL inhibition assay that resulted in IC<sub>50</sub> values of 12.73, 21.7, 34.82 and 9.26 µg/mL, respectively.

Consequently, based on the potent PL inhibition profile, August sample was selected for large scale collection of leaves. Around 30 kgs of fresh *T. divaricata* leaves were collected during August 2014. The leaves were washed with water to remove any dust, and then subjected to shade drying at room temperature. After ensuring complete dryness, the leaves were crushed and sieved using a BSS No. 10 mesh to obtain 6 kgs of dry powder. The leaf powder was then subjected to exhaustive ultrasonic extraction. The extraction was carried out in batches of 200 g using hexane (500 mL). The leaf material was then dried and further subjected to extraction with methanol (500 mL). The resultant hexane and methanol extracts were pooled and concentrated *in vacuo* to yield 0.28 and 1.4 kgs of crude hexane and methanol extracts, respectively (Fig. 5.3).

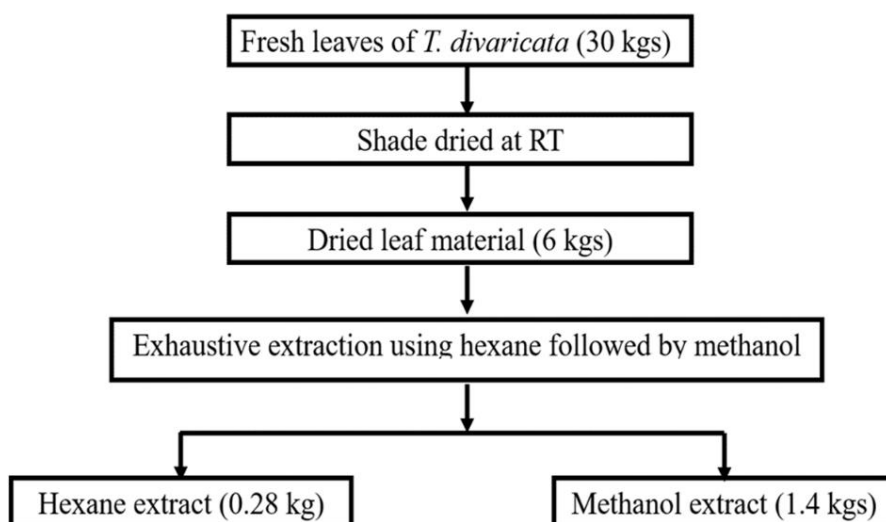


**Fig. 5.3.** Schematic flow representing processing and extraction of *T. divaricata* leaves

## 5.4 | Bioassay guided fractionation

### 5.4.1 | Liquid-liquid partition

In order to identify the PL inhibitory NP lead(s), the crude methanol extract was subjected for liquid-liquid partitioning. The methanol extract (1.4 kgs) was dissolved/suspended in 2 L of water and subjected to sequential extraction with hexane ( $\approx$  20 L), dichloromethane ( $\approx$ 10 L) and ethyl acetate ( $\approx$ 10 L) through the aid of liquid-liquid partition in separatory funnels (Fig. 5.4). The residual aqueous phase was subjected to the preparation of alkaloid rich fraction (ARF) using procedure reported in literature [22]. Briefly, the aqueous phase was acidified to pH 4 using 5% HCl, to convert the alkaloids into their respective salt derivatives. This aqueous phase was extracted with chloroform ( $\approx$  10 L) in a separatory funnel and the residual aqueous phase was basified to pH 9 using 25% ammonia solution. The basified aqueous phase was then extracted using chloroform ( $\approx$  10 L) in a separatory funnel. This alkaloid rich chloroform phase was collected and evaporated to dryness in a rotavapor to obtain the ARF. Various fractions obtained through liquid-liquid partition were then subjected to PL inhibition assay. The respective weights and the results of PL inhibition are represented in Fig. 5.4. The hexane and ethyl acetate fractions exhibited poor PL inhibition, while the dichloromethane and the alkaloid rich fractions exhibited potential inhibitory activity.

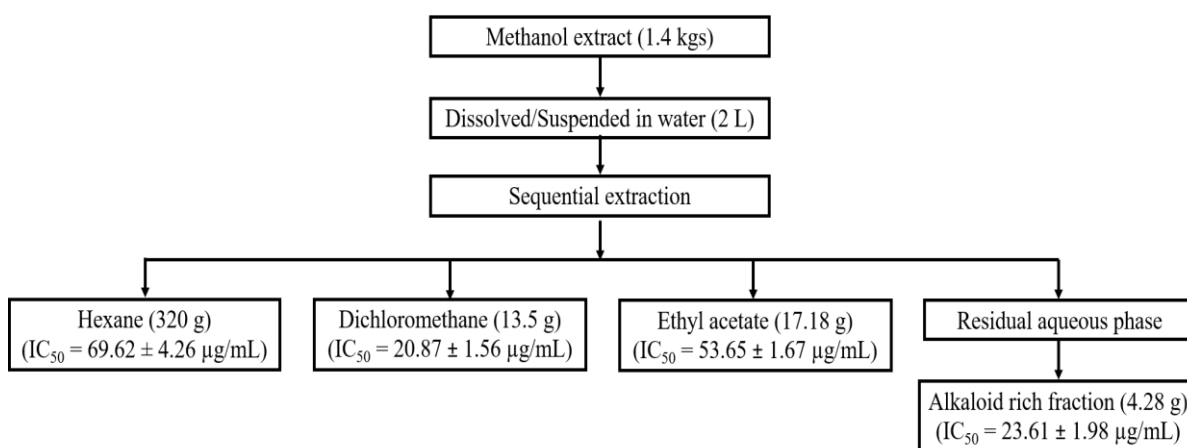


**Fig. 5.4.** Schematic flow representing the weights of various fractions obtained through liquid- liquid partition and their PL inhibitory activities ( $IC_{50}$  values are represented as mean  $\pm$  SEM).

### 5.4.2 | Column chromatography

Considering the better potential of dichloromethane fraction in PL inhibition, column chromatography was performed using the parameters detailed in Table 5.4.

## Chapter 5

**Table 5.4.** Column dimensions and other parameters used in column chromatography

Parameter	Condition	Parameter	Condition
Stationary phase	Silica gel 60-120		- Hexane → DCM
Sample loaded	12 g on 120 g silica		(at 10% increment)
Column dimensions	100 cm (L) x 6 cm (D)		- DCM → Ethyl acetate
Column packed	40 cms (600 g Silica)	<b>Gradient</b>	(at 5% increment)
Elution method	Gradient		- Ethyl acetate → Methanol
Gradient and fraction volume	400 and 100 mL		(up to 30% at 2.5% increment)
Total no of fractions	210		- Ethyl acetate: methanol (50:50 %) for final wash

A total of 210 fractions were obtained, that were pooled based on the TLC profiles to obtain 11 fractions {DF<sub>1</sub> - DF<sub>10</sub> and final wash} (Fig. 5.5). Of these, fractions DF<sub>5</sub> and DF<sub>10</sub> produced white and brown precipitates respectively and were labelled as DF<sub>5P</sub> and DF<sub>10P</sub>. All these fractions were evaluated for PL inhibition assay. As summarised in Fig. 5.5, fraction DF<sub>10P</sub> exhibited potential PL inhibition with an IC<sub>50</sub> value of 4.28 µg/mL. A TLC analysis of DF<sub>10P</sub> highlighted the presence of a single alkaloid as the major constituent apart from a minor non-alkaloidal impurity. Further DF<sub>10P</sub> was purified by recrystallization using ethyl acetate to give yellow prisms (11 mg). A mass analysis using LC-MS/MS (ESI mode) indicated the compound to be conophylline i.e Mass calculated for C<sub>44</sub>H<sub>51</sub>N<sub>4</sub>O<sub>10</sub> [M+H]<sup>+</sup> 795.36, Found 795.45. The compound was further confirmed by matching the λ<sub>max</sub> (280 nm) and R<sub>f</sub> value (0.38, CHCl<sub>3</sub>: MeOH; 9:1, v/v) using HPTLC with the reference standard of conophylline available in the laboratory repository.

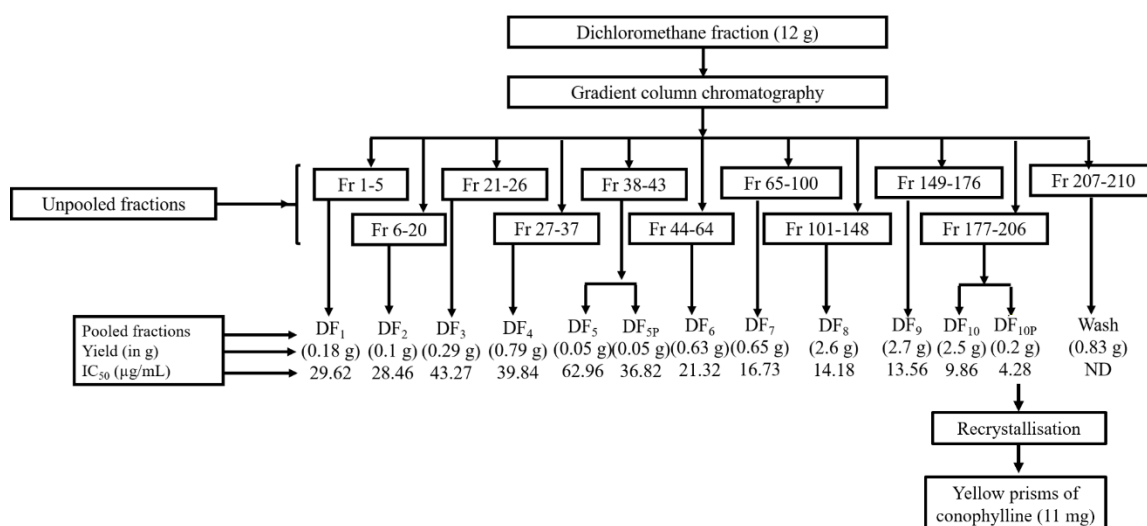


**Fig. 5.5.** A schematic flow summarising the yields and the PL inhibitory activities of various fractions obtained through the column chromatography of the dichloromethane fraction

## 5.4.3 / PL inhibition assay and enzyme kinetics

To evaluate the PL inhibitory activity and kinetics, stock solutions of orlistat (standard) and conophylline were prepared in DMSO at linear concentrations ranging from 7.8 – 1000  $\mu\text{g}/\text{mL}$ . Conophylline exhibited an  $\text{IC}_{50}$  of  $3.31 \pm 0.19 \mu\text{M}$  ( $K_i = 1.60 \mu\text{M}$ ) while orlistat exhibited an  $\text{IC}_{50}$  of  $0.99 \pm 0.11 \mu\text{M}$  ( $K_i = 0.59 \mu\text{M}$ ). These results from the PL inhibition assay indicated conophylline to possess a potent activity comparable to orlistat (Fig. 5.6).

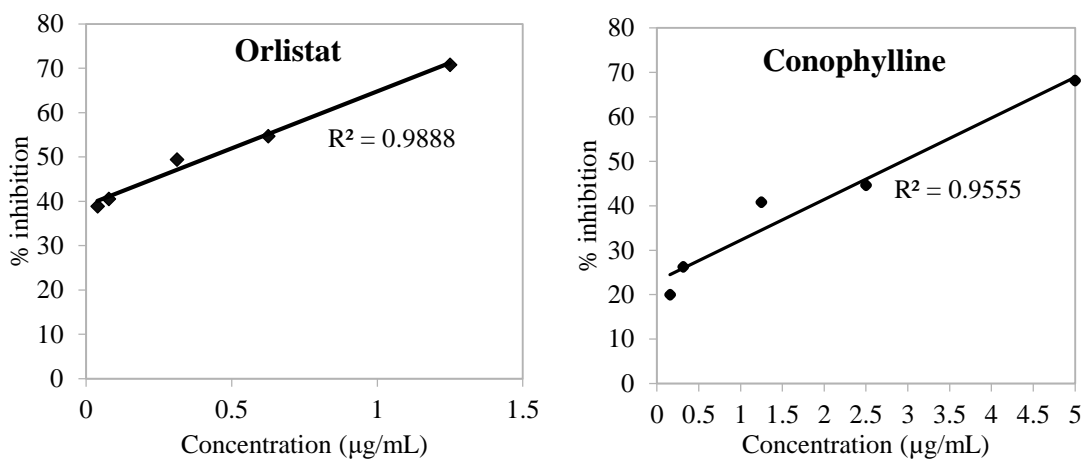


**Fig. 5.6.** Linear regression curves obtained from PL inhibition assay for orlistat and conophylline

Moreover, enzyme kinetics of conophylline and orlistat indicated that both the analogues exhibited a reversible competitive inhibition. As represented in Fig. 5.7, the plots converged at y-intercept, while  $K_m$  (slope of the plots) increased with the inhibitor concentration. These representations are an indication of competitive reversible inhibition [23,24].

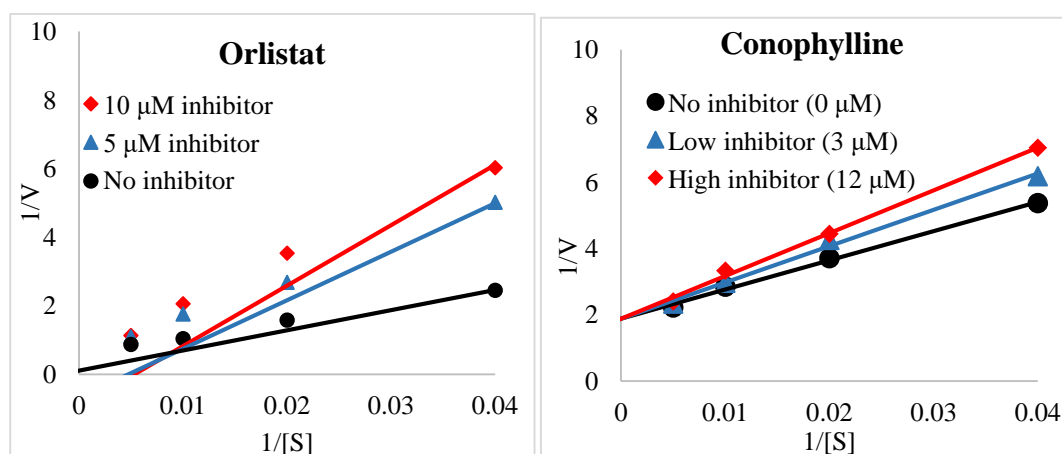


**Fig. 5.7.** Lineweaver-Burk plots of orlistat and conophylline representing reversible competitive inhibition

## 5.4.4 / Molecular docking and MD simulations

A total of 38 alkaloids reported from the leaves of *T. divaricata* were subjected to molecular docking studies using Molegro Virtual Docker 6.0. Of the top four scoring molecules, conophylline, conophyllinine and conophyllidine belonged to the furan bridged bis-indole sub class, while taberhanine was the monomeric counterpart of these three bis-indoles. Among these, conophylline exhibited the most potential MolDock score of -143.382 kcal/mol. Further, a significant variation in the MolDock scores was observed among the dimers and monomers. As represented in Fig. 5.8 and Table 5.5, taberhanine exhibited a significant variation in the MolDock score (-113.252 kcal/mol) compared to the dimers.

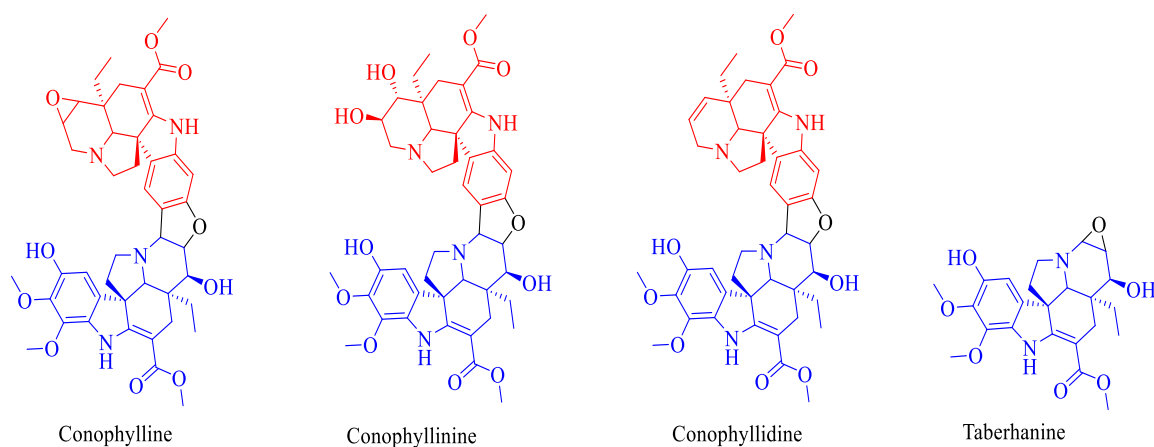


**Fig. 5.8.** Structures of conophylline, conophyllinine, conophyllidine and taberhanine

In an attempt to understand the better MolDock scores of dimeric scaffolds over the monomer, the docking interactions and the binding poses of these molecules with the active site of the Human PL was analysed. A significant variation was observed with the hydrophobic interactions, wherein the dimers exhibited comparatively extended hydrophobic interactions with Ile 78, Ile 209, Val 210, Leu 213 of the lid domain that was not observed with taberhanine. Previous literature suggested the role of hydrophobic moieties in the ligands to potentiate the PL inhibition activity through extended interactions with the lid domain [25,26]. The fact was further confirmed through MD simulations wherein the dimers possessed a stable RMSD throughout the simulation and exhibited a higher degree of hydrophobic interactions that was not seen with taberhanine (Fig. 5.9 and Table 5.6).

## Chapter 5

**Table 5.5.** Summary of docking scores and interactions exhibited by top four scoring molecules (Common interactions in bold)

Ligand	MolDock Score (kcal/mol)	H-bond interactions	$\pi$ - $\pi$ interactions	Hydrophobic interactions
Conophylline	-143.382	<b>Phe 77, Ser 152, Leu 153,</b> Glu 179, Phe 215	<b>Tyr 114,</b> His 263	<b>Phe 77, Tyr 114, Ala 178, Pro 180, Phe 215,</b> Leu 153, Ile 209, Val 210, Leu 213, His 263, Leu 264
Conophyllinine	-137.553	<b>Phe 77, Ser 152, Leu 153,</b> Glu 179, Phe 215	<b>Tyr 114,</b> His 263	<b>Phe 77, Tyr 114, Ala 178, Pro 180, Phe 215,</b> Trp 106, Ile 209, Leu 213, His 263, Leu 264
Conophyllidine	-133.011	<b>Phe 77, Ser 152, Leu 153</b>	<b>Tyr 114,</b> Phe 215	<b>Phe 77, Tyr 114, Ala 178, Pro 180, Phe 215,</b> Ile 78, Ile 209, Leu 213, Ala 260, His 263, Leu 264
Taberhanine	-113.252	<b>Phe 77, Ser 152, Leu 153</b>	<b>Tyr 114</b>	<b>Phe 77, Tyr 114, Ala 178, Pro 180, Phe 215</b>

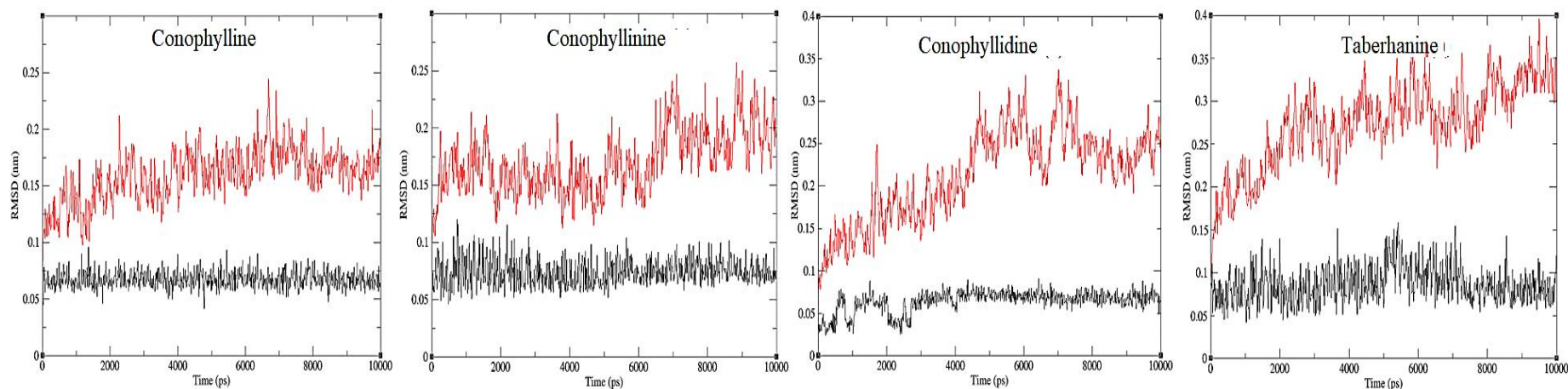


**Fig. 5.9.** Backbone RMSD (in red) and ligand RMSD (in black) of conophylline, conophyllinine, conophyllidine and taberhanine



## Chapter 5

**Table 5.6.** Summary of hydrophobic interactions exhibited by top four scoring molecules during MD simulations

Time frame	Conophylline	Conophyllinine	Conophyllidine	Taberhanine
0 ns	Phe 77, Tyr 114, Pro 180, Ile 209, Phe 215, Ala 259, Ala 260	Phe 77, Tyr 114, Pro 180, Ile 209, Leu 213, Phe 215, His 263	His 151, Pro 180, Ile 209, Ala 259, His 263	Phe 77
1 ns	Tyr 114, Ala 178, Pro 180, Phe 215	Ile 78, Tyr 114, Ala 259, Ala 260, His 263	Pro 180, Ile 209, Phe 215, Ala 259, His 263	Phe 77, Tyr 114
2 ns	Ala 178, Pro 180, Ile 209, Leu 213, Phe 215	Phe 77, Phe 215, Ala 259, Ala 260, His 263	Phe 77, Phe 215, His 263	Phe 77, Tyr 114
3 ns	Tyr 114, Pro 180, Phe 215	Phe 77, Phe 215, His 263	Tyr 114, Leu 153, Ala 178, Phe 215	Phe 77
4 ns	Phe 77, Tyr 114, Pro 180, Leu 213, Phe 215	Phe 215, Ala 259, Ala 260, His 263	Ile 178, Phe 215, His 263	Ile 78, Arg 256, Asp 259
5 ns	Pro 24, Phe 77, Tyr 114, Pro 180, Ile 209, Phe 215	Phe 215, Ala 259, Ala 260, His 263	Phe 77, Pro 180, Phe 215, His 263	Ile 78, Arg 256, Asp 259
6 ns	Phe 77, Tyr 114, Pro 180, Ile 209, Leu 213, Phe 215	Phe 77, Tyr 114, Phe 215, His 263	Tyr 114, Ala 178, Phe 215	Ile 78, Arg 256, Asp 259
7 ns	Ile 209, Leu 213, Phe 215	Phe 77, Ile 78, Leu 153, Pro 180, Phe 215, His 263	Pro 24, Tyr 114, Ala 178, Cys 181, Phe 215	Ile 78, Arg 256
8 ns	Tyr 114, Pro 180, Ile 209, Leu 213, Phe 215	Phe 77, Phe 215, His 263	Pro 24, Tyr 114, Ala 178, Cys 181, Phe 215	Phe 77, Ile 78, Arg 256, Asp 259
9 ns	Tyr 114, Pro 180, Ile 209, Leu 213, Phe 215	Phe 77, Tyr 114, Ala 178, Pro 180, Phe 215, His 263	Pro 24, Leu 25, Phe 215	Ile 78, Arg 256, Asp 259
10 ns	Phe 77, Tyr 114, Ile 209, Leu 213, Phe 215	Phe 77, Tyr 114, Ala 178, Pro 180, Phe 215, His 263	Pro 24, Leu 25, Tyr 114, Cy 181	Ile 78, Arg 256, Asp 259

### 5.4.5 / Method development, validation and quantification of conophylline

The results from the *in vitro* PL inhibition assay indicated anti-obesity potential of conophylline, while the reports from the previous literature cited its anti-diabetic potential through induction of  $\beta$ -cell differentiation [11]. These results proved the importance of conophylline (**1**) as a multi-faceted NP lead against metabolic disorders. Nevertheless, there are no methods reported for the quantification of conophylline from the leaves of *T. divaricata*. Hence, the present study was aimed **a**) to develop and validate a new High-Performance Thin Layer Chromatography (HPTLC) method for the quantification of conophylline in the leaves of *T. divaricata*; **b**) to understand the role of seasonal variation and extraction techniques on the extractive yield of conophylline, and its correlation to PL inhibition that would validate its potential.

#### 5.4.5.1 / Materials and methods

##### Sample Preparation

For quantification of conophylline, a set of 12 methanol extracts from *T. divaricata* leaves obtained from four seasons and subjected to three extraction techniques were processed to obtain the respective ARFs. (See section 4.1 and 5.4.1)

##### HPTLC Densitometry

Conophylline was quantified in these 12 ARFs with the aid of a HPTLC System (CAMAG, Switzerland), equipped with Linomat 5 sample applicator, Hamilton syringe (100  $\mu$ L), Twin trough development chamber (20 x 20 cm) and TLC scanner 3, operated through winCATS (v 1.4.10) software. Chromatography of the 12 ARF samples was performed in triplicate on TLC plates (8 cm  $\times$  15 cm). Prior to the experiments, the TLC plates were washed with methanol and activated at 120°C for 20 min. Sample solutions (5  $\mu$ L) were applied in the form of 5 mm bands at 10 mm and 20 mm from the lower and left edges respectively, and 10 mm space between two bands. Linear ascending development was carried out in pre-saturated vertical twin trough glass chamber saturated with the mobile phase. The mobile phase consisted of chloroform : methanol (90:10 % v/v) and TLC separation of conophylline was achieved without interference from sample matrix components under laboratory conditions (temperature 25  $\pm$  2°C and relative humidity 60%). The plates were scanned and quantified densitometrically at 280 nm using TLC Scanner 3. The scanning was performed in the absorption mode, with a slit width of 3.00 mm  $\times$  0.1 mm, scanning speed 20 mm/s and data resolution of 100  $\mu$ m/step. Savitsky Golay-7 was used for data filtering and the lowest slope for baseline correction to integrate the area.

### *Method development and validation*

To develop the HPTLC method, various solvents with varying polarity were used and preliminary trials were taken to optimise the mobile phase composition and to achieve desirable peak properties such as peak area, tailing factor, height etc. The validation of the developed HPTLC method was performed as per the Q2 (R1) guidelines of International Conference on Harmonization (ICH) for Instrumental Precision, Specificity, Sensitivity, Linearity, Precision, Accuracy, and Robustness [27]. Instrumental precision for Scanner 3 was evaluated by scanning a single spot of conophylline (500 ng/spot) seven times ( $n=7$ ). Linomat 5 sample applicator was checked for its suitability by spotting conophylline (500 ng/spot) seven times ( $n=7$ ). The specificity of the developed method was established by analysing the sample solutions containing conophylline in relation to interferences from other compounds of the ARF. The sensitivity of the developed method was established by determining the Limit of Detection (LOD) and Limit of Quantification (LOQ). For this, a series of concentrations (10-400 ng/spot) of standard conophylline were spotted and the Signal to Noise (S/N) ratio was analysed. LOD was calculated as 3.3 times the noise level, while LOQ was calculated as 10 times the noise level. The linearity was evaluated at different concentration levels (150-1800 ng/spot) of standard conophylline by application of 5  $\mu$ L of the respective stocks (30-360 ng/ $\mu$ L). The experiment was performed thrice ( $n=3$ ), and the calibration curves were obtained by plotting peak area (Y-axis) Vs. concentration of spot applied (X-axis). Precision was evaluated intra-day ( $n=3$ ) and inter-day ( $n=3$ ) at three levels using low (300 ng/spot), medium (1000 ng/spot), and high (1800 ng/spot) concentrations of the calibration curve and the obtained peak areas were used to calculate % RSD (Relative Standard Deviation). The accuracy of the developed method was evaluated by performing recovery studies for each sample. Three concentration levels (80%, 100% and 120%) of standard conophylline were spiked into pre-analysed samples containing 800 ng conophylline and the % recovery of conophylline was calculated ( $n=3$ ). The robustness of the method was evaluated by implementing small changes in mobile phase polarity, mobile phase volume, saturation time of the development chamber and solvent front position. Each experiment was carried out thrice ( $n=3$ ) and the amount of conophylline and its % RSD were calculated.

### *5.4.5.2 | Results and discussion*

#### *Method development and validation*

In the present study, the mobile phase composition was optimized using various solvents with varying polarity (Fig. 5.10), and an overall better profile of the ARFs were

## Chapter 5

obtained with chloroform: methanol (90:10 %v/v) as mobile phase, run on a 10 cm length TLC plate. However, conophylline was still found to be interfered by an unknown compound, that was further resolved by increasing the plate length to 15 cm (Fig. 5.11). Further, when the saturation time of the development chamber was 15 min, an edging effect was observed, and was further resolved by optimizing the chamber saturation time to 30 min.

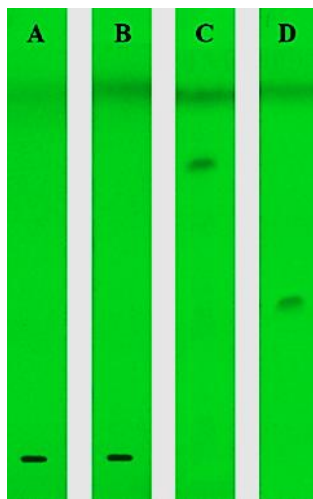


**Fig. 5.10.** TLC of conophylline in different mobile phases. (A) Hexane: ethyl acetate (50:50 %v/v); (B) Hexane: Ethyl acetate (10:90 %v/v); (C) Chloroform: Methanol (80:20 %v/v); (D) Chloroform: Methanol (90:10 %v/v). (conophylline did not elute in mobile phases A and B, while in C and D, it exhibited  $R_f$  of 0.76 and 0.38, respectively)

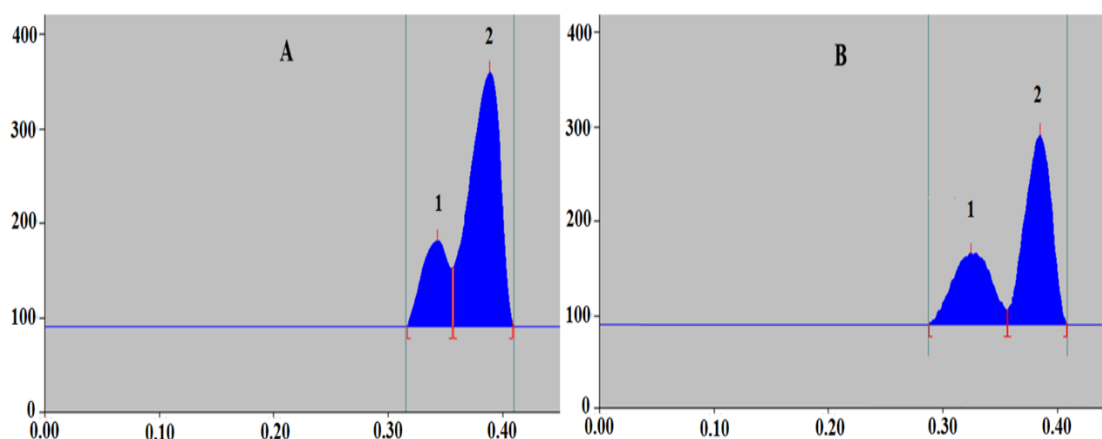


**Fig. 5.11.** (A) Unresolved chromatogram with 10 cm length TLC plate (solvent run length - 8 cm); (B) Resolved chromatogram with 15 cm length TLC plate (solvent run length - 13 cm). Peak 1 (interfering compound) and Peak 2 (conophylline)

## Chapter 5

The developed method was validated for various parameters and are summarized in Table 5.7. Conophylline exhibited a Retardation factor ( $R_f$ ) of 0.38 with no interferences from other compounds in the sample (Fig. 5.12).

**Table 5.7.** Summary of the validated HPTLC parameters for conophylline

S. No.	Parameter	Range
1	Instrumental precision (% CV, $n=7$ )	Linomat 5 (1.81); Scanner 3 (2.66)
2	Specificity ( $n=8$ )	Specific with $R_f$ of $0.38 \pm 0.01$
3	Limit of Detection (LOD)	40 ng/spot
4	Limit of Quantification (LOQ)	150 ng/spot
5	Linearity range	150-1800 ng/spot
6	Regression equation ( $r^2$ )	$y = 111.78 + 3.2745x$ (0.9985)
7	Precision - % RSD range (Intra-day; Inter-Day)	0.22-1.39%; 0.55-1.94%
8	Accuracy (% average recovery range)	96-102%
9	Robustness (% RSD Range)	0.58-1.77%

CV - Co-efficient of Variation;  $n$  – number of replicates; RSD – Relative Standard Deviation

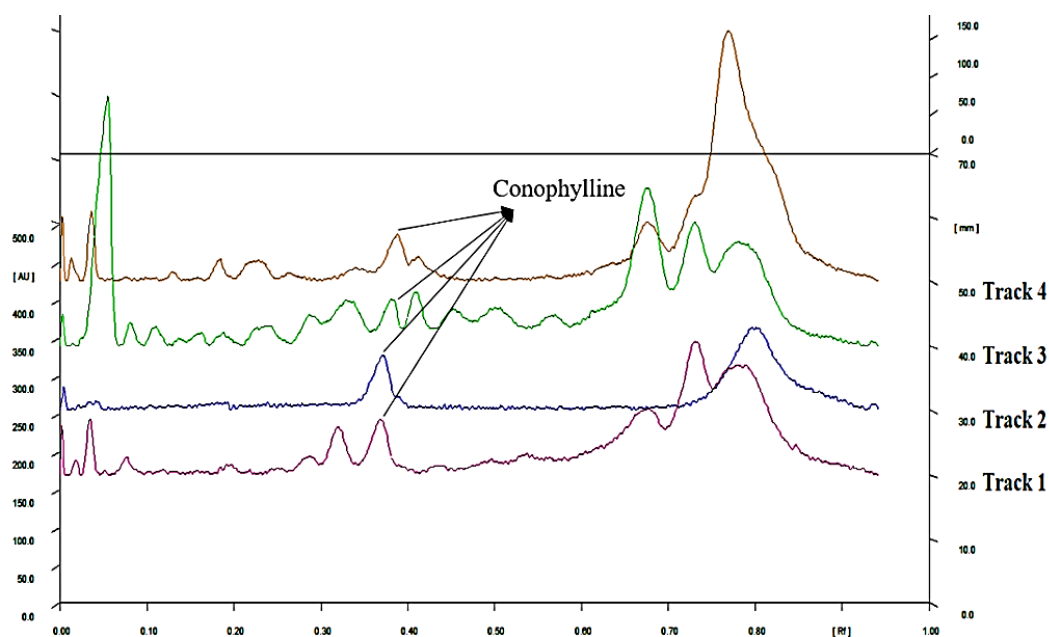


**Fig. 5.12.** HPTLC chromatograms of standard conophylline and ARFs from August samples of *T. divaricata* leaves. Track details - 1: Ultrasonic extraction, 2: standard conophylline, 3: Hot percolation, 4: Cold maceration; Mobile phase – Chloroform : methanol (90:10 % v/v)

The sensitivity of the method was evaluated by calculating LOD and LOQ of standard conophylline, which were found to be 40 and 150 ng/spot, respectively. Standard conophylline was spotted in the range of 150-1800 ng/spot which resulted in good linearity ( $r^2 = 0.9985$ ) with the regression equation  $y = 111.78 + 3.2745x$  (Fig. 5.13 and Table 5.8).

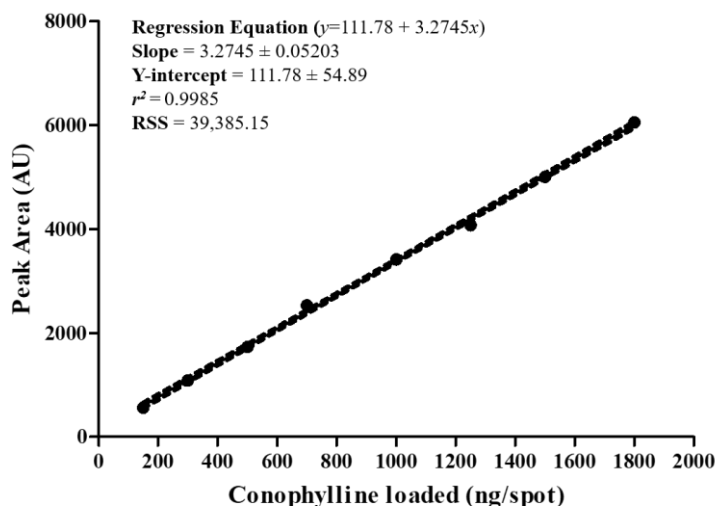


**Fig. 5.13.** Regression plot representing the linearity of the validated HPTLC method.  
 [RSS – Residual Sum of Squares. All values are expressed as mean  $\pm$  SEM ( $n = 3$ )]

**Table 5.8.** Mean areas and their % RSD at various concentrations of conophylline

Conophylline (ng/spot)	Mean area (AU)	SD	% RSD
	( $n=3$ )		
150	565.77	8.79	1.55
300	1086.40	17.58	1.62
500	1734.86	9.30	0.54
700	2534.93	41.01	1.62
1000	3417.30	25.31	0.74
1250	4073.93	43.25	1.06
1500	5005.50	22.88	0.46
1800	6052.13	32.54	0.54

ng – nanogram; AU – Absorbance units;  $n$  – number of replicates; SD – Standard Deviation; RSD – Relative Standard Deviation

The precision of the developed method was evaluated for intra- and inter-day, wherein the % RSD existed in the range 0.22-1.94% (Table 5.9). The accuracy of the developed method was performed by spiking three known concentrations of conophylline into pre-analysed ARF samples. The % average recovery existed in the range of 96-102% (Table 5.10). Finally, the robustness of the developed method was validated by including slight changes in the mobile phase polarity, mobile phase volume, solvent front position and saturation time of the development chamber. Conophylline exhibited  $R_f$  of 0.76 and 0.09 respectively, with 80:20 and 95:05% v/v of chloroform : methanol, while the % RSD existed in the range of 0.58-1.77% (Table 5.11).

## Chapter 5

**Table 5.9.** Summary of intra- and inter-day precision studies

Conophylline Spotted (ng/spot)	Amount Detected (ng) ± SD	% RSD	Conophylline Spotted (ng/spot)	Amount Detected (ng) ± SD	% RSD
<b>Intra-Day (n=3)</b>			<b>Inter-Day (n=3)</b>		
300	292.54 ± 4.08	1.39	300	294.88 ± 5.61	1.94
1000	1015.90 ± 4.33	0.43	1000	1011.93 ± 5.72	0.56
1800	1824.31 ± 2.68	0.15	1800	1841.17 ± 4.58	0.79

ng – nanogram; n – number of replicates; SD – Standard Deviation; RSD – Relative Standard Deviation

**Table 5.10.** Accuracy study of the developed method summarizing the % recovery values

ARF sample <sup>a</sup>	Conophylline analysed (ng)	Conophylline added (ng)	Conophylline recovered (ng)	% Recovery ± SD (n=3)
Nov-UE	800	640	602.90	94.20 ± 2.76
	800	800	836.08	104.51 ± 4.38
	800	960	955.26	99.51 ± 4.65
% Average Recovery ± SD				99.41 ± 3.93
Nov-HP	800	640	655.82	102.47 ± 3.46
	800	800	764.90	95.61 ± 1.89
	800	960	925.74	96.43 ± 4.78
% Average Recovery ± SD				98.17 ± 3.38
Nov-CM	800	640	661.47	103.36 ± 3.17
	800	800	779.81	97.48 ± 4.81
	800	960	1005.65	104.76 ± 4.68
% Average Recovery ± SD				101.86 ± 4.22
Feb-UE	800	640	614.03	95.94 ± 1.57
	800	800	802.42	100.30 ± 3.25
	800	960	941.12	98.03 ± 3.38
% Average Recovery ± SD				98.09 ± 2.73
Feb-HP	800	640	685.03	107.04 ± 1.43
	800	800	774.13	96.77 ± 1.87
	800	960	901.28	93.88 ± 1.62
% Average Recovery ± SD				99.23 ± 1.64
Feb-CM	800	640	640.85	100.13 ± 4.46
	800	800	784.15	98.02 ± 4.78
	800	960	955.23	99.50 ± 1.99
% Average Recovery ± SD				99.22 ± 3.74
May-UE	800	640	621.68	97.14 ± 2.86
	800	800	782.14	97.77 ± 1.14
	800	960	946.27	98.57 ± 3.12

## Chapter 5

			% Average Recovery ± SD	97.83 ± 2.37
May-HP	800	640	625.48	97.73 ± 3.28
	800	800	812.96	101.62 ± 3.46
	800	960	965.32	100.55 ± 2.78
			% Average Recovery ± SD	99.97 ± 3.17
May-CM	800	640	652.86	102.01 ± 1.89
	800	800	806.14	100.77 ± 2.12
	800	960	952.38	99.21 ± 3.48
			% Average Recovery ± SD	100.66 ± 2.50
Aug-UE	800	640	625.16	97.68 ± 2.99
	800	800	768.76	96.09 ± 4.83
	800	960	926.97	96.56 ± 4.66
			% Average Recovery ± SD	96.78 ± 4.16
Aug-HP	800	640	670.80	104.81 ± 4.83
	800	800	783.37	97.92 ± 1.84
	800	960	910.51	94.84 ± 1.60
			% Average Recovery ± SD	99.19 ± 2.76
Aug-CM	800	640	633.84	99.04 ± 2.66
	800	800	788.48	98.56 ± 4.74
	800	960	947.65	98.71 ± 4.22
			% Average Recovery ± SD	98.77 ± 3.87

<sup>a</sup>For the sample codes, the first three letters represent the respective months (Nov – November 2013; Aug – August 2014; Feb – February 2014; May – May 2014), while the next two letters represent the extraction technique (UE – Ultrasonic extraction; HP – Hot percolation; CM – Cold maceration).

**Table 5.11.** Summary of robustness results of the developed method

Parameter	Conophylline		% RSD
	Spotted (ng)	Detected (ng)*	
Mobile phase composition Chloroform : Methanol (80 : 20 %v/v)	600	590.42 ± 6.78	1.15
Mobile phase composition Chloroform : Methanol (95 : 05 %v/v)	600	589.64 ± 7.33	1.24
Mobile phase volume (32 mL)	600	597.33 ± 1.89	0.32
Mobile phase volume (48 mL)	600	581.55 ± 6.05	1.04
Development chamber saturation time (20 min)	600	596.69 ± 2.34	0.39
Development chamber saturation time (40 min)	600	588.71 ± 5.99	1.02
Solvent front position (135 mm)	600	586.59 ± 6.48	1.10
Solvent front position (145 mm)	600	586.65 ± 4.44	0.76

<sup>a</sup>Values represented as mean ± SD ( $n=3$ ).



### *Conophylline quantification in the ARFs*

To date, there are no reports on identification and quantification of conophylline in *T. divaricata* from Indian origin. However, conophylline was quantified using HPLC in *T. divaricata* leaves from Japanese origin, wherein the extractive value of conophylline was found to be 0.35 mg (per 1 g of crude extract) when subjected to extraction with 0.1 M citric acid, dissolved in 20% aqueous ethanol [28].

In the present study, conophylline was quantified in 12 ARF samples using the validated HPTLC method to understand the role of seasonal variations and extraction techniques on the extractive value of conophylline. As represented in Fig. 5.14, the biosynthesis of conophylline was highest in August (11.27-35.57 mg/g), followed by November (7.29-18.02 mg/g) and February (4.14-12.65 mg/g). Conophylline was found very low during May, with the content ranging from 2.14 - 6.73 mg/g of ARF. Conophylline, a bis-indole alkaloid is produced by the dimerization of its mono-indole alkaloid precursor, taberhanine [29]. Conophylline, a bis-indole alkaloid is produced by the dimerization of its mono-indole alkaloid precursor, taberhanine [29]. Similar studies were reported earlier, wherein the dimerization of alkaloids majorly occurred during a particular season. For example, the dimeric carbazole alkaloids of *Murraya euchrestifolia* (Rutaceae) viz., bis-7-hydroxygirinimbine-A and bis-7-hydroxygirinimbine-B, were found only during winter [30]. Similarly, the biosynthesis of dimeric alkaloids, anhydrovinblastine and vinblastine occurred during the flowering season of *Catharanthus roseus* (Apocynaceae), a closely related plant to *T. divaricata* [31].

Further, the extractive value of conophylline was significantly higher with UE ( $p < 0.05$ ) irrespective of the seasons (Fig. 5.14). The highest extractive value of conophylline was identified in August sample, subjected to UE (35.57 mg/g of ARF). Ultrasonic extraction acts directly in the cell matrix, in contrast to the conventional techniques wherein the extraction mechanism majorly involves diffusion of the chemical components into the solvent through cell wall. The energy produced during an ultrasound initially generates cavitation bubbles, which implode resulting in micro-jets. These micro-jets are powerful enough to provoke fissions in cell walls, leading to fragmentation and erosion of the plant matrix, thus aiding in solvent penetration. Further, the micro-jets create turbulences in the cell matrix, enhancing the solubility of the chemical components [32]. The present study was in accordance to the previous literature, wherein ultrasonic extraction was proved to be advantageous in obtaining higher extractive yield (about 2-3 fold) of conophylline compared with the conventional methods.

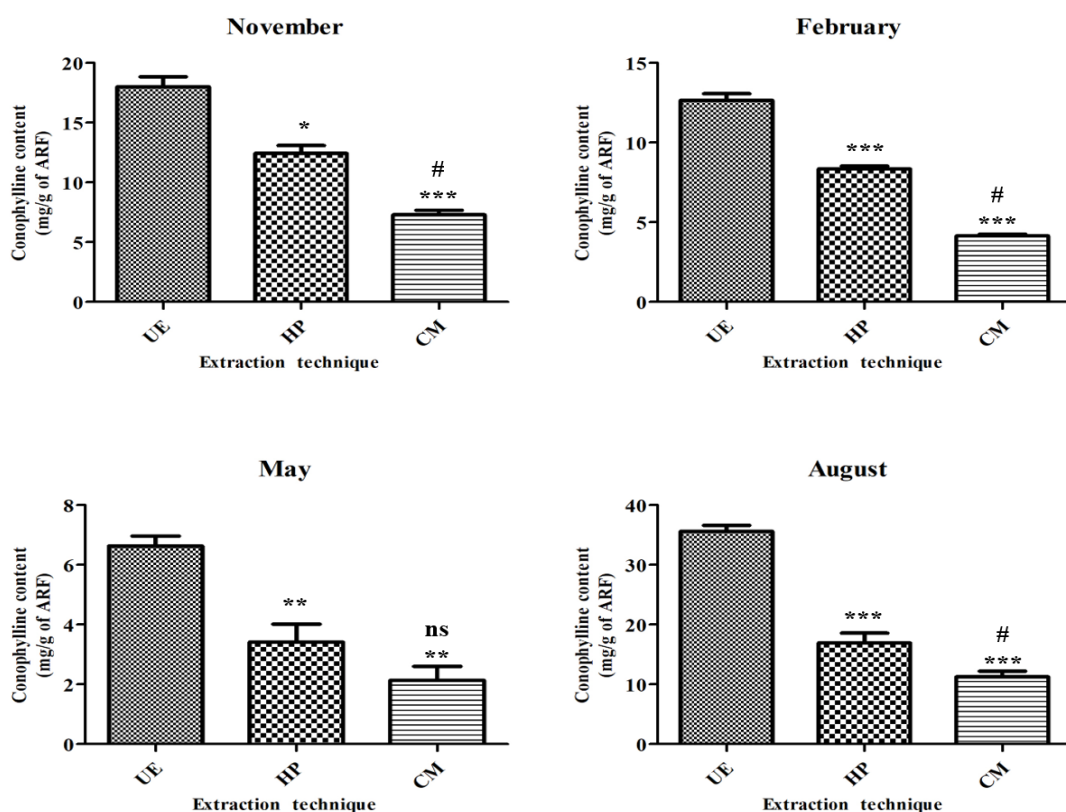


**Fig. 5.14.** Representation of extractive yields of conophylline (mg/g) in different ARF samples. All the values were represented as mean  $\pm$  SEM (n=3). **November** - \*  $p < 0.05$  Vs. UE, \*\*\*  $p < 0.001$  Vs. UE, #  $p < 0.01$  Vs. HP; **February** - \*\*\*  $p < 0.001$  Vs. UE, #  $p < 0.001$  Vs. HP; **May** - \*\*  $p < 0.01$  Vs. UE, ns – not significant Vs. HP; **August** - \*\*\*  $p < 0.001$  Vs. UE, #  $p < 0.05$  Vs. HP.

#### PL inhibition assay

The PL inhibitory activity of the 12 ARF samples are summarized in Fig. 5.15. The UE subjected samples exhibited potential PL inhibitory activity ( $IC_{50} < 20 \mu\text{g/mL}$ ), with an exception for May-UE, which exhibited a moderate PL inhibitory activity of  $31.19 \mu\text{g/mL}$ . Further, all the HP subjected samples exhibited a moderate PL inhibitory activity ranging from  $21.48 - 35.98 \mu\text{g/mL}$ . However, CM subjected samples exhibited poor activity ( $> 50 \mu\text{g/mL}$ ). The PL inhibitory activities of the ARF samples, obtained with similar extraction technique, did not exhibit significant variation, with an exception for the May-UE sample. However, a significant variation in PL inhibitory activity was identified among different extraction techniques, highlighting the fact that the extraction of bioactive compounds was highest with UE.

The fact can be further confirmed wherein the PL inhibitory activity of the ARF samples exhibited significant correlation to their respective conophylline content ( $p < 0.05$ , Pearson's  $r = -0.7152$ ,  $r^2 = 0.5115$ ; calculated using Pearson Correlation Analysis). Aug-UE sample (containing the highest extractive value of conophylline of 35.57 mg/g) exhibited a potent PL inhibition of 7.86  $\mu\text{g/mL}$ , while May-CM, with lowest extractive value of conophylline (2.14 mg/g) exhibited poor PL inhibition ( $\text{IC}_{50} = 61.08 \mu\text{g/mL}$ ).

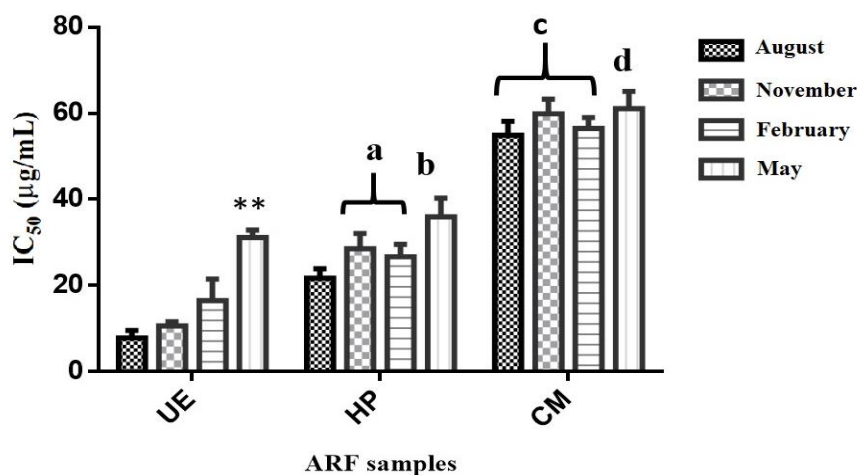


**Fig. 5.15.** Representation of PL inhibitory activity of different ARF samples. All the values represented as mean  $\pm$  SEM ( $n=3$ ). \*\*  $p < 0.01$  Vs. UE of August and November; <sup>a</sup>  $p < 0.05$  Vs. UE of August and November; <sup>b</sup>  $p < 0.05$  Vs. UE of August, November and February; <sup>c</sup>  $p < 0.001$  Vs. UE and HP of August, November and February; <sup>d</sup>  $p < 0.001$  Vs. May-UE and May-HP.

To summarize, the present chapter focussed on the identification of NP lead that would exhibit potent PL inhibition. The methanol extract from the leaves of *T. divaricata* was subjected to bioassay guided fractionation, owing to its potential PL inhibition. Further studies that involved fractionation and column chromatography resulted in the isolation and identification of conophylline as potent NP lead, that exhibited an  $\text{IC}_{50}$  value of 3.31  $\mu\text{M}$  with a competitive reversible inhibition comparable to the standard drug, orlistat ( $\text{IC}_{50} = 0.99 \mu\text{M}$ ). Molecular modelling studies and HPTLC quantification data further supported the PL inhibitory potential of conophylline, wherein it exhibited a stable binding conformation with a MolDock score of -143.382 kcal/mol, while its quantification data exhibited a significant correlation with PL inhibitory profiles of the 12 ARF samples.

### References

- [1] H. Kumari, R. Pushpan, K. Nishteswar, Medohara and Lekhaniya dravyas (anti-obesity and hypolipidemic drugs) in *Ayurvedic* classics: A critical review, *Ayu*. 34 (2013) 11–16.
- [2] C. V Chandrasekaran, M.A. Vijayalakshmi, K. Prakash, V.S. Bansal, J. Meenakshi, A. Amit, Review article: Herbal approach for obesity management, *Am. J. Plant Sci*. 3 (2012) 1003–1014.
- [3] W. Pratchayasakul, A. Pongchaidecha, N. Chattipakorn, S. Chattipakorn, Ethnobotany & ethnopharmacology of *Tabernaemontana divaricata*, *Indian J. Med. Res.* 127 (2008) 317–335.
- [4] D. Tarak, N.D. Namsa, S. Tangjang, S.C. Arya, B. Rajbonshi, P.K. Samal, M. Mandal, An inventory of the ethnobotanicals used as anti-diabetic by a rural community of Dhemaji district of Assam, Northeast India, *J. Ethnopharmacol.* 138 (2011) 345–350.
- [5] S.K. Kanthlal, V. Suresh, G. Arunachalam, F.P. Royal, S. Kameshwaran, Anti-obesity and hypolipidemic activity of methanol extract of *Tabernaemontana divaricata* on atherogenic diet induced obesity in rats, *Int. Res. J. Pharm.* 3 (2012) 157–161.
- [6] S. Atsumi, A. Nagasawa, T. Koyano, T. Kowithayakornd, K. Umezawa, Suppression of TGF- $\beta$  signaling by conophylline via upregulation of c-Jun expression, *Cell. Mol. Life Sci.* 60 (2003) 2516–2525.
- [7] T. Ogata, L. Li, S. Yamada, Y. Yamamoto, Y. Tanaka, I. Takei, K. Umezawa, I. Kojima, Promotion of  $\beta$ -cell differentiation by conophylline in fetal and neonatal rat pancreas, *Diabetes.* 53 (2004) 2596–2602.
- [8] J. Gohda, J.I. Inoue, K. Umezawa, Down-regulation of TNF- $\alpha$  receptors by conophylline in human T-cell leukemia cells, *Int. J. Oncol.* 23 (2003) 1373–1379.
- [9] T. Irie, K. Kubushiro, K. Suzuki, K. Tsukazaki, K. Umezawa, S. Nozawa, Inhibition of attachment and chemotactic invasion of uterine endometrial cancer cells by a new vinca alkaloid, conophylline, *Anticancer Res.* 19 (1999) 3061–3066.
- [10] H. Takatsuna, K. Umezawa, Screening of bioactive metabolites for pancreatic regeneration chemotherapy, *Biomed. Pharmacother.* 58 (2004) 610–613.
- [11] I. Kojima, K. Umezawa, Conophylline: A novel differentiation inducer for pancreatic  $\beta$  cells, *Int. J. Biochem. Cell Biol.* 38 (2006) 923–930.
- [12] A. Quevauviller, O. Foussard-Blanpin, D. Coignard, An alkaloid of *Phyllanthus discoides* (Euphorbiaceae) phyllalbine, a central and peripheral sympathomimetic,

- Therapie. 20 (1965) 1033–1041.
- [13] T.A. Van Beek, R. Verpoorte, A.B. Svendsen, A.J.M. Leeuwenberg, N.G. Bisset, *Tabernaemontana* L.(Apocynaceae): A review of its taxonomy, phytochemistry, ethnobotany and pharmacology, *J. Ethnopharmacol.* 10 (1984) 1–156.
- [14] G. Zetler, Some pharmacological properties of 12 natural and 11 partially synthetically derived indole alkaloids from tropical Apocyanaceae of the sub-tribe *Tabernaemontaninae*, *Arzneimittelforschung.* 14 (1964) 1277–1286.
- [15] G. Zetler, E. Lenschow, W. Prenger-Berninghoff, Action of 11 indole alkaloids on the guinea pig heart *in vivo* and *in vitro*, compared with those of 2 synthetic azepinoindoles, quinidine and quindonium, *Naunyn. Schmiedeberg's. Arch. Exp. Pathol. Pharmacol.* 260 (1968) 26–49.
- [16] M.J. Fyfe, S. Loftfield, I.D. Goldman, A reduction in energy-dependent amino acid transport by microtubular inhibitors in ehrlich ascites tumor cells, *J. Cell. Physiol.* 86 (1975) 201–211.
- [17] A.M.E. Raymond-Hamet, Is the true white ginseng of Korea endowed with the specific sympathicosthenic activity of most excitant drugs, *CR Hebd Seances Acad Sci.* 255 (1962) 3269–3271.
- [18] E. Okuyama, L. H. Gao, M. Yamazaki, Analgesic components from Bornean medicinal plants, *Tabernaemontana pauciflora* Blume and *Tabernaemontana pandacaqui* Poir, *Chem. Pharm. Bull.* 40 (1992) 2075–2079.
- [19] M.T. Andrade, J.A. Lima, A.C. Pinto, C.M. Rezende, M.P. Carvalho, R.A. Epifanio, Indole alkaloids from *Tabernaemontana australis* (Müell. Arg) Miers that inhibit acetylcholinesterase enzyme, *Bioorg. Med. Chem.* 13 (2005) 4092–4095.
- [20] R.D. Singh, Gopichand, R.L. Meena, B. Sharma, B. Singh, V.K. Kaul, P.S. Ahuja, Seasonal variation of bioactive components in *Valeriana jatamansi* from Himachal Pradesh, India, *Ind. Crops Prod.* 32 (2010) 292–296.
- [21] N. Manika, S. Singh, R.K. Verma, G.D. Bagchi, Extraction efficacy, stability assessment and seasonal variation of bioactive ‘gymnemagenin’ in *Gymnema sylvestre*, *Ind. Crops Prod.* 44 (2013) 572–576.
- [22] T.S. Kam, K.Y. Loh, C. Wei, Conophylline and conophyllidine: New dimeric alkaloids from *Tabernaemontana divaricata*, *J. Nat. Prod.* 56 (1993) 1865–1871.
- [23] H. Lineweaver, D. Burk, The determination of enzyme dissociation constants, *J. Am. Chem. Soc.* 56 (1934) 658–666.
- [24] P.K. Robinson, *Enzymes: Principles and biotechnological applications*, Essays

- Biochem. 59 (2015) 1–41.
- [25] H. van Tilbeurgh, M.P. Egloff, C. Martinez, N. Rugani, R. Verger, C. Cambillau, Interfacial activation of the lipase-procolipase complex by mixed micelles revealed by X-ray crystallography, *Nature*. 362 (1993) 814–820.
- [26] V. Point, K.V.P.P. Kumar, S. Marc, V. Delorme, G. Parsiegla, S. Amara, F. Carrière, G. Buono, F. Fotiadu, S. Canaan, Analysis of the discriminative inhibition of mammalian digestive lipases by 3-phenyl substituted 1, 3, 4-oxadiazol-2-(3*H*)-ones, *Eur. J. Med. Chem.* 58 (2012) 452–463.
- [27] ICH Guideline Q2 (R1), November 2005. Validation of analytical procedures: Text and methodology.
- [28] K. Umezawa, M. Fujii, Aqueous solution of conophylline and/or conophyllidine. US 8178135 B2. filed March 5, 2007, issued May 15, 2012.
- [29] T.S. Kam, H.S. Pang, T.M. Lim, Biologically active indole and bisindole alkaloids from *Tabernaemontana divaricata*, *Org. Biomol. Chem.* 1 (2003) 1292–1297.
- [30] T.S. Wu, M.L. Wang, P.L. Wu, Seasonal variations of carbazole alkaloids in *Murraya euchrestifolia*, *Phytochemistry*. 43 (1996) 785–789.
- [31] Q. Pan, M.Z. Saiman, N.R. Mustafa, R. Verpoorte, K. Tang, A simple and rapid HPLC-DAD method for simultaneously monitoring the accumulation of alkaloids and precursors in different parts and different developmental stages of *Catharanthus roseus* plants, *J. Chromatogr. B.* 1014 (2016) 10–16.
- [32] S. Chemat, A. Aissa, A. Boumechhour, O. Arous, H. Ait-Amar, Extraction mechanism of ultrasound assisted extraction and its effect on higher yielding and purity of artemisinin crystals from *Artemisia annua* L. leaves, *Ultrason. Sonochem.* 34 (2017) 310–316.

## 6 | Synthesis - Series I - Carbazolyl Oxoacetamide Analogues

## 6.1 | Rationale

Fractionation and column chromatography of the most active dichloromethane fraction of methanol extract from *T. divaricata* leaves resulted in the isolation and identification of conophylline as a potential NP lead for PL inhibition. Nevertheless, an *in-silico* analysis of conophylline in the active site of Human PL highlighted, a high degree of unfavourable steric interactions (Fig. 6.1). Further, conophylline lacked a reactive ester group, a structural feature that would interact with the Ser152 of the active site. As represented in Fig. 6.2, conophylline possessed a simple methyl ester in contrast to orlistat that possessed a highly reactive  $\beta$ -lactone. This fact can be further confirmed with the previous literature on the PL inhibitory activity of carbazole alkaloids *viz.*, mahanimbine (**76**) and koenimbine (**77**) [1], wherein these molecules possessed moderate to low PL inhibitory potential and did not contain an ester or ester mimicking group essential for potential PL inhibition (Fig. 6.1).

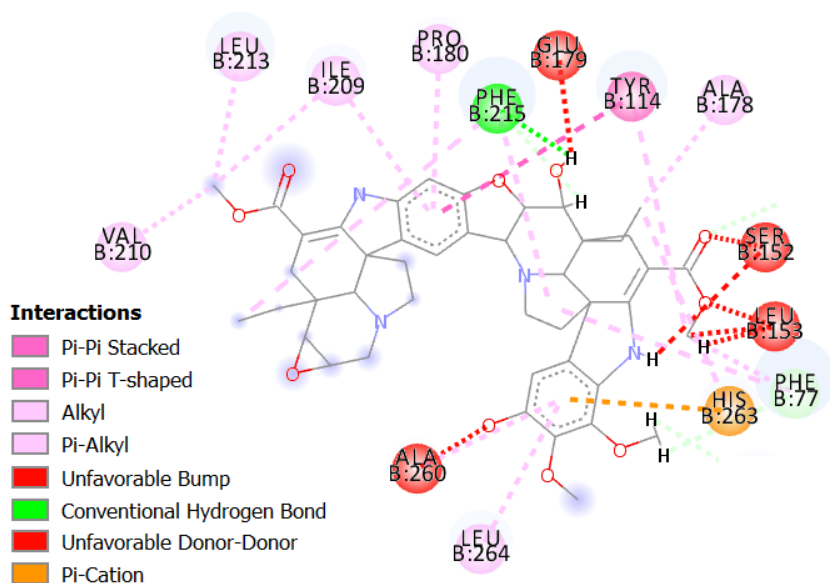


**Fig. 6.1.** 2D pose of conophylline highlighting the unfavourable steric interactions (in red)

Literature review highlighted that scaffolds including fluorinated ketones,  $\alpha$ -keto esters,  $\alpha$ -ketoamides and 1,2-diketones have been found to possess reactive carbonyl groups that act as an electrophile for Ser152 [2,3]. Further, the role of  $\alpha$ -ketoamides as an ester mimicking group has been previously described, where the replacement of ester with the ketoamide in the triacylglycerol analogues led to potential PL inhibition [4–6].

Based on the above literature, we hypothesized the design of conophylline inspired carbazolyl oxoacetamide analogues to possess potential PL inhibitory activity. These

## Chapter 6

analogues can be considered as pharmacophoric hybrid of the carbazole scaffold (present in conophylline) and  $\alpha$ -ketoamide functionality, present in a single molecule (Fig. 6.2). These analogues were designed with an aim to remove the high degree of unfavourable steric interactions found in conophylline as well as to include the reactive carbonyl group. A series of 24 carbazolyl oxoacetamide analogues were synthesised and evaluated for their PL inhibitory activity.

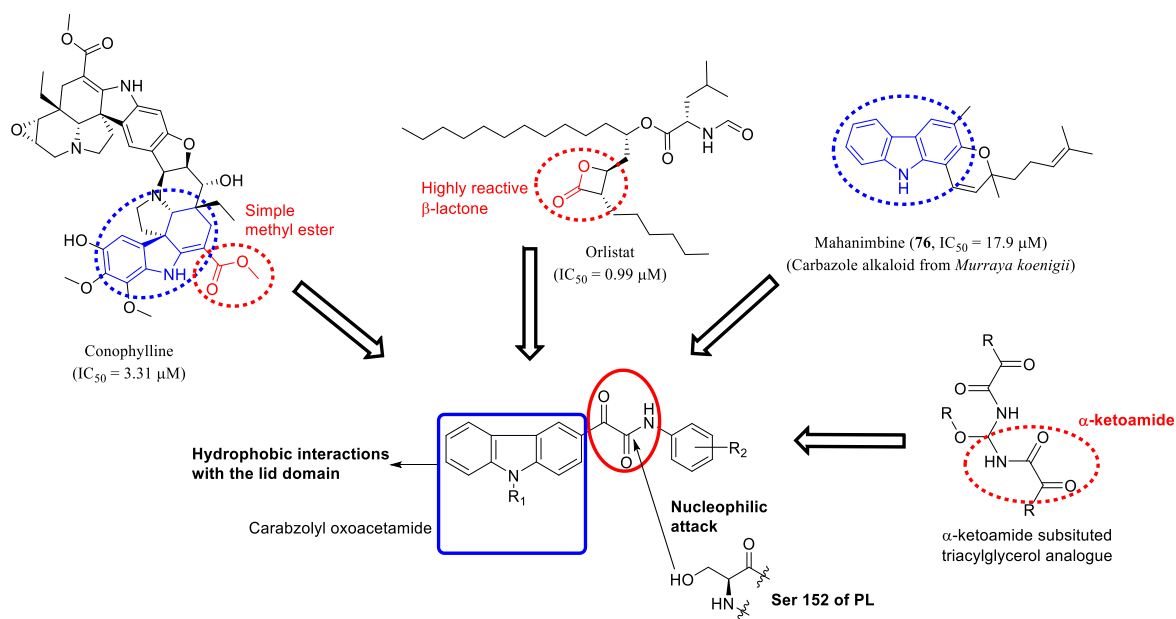


**Fig. 6.2.** Rationale for selecting carbazolyl oxoacetamide analogues as PL inhibitors

### 6.2 | Synthesis and Characterization

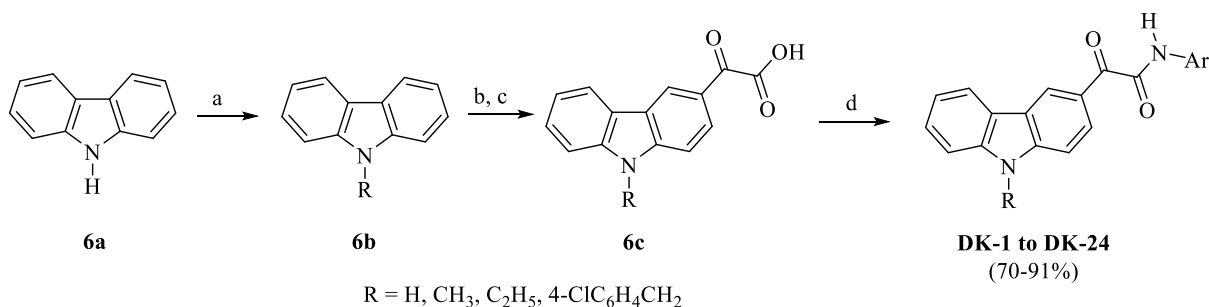
The synthesis of all the analogues were carried out as per the procedure detailed in Scheme 6.1 in collaboration with Prof. Dalip Kumar, Department of Chemistry, BITS Pilani (Pilani Campus) [7]. Initially, carbazole **6a** was allowed to react with various alkyl or aryl halides to obtain the respective N-substituted carbazole analogues (**6b**). The unsubstituted and the substituted carbazoles (**6a** and **6b**) were then allowed to react with ethyl chlorooxacetate in the presence of anhydrous  $\text{AlCl}_3$ , followed by ester hydrolysis using  $\text{LiOH}$  to afford the respective carbazolyl oxoacetic acid analogue **6c** in good yield (Scheme 6.1).

Further, the reaction of the oxoacetic acid analogues **6c** with various aryl/heteroarylamines in the presence of HATU were carried out in a CEM focused microwave at  $70^\circ\text{C}$  for 45 min. Upon completion of the reaction, as confirmed by TLC, reaction contents were poured into ice-cold water (30 mL) and stirred for 20 min at  $25^\circ\text{C}$ . The suspension so obtained was filtered, dried and purified through column chromatography



on silica gel using ethyl acetate:hexane (3:7) as eluent to afford **DK-1** to **DK-24** as pure yellow coloured solids in 70-91% yields (Scheme 6.1).

Structures of the synthesized carbazolyl oxoacetamides were well characterized using NMR ( $^1\text{H}$  and  $^{13}\text{C}$ ), IR and HRMS. In the  $^1\text{H}$  NMR spectra, the amide proton resonated between 9 and 10 ppm (with  $\text{CDCl}_3$ ) and 11-12 ppm (with  $\text{DMSO}-d_6$ ). For the N-unsubstituted analogues **DK-12** to **DK-17**, the -NH proton of the carbazole resonated around 9 ppm or 11-12 ppm (**DK-17**). For the 4-chlorobenzyl substituted analogues (**DK-1** to **DK-11**), the methylene protons resonated between 5-6 ppm. Further, for the N-ethyl (- $\text{CH}_2\text{-CH}_3$ ) substituted analogues **DK-20** to **DK-24**, the methyl protons appeared as a triplet between 1-2 ppm, while the - $\text{CH}_2$  protons appeared as a quartet between 4-5 ppm. Finally, for the N-methyl substituted analogues **DK-18** and **DK-19**, the N-methyl protons appeared as a singlet between 3-4 ppm. In  $^{13}\text{C}$  NMR spectra, carbons of carbonyl and amide functionalities were resonated at  $\sim 180$  (CO) and  $\sim 160$  ppm (NHCO). In the IR spectra, the amide -NH stretch was observed at  $3100\text{-}3500\text{ cm}^{-1}$ , while the characteristic peaks at  $1640\text{-}1690$  and  $1670\text{-}1820\text{ cm}^{-1}$  were assigned to the made carbonyl and the  $\alpha$ -keto functionalities, respectively.



**Scheme 6.1.** Reagents and conditions: (a) KOH,  $\text{CH}_3\text{I}/\text{C}_2\text{H}_5\text{I}/4\text{-ClC}_6\text{H}_4\text{CH}_2\text{Cl}$ , DMF, RT, 13 h; (b)  $\text{Cl}(\text{CO})_2\text{OEt}$ ,  $\text{AlCl}_3$ , DCM,  $0^\circ\text{C}$  to RT, 3 h; (c) LiOH, THF:H<sub>2</sub>O (1:1), RT, 2 h; (d)  $\text{ArNH}_2$ , HATU, DIPEA, DMF,  $70^\circ\text{C}$ , 45 min, MW (100 watt).

**2-(9-(4-Chlorobenzyl)-9H-carbazol-3-yl)-2-oxo-N-phenylacetamide (DK-1)**

Yield 70%; Yellow solid; m.p:  $191\text{-}193^\circ\text{C}$ ;  $^1\text{H}$  NMR (400 MHz,  $\text{CDCl}_3$ )  $\delta$  9.47 (d,  $J = 1.3$  Hz, 1H), 9.15 (s, 1H), 8.58 (dd,  $J = 8.8, 1.7$  Hz, 1H), 8.25 (dd,  $J = 7.6, 1.1$  Hz, 1H), 7.78 (dd,  $J = 8.6, 1.0$  Hz, 2H), 7.54-7.50 (m, 1H), 7.45 (dd,  $J = 8.3, 7.5$  Hz, 3H), 7.41-7.36 (m, 3H), 7.26 (t,  $J = 2.6$  Hz, 2H), 7.08 (d,  $J = 8.6$  Hz, 2H), 5.55 (s, 2H);  $^{13}\text{C}$  NMR (100 MHz,  $\text{CDCl}_3$ )  $\delta$  185.9, 160.0, 144.2, 141.2, 136.9, 134.6, 133.7, 129.8, 129.3, 129.2, 127.7, 127.0, 126.2, 125.2, 125.0, 123.6, 123.1, 121.1, 121.1, 120.0, 109.5, 108.8, 46.24; IR (KBr,  $\nu$ ,  $\text{cm}^{-1}$ ): 3335,

3090, 3052, 2916, 1682, 1653, 1589, 1520, 1435, 1307, 1250, 1134, 1011, 825, 795; HRMS (ESI<sup>+</sup>) Calculated for C<sub>27</sub>H<sub>20</sub>ClN<sub>2</sub>O<sub>2</sub> [M + H]<sup>+</sup>, 439.1213; Found 439.1208.

**2-(9-(4-Chlorobenzyl)-9H-carbazol-3-yl)-2-oxo-N-(p-tolyl)acetamide (DK-2)**

Yield 72%; Yellow solid; m.p: 172-173°C; <sup>1</sup>H NMR (400 MHz, CDCl<sub>3</sub>) δ 9.48 (d, *J* = 1.6 Hz, 1H), 9.09 (s, 1H), 8.58 (dd, *J* = 8.8, 1.7 Hz, 1H), 8.27-8.23 (m, 1H), 7.67-7.64 (m, 2H), 7.53-7.49 (m, 1H), 7.44-7.35 (m, 3H), 7.26 (t, *J* = 2.2 Hz, 3H), 7.24 (s, 1H), 7.09 (d, *J* = 8.6 Hz, 2H), 5.55 (s, 2H), 2.39 (s, 3H); <sup>13</sup>C NMR (100 MHz, CDCl<sub>3</sub>) δ 186.0, 159.9, 144.2, 141.1, 134.9, 134.6, 134.3, 133.7, 129.9, 129.7, 129.2, 127.7, 126.9, 126.1, 125.1, 123.6, 123.1, 121.1, 121.0, 119.9, 109.5, 108.7, 46.2, 21.0; IR (KBr, ν, cm<sup>-1</sup>): 3325, 3094, 3055, 2916, 1682, 1651, 1620, 1582, 1520, 1443, 1327, 1265, 1149; HRMS (ESI<sup>+</sup>) Calculated for C<sub>28</sub>H<sub>22</sub>ClN<sub>2</sub>O<sub>2</sub> [M + H]<sup>+</sup>, 453.1369; Found 453.1365.

**2-(9-(4-Chlorobenzyl)-9H-carbazol-3-yl)-2-oxo-N-(3-methoxyphenyl)acetamide (DK-3)**

Yield 73%; Yellow solid; m.p: 106-107°C; <sup>1</sup>H NMR (400 MHz, CDCl<sub>3</sub>) δ 9.43 (s, 1H), 9.11 (s, 1H), 8.57-8.54 (m, 1H), 8.23 (d, *J* = 7.7 Hz, 1H), 7.52-7.46 (m, 2H), 7.40-7.33 (m, 3H), 7.31-7.28 (m, 2H), 7.24-7.19 (m, 2H), 7.06 (d, *J* = 8.3 Hz, 2H), 6.77 (dd, *J* = 7.8, 1.6 Hz, 1H), 5.52 (s, 2H), 3.87 (s, 3H); <sup>13</sup>C NMR (100 MHz, CDCl<sub>3</sub>) δ 185.8, 160.3, 159.9, 144.2, 141.1, 138.1, 134.6, 133.7, 129.9, 129.7, 129.2, 127.7, 126.9, 126.1, 124.9, 123.5, 123.1, 121.1, 121.0, 112.2, 111.1, 109.5, 108.7, 105.5, 55.4, 46.2; IR (KBr, ν, cm<sup>-1</sup>): 3333, 3055, 2932, 2862, 1693, 1659, 1589, 1528, 1381, 1335, 1265, 1203, 1142, 1088, 1041, 849, 795, 725, 687, 679; HRMS (ESI<sup>+</sup>) Calculated for C<sub>28</sub>H<sub>22</sub>ClN<sub>2</sub>O<sub>3</sub> [M + H]<sup>+</sup>, 469.1319; Found 469.1313.

**2-(9-(4-Chlorobenzyl)-9H-carbazol-3-yl)-2-oxo-N-(4-methoxyphenyl)acetamide (DK-4)**

Yield 72%; Yellow solid; m.p: 168-170°C; <sup>1</sup>H NMR (400 MHz, CDCl<sub>3</sub>) δ 9.45 (d, *J* = 1.5 Hz, 1H), 9.04 (s, 1H), 8.56 (dd, *J* = 8.8, 1.7 Hz, 1H), 8.22 (d, *J* = 7.7 Hz, 1H), 7.69-7.65 (m, 2H), 7.51-7.47 (m, 1H), 7.42-7.32 (m, 4H), 7.25-7.23 (m, 1H), 7.06 (d, *J* = 8.5 Hz, 2H), 6.97-6.94 (m, 2H), 5.52 (s, 2H), 3.84 (s, 3H); <sup>13</sup>C NMR (100 MHz, CDCl<sub>3</sub>) δ 186.1, 159.8, 157.0, 144.2, 141.1, 134.6, 133.7, 130.1, 129.7, 129.2, 127.7, 126.9, 126.1, 125.1, 123.6, 123.1, 121.6, 121.1, 121.0, 114.4, 109.5, 108.7, 55.5, 46.2; IR (KBr, ν, cm<sup>-1</sup>): 3348, 3055, 2924, 1682, 1643, 1620, 1582, 1528, 1443, 1327, 1250, 1149; HRMS (ESI<sup>+</sup>) Calculated for C<sub>28</sub>H<sub>22</sub>ClN<sub>2</sub>O<sub>3</sub> [M + H]<sup>+</sup>, 469.1319; Found 469.1310.

**2-(9-(4-Chlorobenzyl)-9H-carbazol-3-yl)-2-oxo-N-(3,4-dimethoxyphenyl)acetamide (DK-5)**

Yield 70%; Yellow solid; m.p: 136-137°C; <sup>1</sup>H NMR (400 MHz, CDCl<sub>3</sub>) δ 9.43 (s, 1H), 9.08 (s, 1H), 8.56 (d, *J* = 8.7 Hz, 1H), 8.23 (d, *J* = 7.7 Hz, 1H), 7.55 (d, *J* = 2.0 Hz, 1H), 7.49 (t,

$J = 7.7$  Hz, 1H), 7.40-7.33 (m, 3H), 7.24 (s, 2H), 7.16 (dd,  $J = 8.5, 2.1$  Hz, 1H), 7.06 (d,  $J = 8.2$  Hz, 2H), 6.89 (d,  $J = 8.6$  Hz, 1H), 5.51 (s, 2H), 3.96 (s, 3H), 3.90 (s, 3H);  $^{13}\text{C}$  NMR (100 MHz,  $\text{CDCl}_3$ )  $\delta$  186.0, 159.7, 149.2, 146.5, 144.2, 141.1, 134.6, 133.7, 130.6, 129.7, 129.2, 127.7, 126.9, 126.1, 125.1, 123.6, 123.1, 121.1, 121.0, 112.1, 111.4, 109.5, 108.7, 104.5, 56.1, 56.0, 46.2; IR (KBr,  $\nu$ ,  $\text{cm}^{-1}$ ): 3317, 3055, 2924, 2847, 1690, 1651, 1589, 1520, 1458, 1412, 1381, 1335, 1242, 1203, 1134, 1026, 849, 795, 748, 663, 602, 540; HRMS (ESI<sup>+</sup>) Calculated for  $\text{C}_{29}\text{H}_{24}\text{ClN}_2\text{O}_4$   $[\text{M} + \text{H}]^+$ , 499.1424; Found 499.1424.

**2-(9-(4-Chlorobenzyl)-9H-carbazol-3-yl)-2-oxo-N-(3,4,5-trimethoxyphenyl)acetamide (DK-6)**

Yield 71%; Yellow solid; m.p: 183-184°C;  $^1\text{H}$  NMR (400 MHz,  $\text{CDCl}_3$ )  $\delta$  9.43 (s, 1H), 9.15 (s, 1H), 8.57 (dd,  $J = 8.8, 1.6$  Hz, 1H), 8.25 (d,  $J = 7.6$  Hz, 1H), 7.55-7.49 (m, 1H), 7.40 (t,  $J = 8.6$  Hz, 3H), 7.29-7.25 (m, 3H), 7.08 (d,  $J = 8.6$  Hz, 3H), 5.53 (s, 2H), 3.94 (s, 6H), 3.89 (s, 3H);  $^{13}\text{C}$  NMR (100 MHz,  $\text{CDCl}_3$ )  $\delta$  185.8, 159.9, 153.5, 144.2, 141.1, 135.3, 134.6, 133.7, 133.0, 129.7, 129.1, 127.7, 127.0, 126.0, 124.9, 123.5, 123.1, 121.1, 121.0, 109.5, 108.8, 97.5, 61.0, 56.2, 46.2; IR (KBr,  $\nu$ ,  $\text{cm}^{-1}$ ): 3356, 2932, 1690, 1651, 1597, 1528, 1504, 1450, 1412, 1373, 1335, 1296, 1250, 1126, 1011, 802; HRMS (ESI<sup>+</sup>) Calculated for  $\text{C}_{30}\text{H}_{26}\text{ClN}_2\text{O}_5$   $[\text{M} + \text{H}]^+$ , 529.1530; Found 529.1531.

**2-(9-(4-Chlorobenzyl)-9H-carbazol-3-yl)-2-oxo-N-(4-fluorophenyl)acetamide (DK-7)**

Yield 75%; Yellow solid; m.p: 202-203°C;  $^1\text{H}$  NMR (400 MHz,  $\text{CDCl}_3$ )  $\delta$  9.43 (d, 1.5 Hz, 1H), 9.13 (s, 1H), 8.55 (dd,  $J = 8.8, 1.6$  Hz, 1H), 8.22 (d,  $J = 7.7$  Hz, 1H), 7.74-7.71 (m, 2H), 7.53-7.46 (m, 1H), 7.40-7.33 (m, 3H), 7.24 (s, 2H), 7.14-7.03 (m, 4H), 5.51 (s, 2H);  $^{13}\text{C}$  NMR (100 MHz,  $\text{CDCl}_3$ )  $\delta$  185.7, 159.9, 144.2, 141.2, 134.6, 133.7, 133.0, 129.7, 129.2, 127.7, 126.2, 124.9, 123.6, 123.1, 121.8, 121.1, 116.1, 115.9, 113.4, 109.5, 108.8, 46.2; IR (KBr,  $\nu$ ,  $\text{cm}^{-1}$ ): 3310, 3055, 2935, 1690, 1651, 1589, 1535, 1497, 1381, 1335, 1265, 1211, 1142, 833, 705; HRMS (ESI<sup>+</sup>) Calculated for  $\text{C}_{27}\text{H}_{19}\text{ClFN}_2\text{O}_2$   $[\text{M} + \text{H}]^+$ , 457.1031; Found 457.1020.

**2-(9-(4-Chlorobenzyl)-9H-carbazol-3-yl)-2-oxo-N-(pyridin-4-yl)acetamide (DK-8)**

Yield 91%; Yellow solid; m.p: 116-118°C;  $^1\text{H}$  NMR (400 MHz,  $\text{CDCl}_3$ )  $\delta$  9.40 (s, 1H), 9.32 (s, 1H), 8.61 (d,  $J = 5.0$  Hz, 2H), 8.53 (dd,  $J = 8.8, 1.4$  Hz, 1H), 8.22 (d,  $J = 7.5$  Hz, 1H), 7.69 (d,  $J = 6.1$  Hz, 2H), 7.50 (t,  $J = 7.4$  Hz, 1H), 7.31-7.35 (m, 3H), 7.24 (t,  $J = 4.8$  Hz, 2H), 7.06 (d,  $J = 8.3$  Hz, 2H), 5.52 (s, 2H);  $^{13}\text{C}$  NMR (100 MHz,  $\text{CDCl}_3$ )  $\delta$  184.6, 160.5, 151.0, 144.4, 143.8, 141.2, 134.5, 133.8, 129.8, 129.2, 127.7, 127.2, 126.2, 124.5, 123.5, 123.3, 121.2, 121.1, 113.8, 109.6, 108.9, 46.3; IR (KBr,  $\nu$ ,  $\text{cm}^{-1}$ ): 3340, 2924, 1696, 1659, 1489,

1327, 1265, 1142, 1021, 803; HRMS (ESI<sup>+</sup>) Calculated for C<sub>26</sub>H<sub>19</sub>ClN<sub>3</sub>O<sub>2</sub> [M + H]<sup>+</sup>, 440.1166; Found 440.1171.

***2-(9-(4-Chlorobenzyl)-9H-carbazol-3-yl)-2-oxo-N-(4-(dimethylamino)phenyl)acetamide (DK-9)***

Yield 71%; Yellow solid; m.p: 211-213°C; <sup>1</sup>H NMR (400 MHz, CDCl<sub>3</sub>) δ 9.46 (d, *J* = 1.3 Hz, 1H), 8.98 (s, 1H), 8.56 (dd, *J* = 8.8, 1.7 Hz, 1H), 8.24-8.21 (m, 1H), 7.63-7.60 (m, 2H), 7.50-7.46 (m, 1H), 7.42-7.30 (m, 4H), 7.24 (s, 1H), 7.06 (d, *J* = 8.6 Hz, 2H), 6.79-6.76 (m, 2H), 5.52 (s, 2H), 2.97 (s, 6H); IR (KBr, ν, cm<sup>-1</sup>): 3333, 3047, 2924, 2854, 2800, 1674, 1643, 1582, 1520, 1443, 1350, 1265, 1136, 1011, 949, 895, 825, 795, 748, 694, 617; HRMS (ESI<sup>+</sup>) Calculated for C<sub>29</sub>H<sub>25</sub>ClN<sub>3</sub>O<sub>2</sub> [M + H]<sup>+</sup>, 482.1635; Found 482.1621.

***2-(9-(4-Chlorobenzyl)-9H-carbazol-3-yl)-2-oxo-N-(quinolin-6-yl)acetamide (DK-10)***

Yield 70%; Yellow solid; m.p: 129-131°C; <sup>1</sup>H NMR (400 MHz, CDCl<sub>3</sub>) δ 9.44 (d, *J* = 1.3 Hz, 2H), 8.89 (dd, *J* = 4.3, 1.6 Hz, 1H), 8.61-8.55 (m, 2H), 8.25-8.18 (m, 2H), 8.16 (d, *J* = 9.0 Hz, 1H), 7.79 (dd, *J* = 9.0, 2.4 Hz, 1H), 7.52-7.41 (m, 2H), 7.41-7.30 (m, 3H), 7.23 (t, *J* = 2.1 Hz, 2H), 7.05 (d, *J* = 8.5 Hz, 2H), 5.49 (s, 2H); <sup>13</sup>C NMR (100 MHz, CDCl<sub>3</sub>) δ 185.4, 160.3, 149.5, 145.4, 144.3, 141.1, 136.4, 134.9, 134.5, 133.7, 130.2, 130.1, 129.8, 129.2, 128.8, 127.7, 127.1, 126.2, 124.8, 123.5, 123.4, 123.2, 121.9, 121.1, 116.5, 109.5, 108.8, 46.2; IR (KBr, ν, cm<sup>-1</sup>): 3356, 2932, 1690, 1651, 1597, 1528, 1504, 1450, 1412, 1373, 1335, 1296, 1250, 1126, 1011, 802; HRMS (ESI<sup>+</sup>) Calculated for C<sub>30</sub>H<sub>21</sub>ClN<sub>3</sub>O<sub>2</sub> [M + H]<sup>+</sup>, 490.1322; Found 490.1327.

***2-(9-(4-Chlorobenzyl)-9H-carbazol-3-yl)-2-oxo-N-(5-methylthiazol-2-yl)acetamide (DK-11)***

Yield 74%; Yellow solid; m.p: 178-179°C; <sup>1</sup>H NMR (400 MHz, CDCl<sub>3</sub>) δ 10.63 (s, 1H), 9.48 (d, *J* = 1.3 Hz, 1H), 8.60 (dd, *J* = 8.8, 1.5 Hz, 1H), 8.25 (d, *J* = 8.2 Hz, 1H), 7.52 (t, *J* = 7.3 Hz, 1H), 7.46-7.32 (m, 4H), 7.26 (s, 1H), 7.08 (d, *J* = 8.3 Hz, 2H), 6.70 (s, 1H), 5.53 (s, 2H), 2.44 (s, 3H); <sup>13</sup>C NMR (100 MHz, CDCl<sub>3</sub>) δ 182.9, 159.3, 156.1, 148.4, 144.4, 141.2, 134.5, 133.8, 129.7, 129.2, 128.7, 127.7, 127.1, 126.2, 124.6, 123.5, 123.3, 121.2, 109.6, 109.2, 108.9, 46.3, 17.1; IR (KBr, ν, cm<sup>-1</sup>): 3317, 3055, 2932, 1690, 1651, 1589, 1528, 1489, 1257, 1142, 1011, 802; HRMS (ESI<sup>+</sup>) Calculated for C<sub>25</sub>H<sub>19</sub>ClN<sub>3</sub>O<sub>2</sub>S [M + H]<sup>+</sup>, 460.0886; Found 460.0888.

***2-(9H-Carbazol-3-yl)-2-oxo-N-phenylacetamide (DK-12)***

Yield 70%; Yellow solid; m.p: 221-222°C; <sup>1</sup>H NMR (400 MHz, CDCl<sub>3</sub>) δ 9.41 (s, 1H), 9.12 (s, 1H), 8.55 (dd, *J* = 8.7, 1.5 Hz, 1H), 8.43 (s, 1H), 8.18 (d, *J* = 7.7 Hz, 1H), 7.76 (d, *J* = 7.7 Hz, 2H), 7.53-7.46 (m, 3H), 7.43 (t, *J* = 7.9 Hz, 2H), 7.36-7.30 (m, 1H), 7.21 (t, *J* = 7.4 Hz,

1H);  $^{13}\text{C}$  NMR (100 MHz,  $\text{CDCl}_3$ )  $\delta$  187.4, 162.4, 143.9, 140.6, 137.5, 128.8, 128.3, 126.4, 125.1, 124.6, 124.0, 123.1, 122.8, 120.4, 120.2, 120.0, 111.4, 110.9; IR (KBr,  $\nu$ ,  $\text{cm}^{-1}$ ): 3348, 3055, 2932, 1674, 1651, 1589, 1528, 1443, 1335, 1296, 1265, 1257, 1165, 1134, 1011, 787, 748, 687, 602, 548; HRMS (ESI $^+$ ) Calculated for  $\text{C}_{20}\text{H}_{15}\text{N}_2\text{O}_2$   $[\text{M} + \text{H}]^+$ , 315.1133; Found 315.1129.

***2-(9H-Carbazol-3-yl)-2-oxo-N-(3-methoxyphenyl)acetamide (DK-13)***

Yield 72%; Yellow solid; m.p: 171-173°C;  $^1\text{H}$  NMR (400 MHz,  $\text{CDCl}_3$ )  $\delta$  9.40 (s, 1H), 9.10 (s, 1H), 8.55 (dd,  $J = 8.7, 1.4$  Hz, 1H), 8.43 (s, 1H), 8.18 (d,  $J = 7.8$  Hz, 1H), 7.49 (dd,  $J = 8.5, 3.8$  Hz, 3H), 7.35-7.29 (m, 2H), 7.22 (d,  $J = 8.0$  Hz, 1H), 6.77 (dd,  $J = 7.9, 1.8$  Hz, 1H), 6.38-6.21 (m, 1H), 3.87 (s, 3H); IR (KBr,  $\nu$ ,  $\text{cm}^{-1}$ ): 3379, 3317, 3070, 2962, 2831, 1690, 1651, 1597, 1535, 1497, 1450, 1335, 1242, 1203, 1149, 1034, 795, 687; HRMS (ESI $^+$ ) Calculated for  $\text{C}_{21}\text{H}_{17}\text{N}_2\text{O}_3$   $[\text{M} + \text{H}]^+$ , 345.1239; Found 345.1237.

***2-(9H-Carbazol-3-yl)-2-oxo-N-(4-methoxyphenyl)acetamide (DK-14)***

Yield 70%; Yellow solid; m.p: 199-201°C;  $^1\text{H}$  NMR (400 MHz,  $\text{CDCl}_3$ )  $\delta$  9.41 (s, 1H), 9.04 (s, 1H), 8.54 (dd,  $J = 8.7, 1.7$  Hz, 1H), 8.43 (s, 1H), 8.17 (d,  $J = 7.8$  Hz, 1H), 7.71-7.67 (m, 1H), 7.67-7.65 (m, 1H), 7.48 (dd,  $J = 5.8, 2.1$  Hz, 3H), 7.34-7.30 (m, 1H), 6.98-6.96 (m, 1H), 6.96-6.93 (m, 1H), 3.84 (s, 3H); IR (KBr,  $\nu$ ,  $\text{cm}^{-1}$ ): 3294, 3256, 3094, 2962, 2831, 1692, 1659, 1597, 1504, 1450, 1412, 1335, 1281, 1234, 1134, 1103, 1011, 802, 795, 679; HRMS (ESI $^+$ ) Calculated for  $\text{C}_{21}\text{H}_{17}\text{N}_2\text{O}_3$   $[\text{M} + \text{H}]^+$ , 345.1239; Found 345.1238.

***2-(9H-Carbazol-3-yl)-2-oxo-N-(3,4-dimethoxyphenyl)acetamide (DK-15)***

Yield 71%; Yellow solid; m.p: 202-203°C;  $^1\text{H}$  NMR (400 MHz,  $\text{CDCl}_3$ )  $\delta$  9.41 (s, 1H), 9.07 (s, 1H), 8.55 (dd,  $J = 8.7, 1.7$  Hz, 1H), 8.43 (s, 1H), 8.18 (d,  $J = 7.8$  Hz, 1H), 7.56 (d,  $J = 2.4$  Hz, 1H), 7.51-7.45 (m, 3H), 7.35-7.31 (m, 1H), 7.16 (dd,  $J = 8.6, 2.4$  Hz, 1H), 6.90 (d,  $J = 8.6$  Hz, 1H), 3.96 (s, 3H), 3.91 (s, 3H);  $^{13}\text{C}$  NMR (100 MHz,  $\text{CDCl}_3$ )  $\delta$  186.0, 159.7, 149.2, 146.5, 143.4, 139.9, 130.6, 129.6, 126.9, 126.1, 125.1, 123.6, 123.3, 120.9, 120.7, 112.1, 111.4, 111.1, 110.5, 104.4, 56.1, 56.0; IR (KBr,  $\nu$ ,  $\text{cm}^{-1}$ ): 3472, 3286, 3086, 2924, 2839, 1692, 1659, 1589, 1450, 1335, 1219, 1134, 1018, 849, 795, 733, 671, 617; HRMS (ESI $^+$ ) Calculated for  $\text{C}_{22}\text{H}_{19}\text{N}_2\text{O}_4$   $[\text{M} + \text{H}]^+$ , 375.1344; Found 375.1348.

***2-(9H-Carbazol-3-yl)-2-oxo-N-(3,4,5-trimethoxyphenyl)acetamide (DK-16)***

Yield 72%; Yellow solid; m.p: 207-208°C;  $^1\text{H}$  NMR (400 MHz,  $\text{CDCl}_3$ )  $\delta$  9.39 (s, 1H), 9.08 (s, 1H), 8.55 (dd,  $J = 8.7, 1.7$  Hz, 1H), 8.47 (s, 1H), 8.19 (d,  $J = 7.8$  Hz, 1H), 7.51-7.45 (m, 3H), 7.35-7.31 (m, 1H), 7.07 (s, 2H), 3.93 (s, 6H), 3.86 (s, 3H);  $^{13}\text{C}$  NMR (100 MHz,  $\text{CDCl}_3$ )  $\delta$  185.9, 160.0, 153.5, 143.5, 140.0, 135.3, 133.1, 129.5, 126.9, 126.1, 124.9, 123.6, 123.3,

120.9, 120.8, 111.1, 110.6, 97.6, 61.0, 56.2; IR (KBr,  $\nu$ ,  $\text{cm}^{-1}$ ): 3340, 3301, 3055, 2932, 2839, 1690, 1651, 1597, 1528, 1458, 1412, 1373, 1335, 1234, 1203, 1126, 995, 802, 733, 617; HRMS (ESI<sup>+</sup>) Calculated for C<sub>23</sub>H<sub>21</sub>N<sub>2</sub>O<sub>5</sub> [M + H]<sup>+</sup>, 405.1450; Found 405.1451.

**2-(9H-Carbazol-3-yl)-2-oxo-N-(pyridin-4-yl)acetamide (DK-17)**

Yield 71%; Yellow solid; m.p > 300°C; <sup>1</sup>H NMR (400 MHz, DMSO-*d*<sub>6</sub>)  $\delta$  11.97 (s, 1H), 11.34 (s, 1H), 8.91 (d, *J* = 1.4 Hz, 1H), 8.56 (d, *J* = 6.0 Hz, 2H), 8.31 (d, *J* = 7.8 Hz, 1H), 8.10 (dd, *J* = 8.6, 1.7 Hz, 1H), 7.78 (d, *J* = 6.3 Hz, 2H), 7.66 (d, *J* = 8.6 Hz, 1H), 7.59 (d, *J* = 8.1 Hz, 1H), 7.49 (t, *J* = 8.2 Hz, 1H), 7.27 (t, *J* = 7.9 Hz, 1H); <sup>13</sup>C NMR (100 MHz, DMSO-*d*<sub>6</sub>)  $\delta$  188.6, 165.8, 151.1, 145.2, 144.2, 141.0, 128.1, 127.3, 124.7, 123.6, 123.0, 123.2, 121.5, 120.6, 114.6, 112.2, 112.0; IR (KBr,  $\nu$ ,  $\text{cm}^{-1}$ ): 3286, 3217, 3094, 2962, 2800, 1705, 1659, 1605, 1566, 1489, 1420, 1342, 1311, 1250, 1196, 1157, 1126, 1011, 802, 787, 748, 679; HRMS (ESI<sup>+</sup>) Calculated for C<sub>19</sub>H<sub>14</sub>N<sub>3</sub>O<sub>2</sub> [M + H]<sup>+</sup>, 316.1086; Found 316.1085.

**2-(9-Methyl-9H-carbazol-3-yl)-2-oxo-N-phenylacetamide (DK-18)**

Yield 78%; Yellow solid; m.p: 165-166°C; <sup>1</sup>H NMR (400 MHz, CDCl<sub>3</sub>)  $\delta$  9.40 (d, *J* = 1.4 Hz, 1H), 9.18 (s, 1H), 8.60 (dd, *J* = 8.8, 1.7 Hz, 1H), 8.19 (d, *J* = 7.7 Hz, 1H), 7.79 (d, *J* = 7.6 Hz, 2H), 7.56 (t, *J* = 8.2 Hz, 1H), 7.47-7.41 (m, 4H), 7.35 (t, *J* = 7.9 Hz, 1H), 7.23 (t, *J* = 7.4 Hz, 1H), 3.87 (s, 3H); <sup>13</sup>C NMR (100 MHz, CDCl<sub>3</sub>)  $\delta$  185.8, 160.2, 144.6, 141.7, 136.9, 129.5, 129.2, 126.7, 126.0, 125.1, 124.4, 123.3, 122.7, 120.8, 120.6, 120.0, 109.1, 108.4, 29.4; IR (KBr,  $\nu$ ,  $\text{cm}^{-1}$ ): 3333, 2924, 2854, 1682, 1643, 1610, 1528, 1443, 1366, 1304, 1257, 1149, 1026, 895; MS (ESI<sup>+</sup>) Calculated for C<sub>21</sub>H<sub>17</sub>N<sub>2</sub>O<sub>2</sub> [M + H]<sup>+</sup>, 329.12; Found 329.12.

**2-(9-Methyl-9H-carbazol-3-yl)-2-oxo-N-(3,4,5-trimethoxyphenyl)acetamide (DK-19)**

Yield 80%; Yellow solid; m.p: 187-188°C; <sup>1</sup>H NMR (400 MHz, CDCl<sub>3</sub>)  $\delta$  9.35 (d, *J* = 1.6 Hz, 1H), 9.17 (s, 1H), 8.57 (dd, *J* = 8.8, 1.6 Hz, 1H), 8.18 (d, *J* = 7.7 Hz, 1H), 7.54 (t, *J* = 8.2 Hz, 1H), 7.43-7.38 (m, 2H), 7.34 (t, *J* = 7.2 Hz, 1H), 7.08 (s, 2H), 3.92 (s, 6H), 3.88 (s, 3H), 3.84 (s, 3H); <sup>13</sup>C NMR (100 MHz, CDCl<sub>3</sub>)  $\delta$  185.7, 160.1, 153.4, 144.5, 141.6, 135.2, 133.1, 129.4, 126.7, 125.9, 124.3, 123.2, 122.7, 120.8, 120.5, 109.1, 108.4, 97.5, 61.0, 56.2, 29.3; IR (KBr,  $\nu$ ,  $\text{cm}^{-1}$ ): 3310, 2924, 2854, 1683, 1659, 1607, 1589, 1504, 1450, 1373, 1327, 1227, 1126, 895; MS (ESI<sup>+</sup>) Calculated for C<sub>24</sub>H<sub>23</sub>N<sub>2</sub>O<sub>5</sub> [M + H]<sup>+</sup>, 419.16; Found 419.18.

**2-(9-Ethyl-9H-carbazol-3-yl)-2-oxo-N-phenylacetamide (DK-20)**

Yield 82%; Yellow solid; m.p 159-160°C; <sup>1</sup>H NMR (400 MHz, CDCl<sub>3</sub>)  $\delta$  9.44 (d, *J* = 1.3 Hz, 1H), 9.18 (s, 1H), 8.62 (dd, *J* = 8.8, 1.7 Hz, 1H), 8.22 (d, *J* = 7.7 Hz, 1H), 7.79 (d, *J* = 7.6 Hz, 2H), 7.59-7.53 (m, 1H), 7.49-7.43 (m, 4H), 7.35 (t, *J* = 7.4 Hz, 1H), 7.26-7.21 (m, 1H), 4.42 (q, *J* = 7.2 Hz, 2H), 1.50 (t, *J* = 7.3 Hz, 3H); <sup>13</sup>C NMR (100 MHz, CDCl<sub>3</sub>)  $\delta$  185.8, 160.2, 143.7, 140.7, 136.9, 129.5, 129.2, 126.6, 126.2, 125.1, 124.3, 123.5, 122.9, 121.0,

120.5, 119.9, 109.1, 108.4, 37.9, 13.8; IR (KBr,  $\nu$ ,  $\text{cm}^{-1}$ ): 3310, 2924, 2854, 1690, 1643, 1589, 1535, 1497, 1443, 1381, 1335, 1257, 1149, 756; MS (ESI<sup>+</sup>) Calculated for  $\text{C}_{22}\text{H}_{19}\text{N}_2\text{O}_2$  [M + H]<sup>+</sup>, 343.14; Found 343.19.

***2-(9-ethyl-9H-carbazol-3-yl)-2-oxo-N-(3,4-Dimethoxyphenyl)acetamide (DK-21)***

Yield 85%; Yellow solid; m.p: 110-111°C; <sup>1</sup>H NMR (400 MHz,  $\text{CDCl}_3$ )  $\delta$  9.41 (d,  $J = 1.4$  Hz, 1H), 9.15 (s, 1H), 8.60 (dd,  $J = 8.8, 1.6$  Hz, 1H), 8.20 (d,  $J = 7.7$  Hz, 1H), 7.58 (d,  $J = 2.4$  Hz, 1H), 7.54 (t,  $J = 7.2$  Hz, 1H), 7.44 (t,  $J = 8.6$  Hz, 2H), 7.34 (t,  $J = 7.4$  Hz, 1H), 7.18 (dd,  $J = 8.6, 2.4$  Hz, 1H), 6.90 (d,  $J = 8.7$  Hz, 1H), 4.39 (q,  $J = 7.2$  Hz, 2H), 3.98 (s, 3H), 3.92 (s, 3H), 1.47 (t,  $J = 7.2$  Hz, 3H); <sup>13</sup>C NMR (100 MHz,  $\text{CDCl}_3$ )  $\delta$  185.9, 160.0, 149.2, 146.4, 143.6, 140.6, 130.6, 129.4, 126.6, 126.1, 124.4, 123.5, 122.9, 121.0, 120.4, 112.0, 111.3, 109.1, 108.3, 104.4, 61.0, 56.0, 37.9, 13.8; IR (KBr,  $\nu$ ,  $\text{cm}^{-1}$ ): 3338, 2924, 2854, 1724, 1659, 1589, 1443, 1381, 1327, 1250, 1142, 1026, 768; MS (ESI<sup>+</sup>) Calculated for  $\text{C}_{24}\text{H}_{23}\text{N}_2\text{O}_4$  [M + H]<sup>+</sup>, 403.16; Found 403.21.

***2-(9-Ethyl-9H-carbazol-3-yl)-2-oxo-N-(3,4,5-trimethoxyphenyl)acetamide (DK-22)***

Yield 86%; Yellow solid; m.p: 175-176°C; <sup>1</sup>H NMR (400 MHz,  $\text{CDCl}_3$ )  $\delta$  9.39 (d,  $J = 1.4$  Hz, 1H), 9.18 (s, 1H), 8.59 (dd,  $J = 8.8, 1.6$  Hz, 1H), 8.20 (d,  $J = 7.7$  Hz, 1H), 7.54 (t,  $J = 7.7$  Hz, 1H), 7.47-7.41 (m, 2H), 7.34 (t,  $J = 7.7$  Hz, 1H), 7.10 (s, 2H), 4.38 (q,  $J = 7.2$  Hz, 2H), 3.93 (s, 6H), 3.88 (s, 3H), 1.47 (t,  $J = 7.2$  Hz, 3H); <sup>13</sup>C NMR (100 MHz,  $\text{CDCl}_3$ )  $\delta$  185.7, 160.1, 153.5, 143.6, 140.6, 135.2, 133.1, 129.4, 126.6, 126.0, 124.2, 123.4, 122.9, 121.0, 120.5, 109.1, 108.3, 97.6, 61.0, 56.2, 37.9, 13.8; IR (KBr,  $\nu$ ,  $\text{cm}^{-1}$ ): 3279, 2932, 2854, 1736, 1659, 1607, 1589, 1504, 1450, 1389, 1342, 1234, 1126, 1049, 995; MS (ESI<sup>+</sup>) Calculated for  $\text{C}_{25}\text{H}_{25}\text{N}_2\text{O}_5$  [M + H]<sup>+</sup>, 433.17; Found 433.18.

***2-(9-ethyl-9H-carbazol-3-yl)-2-oxo-N-(4-(dimethylamino)phenyl)acetamide (DK-23)***

Yield 73%; Yellow solid; m.p: 173-174°C; <sup>1</sup>H NMR (400 MHz,  $\text{CDCl}_3$ )  $\delta$  9.45 (d,  $J = 1.3$  Hz, 1H), 9.04 (s, 1H), 8.63 (dd,  $J = 8.8, 1.6$  Hz, 1H), 8.21 (d,  $J = 7.7$  Hz, 1H), 7.65 (d,  $J = 9.0$  Hz, 2H), 7.55 (t,  $J = 7.6$  Hz, 1H), 7.49-7.43 (m, 2H), 7.34 (t,  $J = 7.0$  Hz, 1H), 6.80 (d,  $J = 9.0$  Hz, 2H), 4.41 (q,  $J = 7.2$  Hz, 2H), 2.99 (s, 6H), 1.49 (t,  $J = 7.2$  Hz, 3H); <sup>13</sup>C NMR (100 MHz,  $\text{CDCl}_3$ )  $\delta$  186.3, 159.8, 148.3, 143.6, 140.6, 129.5, 126.7, 126.6, 126.1, 124.7, 123.6, 122.8, 121.4, 121.0, 120.4, 112.9, 109.1, 108.3, 40.8, 37.9, 13.8; IR (KBr,  $\nu$ ,  $\text{cm}^{-1}$ ): 3290, 2924, 2854, 1723, 1666, 1582, 1448, 1350, 1234, 1126, 1065, 895; MS (ESI<sup>+</sup>) Calculated for  $\text{C}_{24}\text{H}_{24}\text{N}_3\text{O}_2$  [M + H]<sup>+</sup>, 386.18; Found 386.24.

***2-(9-Ethyl-9H-carbazol-3-yl)-2-oxo-N-(quinolin-6-yl)acetamide (DK-24)***

Yield 78%; Yellow solid; m.p: 191-192°C; <sup>1</sup>H NMR (400 MHz,  $\text{CDCl}_3$ )  $\delta$  9.49 (s, 1H), 9.42 (d,  $J = 1.3$  Hz, 1H), 8.89 (dd,  $J = 4.2, 1.7$  Hz, 1H), 8.64-8.56 (m, 2H), 8.19 (t,  $J = 7.1$  Hz,

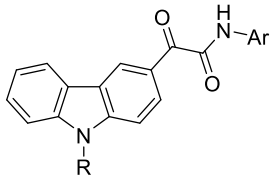
## Chapter 6

2H), 8.14 (d,  $J = 8.0$  Hz, 1H), 7.80 (dd,  $J = 9.0, 2.4$  Hz, 1H), 7.57-7.52 (m, 1H), 7.47-7.40 (m, 3H), 7.34 (t,  $J = 7.5$  Hz, 1H), 4.37 (q,  $J = 7.2$  Hz, 2H), 1.47 (t,  $J = 7.3$  Hz, 3H);  $^{13}\text{C}$  NMR (100 MHz,  $\text{CDCl}_3$ )  $\delta$  185.3, 160.5, 149.8, 145.8, 143.7, 140.6, 136.0, 134.9, 130.5, 129.5, 128.8, 126.7, 126.2, 124.2, 123.4, 123.2, 122.9, 121.8, 121.0, 120.6, 116.5, 109.2, 108.4, 37.9, 13.8; IR (KBr,  $\nu$ ,  $\text{cm}^{-1}$ ): 3348, 2924, 2854, 1690, 1651, 1582, 1466, 1327, 1234, 1126, 1065, 887; MS (ESI<sup>+</sup>) Calculated for  $\text{C}_{25}\text{H}_{20}\text{N}_3\text{O}_2$   $[\text{M} + \text{H}]^+$ , 394.15; Found 394.16.

### 6.3 | PL inhibition assay and enzyme kinetics

The procedure for PL inhibition assay and kinetics was performed as per the protocol detailed in chapter 4. Stock solutions of the synthesised analogues were prepared in DMSO at linear concentrations ranging from 1.56 - 2000  $\mu\text{g}/\text{mL}$ . Enzyme inhibition kinetics were performed for the most active analogues **DK-5**, **DK-6** and **DK-16**, each at three different concentrations (0, 5 and 10  $\mu\text{M}$ ). The PL inhibitory profiles of all the analogues are summarized in Table 6.1. Most of the analogues exhibited potential (< 25  $\mu\text{M}$ ) to moderate (25-50  $\mu\text{M}$ ) activity, while only one analogue (**DK-23**) displayed poor activity (> 50  $\mu\text{M}$ ). Analogue **DK-5** exhibited the most potent activity against PL, with an  $\text{IC}_{50}$  of 6.31  $\mu\text{M}$ , followed by **DK-6** and **DK-16** ( $\text{IC}_{50}$  8.72 and 9.58  $\mu\text{M}$ , respectively).

**Table 6.1.** *In vitro* PL inhibitory activities of carbazolyl oxoacetamide analogues **DK-1** to **DK-24**



#	R	Ar	$\text{IC}_{50}$ ( $\mu\text{M}$ )*
<b>DK-1</b>	4-Chlorobenzyl	Phenyl	13.91 $\pm$ 2.10
<b>DK-2</b>	4-Chlorobenzyl	4-Methylphenyl	13.53 $\pm$ 1.67
<b>DK-3</b>	4-Chlorobenzyl	3-Methoxyphenyl	26.61 $\pm$ 0.97
<b>DK-4</b>	4-Chlorobenzyl	4-Methoxyphenyl	14.83 $\pm$ 2.17
<b>DK-5</b>	4-Chlorobenzyl	3,4-Dimethoxyphenyl	<b>6.31 0.56</b>
<b>DK-6</b>	4-Chlorobenzyl	3,4,5-Trimethoxyphenyl	<b>8.72 0.47</b>
<b>DK-7</b>	4-Chlorobenzyl	4-Fluorophenyl	27.98 $\pm$ 2.25
<b>DK-8</b>	4-Chlorobenzyl	4-Pyridyl	19.87 $\pm$ 1.08
<b>DK-9</b>	4-Chlorobenzyl	<i>N,N</i> -dimethylaminophenyl	14.78 $\pm$ 1.50
<b>DK-10</b>	4-Chlorobenzyl	6-Quinolyl	23.05 $\pm$ 2.49
<b>DK-11</b>	4-Chlorobenzyl	2-(5-Methyl)thiazolyl	32.76 $\pm$ 6.05
<b>DK-12</b>	H	Phenyl	29.73 $\pm$ 5.62
<b>DK-13</b>	H	3-Methoxyphenyl	33.02 $\pm$ 2.30



## Chapter 6

<b>DK-14</b>	H	4-Methoxyphenyl	19.31 ± 0.80
<b>DK-15</b>	H	3,4-Dimethoxyphenyl	44.12 ± 5.18
<b>DK-16</b>	<b>H</b>	<b>3,4,5-Trimethoxyphenyl</b>	<b>9.58 ± 1.24</b>
<b>DK-17</b>	H	4-Pyridyl	29.35 ± 2.17
<b>DK-18</b>	Methyl	Phenyl	36.18 ± 1.88
<b>DK-19</b>	Methyl	3,4,5-Trimethoxyphenyl	23.12 ± 2.06
<b>DK-20</b>	Ethyl	Phenyl	24.22 ± 0.30
<b>DK-21</b>	Ethyl	3,4-Dimethoxyphenyl	16.37 ± 2.09
<b>DK-22</b>	Ethyl	3,4,5-Trimethoxyphenyl	11.37 ± 1.12
<b>DK-23</b>	Ethyl	<i>N,N</i> -dimethylaminophenyl	56.18 ± 4.34
<b>DK-24</b>	Ethyl	6-Quinolyl	15.48 ± 1.87
<b>Orlistat</b>	-	-	0.99 ± 0.11

\* All the experiments were performed in triplicate and the values are represented as mean ± SEM

Further, enzyme kinetics study for **DK-5**, **DK-6** and **DK-16** indicated that the carbazolyl oxoacetamide analogues exhibited a reversible competitive inhibition similar to orlistat and conophylline (See 4.2 in chapter 4). As shown in Fig. 6.3 and Table 6.2, the plots converged at y-intercept while the  $K_m$  value increased in proportion to the inhibitor concentration. These graphical representations from the Lineweaver-Burk plots (Fig. 6.3) represented reversible competitive inhibition, indicating that these analogues were bound to the active site of the PL during the inhibition.

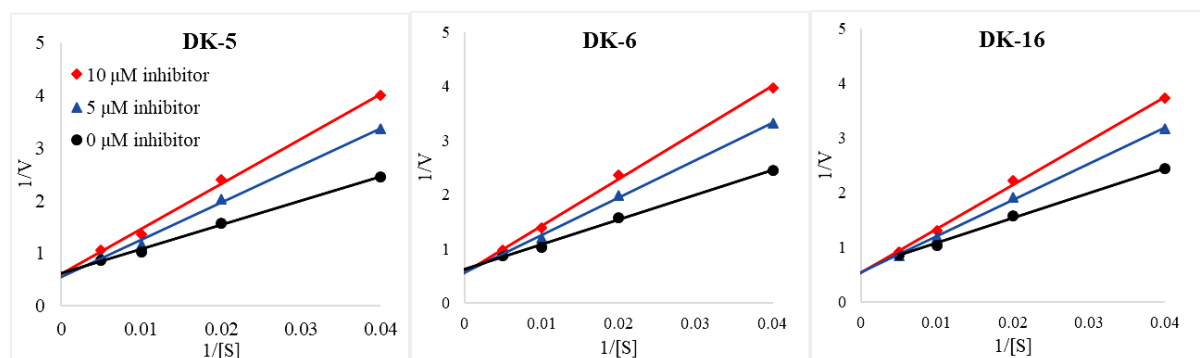


**Fig. 6.3.** Double reciprocal Lineweaver-Burk plots of analogues **DK-5**, **DK-6** and **DK-16**

**Table 6.2.**  $V_{max}$ ,  $K_m$  and  $K_i$  values calculated from Lineweaver-Burk plots at different inhibitory concentrations [I] of **DK-5**, **DK-6** and **DK-16**

Analogue	$K_m$ (in $\mu\text{M}$ ) at different inhibitor concentrations [I]			$V_{max}$ ( $\mu\text{M}/\text{min}$ )	$K_i$ ( $\mu\text{M}$ )
	0 $\mu\text{M}$	5 $\mu\text{M}$	10 $\mu\text{M}$		
<b>DK-5</b>	74.01	129.14	154.20	1.74	3.77
<b>DK-6</b>	74.03	123.73	150.92	1.73	5.20
<b>DK-16</b>	74.01	122.77	141.92	1.78	5.72

### 6.4 | Structure activity relationship

A preliminary structure-activity relationship of the screened analogues was analysed based on their PL inhibitory activity. As shown in Figure 6.4, the potential of the analogues to inhibit PL varied with respect to the substitutions on the carbazolyl and amide nitrogen *viz.*, R and Ar respectively. The presence of aromatic benzyl group on the carbazolyl nitrogen increased the PL inhibition activity of analogues. This might be attributed to an increase in the hydrophobic density on the carbazole, which in turn resulted in stronger hydrophobic interactions with the lid domain. Similarly, the presence of an electron-donating group on the amide nitrogen potentiated the PL inhibitory activity of the analogues. 3,4-Dimethoxy and 3,4,5-trimethoxy analogues exhibited comparatively stronger inhibition activity when compared to other analogues.

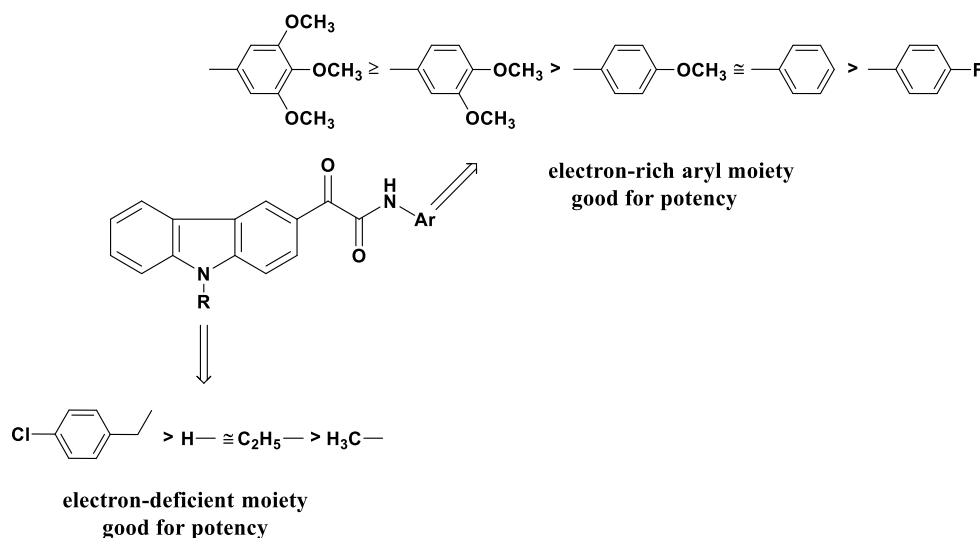


**Fig. 6.4.** Structure-activity relationship for carbazolyl oxoacetamide analogues **DK-1** to **DK-24**

### 6.5 | Molecular modelling studies

A total of 24 carbazolyl oxoacetamide analogues were subjected to molecular docking studies on human PL (PDB ID: 1LPB) while MD simulation was conducted for **DK-5** in complex with PL. The MolDock scores and the various interactions exhibited by the carbazolyl oxoacetamides are summarized in Table 6.3. Analogue **DK-5** possessed a top docking score of -151.21 kcal/mol. Moreover, the MolDock score was in alignment with the  $IC_{50}$  values of the *in vitro* assay, validating the docking parameters.

As represented in Table 6.3 and Figure 6.5, the ligands exhibited  $\pi$ - $\pi$  stacking interactions with amino acids of the lid domain in addition to H-bond interaction with Phe 77. Further, the presence of aromatic group (4-chlorobenzyl substitution) on carbazole nitrogen facilitated an additional  $\pi$ - $\pi$  interaction with Tyr 114 as evident from binding pose

## Chapter 6

analysis. Moreover, the reactive carbonyl group of the oxoacetamide existed near to the Ser152 as observed with most of the ligands. As represented in Fig. 6.6, the reactive carbonyl group of **DK-5** existed at a distance of 4.45 Å from Ser152 of the active site. These findings are in accordance to the rationale of the study, validating the hypothesis.

**Table 6.3.** MolDock scores and interaction summary of carbazolyl oxoacetamide analogues **DK-1** to **DK-24** with the active site of PL

Analogue	MolDock score*	H-bond	$\pi$ - $\pi$ stacking interactions	$\pi$ -cation
<b>DK-1</b>	-150.44	Phe 77	Phe 77, His 263	Arg 256
<b>DK-2</b>	-146.89	Phe 77	Phe 77, His 263	Arg 256
<b>DK-3</b>	-135.41	-	Phe 77	Arg 256
<b>DK-4</b>	-149.62	Phe 77	Phe 77, Tyr 114, His 263	Arg 256
<b>DK-5</b>	<b>-151.21</b>	<b>Phe 77, Ser 152</b>	<b>Phe 77, Tyr 114</b>	<b>Arg 256</b>
<b>DK-6</b>	<b>-150.99</b>	<b>Phe 77, Ser 152</b>	<b>Phe 77, Tyr 114, His 263</b>	<b>Arg 256</b>
<b>DK-7</b>	-134.27	His 263	Phe 77	Arg 256
<b>DK-8</b>	-133.84	-	Phe 77, Tyr 114, Phe 215	-
<b>DK-9</b>	-142.12	Phe 77	Phe 77, His 263	-
<b>DK-10</b>	-137.15	-	Phe 77, Tyr 114, Phe 215	-
<b>DK-11</b>	-126.32	Phe 77	Phe 77, His 263	Arg 256
<b>DK-12</b>	-124.10	His 263	Tyr 114	-
<b>DK-13</b>	-126.72	Phe 77	His 263	Arg 256
<b>DK-14</b>	-135.76	Phe 77	His 263	Arg 256
<b>DK-15</b>	-114.70	Phe 77	His 151, Phe 215, His 263	-
<b>DK-16</b>	<b>-145.39</b>	<b>Phe 77</b>	<b>Phe 77, His 151</b>	<b>-</b>
<b>DK-17</b>	-126.11	Phe 77	His 263, Arg 256	-
<b>DK-18</b>	-124.85	Phe 77	Phe 77	-
<b>DK-19</b>	-135.83	Phe 77	Phe 77	Arg 256
<b>DK-20</b>	-128.57	Phe 77	His 263	Arg 256
<b>DK-21</b>	-132.65	Phe 77	His 263	-
<b>DK-22</b>	-135.02	Phe 77	Phe 77, His 263	Arg 256
<b>DK-23</b>	-133.65	Phe 77	Phe 77, His 263	Arg 256
<b>DK-24</b>	-134.39	Phe 77	His 263	Arg 256
<b>Orlistat</b>	-150.44	His 151, Ser 152	-	-

\* MolDock scores are represented in kcal/mol.

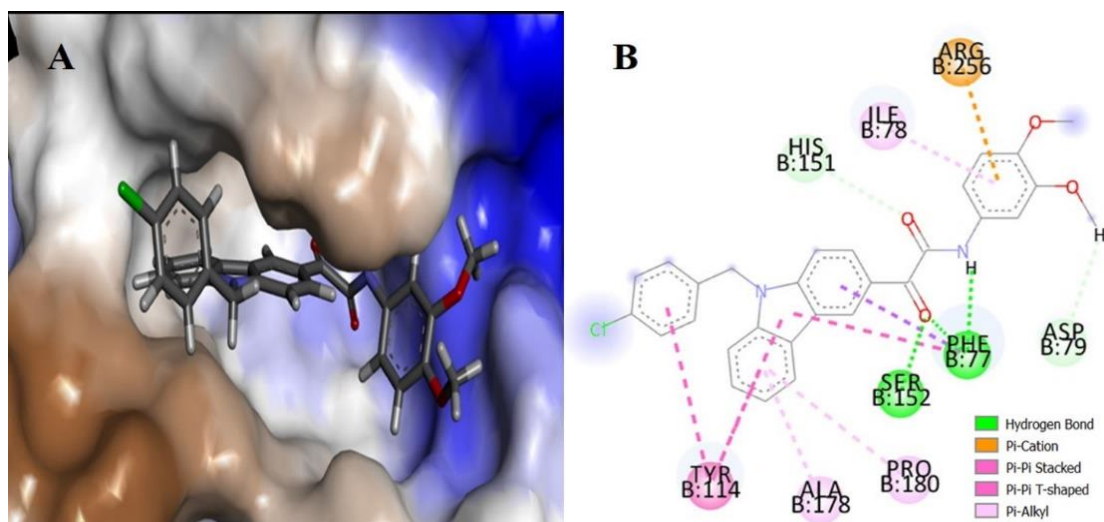


**Fig. 6.5.** (A) Representation of **DK-5** in the binding pocket of PL (brown region indicates hydrophobic lid domain); (B) 2D interaction diagram of **DK-5** with PL

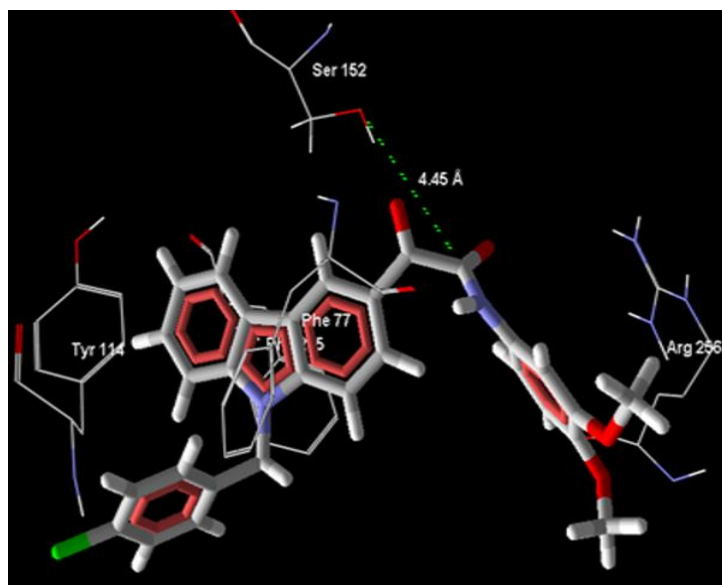


**Fig. 6.6.** 3D pose of **DK-5** in the active site of PL highlighting the distance of the reactive carbonyl group from Ser152

Moreover, most of the ligands exhibited an additional  $\pi$ -cation interaction with Arg 256. Literature study revealed that Arg 256 plays a key role in the transformation of PL from closed to an open lid conformation. Lowe *et al.* reported that Arg 256 and Asp 257 makes a salt bridge with Tyr 267 and Lys 268 in the open lid conformation [8,9]. Further, the role of  $\pi$ -cation interaction with Arg 256 in potentiating the activity was established in previous reports [10,11]. This fact is in correlation to the structure-activity relationship mentioned

above, wherein the ring deactivating groups on the aryl ring of the amide nitrogen resulted in moderate to poor PL inhibitory activity.

Docking studies provided a preliminary idea of the ligand interactions with PL. To further understand the ligand behaviour in motion, a 10 ns MD simulation was performed for **DK-5** in complex with PL. The RMSD of the protein backbone remained stable during the entire run with a maximum deviation of 2.5 Å recorded around 8 ns (Fig. 6.7A), while a stable radius of gyration indicated no structural changes in the protein (Fig. 6.7B). Further, as represented in Fig. 6.7C, the ligand remained very stable during the first 4 ns (RMSD < 2 Å), then slightly deviated by 0.5 Å during the next 3 ns and achieved a final RMSD of 4 Å in the last 3 ns.

A summary of the various interactions exhibited by the ligand **DK-5** with the active site during the MD simulation is detailed under Table 6.4. The ligand made stable H-bond interactions with Phe 77 during the first 3 ns apart from the  $\pi$ -cationic interactions with Asp 79 and Arg 256, and hydrophobic interactions with the amino acids of the lid domain. Furthermore, the  $\pi$ - $\pi$  stacking interactions with the lid domain remained stable during the entire run, substantiating the role of aromatic wings for potential PL inhibitory activity of the ligand.

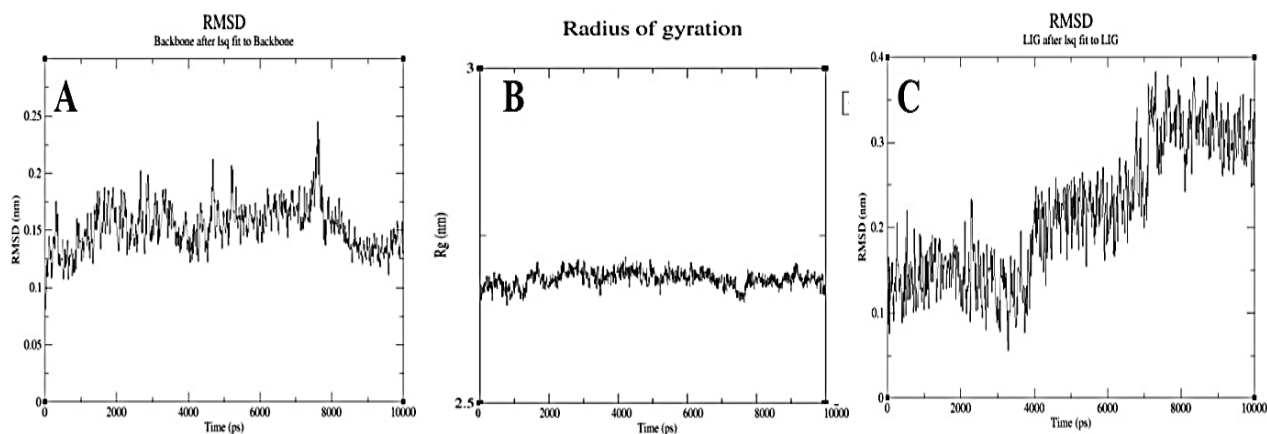


**Fig. 6.7.** (A) RMSD of the backbone; (B) Radius of gyration of the protein and (C) RMSD of the ligand (**DK-5**) retrieved through 10 ns MD trajectory

## Chapter 6

**Table 6.4.** Interaction chart of **DK-5** with the active site of PL at different time frames during MD simulation

Time Frame (ns)	H-bond	$\pi$ - $\pi$ stacking	$\pi$ -charge interactions
0	Phe 77	Phe 77, Phe 215	Asp 79, Arg 256
1	Phe 77	Phe 77, Phe 215, His 263	Asp 79, Arg 256
2	Phe 77	Phe 77, Phe 215	Asp 79, Arg 256
3	Phe 77, Ser 152	Phe 77, Phe 215, His 263	Asp 79, Arg 256
4	-	Phe 77, Tyr 114, Phe 215	-
5	Arg 256	Phe 77, Phe 215	-
6	-	Phe 77	Arg 256
7	-	Phe 77, Phe 215	-
8	Trp 252, Arg 256	Phe 77, Tyr 114, Phe 215	-
9	Trp 252, Arg 256	Phe 77, Tyr 114, Phe 215	-
10	-	Tyr 114	Arg 256

To summarize, a series of 24 carbazolyl oxoacetamide analogues have been synthesised and screened *in vitro* to determine their PL inhibition activity. From the series, Analogue **DK-5** was found to be the most active inhibitor of PL with an  $IC_{50}$  of 6.31  $\mu$ M, followed by **DK-6** ( $IC_{50}$  = 8.72  $\mu$ M) and **DK-16** ( $IC_{50}$  = 9.58  $\mu$ M). Furthermore, these three active analogues exhibited competitive inhibition as evidenced through enzyme kinetics. Molecular docking studies validated the rationale for selecting the carbazolyl oxoacetamides as PL inhibitors. A 10 ns MD simulation of the top scoring molecule, **DK-5** in complex with PL, highlighted a stable conformation of the ligand with maximum RMSD of 4 Å.

### References

- [1] R. Birari, S.K. Roy, A. Singh, K.K. Bhutani, Pancreatic lipase inhibitory alkaloids of *Murraya koenigii* leaves., *Nat. Prod. Commun.* 4 (2009) 1089–1092.
- [2] W. Han, Z. Hu, X. Jiang, C.P. Decicco,  $\alpha$ -Ketoamides,  $\alpha$ -ketoesters and  $\alpha$ -diketones as HCV NS3 protease inhibitors, *Bioorg. Med. Chem. Lett.* 10 (2000) 711–713.
- [3] C. Steuer, C. Gege, W. Fischl, K.H. Heinonen, R. Bartenschlager, C.D. Klein, Synthesis and biological evaluation of  $\alpha$ -ketoamides as inhibitors of the Dengue virus protease with antiviral activity in cell-culture, *Bioorg. Med. Chem.* 19 (2011) 4067–4074.
- [4] S. Kotsovolou, A. Chiou, R. Verger, G. Kokotos, Bis-2-oxo amide triacylglycerol analogues: A novel class of potent human gastric lipase inhibitors, *J. Org. Chem.* 66 (2001) 962–967.
- [5] A. Chiou, T. Markidis, V. Constantinou-Kokotou, R. Verger, G. Kokotos, Synthesis and study of a lipophilic  $\alpha$ -keto amide inhibitor of pancreatic lipase, *Org. Lett.* 2 (2000) 347–350.
- [6] G. Kokotos, R. Verger, A. Chiou, Synthesis of 2-oxo amide triacylglycerol analogues and study of their inhibition effect on pancreatic and gastric Lipases, *Chem. Eur. J.* 6 (2000) 4211–4217.
- [7] P.O.V. Reddy, M.P. Tantak, R. Valdez, R.P. Singh, O.M. Singh, R. Sadana, D. Kumar, Synthesis and biological evaluation of novel carbazolyl glyoxamides as anticancer and antibacterial agents, *RSC Adv.* 6 (2016) 9379–9386.
- [8] M.E. Lowe, The triglyceride lipases of the pancreas, *J. Lipid Res.* 43 (2002) 2007–2016.
- [9] M.E. Lowe, Pancreatic triglyceride lipase and colipase: Insights into dietary fat digestion, *Gastroenterology.* 107 (1994) 1524–1536.
- [10] S.N.C. Sridhar, D. Bhurta, D. Kantiwal, G. George, V. Monga, A.T. Paul, Design, synthesis, biological evaluation and molecular modelling studies of novel diaryl substituted pyrazolyl thiazolidinediones as potent pancreatic lipase inhibitors, *Bioorg. Med. Chem. Lett.* 27 (2017) 3749–3754.
- [11] R.B. Birari, S. Gupta, C.G. Mohan, K.K. Bhutani, Antiobesity and lipid lowering effects of *Glycyrrhiza* chalcones: Experimental and computational studies, *Phytomedicine.* 18 (2011) 795–801.

## 7 | Synthesis - Series II - Indolyl Oxoacetamide Analogues (Part 1)

## 7.1 | Rationale

Carbazolyl oxoacetamide analogues (chapter 6) exhibited a moderate to potential PL inhibitory profile, with the most active analogue **DK-5** that exhibited an  $IC_{50}$  value of 6.31  $\mu$ M. Further, molecular modelling studies indicated the absence of any unfavourable steric bumps with **DK-5**, in contrast to conophylline (Fig. 7.1). Nevertheless, a lower PL inhibitory potential of **DK-5** compared to conophylline ( $IC_{50} = 3.31 \mu$ M) can be attributed to three drawbacks, as determined through *in silico* analysis of the docking poses of orlistat, conophylline and **DK-5**; i) A greater interaction distance between the reactive carbonyl group of the ketoamide and Ser152 of the active site (Fig. 7.1); ii) A lesser intensity of hydrophobic interactions exhibited by **DK-5** in comparison to conophylline and orlistat, and iii) the strength of the  $\pi$ -cation interaction with Arg 256.

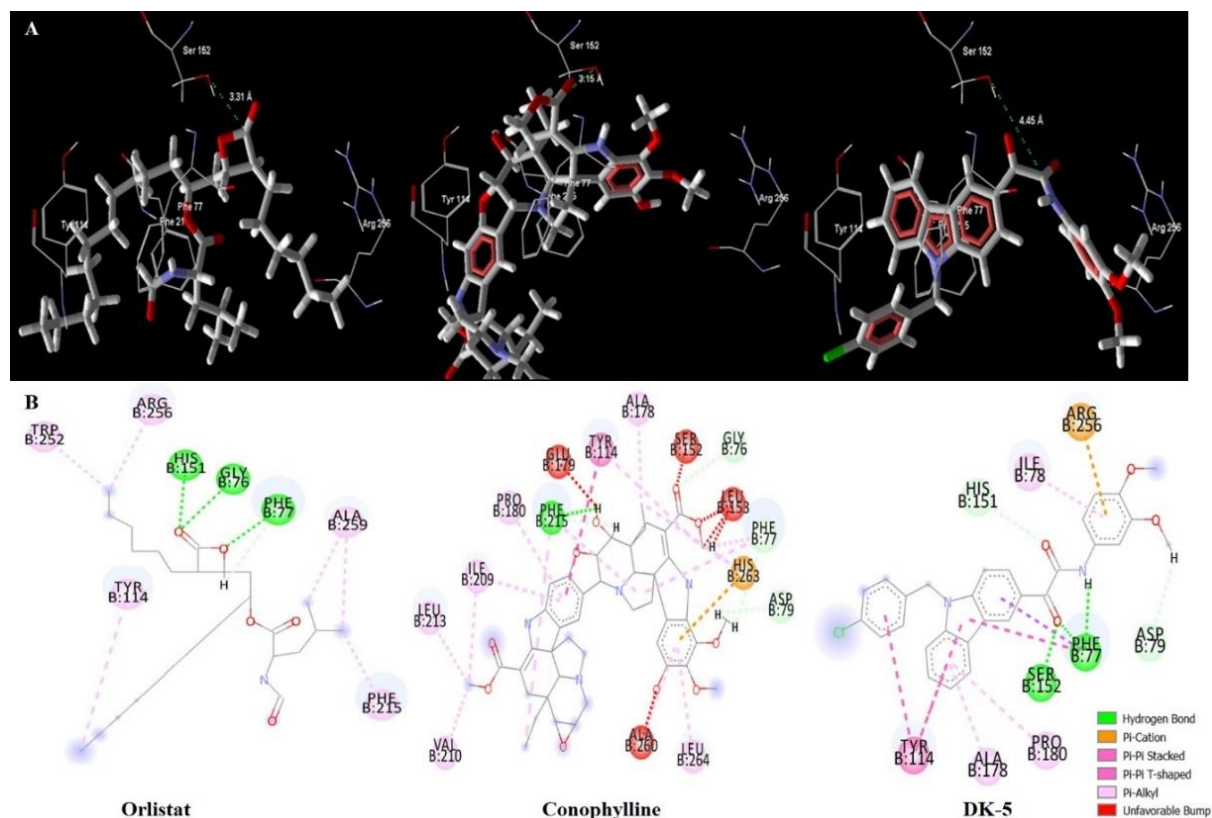


**Fig. 7.1.** (A) 3D poses of orlistat, conophylline and **DK-5** highlighting the distance of reactive carbonyl from Ser152 (3.31, 3.15 and 4.45 Å, respectively); (B) 2D interactions highlighting no unfavourable steric bumps and low degree of hydrophobic interactions in **DK-5**.

Thus, the present chapter is focussed on understanding the variability in PL inhibitory activity, that would be the result of reduction in the interaction distance of the reactive



carbonyl group and Ser152. In a preliminary docking study, replacement of carbazole scaffold of **DK-5** with an indole scaffold (indole counterpart) exhibited a reduced interaction distance of 3.42 Å between the reactive carbonyl group and Ser152 as compared to 4.45 Å (Fig. 7.2). Based on this observation, we hypothesized that the replacement of carbazole scaffold with an indole scaffold would result in potent PL inhibitors. Accordingly, a series of 39 indolyl oxoacetamide analogues were synthesised and evaluated for their PL inhibitory potential.

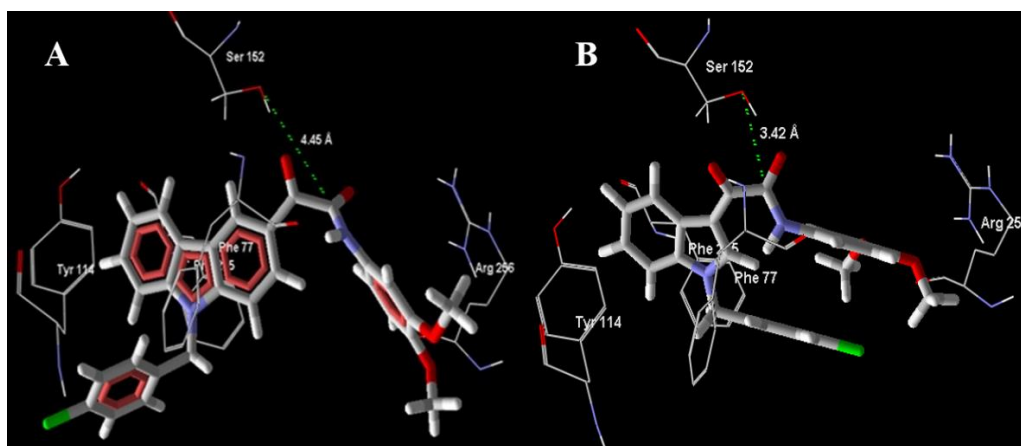


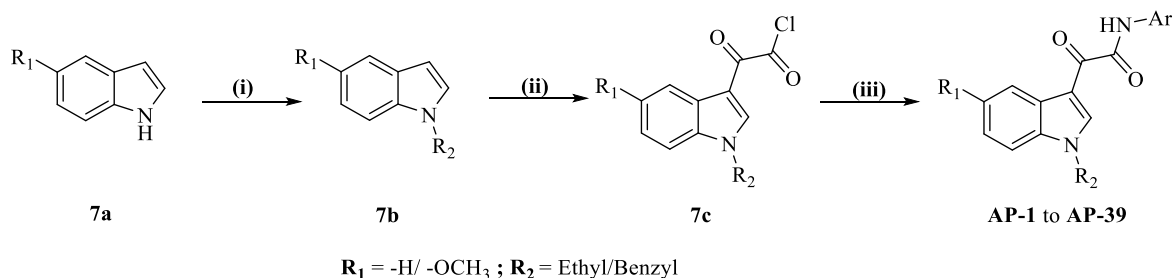
**Fig. 7.2.** Rationale for designing indolyl oxoacetamide analogues as PL inhibitors. The interaction distance has reduced from 4.45 Å in **DK-5** (A) to 3.42 Å for the indole counterpart of **DK-5** (B).

## 7.2 | Synthesis and Characterization

The synthesis of all the final analogues **AP-1** to **AP-39** were carried out as per the procedure detailed in Scheme 7.1 [1–3]. Briefly, to 10 mL DMF taken in a 100 mL round bottomed flask, 25.6 mmol of KOH was added and stirred vigorously for 15 minutes at room temperature. To this, 8.5 mmol of indole/5-methoxyindole (**7a**) was added and the stirring was continued. After 30 minutes, a solution of appropriate halide (8.5 mmol in 5 mL DMF) was added dropwise for over 5 minutes to the reaction mixture, and the stirring was continued overnight. The reaction mixture was then transferred to ice-cold water. The N-benzyl and N-ethyl substituted indole analogues (**7b**) were obtained as crude precipitates and oily liquid, respectively. The N-benzyl substituted indole analogues were purified by recrystallization from ethanol, while the N-ethyl substituted indole was extracted using chloroform and purified through column chromatography.

The indole analogues (**7a** and **7b**) (2.5 mmol) were then stirred at 0°C for 30 minutes in 5 mL diethylether. To this, oxalyl chloride (2.5 mmol) was added dropwise for a period of over 5 min, and the reaction was continued at 0°C for 15 minutes. The obtained yellow

precipitate of glyoxylyl chloride analogue (**7c**) was either filtered or dried *in vacuo*, washed with cold ether, and transferred immediately to a solution of THF containing appropriate amount of aniline analogue, followed by addition of triethylamine (7.5 mmol). The reaction was continued at room temperature for 2 hours, and THF was removed *in vacuo* to yield crude glyoxylamide analogues. The crude precipitate was then re-crystallized from ethanol to obtain analogues **AP-1** to **AP-39** in 68-94% yields.



**Scheme 7.1.** Reagents and conditions: (i) Benzyl chloride/Ethyl bromide, KOH, DMF, RT, 12 h; (ii) (COCl)<sub>2</sub>, Et<sub>2</sub>O, 0°C, 30 min; (iii) Ar-NH<sub>2</sub>, TEA, THF, RT, 2 h.

Structures of the synthesized indolyl oxoacetamide analogues, **AP-1** to **AP-39**, were well characterized using NMR (<sup>1</sup>H and <sup>13</sup>C), IR and HRMS. In the <sup>1</sup>H NMR, the -NH protons of amide functionality resonated at 10-11 ppm, while the proton at C<sub>2</sub> adjacent to the indole nitrogen resonated at 8-9 ppm. In addition, for the unsubstituted indole analogues **AP-1** to **AP-15**, the -NH proton of the indole appeared as a singlet above 12 ppm. For, the N-benzyl substituted analogues **AP-16** to **AP-24** and **AP-34** to **AP-39**, the methylene protons appeared as a singlet between 5-6 ppm. Further, for the N-ethyl (-CH<sub>2</sub>-CH<sub>3</sub>) substituted analogues **AP-25** to **AP-33**, the methyl protons appeared as a triplet between 1-2 ppm, while the -CH<sub>2</sub> protons appeared as a quartet between 4-5 ppm. Further, the -OCH<sub>3</sub> protons of the 5-methoxyindole analogues, **AP-9** to **AP-15** and **AP-34** to **AP-39** resonated as singlets around 3-4 ppm. In the <sup>13</sup>C NMR, the carbons of carbonyl and amide functionalities were resonated at ~180 (CO) and ~160 ppm (NHCO). In the IR spectra, the amide -NH stretch was observed at 3600-3700 cm<sup>-1</sup>, while the characteristic peaks at 1600-1800 cm<sup>-1</sup> were assigned to the carbonyl functionalities

#### **2-(1H-indol-3-yl)-2-oxo-N-phenylacetamide (AP-1)**

Yield 89%; Creamy white solid; m.p: 248-250°C; <sup>1</sup>H NMR (400 MHz, DMSO-*d*<sub>6</sub>) δ 12.37 (s, 1H), 10.70 (s, 1H), 8.78 (s, 1H), 8.34-8.27 (m, 1H), 7.88 (d, *J* = 7.4 Hz, 2H), 7.61-7.54 (m, 1H), 7.39 (t, *J* = 8.0 Hz, 2H), 7.30 (dd, *J* = 6.1, 3.2 Hz, 2H), 7.15 (t, *J* = 7.4 Hz, 1H); <sup>13</sup>C NMR (100 MHz, DMSO-*d*<sub>6</sub>) δ 182.4, 162.8, 139.1, 138.5, 136.9, 129.2, 126.6, 124.6,

124.0, 123.1, 121.6, 120.7, 113.1, 112.4; IR (KBr,  $\nu$ ,  $\text{cm}^{-1}$ ): 3742, 3294, 2569, 2361, 1913, 1674, 1612, 1504, 1443, 1319, 1242, 1072, 996, 957, 864, 810, 687, 501, 455; HRMS (ESI<sup>+</sup>) calculated for  $\text{C}_{16}\text{H}_{13}\text{N}_2\text{O}_2$  [ $\text{M}+\text{H}^+$ ], 265.0899; Found 265.0788.

***2-(1H-indol-3-yl)-2-oxo-N-(p-tolyl)acetamide (AP-2)***

Yield 81%; Light brown solid; m.p: 225-227°C; <sup>1</sup>H NMR (400 MHz, DMSO-*d*<sub>6</sub>)  $\delta$  12.34 (s, 1H), 10.58 (s, 1H), 8.78 (s, 1H), 8.32-8.24 (m, 1H), 7.79 (d,  $J = 7.4$  Hz, 2H), 7.60-7.52 (m, 1H), 7.34-7.25 (m, 2H), 6.96 (d,  $J = 7.4$  Hz, 2H), 3.36 (s, 3H); <sup>13</sup>C NMR (100 MHz, DMSO-*d*<sub>6</sub>)  $\delta$  182.5, 162.3, 156.3, 139.0, 136.8, 131.6, 126.6, 124.0, 123.1, 122.1, 121.6, 114.3, 113.1, 112.4, 51.6; IR (KBr,  $\nu$ ,  $\text{cm}^{-1}$ ): 3757, 3402, 2963, 2353, 1883, 1821, 1574, 1435, 1242, 1126, 1011, 818, 640, 471, 417; HRMS (ESI<sup>+</sup>) calculated for  $\text{C}_{17}\text{H}_{15}\text{N}_2\text{O}_2$  [ $\text{M}+\text{H}^+$ ], 279.1128; Found 279.1114.

***2-(1H-indol-3-yl)-2-oxo-N-(3,4-dimethylphenyl)acetamide (AP-3)***

Yield 81%; Greenish yellow solid; m.p: 230-232°C; <sup>1</sup>H NMR (400 MHz, DMSO-*d*<sub>6</sub>)  $\delta$  12.34 (s, 1H), 10.50 (s, 1H), 8.78 (s, 1H), 8.32-8.25 (m, 1H), 7.68 (s, 1H), 7.56 (d,  $J = 6.5$  Hz, 2H), 7.29 (dd,  $J = 6.0, 3.2$  Hz, 2H), 7.12 (d,  $J = 8.2$  Hz, 1H), 2.23 (s, 3H), 2.20 (s, 3H); <sup>13</sup>C NMR (100 MHz, DMSO-*d*<sub>6</sub>)  $\delta$  181.3, 161.9, 138.3, 137.7, 136.3, 136.8, 134.4, 129.5, 126.3, 123.6, 122.8, 122.4, 121.6, 118.4, 114.9, 112.5, 19.6, 18.7; IR (KBr,  $\nu$ ,  $\text{cm}^{-1}$ ) 3935, 3341, 2978, 2361, 1913, 1682, 1497, 1443, 1327, 1242, 1111, 995, 957, 826, 725, 694, 656, 501; HRMS (ESI<sup>+</sup>) calculated for  $\text{C}_{18}\text{H}_{17}\text{N}_2\text{O}_2$  [ $\text{M}+\text{H}^+$ ], 293.1285; Found 293.1278.

***2-(1H-indol-3-yl)-2-oxo-N-(4-methoxyphenyl)acetamide (AP-4)***

Yield 81%; Greenish yellow solid; m.p: 231-233°C; <sup>1</sup>H NMR (400 MHz, DMSO-*d*<sub>6</sub>)  $\delta$  12.34 (s, 1H), 10.59 (s, 1H), 8.77 (s, 1H), 8.36-8.22 (m, 1H), 7.76 (d,  $J = 8.4$  Hz, 2H), 7.61-7.53 (m, 1H), 7.28 (dd,  $J = 6.1, 3.1$  Hz, 2H), 7.18 (d,  $J = 8.2$  Hz, 2H), 2.29 (s, 3H); <sup>13</sup>C NMR (100 MHz, DMSO-*d*<sub>6</sub>)  $\delta$  182.1, 162.7, 139.8, 137.6, 136.0, 133.6, 129.5, 126.9, 123.8, 122.9, 121.6, 120.6, 113.4, 112.4, 21.0; IR (KBr,  $\nu$ ,  $\text{cm}^{-1}$ ): 3765, 2361, 1875, 1420, 1342, 1250, 1119, 1034, 818, 725, 679, 501, 424; HRMS (ESI<sup>+</sup>) calculated for  $\text{C}_{17}\text{H}_{15}\text{N}_2\text{O}_3$  [ $\text{M}+\text{H}^+$ ], 295.1077; Found 295.1064.

***2-(1H-indol-3-yl)-2-oxo-N-(4-methoxybenzyl)acetamide (AP-5)***

Yield 91%; White solid; m.p: 158-160°C; <sup>1</sup>H NMR (400 MHz, DMSO-*d*<sub>6</sub>)  $\delta$  12.31 (s, 1H), 9.24 (t,  $J = 6.3$  Hz, 1H), 8.77 (s, 1H), 8.34-8.07 (m, 1H), 7.69-7.45 (m, 2H), 7.45-7.13 (m, 3H), 6.90 (d,  $J = 3.2$  Hz, 2H), 4.36 (d,  $J = 6.1$  Hz, 2H), 3.73 (s, 3H); <sup>13</sup>C NMR (100 MHz, DMSO-*d*<sub>6</sub>)  $\delta$  182.6, 163.9, 158.7, 138.9, 136.7, 131.4, 129.2, 126.6, 124.3, 123.3, 121.7, 114.1, 113.0, 112.8, 55.5, 41.9; IR (KBr,  $\nu$ ,  $\text{cm}^{-1}$ ): 3757, 3271, 2577, 2369, 1736, 1612, 1497,

1412, 1319, 1242, 1134, 1034, 833, 733, 664, 517, 424; HRMS (ESI<sup>+</sup>) calculated for C<sub>18</sub>H<sub>17</sub>N<sub>2</sub>O<sub>3</sub> [M+H<sup>+</sup>], 309.1234; Found 309.1225.

**2-(1*H*-indol-3-yl)-2-oxo-*N*-(3,4,5-trimethoxyphenyl)acetamide (AP-6)**

Yield 81%; Light brown solid; m.p: 201-203°C; <sup>1</sup>H NMR (400 MHz, DMSO-*d*<sub>6</sub>) δ 12.38 (s, 1H), 10.58 (s, 1H), 8.84 (s, 1H), 8.29 (dd, *J* = 6.1, 3.1 Hz, 1H), 7.57 (dd, *J* = 6.1, 3.1 Hz, 1H), 7.35 (s, 2H), 7.30 (dd, *J* = 6.1, 3.2 Hz, 2H), 3.78 (s, 6H), 3.65 (s, 3H); <sup>13</sup>C NMR (100 MHz, DMSO-*d*<sub>6</sub>) δ 182.0, 162.3, 153.1, 139.2, 136.8, 134.6, 134.5, 126.7, 124.0, 123.2, 121.7, 113.1, 112.3, 98.4, 60.5, 56.2; IR (KBr, ν, cm<sup>-1</sup>): 3402, 2832, 2353, 2099, 1867, 1574, 1412, 1342, 1227, 1126, 1103, 818, 671, 463; HRMS (ESI<sup>+</sup>) calculated for C<sub>19</sub>H<sub>19</sub>N<sub>2</sub>O<sub>5</sub> [M+H<sup>+</sup>], 355.1288; Found 355.1278.

**2-(1*H*-indol-3-yl)-2-oxo-*N*-(4-bromophenyl)acetamide (AP-7)**

Yield 84%; Yellowish white solid; m.p: 282-285°C; <sup>1</sup>H NMR (400 MHz, DMSO-*d*<sub>6</sub>) δ 12.38 (s, 1H), 10.86 (s, 1H), 8.77 (s, 1H), 8.34-8.25 (m, 1H), 7.86 (d, *J* = 8.9 Hz, 2H), 7.62-7.52 (m, 3H), 7.35-7.26 (m, 2H); <sup>13</sup>C NMR (100 MHz, DMSO-*d*<sub>6</sub>) δ 182.0, 162.8, 139.1, 137.9, 136.8, 132.0, 126.6, 124.0, 123.2, 122.6, 121.6, 116.5, 113.1, 112.3; IR (KBr, ν, cm<sup>-1</sup>): 3750, 3310, 2978, 2369, 1890, 1659, 1582, 1443, 1242, 1142, 1011, 872, 818, 741, 656, 501; HRMS (ESI<sup>+</sup>) calculated for C<sub>16</sub>H<sub>12</sub>BrN<sub>2</sub>O<sub>2</sub> [M+H<sup>+</sup>], 343.0004; Found 343.0043

**2-(1*H*-indol-3-yl)-2-oxo-*N*-(3,4-dichlorophenyl)acetamide (AP-8)**

Yield 94%; Pale yellow solid; m.p: 282-284°C; <sup>1</sup>H NMR (400 MHz, DMSO-*d*<sub>6</sub>) δ 12.41 (s, 1H), 11.03 (s, 1H), 8.80 (s, 1H), 8.34-8.23 (m, 2H), 7.85 (dd, *J* = 8.8, 2.5 Hz, 1H), 7.65 (d, *J* = 8.9 Hz, 1H), 7.61-7.52 (m, 1H), 7.35-7.26 (m, 2H); <sup>13</sup>C NMR (100 MHz, DMSO-*d*<sub>6</sub>) δ 181.5, 162.9, 139.3, 138.7, 136.8, 131.4, 131.1, 126.6, 126.2, 124.1, 123.3, 121.9, 121.6, 120.8, 113.1, 112.2; IR (KBr, ν, cm<sup>-1</sup>): 3927, 3372, 2978, 2353, 1883, 1690, 1574, 1497, 1435, 1227, 1126, 1018, 926, 802, 741, 640; HRMS (ESI<sup>+</sup>) calculated for C<sub>16</sub>H<sub>11</sub>Cl<sub>2</sub>N<sub>2</sub>O<sub>2</sub> [M+H<sup>+</sup>], 333.0192; Found 333.0177.

**2-(1*H*-indol-3-yl)-2-oxo-*N*-(4-fluorophenyl)acetamide (AP-9)**

Yield 84%; Pale yellow solid; m.p: 268-270°C; <sup>1</sup>H NMR (400 MHz, DMSO-*d*<sub>6</sub>) δ 12.40 (s, 1H), 10.81 (s, 1H), 8.81 (s, 1H), 8.45-8.18 (m, 1H), 7.93 (dd, *J* = 8.7, 4.8 Hz, 2H), 7.66-7.50 (m, 1H), 7.42-7.06 (m, 4H); <sup>13</sup>C NMR (100 MHz, DMSO-*d*<sub>6</sub>) δ 182.2, 162.6, 160.2, 157.8, 139.1, 136.8, 134.9, 126.6, 124.0, 123.2, 122.6, 121.7, 115.9, 113.1; IR (KBr, ν, cm<sup>-1</sup>): 3726, 3140, 2554, 2369, 1883, 1751, 1674, 1574, 1497, 1412, 1242, 1142, 1011, 818, 656, 486; HRMS (ESI<sup>+</sup>) calculated for C<sub>16</sub>H<sub>12</sub>FN<sub>2</sub>O<sub>2</sub> [M+H<sup>+</sup>], 283.0877; Found 283.0862.

### **2-(5-methoxy-1H-indol-3-yl)-2-oxo-N-(3,4-dimethylphenyl)acetamide (AP-10)**

Yield 93%; Brownish yellow solid; m.p: 210-212°C; <sup>1</sup>H NMR (400 MHz, DMSO-*d*<sub>6</sub>) δ 12.24 (s, 1H), 10.49 (s, 1H), 8.70 (s, 1H), 7.81 (d, *J* = 2.5 Hz, 1H), 7.67 (d, *J* = 2.1 Hz, 1H), 7.55 (d, *J* = 2.2 Hz, 1H), 7.46 (d, *J* = 8.8 Hz, 1H), 7.12 (d, *J* = 8.2 Hz, 1H), 6.93 (dd, *J* = 8.8, 2.6 Hz, 1H), 3.82 (s, 3H), 2.23 (s, 3H), 2.20 (s, 3H); <sup>13</sup>C NMR (100 MHz, DMSO-*d*<sub>6</sub>) δ 182.3, 162.6, 156.5, 138.9, 136.8, 136.2, 132.5, 131.5, 130.0, 127.6, 121.7, 118.1, 113.8, 113.4, 112.3, 103.7, 55.7, 20.1, 19.3; IR (KBr, ν, cm<sup>-1</sup>): 3935, 3719, 3672, 2970, 2353, 2129, 2006, 1813, 1582, 1435, 1342, 1111, 1057, 995, 679, 501, 455; HRMS (ESI<sup>+</sup>) calculated for C<sub>19</sub>H<sub>19</sub>N<sub>2</sub>O<sub>3</sub> [M+H<sup>+</sup>], 323.1390; Found 323.1375.

### **2-(5-methoxy-1H-indol-3-yl)-2-oxo-N-(4-methoxyphenyl)acetamide (AP-11)**

Yield 82%; Greenish yellow solid; m.p: 242-244°C; <sup>1</sup>H NMR (400 MHz, DMSO-*d*<sub>6</sub>) δ 12.24 (s, 1H), 10.56 (s, 1H), 8.73 (d, *J* = 2.8 Hz, 1H), 7.92-7.71 (m, 3H), 7.47 (d, *J* = 8.8 Hz, 1H), 7.02-6.88 (m, 3H), 3.82 (s, 3H), 3.75 (s, 3H); <sup>13</sup>C NMR (100 MHz, DMSO-*d*<sub>6</sub>) δ 182.3, 162.3, 156.5, 156.3, 138.9, 131.6, 131.5, 127.6, 122.0, 114.3, 113.8, 113.3, 112.3, 103.8, 55.7, 55.6; IR (KBr, ν, cm<sup>-1</sup>): 3750, 3418, 2978, 2369, 1805, 1651, 1558, 1420, 1296, 1142, 1018, 1011, 818, 656, 463, 424; HRMS (ESI<sup>+</sup>) calculated for C<sub>18</sub>H<sub>17</sub>N<sub>2</sub>O<sub>4</sub> [M+H<sup>+</sup>], 325.1183; Found 325.1169.

### **2-(5-methoxy-1H-indol-3-yl)-2-oxo-N-(4-methoxybenzyl)acetamide (AP-12)**

Yield 94%; Light brown solid; m.p: 201-203°C; <sup>1</sup>H NMR (400 MHz, DMSO-*d*<sub>6</sub>) δ 12.15 (s, 1H), 9.20 (t, *J* = 6.3 Hz, 1H), 8.69 (s, 1H), 7.75 (d, *J* = 2.57 Hz, 1H), 7.44 (d, *J* = 8.8 Hz, 1H), 7.26 (d, *J* = 8.0 Hz, 2H), 6.94-6.86 (m, 3H), 4.35 (d, *J* = 6.3 Hz, 2H), 3.80 (s, 3H), 3.73 (s, 3H); <sup>13</sup>C NMR (100 MHz, DMSO-*d*<sub>6</sub>) δ 182.4, 164.0, 158.7, 156.4, 138.8, 131.4, 131.4, 129.1, 127.6, 114.1, 113.7, 113.3, 112.3, 103.8, 55.7, 55.5, 41.9; IR (KBr, ν, cm<sup>-1</sup>): 3767, 3242, 2926, 2717, 2362, 2138, 1992, 1876, 1814, 1582, 1443, 1250, 1135, 1027, 818, 486; HRMS (ESI<sup>+</sup>) calculated for C<sub>19</sub>H<sub>19</sub>N<sub>2</sub>O<sub>4</sub> [M+H<sup>+</sup>], 339.1339; Found 339.1324.

### **2-(5-methoxy-1H-indol-3-yl)-2-oxo-N-(3,4,5-trimethoxyphenyl)acetamide (AP-13)**

Yield 86%; Brownish yellow solid; m.p: 207-209°C; <sup>1</sup>H NMR (400 MHz, DMSO-*d*<sub>6</sub>) δ 12.27 (s, 1H), 10.56 (s, 1H), 8.76 (d, *J* = 3.0 Hz, 1H), 7.81 (s, 1H), 7.46 (d, *J* = 8.8 Hz, 1H), 7.34 (s, 2H), 6.93 (d, *J* = 8.8 Hz, 1H), 3.82 (s, 3H), 3.78 (s, 6H), 3.36 (s, 3H); <sup>13</sup>C NMR (100 MHz, DMSO-*d*<sub>6</sub>) δ 181.8, 162.4, 156.5, 153.1, 139.1, 134.6, 134.5, 131.5, 127.7, 113.9, 113.4, 112.2, 103.8, 98.4, 60.5, 56.2, 55.7; IR (KBr, ν, cm<sup>-1</sup>): 3935, 3696, 2955, 2361, 2021, 1579, 1443, 1126, 1049, 995, 872, 679, 656, 455; HRMS (ESI<sup>+</sup>) calculated for C<sub>20</sub>H<sub>21</sub>N<sub>2</sub>O<sub>6</sub> [M+H<sup>+</sup>], 385.1394; Found 385.1385.

**2-(5-methoxy-1H-indol-3-yl)-2-oxo-N-(3,4-dichlorophenyl)acetamide (AP-14)**

Yield 87%; Yellow solid; m.p: 272-274°C; <sup>1</sup>H NMR (400 MHz, DMSO-*d*<sub>6</sub>) δ 12.32 (s, 1H), 11.01 (s, 1H), 8.73 (s, 1H), 8.26 (s, 1H), 7.88-7.78 (m, 2H), 7.63 (d, *J* = 8.8 Hz, 1H), 7.47 (d, *J* = 8.8 Hz, 1H), 6.93 (d, *J* = 8.8, 2.6 Hz, 1H), 3.82 (s, 3H); <sup>13</sup>C NMR (100 MHz, DMSO-*d*<sub>6</sub>) δ 181.2, 162.9, 156.6, 139.1, 138.7, 131.5, 131.4, 131.1, 127.6, 126.2, 121.8, 120.7, 113.9, 113.4, 112.1, 103.8, 55.7; IR (KBr  $\nu$ , cm<sup>-1</sup>): 3742, 3341, 2832, 2361, 1697, 1566, 1504, 1404, 1265, 1250, 1188, 1119, 1034, 818, 679; HRMS (ESI<sup>+</sup>) calculated for C<sub>17</sub>H<sub>13</sub>Cl<sub>2</sub>N<sub>2</sub>O<sub>3</sub> [M+H<sup>+</sup>], 363.0298; Found 363.0287.

**2-(5-methoxy-1H-indol-3-yl)-2-oxo-N-(4-fluorophenyl)acetamide (AP-15)**

Yield 82%; Greenish yellow solid; m.p: 242-245°C; <sup>1</sup>H NMR (400 MHz, DMSO-*d*<sub>6</sub>) δ 12.32 (s, 1H), 10.76 (s, 1H), 8.73 (s, 1H), 7.96-7.86 (m, 2H), 7.83 (d, *J* = 2.5 Hz, 1H), 7.49 (d, *J* = 8.8 Hz, 1H), 7.23 (m, 2H), 6.93 (dd, *J* = 8.8, 2.5 Hz, 1H), 3.82 (s, 3H); <sup>13</sup>C NMR (100 MHz, DMSO-*d*<sub>6</sub>) δ 181.8, 162.7, 160.2, 157.8, 156.5, 139.4, 135.0, 131.9, 127.8, 122.5, 115.9, 114.0, 113.3, 103.8, 55.6; IR (KBr,  $\nu$ , cm<sup>-1</sup>): 3719, 3163, 2832, 2353, 1666, 1574, 1412, 1265, 1227, 1142, 1026, 926, 810, 664, 486, 424; HRMS (ESI<sup>+</sup>) calculated for C<sub>17</sub>H<sub>14</sub>FN<sub>2</sub>O<sub>3</sub> [M+H<sup>+</sup>], 313.0983; Found 313.0970.

**2-(1-benzyl-1H-indol-3-yl)-2-oxo-N-phenylacetamide (AP-16)**

Yield 86%; Creamy white solid; m.p: 142-143°C; <sup>1</sup>H NMR (400 MHz, DMSO-*d*<sub>6</sub>) δ 10.70 (s, 1H), 9.01 (s, 1H), 8.44-8.22 (m, 1H), 7.99-7.80 (m, 2H), 7.69-7.57 (m, 1H), 7.47-7.26 (m, 9H), 7.16 (t, *J* = 7.4 Hz, 1H), 5.63 (s, 2H); <sup>13</sup>C NMR (100 MHz, DMSO-*d*<sub>6</sub>) δ 182.2, 162.6, 141.7, 138.4, 137.1, 136.8, 129.2, 129.2, 128.3, 127.8, 127.3, 124.7, 124.2, 123.6, 121.9, 120.7, 112.1, 111.7, 50.3; IR (KBr,  $\nu$ , cm<sup>-1</sup>): 3935, 3572, 2353, 2122, 2021, 1821, 1589, 1504, 1435, 1381, 1342, 1242, 1150, 1049, 872, 679, 494, 424; HRMS (ESI<sup>+</sup>) calculated for C<sub>23</sub>H<sub>19</sub>N<sub>2</sub>O<sub>2</sub> [M+H<sup>+</sup>], 355.1441; Found 355.1428.

**2-(1-benzyl-1H-indol-3-yl)-2-oxo-N-(*p*-tolyl)acetamide (AP-17)**

Yield 88%; Off-white solid; m.p: 160-162°C; <sup>1</sup>H NMR (400 MHz, DMSO-*d*<sub>6</sub>) δ 10.64 (s, 1H), 9.02 (s, 1H), 8.37-8.28 (m, 1H), 7.77 (d, *J* = 8.5 Hz, 2H), 7.67-7.58 (m, 1H), 7.40-7.24 (m, 7H), 7.19 (d, *J* = 8.2 Hz, 2H), 5.62 (s, 2H), 2.29 (s, 3H); <sup>13</sup>C NMR (100 MHz, DMSO-*d*<sub>6</sub>) δ 182.2, 162.6, 141.7, 137.1, 136.7, 135.9, 133.7, 129.7, 129.2, 128.3, 127.8, 127.3, 124.1, 123.6, 122.0, 120.6, 112.1, 111.7, 50.3, 21.0; IR (KBr,  $\nu$ , cm<sup>-1</sup>): 3942, 3373, 2978, 2361, 2129, 2029, 1813, 1659, 1582, 1435, 1165, 1072, 679, 672, 618, 471; HRMS (ESI<sup>+</sup>) calculated for C<sub>24</sub>H<sub>21</sub>N<sub>2</sub>O<sub>2</sub> [M+H<sup>+</sup>], 369.1598; Found 369.1584.

### **2-(1-benzyl-1H-indol-3-yl)-2-oxo-N-(3,4-dimethylphenyl)acetamide (AP-18)**

Yield 87%; Yellowish white solid; m.p: 180-182°C; <sup>1</sup>H NMR (400 MHz, DMSO-*d*<sub>6</sub>) δ 10.55 (s, 1H), 9.04 (s, 1H), 8.37-8.28 (m, 1H), 7.71 (d, *J* = 2.2 Hz, 1H), 7.67-7.53 (m, 2H), 7.40-7.24 (m, 7H), 7.13 (d, *J* = 8.2 Hz, 1H), 5.62 (s, 2H), 2.23 (s, 3H), 2.20 (s, 3H); <sup>13</sup>C NMR (100 MHz, DMSO-*d*<sub>6</sub>) δ 182.2, 162.4, 141.7, 137.1, 136.8, 136.2, 132.5, 130.2, 130.0, 129.2, 128.3, 127.8, 127.4, 124.1, 123.6, 122.0, 118.2, 116.0, 112.1, 111.9, 50.3, 20.1, 19.3; IR (KBr, ν, cm<sup>-1</sup>): 3726, 3140, 2554, 2369, 1883, 1751, 1674, 1574, 1497, 1412, 1242, 1142, 1011, 818, 656, 486, 417; HRMS (ESI<sup>+</sup>) calculated for C<sub>25</sub>H<sub>23</sub>N<sub>2</sub>O<sub>2</sub> [M+H<sup>+</sup>], 383.1754; Found 383.1744.

### **2-(1-benzyl-1H-indol-3-yl)-2-oxo-N-(4-methoxyphenyl)acetamide (AP-19)**

Yield 91%; Creamy yellow solid; m.p: 170-172°C; <sup>1</sup>H NMR (400 MHz, DMSO-*d*<sub>6</sub>) δ 10.61 (s, 1H), 9.03 (s, 1H), 8.36-8.27 (m, 1H), 7.84-7.75 (m, 2H), 7.67-7.58 (m, 1H), 7.40-7.24 (m, 8H), 7.00-6.91 (m, 1H), 5.62 (s, 2H), 3.76 (s, 3H); <sup>13</sup>C NMR (100 MHz, DMSO-*d*<sub>6</sub>) δ 182.3, 162.1, 156.3, 141.7, 137.1, 136.7, 131.6, 129.2, 128.3, 127.8, 127.4, 124.1, 123.6, 122.1, 121.9, 114.3, 112.1, 111.8, 55.6, 50.3; IR (KBr, ν, cm<sup>-1</sup>): 3927, 3426, 2978, 2369, 2137, 1798, 1558, 1420, 1250, 1157, 1018, 818, 640, 463; HRMS (ESI<sup>+</sup>) calculated for C<sub>24</sub>H<sub>21</sub>N<sub>2</sub>O<sub>3</sub> [M+H<sup>+</sup>], 385.1547; Found 385.1536.

### **2-(1-benzyl-1H-indol-3-yl)-2-oxo-N-(4-methoxybenzyl)acetamide (AP-20)**

Yield 90%; White solid; m.p: 168-170°C; <sup>1</sup>H NMR (400 MHz, DMSO-*d*<sub>6</sub>) δ 9.28 (t, *J* = 6.4 Hz, 1H), 9.01 (d, *J* = 0.8 Hz, 1H), 8.32-8.23 (m, 1H), 7.65-7.56 (m, 1H), 7.39-7.23 (m, 9H), 6.94-6.84 (m, 2H), 5.60 (s, 2H), 4.36 (d, *J* = 6.3 Hz, 2H), 3.73 (s, 3H); <sup>13</sup>C NMR (100 MHz, DMSO-*d*<sub>6</sub>) δ 182.3, 163.7, 158.7, 141.6, 137.1, 136.7, 131.4, 129.2, 129.2, 128.2, 127.8, 127.3, 124.0, 123.4, 122.0, 114.1, 112.0, 112.0, 55.5, 50.2, 42.0; IR (KBr, ν, cm<sup>-1</sup>): 3372, 2963, 2369, 2114, 1883, 1690, 1507, 1427, 1250, 1165, 1003, 802, 687, 447; HRMS (ESI<sup>+</sup>) calculated for C<sub>25</sub>H<sub>23</sub>N<sub>2</sub>O<sub>3</sub> [M+H<sup>+</sup>], 399.1703; Found 399.1691.

### **2-(1-benzyl-1H-indol-3-yl)-2-oxo-N-(3,4,5-trimethoxyphenyl)acetamide (AP-21)**

Yield 83%; Yellow solid; m.p: 180-182°C; <sup>1</sup>H NMR (400 MHz, DMSO-*d*<sub>6</sub>) δ 10.59 (s, 1H), 9.11 (s, 1H), 8.37-8.29 (m, 1H), 7.66-7.57 (m, 1H), 7.39-7.24 (m, 9H), 5.64 (s, 2H), 3.79 (s, 6H), 3.66 (s, 3H); <sup>13</sup>C NMR (100 MHz, DMSO-*d*<sub>6</sub>) δ 181.7, 162.1, 153.1, 141.9, 137.2, 136.7, 134.6, 134.5, 129.2, 128.2, 127.7, 127.4, 124.2, 123.6, 122.0, 112.1, 111.7, 98.5, 60.6, 56.2, 50.3; IR (KBr, ν, cm<sup>-1</sup>): 3935, 3750, 3433, 2361, 2129, 1875, 1558, 1420, 1242, 1096, 1011, 818, 656, 463; HRMS (ESI<sup>+</sup>) calculated for C<sub>26</sub>H<sub>25</sub>N<sub>2</sub>O<sub>5</sub> [M+H<sup>+</sup>], 445.1758; Found 445.1747.

### **2-(1-benzyl-1H-indol-3-yl)-2-oxo-N-(4-bromophenyl)acetamide (AP-22)**

Yield 93%; Off-white solid; m.p: 201-203°C; <sup>1</sup>H NMR (400 MHz, DMSO-*d*<sub>6</sub>) δ 10.89 (s, 1H), 9.02 (s, 1H), 8.45-8.12 (m, 1H), 7.87 (d, *J* = 3.2 Hz, 2H), 7.67-7.61 (m, 1H), 7.58 (d, *J* = 2.2 Hz, 2H), 7.43-7.22 (m, 7H) 5.62 (s, 2H); <sup>13</sup>C NMR (100 MHz, DMSO-*d*<sub>6</sub>) δ 181.7, 162.7, 141.8, 137.9, 137.0, 136.8, 132.0, 129.2, 128.3, 127.8, 127.3, 124.2, 123.7, 122.9, 121.9, 116.6, 112.1, 111.7, 50.3; IR (KBr, ν, cm<sup>-1</sup>): 3950, 3773, 3418, 2932, 2369, 2014, 1690, 1574, 1427, 1204, 1165, 1065, 1011, 818, 733, 656, 463; HRMS (ESI<sup>+</sup>) calculated for C<sub>23</sub>H<sub>18</sub>BrN<sub>2</sub>O<sub>2</sub> [M+H<sup>+</sup>], 433.0546; Found 433.0532.

### **2-(1-benzyl-1H-indol-3-yl)-2-oxo-N-(3,4-dichlorophenyl)acetamide (AP-23)**

Yield 92%; White solid; m.p: 189-190°C; <sup>1</sup>H NMR (400 MHz, DMSO-*d*<sub>6</sub>) δ 11.07 (s, 1H), 9.06 (s, 1H), 8.35-8.31 (m, 1H), 8.30 (d, *J* = 2.4 Hz, 1H), 7.85 (dd, *J* = 8.8, 2.5 Hz, 1H), 7.71-7.58 (m, 2H), 7.40-7.24 (m, 7H), 5.62 (s, 2H); <sup>13</sup>C NMR (100 MHz, DMSO-*d*<sub>6</sub>) δ 181.2, 162.7, 142.0, 138.6, 137.0, 136.8, 131.4, 131.1, 129.2, 128.3, 127.8, 127.3, 126.3, 124.2, 123.7, 122.0, 121.9, 120.8, 112.2, 111.6, 50.3; IR (KBr, ν, cm<sup>-1</sup>): 3757, 3395, 2940, 2369, 2114, 1906, 1821, 1697, 1582, 1381, 1296, 1196, 1165, 818, 694, 463, 409; HRMS (ESI<sup>+</sup>) calculated for C<sub>23</sub>H<sub>17</sub>Cl<sub>2</sub>N<sub>2</sub>O<sub>2</sub> [M+H<sup>+</sup>], 423.0662; Found 423.0651.

### **2-(1-benzyl-1H-indol-3-yl)-2-oxo-N-(4-fluorophenyl)acetamide (AP-24)**

Yield 84%; White solid; m.p: 182-184°C; <sup>1</sup>H NMR (400 MHz, DMSO-*d*<sub>6</sub>) δ 10.83 (s, 1H), 9.03 (s, 1H), 8.38-8.28 (m, 1H), 7.68-7.58 (m, 1H), 7.40-7.18 (m, 11H), 5.62 (s, 2H); <sup>13</sup>C NMR (100 MHz, DMSO-*d*<sub>6</sub>) δ 182.0, 162.4, 158.8, 141.8, 137.0, 134.9, 129.2, 128.3, 127.8, 127.3, 124.2, 123.6, 122.8, 122.0, 115.9, 115.7, 112.1, 111.7, 50.3; IR (KBr, ν, cm<sup>-1</sup>): 3750, 3287, 3148, 2932, 2832, 2353, 1890, 1628, 1574, 1512, 1404, 1219, 1157, 818, 679, 501, 471; HRMS (ESI<sup>+</sup>) calculated for C<sub>23</sub>H<sub>18</sub>FN<sub>2</sub>O<sub>2</sub> [M+H<sup>+</sup>], 373.1347; Found 373.1336.

### **2-(1-ethyl-1H-indol-3-yl)-2-oxo-N-phenylacetamide (AP-25)**

Yield 87%; Creamy white solid; m.p: 111-113°C; <sup>1</sup>H NMR (400 MHz, DMSO-*d*<sub>6</sub>) δ 10.71 (s, 1H), 8.85 (s, 1H), 8.37-8.28 (m, 1H), 7.88 (d, *J* = 7.4 Hz, 2H), 7.74-7.64 (m, 1H), 7.44-7.30 (m, 4H), 7.15 (t, *J* = 7.4 Hz, 1H), 4.38 (q, *J* = 7.2 Hz, 2H), 1.43 (t, *J* = 7.2 Hz, 3H); <sup>13</sup>C NMR (100 MHz, DMSO-*d*<sub>6</sub>) δ 181.9, 162.8, 140.9, 138.5, 136.5, 129.2, 127.3, 124.7, 124.1, 123.5, 121.9, 120.6, 111.7, 111.4, 41.9, 15.6; IR (KBr, ν, cm<sup>-1</sup>): 3823, 3291, 2689, 2355, 2106, 1701, 1555, 1396, 1312, 1219, 1165, 866, 689; HRMS (ESI<sup>+</sup>) calculated for C<sub>18</sub>H<sub>17</sub>N<sub>2</sub>O<sub>2</sub> [M+H<sup>+</sup>], 293.1212; Found 293.1278.

### **2-(1-ethyl-1H-indol-3-yl)-2-oxo-N-(p-tolyl)acetamide (AP-26)**

Yield 84%; Creamy white solid; m.p: 160-162°C; <sup>1</sup>H NMR (400 MHz, DMSO-*d*<sub>6</sub>) δ 10.53 (s, 1H), 8.84 (s, 1H), 8.37-8.28 (m, 1H), 7.79-7.72 (m, 2H), 7.72-7.63 (m, 1H), 7.41-7.29



(m, 2H), 7.19 (d,  $J = 8.2$  Hz, 2H), 4.38 (q,  $J = 7.2$  Hz, 2H), 2.30 (s, 3H), 1.44 (t,  $J = 7.2$  Hz, 3H);  $^{13}\text{C}$  NMR (100 MHz, DMSO- $d_6$ )  $\delta$  182.0, 162.5, 140.9, 136.5, 136.0, 133.7, 129.5, 127.3, 124.0, 123.5, 122.0, 120.6, 111.6, 111.5, 41.9, 15.5, 15.5; IR (KBr,  $\nu$ ,  $\text{cm}^{-1}$ ): 3792, 3277, 2978, 2405, 2318, 1935, 1838, 1614, 1377, 1312, 1219, 1043, 957, 829; HRMS (ESI $^+$ ) calculated for  $\text{C}_{19}\text{H}_{19}\text{N}_2\text{O}_2$  [ $\text{M}+\text{H}^+$ ], 307.1368; Found 307.1434.

**2-(1-ethyl-1H-indol-3-yl)-2-oxo-N-(3,4-dimethylphenyl)acetamide (AP-27)**

Yield 81%; Creamy yellow solid; m.p: 147-149°C;  $^1\text{H}$  NMR (400 MHz, DMSO- $d_6$ )  $\delta$  10.53 (s, 1H), 8.86 (s, 1H), 8.36-8.27 (m, 1H), 7.73-7.64 (m, 2H), 7.56 (dd,  $J = 8.1, 2.3$  Hz, 1H), 7.41-7.29 (m, 2H), 7.12 (d,  $J = 8.2$  Hz, 1H), 4.38 (q,  $J = 7.2$  Hz, 2H), 2.23 (s, 3H), 2.20 (s, 3H), 1.43 (t,  $J = 7.2$  Hz, 3H);  $^{13}\text{C}$  NMR (100 MHz, DMSO- $d_6$ )  $\delta$  182.0, 162.5, 140.9, 136.8, 136.5, 136.2, 132.5, 130.0, 127.3, 124.0, 123.5, 121.9, 121.7, 118.1, 111.6, 111.4, 41.9, 20.1, 19.3, 15.6; IR (KBr,  $\nu$ ,  $\text{cm}^{-1}$ ): 3686, 3312, 2355, 2299, 2106, 1680, 1574, 1504, 1381, 1219, 1184, 991, 789, 602; HRMS (ESI $^+$ ) calculated for  $\text{C}_{20}\text{H}_{21}\text{N}_2\text{O}_2$  [ $\text{M}+\text{H}^+$ ], 321.1525; Found 321.1599.

**2-(1-ethyl-1H-indol-3-yl)-2-oxo-N-(4-methoxyphenyl)acetamide (AP-28)**

Yield 73%; Yellowish green solid; m.p: 178-180°C;  $^1\text{H}$  NMR (400 MHz, DMSO- $d_6$ )  $\delta$  10.51 (s, 1H), 8.89 (s, 1H), 8.34-8.26 (m, 1H), 7.73 (d,  $J = 8.4$  Hz, 2H), 7.72-7.63 (m, 1H), 7.41-7.29 (m, 2H), 7.19 (d,  $J = 8.2$  Hz, 2H), 4.37 (q,  $J = 7.1$  Hz, 2H), 3.80 (s, 3H), 1.44 (t,  $J = 7.1$  Hz, 3H);  $^{13}\text{C}$  NMR (100 MHz, DMSO- $d_6$ )  $\delta$  182.0, 162.2, 156.3, 140.9, 136.4, 131.6, 127.3, 124.0, 123.5, 122.1, 122.0, 114.3, 111.6, 111.5, 55.6, 41.9, 15.5; IR (KBr,  $\nu$ ,  $\text{cm}^{-1}$ ): 3645, 3291, 2830, 2355, 2318, 1711, 1595, 1381, 1222, 1165, 1097, 1022, 851, 799, 673, 440; HRMS (ESI $^+$ ) calculated for  $\text{C}_{19}\text{H}_{19}\text{N}_2\text{O}_3$  [ $\text{M}+\text{H}^+$ ], 323.1317; Found 323.1386.

**2-(1-ethyl-1H-indol-3-yl)-2-oxo-N-(4-methoxybenzyl)acetamide (AP-29)**

Yield 68%; Creamy white solid; m.p: 90-93°C;  $^1\text{H}$  NMR (400 MHz, DMSO- $d_6$ )  $\delta$  10.56 (t,  $J = 6.2$  Hz, 1H), 8.87 (s, 1H), 8.37-8.24 (m, 1H), 7.68 (d,  $J = 8.4$  Hz, 2H), 7.72-7.63 (m, 1H), 7.41-7.29 (m, 2H), 7.17 (d,  $J = 8.2$  Hz, 2H), 4.48 (d,  $J = 6.1$  Hz, 2H), 4.37 (q,  $J = 7.1$  Hz, 2H), 3.80 (s, 3H), 1.44 (t,  $J = 7.1$  Hz, 3H);  $^{13}\text{C}$  NMR (100 MHz, DMSO- $d_6$ )  $\delta$  182.0, 163.8, 158.7, 140.8, 136.4, 131.4, 129.2, 127.3, 123.9, 123.3, 122.0, 114.1, 111.6, 111.5, 55.5, 41.9, 41.8, 15.5; IR (KBr,  $\nu$ ,  $\text{cm}^{-1}$ ): 3736, 3343, 2355, 2334, 1842, 1736, 1504, 1468, 1362, 1184, 1028, 826, 673, 530, 440; HRMS (ESI $^+$ ) calculated for  $\text{C}_{20}\text{H}_{21}\text{N}_2\text{O}_3$  [ $\text{M}+\text{H}^+$ ], 337.1474; Found 337.1535.

**2-(1-ethyl-1H-indol-3-yl)-2-oxo-N-(3,4,5-trimethoxyphenyl)acetamide (AP-30)**

Yield 84%; Creamy yellow solid; m.p: 153-155°C;  $^1\text{H}$  NMR (400 MHz, DMSO- $d_6$ )  $\delta$  10.57 (s, 1H), 8.93 (s, 1H), 8.38-8.29 (m, 1H), 7.73-7.65 (m, 1H), 7.40-7.32 (m, 4H), 4.40 (q,  $J =$

7.2 Hz, 2H), 3.79 (s, 6H), 3.34 (s, 3H), 1.43 (t,  $J = 7.2$  Hz, 3H);  $^{13}\text{C}$  NMR (100 MHz, DMSO- $d_6$ )  $\delta$  181.4, 162.2, 153.1, 141.1, 136.4, 135.6, 134.6, 127.4, 124.1, 123.5, 122.0, 111.6, 111.3, 98.4, 60.6, 56.2, 41.9, 15.6; IR (KBr,  $\nu$ ,  $\text{cm}^{-1}$ ) 3611, 3312, 2340, 2318, 2106, 1736, 1645, 1574, 1412, 1234, 1128, 1007, 829, 652, 633; HRMS (ESI $^+$ ) calculated for  $\text{C}_{21}\text{H}_{23}\text{N}_2\text{O}_5$  [M+H $^+$ ], 383.1529; Found 383.3172.

**2-(1-ethyl-1H-indol-3-yl)-2-oxo-N-(4-bromophenyl)acetamide (AP-31)**

Yield 79%; Light yellow solid; m.p: 178-180°C;  $^1\text{H}$  NMR (400 MHz, DMSO- $d_6$ )  $\delta$  10.87 (s, 1H), 8.84 (s, 1H), 8.36-8.27 (m, 1H), 7.86 (d,  $J = 8.9$  Hz, 2H), 7.74-7.64 (m, 1H), 7.58 (d,  $J = 8.9$  Hz, 2H), 7.41-7.30 (m, 2H), 4.38 (q,  $J = 7.2$  Hz, 2H), 1.43 (t,  $J = 7.2$  Hz, 3H);  $^{13}\text{C}$  NMR (100 MHz, DMSO- $d_6$ )  $\delta$  181.5, 162.8, 141.0, 137.9, 132.0, 127.3, 124.1, 123.6, 119.2, 116.5, 111.7, 100.8, 41.9, 15.5; IR (KBr,  $\nu$ ,  $\text{cm}^{-1}$ ): 3611, 3312, 2922, 2355, 2106, 1857, 1686, 1524, 1418, 1381, 1240, 1150, 1007, 773, 667; HRMS (ESI $^+$ ) calculated for  $\text{C}_{18}\text{H}_{16}\text{BrN}_2\text{O}_2$  [M+H $^+$ ], 371.0317; Found 371.0377.

**2-(1-ethyl-1H-indol-3-yl)-2-oxo-N-(3,4-dichlorophenyl)acetamide (AP-32)**

Yield 91%; Light yellow solid; m.p: 162-163°C;  $^1\text{H}$  NMR (400 MHz, DMSO- $d_6$ )  $\delta$  11.05 (s, 1H), 8.88 (s, 1H), 8.35-8.26 (m, 2H), 7.84 (dd,  $J = 8.9, 2.4$  Hz, 1H), 7.75-7.61 (m, 2H), 7.42-7.30 (m, 2H), 4.39 (q,  $J = 7.2$  Hz, 2H), 1.43 (t,  $J = 7.2$  Hz, 3H);  $^{13}\text{C}$  NMR (100 MHz, DMSO- $d_6$ )  $\delta$  181.0, 162.9, 141.2, 138.6, 136.5, 131.4, 131.1, 127.3, 126.2, 124.2, 123.6, 121.9, 121.9, 120.8, 111.7, 111.2, 41.9, 15.6; IR (KBr,  $\nu$ ,  $\text{cm}^{-1}$ ): 3844, 3567, 3327, 2972, 2355, 2112, 1695, 1574, 1402, 1219, 1134, 1007, 935, 814, 667; HRMS (ESI $^+$ ) calculated for  $\text{C}_{18}\text{H}_{15}\text{Cl}_2\text{N}_2\text{O}_2$  [M+H $^+$ ], 361.0432; Found 361.0493.

**2-(1-ethyl-1H-indol-3-yl)-2-oxo-N-(4-fluorophenyl)acetamide (AP-33)**

Yield 91%; Brown solid; m.p: 150-152°C;  $^1\text{H}$  NMR (400 MHz, DMSO- $d_6$ )  $\delta$  10.81 (s, 1H), 8.85 (s, 1H), 8.36-8.27 (m, 1H), 7.96 – 7.85 (m, 2H), 7.74-7.65 (m, 1H), 7.41-7.30 (m, 2H), 7.29-7.18 (m, 2H), 4.38 (q,  $J = 7.2$  Hz, 2H), 1.43 (t,  $J = 7.2$  Hz, 3H);  $^{13}\text{C}$  NMR (100 MHz, DMSO- $d_6$ )  $\delta$  181.8, 162.6, 160.2, 157.8, 141.0, 136.5, 134.9, 127.3, 124.1, 123.5, 122.5, 121.9, 115.9, 111.7, 41.9, 15.6; IR (KBr,  $\nu$ ,  $\text{cm}^{-1}$ ) 3879, 3611, 3331, 2922, 2355, 2318, 2087, 1857, 1807, 1611, 1412, 1260, 1113, 1057, 814, 652; HRMS (ESI $^+$ ) calculated for  $\text{C}_{18}\text{H}_{16}\text{FN}_2\text{O}_2$  [M+H $^+$ ], 311.1118; Found 311.1176.

**2-(1-benzyl-1H-5-methoxyindol-3-yl)-2-oxo-N-(3,4-dimethylphenyl)acetamide (AP-34)**

Yield 83%; Off-white solid; m.p: 168-170°C;  $^1\text{H}$  NMR (400 MHz, DMSO- $d_6$ )  $\delta$  10.52 (s, 1H), 8.96 (s, 1H), 7.83 (d,  $J = 2.5$  Hz, 1H), 7.70 (s, 1H), 7.60-7.46 (m, 2H), 7.41-7.24 (m, 5H), 7.12 (d,  $J = 8.2$  Hz, 1H), 6.93 (dd,  $J = 9.0, 2.6$  Hz, 1H), 5.58 (s, 2H), 3.81 (s, 3H), 2.23 (s, 3H), 2.20 (s, 3H);  $^{13}\text{C}$  NMR (100 MHz, DMSO- $d_6$ )  $\delta$  182.0, 162.4, 156.8, 141.4, 137.1,

136.8, 136.2, 132.5, 131.0, 130.6, 129.1, 128.4, 128.2, 127.8, 121.7, 118.1, 113.4, 113.0, 111.5, 104.1, 55.7, 50.4, 20.1, 19.3; IR (KBr,  $\nu$ ,  $\text{cm}^{-1}$ ): 3927, 3750, 2932, 2777, 2361, 2006, 1913, 1852, 1713, 1582, 1474, 1435, 1342, 1265, 1165, 1111, 1057; HRMS (ESI<sup>+</sup>) calculated for  $\text{C}_{26}\text{H}_{25}\text{N}_2\text{O}_3$  [M+H<sup>+</sup>], 413.1860; Found 413.1849.

**2-(1-benzyl-1H-5-methoxyindol-3-yl)-2-oxo-N-(4-methoxyphenyl)acetamide (AP-35)**

Yield 89%; Light yellow solid; m.p: 152-154°C; <sup>1</sup>H NMR (400 MHz, DMSO-*d*<sub>6</sub>)  $\delta$  10.58 (s, 1H), 8.95 (s, 1H), 7.86-7.75 (m, 3H), 7.52 (d, *J* = 8.9 Hz, 1H), 7.40-7.24 (m, 5H), 7.02-6.89 (m, 3H), 5.58 (s, 2H), 3.81 (s, 3H), 3.76 (s, 3H); <sup>13</sup>C NMR (100 MHz, DMSO-*d*<sub>6</sub>)  $\delta$  182.0, 162.2, 156.8, 156.3, 141.6, 137.1, 131.6, 131.6, 129.2, 128.4, 128.2, 127.8, 126.8, 122.0, 114.3, 113.3, 113.0, 111.6, 104.2, 55.7, 50.4; IR (KBr,  $\nu$ ,  $\text{cm}^{-1}$ ): 3922, 3775, 3443, 2972, 2500, 2362, 2130, 1822, 1582, 1428, 1119, 1057, 996, 834, 641, 509; HRMS (ESI<sup>+</sup>) calculated for  $\text{C}_{25}\text{H}_{23}\text{N}_2\text{O}_4$  [M+H<sup>+</sup>], 415.1652; Found 415.1641.

**2-(1-benzyl-1H-5-methoxyindol-3-yl)-2-oxo-N-(4-methoxybenzyl)acetamide (AP-36)**

Yield 91%; Light brown solid; m.p: 160-162°C; <sup>1</sup>H NMR (400 MHz, DMSO-*d*<sub>6</sub>)  $\delta$  9.26 (t, *J* = 6.4 Hz 1H), 8.95 (s, 1H), 7.79 (s, 1H), 7.49 (d, *J* = 8.9 Hz, 1H), 7.39-7.24 (m, 7H), 6.97-6.86 (m, 3H), 5.55 (s, 2H), 4.36 (d, *J* = 6.3 Hz, 2H), 3.79 (s, 3H), 3.73 (s, 3H); <sup>13</sup>C NMR (100 MHz, DMSO-*d*<sub>6</sub>)  $\delta$  182.0, 163.8, 158.7, 156.8, 141.5, 138.5, 137.1, 131.5, 131.4, 129.2, 128.4, 128.2, 127.8, 114.1, 113.3, 112.8, 111.7, 104.2, 55.7, 55.5, 50.4, 41.9; IR (KBr,  $\nu$ ,  $\text{cm}^{-1}$ ): 3750, 3132, 2824, 2361, 1690, 1574, 1504, 1396, 1242, 1165, 1042, 856, 802, 648, 517; HRMS (ESI<sup>+</sup>) calculated for  $\text{C}_{26}\text{H}_{25}\text{N}_2\text{O}_4$  [M+H<sup>+</sup>], 429.1809; Found 429.1799.

**2-(1-benzyl-1H-5-methoxyindol-3-yl)-2-oxo-N-(3,4,5-trimethoxyphenyl)acetamide (AP-37)**

Yield 83%; Light yellow solid; m.p: 160-162°C; <sup>1</sup>H NMR (400 MHz, DMSO-*d*<sub>6</sub>)  $\delta$  10.59 (s, 1H), 9.04 (s, 1H), 7.84 (d, *J* = 2.6 Hz, 1H), 7.51 (d, *J* = 8.9 Hz, 1H), 7.39-7.25 (m, 7H), 6.93 (dd, *J* = 8.9, 2.6 Hz, 1H), 5.60 (s, 2H), 3.81 (s, 3H), 3.78 (s, 6H), 3.66 (s, 3H); <sup>13</sup>C NMR (100 MHz, DMSO-*d*<sub>6</sub>)  $\delta$  181.4, 162.1, 156.9, 153.1, 141.8, 137.2, 134.6, 134.5, 131.5, 129.2, 128.5, 128.2, 127.7, 113.4, 113.0, 111.4, 104.2, 98.3, 60.6, 56.2, 55.7, 50.4; IR (KBr,  $\nu$ ,  $\text{cm}^{-1}$ ): 3873, 2986, 2832, 2369, 2106, 1929, 1798, 1643, 1543, 1504, 1342, 1111, 1057, 679, 586, 501, 463; HRMS (ESI<sup>+</sup>) calculated for  $\text{C}_{27}\text{H}_{27}\text{N}_2\text{O}_6$  [M+H<sup>+</sup>], 475.1864; Found 475.1858.

**2-(1-benzyl-1H-5-methoxyindol-3-yl)-2-oxo-N-(3,4-dichlorophenyl)acetamide (AP-38)**

Yield 87%, Creamy yellow solid, m.p: 191-193°C; <sup>1</sup>H NMR (400 MHz, DMSO-*d*<sub>6</sub>)  $\delta$  11.05 (s, 1H), 8.98 (s, 1H), 8.28 (d, *J* = 2.4 Hz, 1H), 7.84 (dd, *J* = 8.7, 2.5 Hz, 2H), 7.65 (d, *J* = 8.8 Hz, 1H), 7.52 (d, *J* = 9.0 Hz, 1H), 7.40-7.24 (m, 5H), 6.94 (dd, *J* = 8.9, 2.6 Hz, 1H), 5.58 (s,

2H), 3.81 (s, 3H);  $^{13}\text{C}$  NMR (100 MHz, DMSO- $d_6$ )  $\delta$  180.9, 162.8, 156.9, 141.8, 138.6, 137.0, 131.6, 131.4, 131.1, 129.2, 128.4, 128.3, 127.8, 126.2, 121.8, 120.7, 113.4, 113.1, 111.3, 104.2, 55.7, 50.5; IR (KBr,  $\nu$ ,  $\text{cm}^{-1}$ ): 3757, 2978, 2770, 2361, 1875, 1713, 1582, 1497, 1342, 1265, 1165, 1057, 864, 679, 463; HRMS (ESI $^{+}$ ) calculated for  $\text{C}_{24}\text{H}_{19}\text{Cl}_2\text{N}_2\text{O}_3$   $[\text{M}+\text{H}^{+}]$ , 453.0767; Found 453.0755.

### 2-(1-benzyl-1H-5-methoxyindol-3-yl)-2-oxo-N-(4-fluorophenyl)acetamide (AP-39)

Yield 86%; White solid; m.p: 197-199°C;  $^1\text{H}$  NMR (400 MHz, DMSO- $d_6$ )  $\delta$  10.82 (s, 1H), 8.96 (s, 1H), 7.97-7.82 (m, 3H), 7.52 (d,  $J = 8.9$  Hz, 1H), 7.40-7.18 (m, 7H), 6.94 (dd,  $J = 8.9, 2.6$  Hz, 1H), 5.57 (s, 2H), 3.81 (s, 3H);  $^{13}\text{C}$  NMR (100 MHz, DMSO- $d_6$ )  $\delta$  181.7, 162.5, 160.2, 157.8, 156.9, 141.6, 137.1, 134.9, 131.6, 129.2, 128.4, 127.8, 122.5, 115.9, 113.4, 113.0, 111.4, 104.1, 55.7, 50.5; IR (KBr,  $\nu$ ,  $\text{cm}^{-1}$ ): 3742, 3140, 2361, 1875, 1674, 1636, 1504, 1389, 1265, 1211, 1057, 833, 664, 501, 424; HRMS (ESI $^{+}$ ) calculated for  $\text{C}_{24}\text{H}_{20}\text{FN}_2\text{O}_3$   $[\text{M}+\text{H}^{+}]$ , 403.1452; Found 403.1439.

### 7.3 | PL inhibition assay and enzyme kinetics

The procedure for PL inhibition assay and kinetics was performed as per the protocol detailed in chapter 4. Stock solutions of the synthesised analogues were prepared in DMSO at linear concentrations ranging from 1.56 - 2000  $\mu\text{g}/\text{mL}$ . The PL inhibitory profiles of all the analogues are summarized in Table 7.1. Most of the analogues exhibited potential ( $> 10$ -25  $\mu\text{M}$ ) to moderate (15-30  $\mu\text{M}$ ) activity. Analogue **AP-37** exhibited the most potent activity against PL, with an  $\text{IC}_{50}$  of 4.53  $\mu\text{M}$ , followed by **AP-21** and **AP-36** (4.92 and 5.12  $\mu\text{M}$ , respectively). Enzyme inhibition kinetics were performed for the most active analogues **AP-21**, **AP-36** and **AP-37**, each at three different concentrations (0, 5 and 10  $\mu\text{M}$ ), which indicated reversible competitive inhibition similar to carbazolyl oxoacetamide analogues (Fig. 7.3 and Table 7.2).

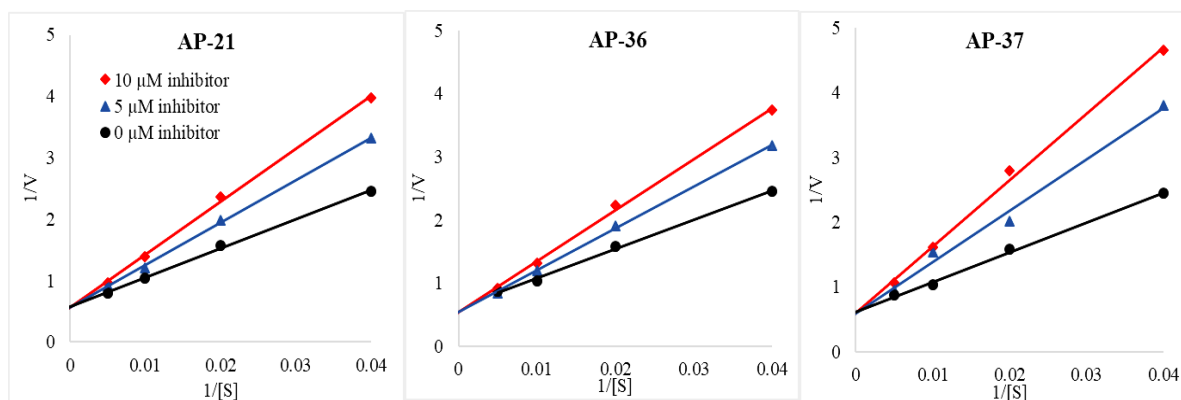


**Fig. 7.3.** Double reciprocal Lineweaver-Burk plots of analogues **AP-21**, **AP-36** and **AP-37** indicating reversible competitive inhibition

## Chapter 7

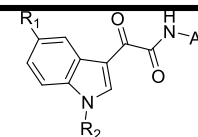


**Table 7.1.** *In vitro* PL inhibitory activities of indolyl oxoacetamide analogues **AP-1** to **AP-39**

#	R <sub>1</sub>	R <sub>2</sub>	Ar	IC <sub>50</sub> (μM)*	#	R <sub>1</sub>	R <sub>2</sub>	Ar	IC <sub>50</sub> (μM)*
<b>AP-1</b>	-H	-H	Phenyl	27.49 ± 1.68	<b>AP-20</b>	-H	Benzyl	4-Methoxybenzyl	5.83 ± 0.64
<b>AP-2</b>	-H	-H	4-Methylphenyl	26.13 ± 0.92	<b>AP-21</b>	-H	Benzyl	<b>3,4,5-Trimethoxyphenyl</b>	<b>4.92 ± 0.29</b>
<b>AP-3</b>	-H	-H	3,4-Dimethylphenyl	26.07 ± 1.14	<b>AP-22</b>	-H	Benzyl	4-Bromophenyl	25.76 ± 0.97
<b>AP-4</b>	-H	-H	4-Methoxyphenyl	23.72 ± 0.67	<b>AP-23</b>	-H	Benzyl	3,4-Dichlorophenyl	26.72 ± 0.79
<b>AP-5</b>	-H	-H	4-Methoxybenzyl	17.39 ± 0.53	<b>AP-24</b>	-H	Benzyl	4-Fluorophenyl	24.18 ± 0.86
<b>AP-6</b>	-H	-H	3,4,5-Trimethoxyphenyl	17.28 ± 0.49	<b>AP-25</b>	-H	Ethyl	Phenyl	21.92 ± 2.18
<b>AP-7</b>	-H	-H	4-Bromophenyl	43.36 ± 1.67	<b>AP-26</b>	-H	Ethyl	4-Methylphenyl	19.73 ± 2.01
<b>AP-8</b>	-H	-H	3,4-Dichlorophenyl	44.27 ± 1.21	<b>AP-27</b>	-H	Ethyl	3,4-Dimethylphenyl	18.85 ± 1.88
<b>AP-9</b>	-H	-H	4-Fluorophenyl	47.62 ± 1.48	<b>AP-28</b>	-H	Ethyl	4-Methoxyphenyl	20.63 ± 2.16
<b>AP-10</b>	-OCH <sub>3</sub>	-H	3,4-Dimethylphenyl	18.26 ± 0.58	<b>AP-29</b>	-H	Ethyl	4-Methoxybenzyl	17.24 ± 1.82
<b>AP-11</b>	-OCH <sub>3</sub>	-H	4-Methoxyphenyl	18.12 ± 0.43	<b>AP-30</b>	-H	Ethyl	3,4,5-Trimethoxyphenyl	12.74 ± 0.38
<b>AP-12</b>	-OCH <sub>3</sub>	-H	4-Methoxybenzyl	17.93 ± 0.39	<b>AP-31</b>	-H	Ethyl	4-Bromophenyl	39.72 ± 2.46
<b>AP-13</b>	-OCH <sub>3</sub>	-H	3,4,5-Trimethoxyphenyl	16.38 ± 0.26	<b>AP-32</b>	-H	Ethyl	3,4-Dichlorophenyl	28.37 ± 1.72
<b>AP-14</b>	-OCH <sub>3</sub>	-H	3,4-Dichlorophenyl	34.62 ± 0.94	<b>AP-33</b>	-H	Ethyl	4-Fluorophenyl	37.68 ± 2.47
<b>AP-15</b>	-OCH <sub>3</sub>	-H	4-Fluorophenyl	37.83 ± 0.98	<b>AP-34</b>	-OCH <sub>3</sub>	Benzyl	3,4-Dimethylphenyl	9.14 ± 0.69
<b>AP-16</b>	-H	Benzyl	Phenyl	18.24 ± 0.74	<b>AP-35</b>	-OCH <sub>3</sub>	Benzyl	4-Methoxyphenyl	6.28 ± 0.24
<b>AP-17</b>	-H	Benzyl	4-Methylphenyl	12.9 ± 0.58	<b>AP-36</b>	-OCH <sub>3</sub>	Benzyl	<b>4-Methoxybenzyl</b>	<b>5.12 ± 0.38</b>
<b>AP-18</b>	-H	Benzyl	3,4-Dimethylphenyl	10.62 ± 0.66	<b>AP-37</b>	-OCH <sub>3</sub>	Benzyl	<b>3,4,5-Trimethoxyphenyl</b>	<b>4.53 ± 0.47</b>
<b>AP-19</b>	-H	Benzyl	4-Methoxyphenyl	10.86 ± 0.71	<b>AP-38</b>	-OCH <sub>3</sub>	Benzyl	3,4-Dichlorophenyl	23.21 ± 0.93
<b>Orlistat</b>				0.99 ± 0.11	<b>AP-39</b>	-OCH <sub>3</sub>	Benzyl	4-Fluorophenyl	19.48 ± 0.76

\* All the experiments were performed in triplicate and the values are represented as mean ± SEM

**Table 7.2.**  $V_{\max}$ ,  $K_m$  and  $K_i$  values calculated from Lineweaver-Burk plots at different inhibitory concentrations [I] of **AP-21**, **AP-36** and **AP-37**

Analogue	$K_m$ (in $\mu\text{M}$ ) at different inhibitor concentrations [I]			$V_{\max}$ ( $\mu\text{M}/\text{min}$ )	$K_i$ ( $\mu\text{M}$ )
	0 $\mu\text{M}$	5 $\mu\text{M}$	10 $\mu\text{M}$		
<b>AP-21</b>	82.27	123.73	154.20	1.789	3.06
<b>AP-36</b>	81.11	122.77	150.92	1.823	3.27
<b>AP-37</b>	81.01	134.63	168.08	1.792	2.70

#### 7.4 | Structure activity relationship

The PL inhibitory activity of the indolyl oxoacetamide analogues **AP-1** to **AP-39** indicated a similar structure activity relationship as observed with the carbazolyl oxoacetamide analogues. As represented in Fig. 7.4, the presence of aromatic benzyl group on the indole significantly increased the PL inhibitory activity of analogues in comparison to the ethyl substitution and the unsubstituted counterparts. Further, an additional methoxysubstitution at the 5<sup>th</sup> position of the indole resulted in slight increase in the PL inhibitory potential. Similarly, the presence of ring activating groups on the aryl ring of the amide nitrogen resulted in better potency of the analogues. Moreover, the presence of a methylene bridge between the aryl extension and the amide nitrogen resulted in potent activity. As represented in Table 7.2, analogues **AP-20** and **AP-36** with 4-methoxybenzyl substitution on the amide nitrogen possessed comparatively potent  $\text{IC}_{50}$  values of 5.83  $\mu\text{M}$  and 5.12  $\mu\text{M}$ , while analogues **AP-19** and **AP-35** with 4-methoxyphenyl substitution exhibited comparatively lower potential ( $\text{IC}_{50}$  values of 10.86  $\mu\text{M}$  and 6.28  $\mu\text{M}$ ).

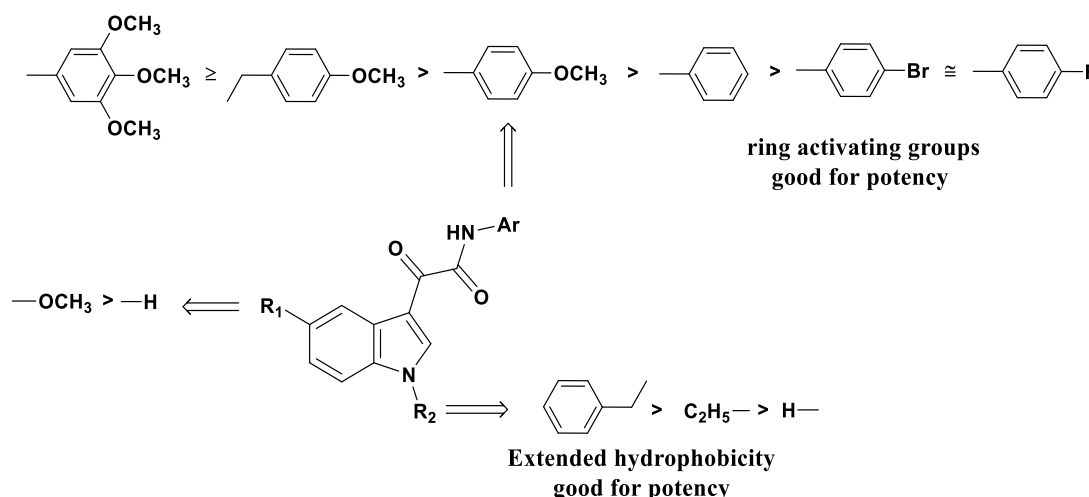


**Fig. 7.4.** Structure-activity relationship for indolyl oxoacetamide analogues **AP-1** to **AP-39**

### 7.5 | Molecular modelling studies

A total of 39 indolyl oxoacetamide analogues were subjected to molecular docking studies while the most active analogues **AP-21**, **AP-36** and **AP-37** were subjected to MD simulations. The MolDock scores and the various interactions exhibited by the indolyl oxoacetamide analogues are summarized in Table 7.3. **AP-37**, the most active analogue from the series possessed a top docking score of -163.052 kcal/mol while **AP-21**, the second most active in the series, exhibited a MolDock score of -153.037 kcal/mol. All the molecules exhibited a consistent H-bond interaction with Phe77 and Ser152, apart from His151 and Leu153. Further, analogues **AP-16** to **AP-24** and **AP-34** to **AP-39**, that possessed N-benzyl substitution exhibited an additional  $\pi$ - $\pi$  stacking interaction with Phe77, that was not observed with other molecules in the series (Table 7.3 and Fig. 7.5).

In addition, the presence of N-benzyl moiety reduced the distance between the N-aryl substitution and Arg 256, favouring the  $\pi$ -cation interaction. The fact also indicated the requirement of carbon linker between the amide NH and the aryl substitution that would favour the Arg 256 interaction. This can be explained by the better potential activity exhibited by **AP-20** and **AP-36** with 4-methoxybenzyl substitution in comparison to **AP-19** and **AP-35** that possessed 4-methoxyphenyl substitution (Table 7.2). A similar phenomenon can be observed with **AP-5** and **AP-12**, that exhibited  $\pi$ -cation interaction with Arg256, which was not seen with **AP-4** and **AP-11**.

A 10 ns MD simulation has been performed for **AP-21**, **AP-36** and **AP-37** in complex with PL and the respective ligand RMSD are represented in Fig. 7.6. Analogue **AP-21** exhibited high degree of deviation throughout the run, with a maximum deviation of 3.5 Å, observed around 3 ns. On the other hand, **AP-36** remained stable during the first 4 ns (RMSD < 2 Å), and then exhibited a sharp deviation during the next 6 ns (with maximum RMSD of 4 Å). **AP-37** was the most stable during the MD run and exhibited an RMSD < 2 Å.

## Chapter 7

**Table 7.3.** MolDock scores and interaction summary of indolyl oxoacetamide analogues **AP-1** to **AP-39** with the active site of PL

Analogue	MolDock Score*	H-bond	$\pi$ - $\pi$ stacking	$\pi$ -cation interactions
<b>AP-1</b>	-117.580	Phe 77, Ser 152, Leu 153, Phe 215	Phe 215	-
<b>AP-2</b>	-119.927	Phe 77, Ser 152, Leu 153, His 263	Tyr 114, Phe 215	-
<b>AP-3</b>	-131.305	Phe 77, Ser 152, Leu 153, Phe 215	Phe 215, His 263	His 263
<b>AP-4</b>	-120.942	Phe 77, Ser 152, Leu 153	Tyr 114, Phe 215	-
<b>AP-5</b>	-124.531	Phe 77, His 263	Phe 77, His 263	Asp 79, Arg 256
<b>AP-6</b>	-140.301	Phe 77, Ser 152, Leu 153, Phe 215	Tyr 114, Phe 215	-
<b>AP-7</b>	-126.141	Phe 77, Ser 152, Leu 153, Phe 215	Phe 215	-
<b>AP-8</b>	-128.118	Phe 77, Ser 152, Leu 153, Phe 215	Tyr 114, Phe 215	-
<b>AP-9</b>	-110.475	Ser 152	Tyr 114	-
<b>AP-10</b>	-141.281	Phe 77, Ser 152, Leu 153, Phe 215	Phe 215	-
<b>AP-11</b>	-141.105	Phe 77, Ser 152, Leu 153, Phe 215	Tyr 114, Phe 215	-
<b>AP-12</b>	-131.126	Phe 77, Ser 152, Phe215	Tyr 114, Phe 215	Asp 79, Arg 256
<b>AP-13</b>	-140.953	Phe 77, Ser 152, Leu 153	Tyr 114, Phe 215	-
<b>AP-14</b>	-144.163	Phe 77, Ser 152, Leu 153, Phe 215	Tyr 114, Phe 215, His 263	-
<b>AP-15</b>	-123.261	Phe 77, Ser 152, Leu 153, Phe 215	Phe 215, His 263	-
<b>AP-16</b>	-127.251	Phe 77, His 151, Ser 152, Leu 153	Phe 77, Tyr 114, Phe 215	Asp 79
<b>AP-17</b>	-133.192	Phe 77, His 151, Ser 152, Leu 153	Phe 77, Tyr 114	Arg 256
<b>AP-18</b>	-148.109	Phe 77, His 151, Ser 152	Phe 77, Phe 215, His 263	Arg 256
<b>AP-19</b>	-136.731	Phe 77, His 151, Ser 152, Leu 153	Phe 77, Tyr 114, Phe 215	Asp 79, Arg 256
<b>AP-20</b>	-145.138	Phe 77, His 151, Ser 152, Leu 153	Phe 77, Tyr 114, Phe 215, His 263	Arg 256, His 263
<b>AP-21</b>	<b>-153.037</b>	<b>Gly 76, Phe 77, His 151, Ser 152</b>	<b>Phe 77, Tyr 114, Phe 215, His 263</b>	<b>Asp 79, Arg 256, His 263</b>
<b>AP-22</b>	-128.188	Phe 77, Ser 152, Leu 153	Phe 77, Tyr 114, His 263	



## Chapter 7

<b>AP-23</b>	-144.217	Gly 76, Phe 77, His 151, Ser 152	Phe 77, Tyr 114, Phe 215, His 263	Asp 79, Arg 256, His 263
<b>AP-24</b>	-129.833	Phe 77, His 151, Ser 152, Leu 153	Phe 77, Tyr 114	-
<b>AP-25</b>	-110.872	Phe 77, His 151, His 263	Tyr 114	
<b>AP-26</b>	-118.676	Phe 77, His 263	Tyr 114, His 263	
<b>AP-27</b>	-121.694	Phe 77, His 263	Tyr 114, His 263	
<b>AP-28</b>	-121.499	Phe 77, His 263	Tyr 114, His 263	Asp 79
<b>AP-29</b>	-117.877	Gly 76, Phe 77, Leu 153	Phe 77, Tyr 114, Phe 215	Asp 79, Arg 256
<b>AP-30</b>	-119.053	Phe 77, Leu 153, Arg 256	Phe 77, Tyr 114, Phe 215	
<b>AP-31</b>	-123.105	Phe 77, Leu 153, His 263	Tyr 114, His 263	
<b>AP-32</b>	-115.959	Phe 77, Leu 153, His 263	Tyr 114, His 263	
<b>AP-33</b>	-119.34	Phe 77, His 263	Tyr 114, His 263	
<b>AP-34</b>	-155.561	Gly 76, Phe 77, His 151, Ser 152	Phe 77, Phe 215, His 263	Asp 79, Arg 256, His 263
<b>AP-35</b>	-160.657	Gly 76, Phe 77, His 151, Ser 152	Phe 77, Phe215, His 263	Asp 79, Arg 256, His 263
<b>AP-36</b>	<b>-160.577</b>	<b>Gly 76, Phe 77, His 151, Ser 152, Leu 153</b>	<b>Phe 77, Tyr 114, Phe 215, His 263</b>	<b>Asp 79, Arg 256</b>
<b>AP-37</b>	<b>-163.052</b>	<b>Gly 76, Phe 77, His 151, Ser 152</b>	<b>Phe 77, Phe 215, His 263</b>	<b>Asp 79, Arg 256, His 263</b>
<b>AP-38</b>	-159.287	Gly 76, Phe 77, His 151, Ser 152, Phe 215	Phe 77, His 263	Asp 79, His 263
<b>AP-39</b>	-136.758	Gly 76, Phe 77, His 151, Ser 152	Phe 77, Phe 215, His 263	Asp 79, His 263

\* MolDock scores are represented in kcal/mol.

## Chapter 7

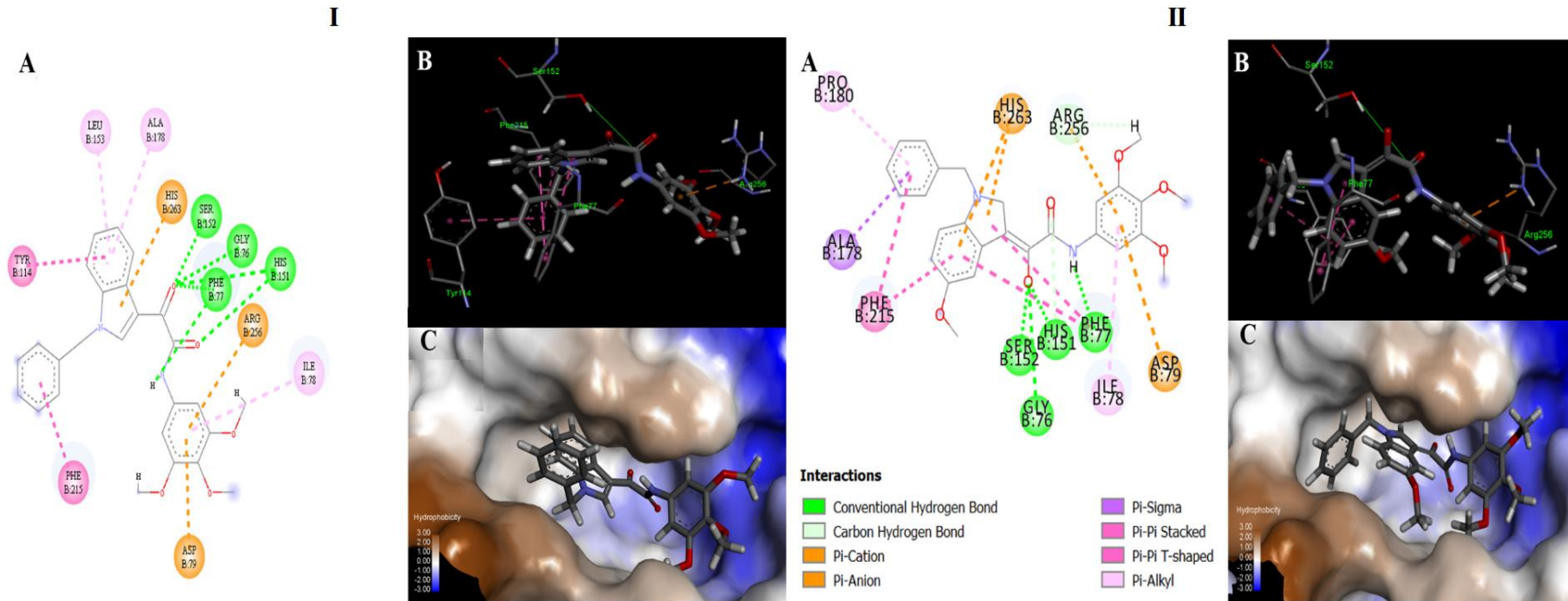


**Fig. 7.5.**(A). 2D interaction diagrams; (B) 3D interaction diagrams (highlighting the lid domain interactions (in pink) and reactive carbonyl position with reference to Ser152 (in green) and (C) binding conformations in the active site of PL of **AP-21** (I) and **AP-37** (II) respectively

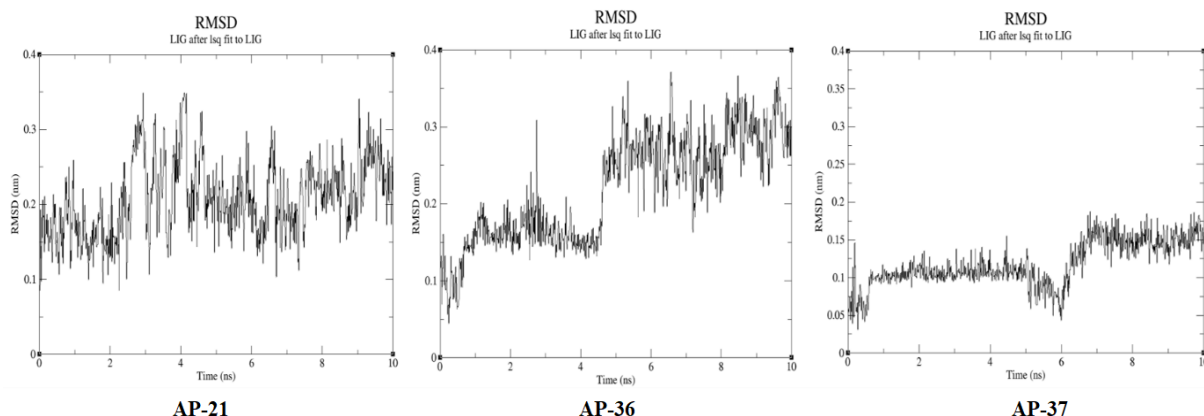


**Fig. 7.6.** RMSD of the ligands **AP-21**, **AP-36** and **AP-37** retrieved through 10 ns MD trajectory

A summary of the various interactions exhibited by **AP-21**, **AP-36** and **AP-37** with the active site during the MD simulation is detailed under Tables 7.4, 7.5 and 7.6, respectively. A similar interaction profile was observed for **AP-21** and **AP-36**, wherein the H-bonds and the  $\pi$ -cation interactions vanished with the initiation of MD. However, the ligands remained stable through  $\pi$ - $\pi$  stackings with Phe77, Tyr114 and Phe215. Conversely, **AP-37** exhibited a significant degree of H-bonds and  $\pi$ -cation interactions with Phe77, Ser152, Asp79 and Arg256 throughout the MD run apart from  $\pi$ - $\pi$  stackings.

**Table 7.4.** Interaction chart of **AP-21** with PL at different time frames during MD simulation

Time Frame (ns)	H-bond	$\pi$ - $\pi$ stacking	$\pi$ -cation interactions
0	Phe 77	Phe 77, Tyr 114, Phe 215	Arg 256
1	-	Phe 77, Tyr 114, Phe 215	-
2	-	Phe 77, Tyr 114, Phe 215	-
3	-	Phe 77, Tyr 114	-
4	-	Phe 77, Tyr 114, Phe 215	-
5	-	Phe 77, Phe 215	-
6	-	Phe 215	-
7	His 263	Phe 77, Phe 215	-
8	-	Phe 77, Phe 215, His 263	-
9	-	Tyr 114, Phe 215, His 263	-
10	-	Phe 77, Phe 215, His 263	-

## Chapter 7

**Table 7.5.** Interaction chart of **AP-36** with PL at different time frames during MD simulation

Time Frame (ns)	H-bond	$\pi$ - $\pi$ stacking	$\pi$ -cation interactions
0	Phe 77, Ser 152	Phe 77, Tyr 114, Phe 215	Arg 256
1	-	Phe 77, Phe 215	-
2	-	Phe 77, Phe 215	-
3	-	Phe 77, Tyr 114	-
4	-	Phe 77, Tyr 114, Phe 215	-
5	-	Phe 77, Phe 215	-
6	-	Phe 215	-
7	-	Phe 77, Phe 215	-
8	-	Phe 77, His 263	-
9	-	Tyr 114, Phe 215	-
10	-	Phe 215	-

**Table 7.6.** Interaction chart of **AP-37** with PL at different time frames during MD simulation.

Time Frame (ns)	H-bond	$\pi$ - $\pi$ stacking	$\pi$ -cation interactions
0	Phe 77, Ser 152	His 263	Asp 79, Arg 256
1	Phe 77, Ser 152	His 263, Phe 215	Asp 79, Arg 256
2	Phe 77, Ser 152	Tyr 114, Phe 215, His 263	Asp 79, Arg 256
3	Phe 77	Tyr 114, Phe 215, His 263	Asp 79, Arg 256
4	Phe 77	Tyr 114, Phe 215, His 263	Asp 79, Arg 256
5	Phe 77	Tyr 114, Phe 215, His 263	Asp 79, Arg 256
6	Phe 77, Ser 152	Tyr 114, His 263	Asp 79
7	-	Phe 77, Phe 215	Arg 256
8	-	Phe 77	-
9	-	Phe 77	Arg 256
10	-	Phe 77	-

In conclusion, a series of 39 indolyl oxoacetamide analogues have been synthesised and screened *in vitro* to determine their PL inhibition activity. The study validated the rationale for replacing the carbazole scaffold with the indole scaffold, that resulted in reduced interaction distance between the reactive carbonyl from Ser152 from 4.45 Å to 3.42 Å. A significant enhancement in the PL inhibitory profile was observed with five analogues, **AP-37**, **AP-21**, **AP-36**, **AP-20** and **AP-35** (IC<sub>50</sub> - 4.53, 4.92, 5.12, 5.83 and 6.28 µM, respectively). These analogues exhibited better potent activity in comparison to **DK-5** (IC<sub>50</sub>

- 6.31  $\mu\text{M}$ ) from the previous series. Molecular docking studies have further supported the rationale wherein the distance of the reactive carbonyl from Ser152 has enhanced the activity.

### References

- [1] M.P. Tantak, L. Klingler, V. Arun, A. Kumar, R. Sadana, D. Kumar, Design and synthesis of bis(indolyl)ketohydrazide-hydrazones: Identification of potent and selective novel tubulin inhibitors, *Eur. J. Med. Chem.* 136 (2017) 184–194.
- [2] M.P. Tantak, V. Gupta, K. Nikhil, V. Arun, R.P. Singh, P.N. Jha, K. Shah, D. Kumar, Sequential one-pot synthesis of bis(indolyl) glyoxylamides: Evaluation of antibacterial and anticancer activities, *Bioorg. Med. Chem. Lett.* 26 (2016) 3167–3171.
- [3] F. Naaz, M.C.P. Pallavi, S. Shafi, N. Mulakayala, M.S. Yar, H.M.S. Kumar, 1, 2, 3-triazole tethered indole-3-glyoxamide derivatives as multiple inhibitors of 5-LOX, COX-2 & tubulin: Their anti-proliferative & anti-inflammatory activity, *Bioorg. Chem.* 81 (2018) 1–20.

## 8 | Synthesis - Series III - Indolyl Oxoacetamide Analogues (Part 2)

## 8.1 | Rationale

The previous chapter 7 validated the hypothesis of replacing carbazole nucleus with an indole nucleus resulting in significant enhancement in the PL inhibitory activity. Nevertheless, the most potent analogue of the series, **AP-37**, exhibited lower PL inhibitory activity ( $IC_{50} = 4.53 \mu M$ ) compared to the NP lead, conophylline ( $IC_{50} = 3.31 \mu M$ ). On the contrary, **AP-37** that possessed a 5-methoxy substitution on the indole, did not exhibit significantly potent activity compared to its unsubstituted counterpart, **AP-21** ( $IC_{50} = 4.92 \mu M$ ), clearly indicating its negligible role in the activity. The lower potency of these analogues can be attributed to the low hydrophobic density on the indole nucleus.

Previously, in chapter 2, the prominent role of prenyl and geranyl substitutions in imparting potential PL inhibitory activity has been identified. Hence, the N-benzyl substitution of **AP-21** was replaced with an N-geranyl, and a preliminary docking was performed. As represented in Fig. 8.1, a high degree of hydrophobic interactions with the lid domain was observed.

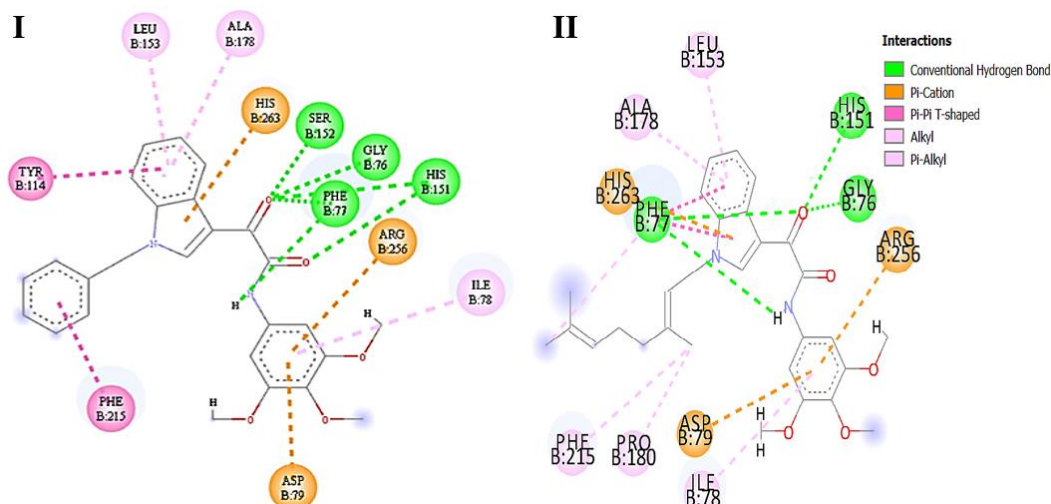


**Fig. 8.1.** 2D interaction poses **AP-21** (I) and its N-geranyl counterpart (II) highlighting dense hydrophobic interactions with the lid domain amino acids (in light pink)

Nevertheless, the intensity of  $\pi$ - $\pi$  stackings was reduced due to the absence of the N-benzyl substitution. Hence, a second prototype was docked with a 5-benzyloxy substitution in place of the 5-methoxy (as seen in **AP-37**) was designed, that also included the N-geranyl moiety (Fig. 8.2).

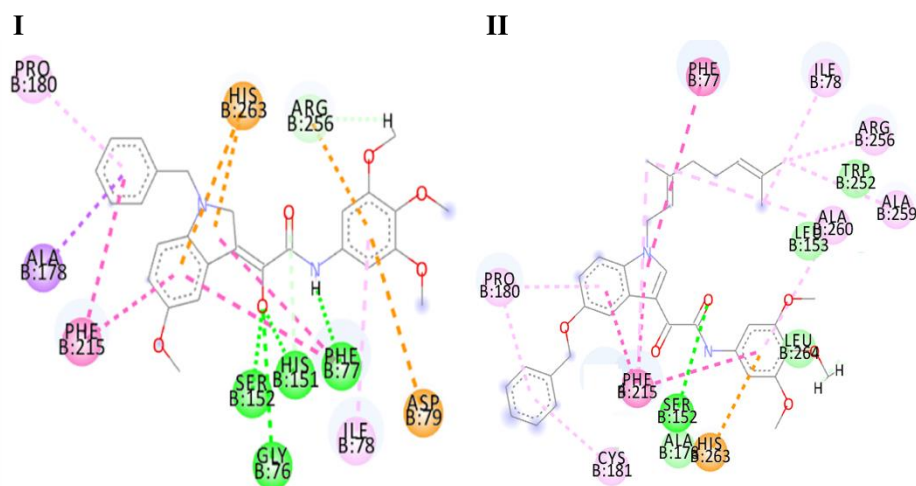


**Fig. 8.2.** 2D interaction pose of **AP-37** (**I**) and its 5-benzyloxy-N-geranyl substituted counterpart (**II**) highlighting an increase in  $\pi$ - $\pi$  stacking density (in dark pink)

Further, the presence of a  $-\text{CH}_2-$  linker between the aryl extension and the amide (as observed with **AP-20** and **AP-36**) resulted in enhanced PL inhibitory activity ( $\text{IC}_{50}$  of 5.83  $\mu\text{M}$  and 5.12  $\mu\text{M}$ , respectively) compared to their counterparts, **AP-19** and **AP-35** ( $\text{IC}_{50}$  10.86  $\mu\text{M}$  and 6.28  $\mu\text{M}$ ) that did not possess the linker. These facts clearly indicated that the PL inhibitory activity of the analogues can also be enhanced through better  $\pi$ -cation interaction with Arg 256.

Considering the above facts, the present chapter is focussed on further structural optimization of the indolyl oxoacetamide analogue with inclusion of various structural modifications (Fig. 8.3) viz;

- An additional aromatic substitution on the benzene ring of the indole (**R<sub>1</sub>**);
- Dense lipophilic groups, such as prenyl and geranyl moieties on the indole nitrogen (**R<sub>2</sub>**);
- Optimizing the carbon linker chain (**n**) and the aryl group on the amide nitrogen (**Ar**) to enhance the  $\pi$ -cation strength with Arg 256

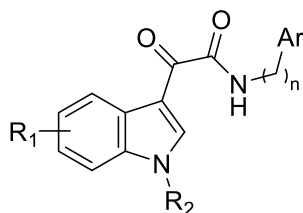


**Fig. 8.3.** General representation of indolyl oxoacetamide analogues highlighting various positions for substitution

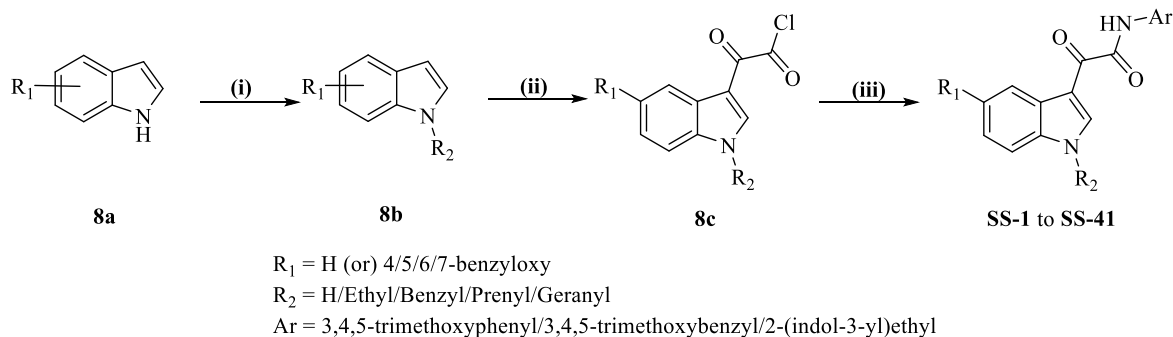
## 8.2 | Synthesis and characterization

The procedure for the synthesis of all the final analogues **SS-1** to **SS-41** were carried out as per the procedure detailed in chapter 7, with minor modifications (Scheme 8.1).

## Chapter 8

Briefly, the N-substitution of ethyl/benzyl/prenyl/geranyl moieties on indole and its various benzyloxy analogues were carried out in the presence of KOH. The obtained product was further proceeded for the synthesis of the respective glyoxylyl chlorides (**8c**) in THF. The reaction time for the synthesis of the glyoxylyl chlorides (**8c**) varied with the benzyloxy substitutions. For instance, the reaction time for 4- and 6-benzyloxy analogues was around 30 min, while this time has extended to 1 h and 3 h, respectively for 5-benzyloxy and 7-benzyloxy analogues. Finally, the glyoxylyl chloride analogues (**8c**) were made to react either with 3,4,5-trimethoxyaniline/3,4,5-trimethoxybenzylamine/tryptamine to yield (55-87%) the final analogues, **SS-1** to **SS-41** respectively.

The structures of the synthesized analogues were well characterized. In the  $^1\text{H}$  NMR, the -NH proton of the amide resonated at 11-12 and 8-9 ppm with  $\text{DMSO-}d_6$  and  $\text{CDCl}_3$  solvents. Further, the amide -NH appeared as a triplet due to the adjacent - $\text{CH}_2$  protons in the trimethoxybenzyl and 2-(1H-indol-3-yl) ethyl substituted analogues, **SS-13** to **SS-41** (with exceptions). For the N-geranyl substitution, the - $\text{CH}_3$  protons resonated at 1.5-2 ppm, while the - $\text{CH}_2$  protons of the benzyloxy extension was resonated at 5-6 ppm. The - $\text{OCH}_3$  protons on the aryl substitution of the amide for analogues **SS-1** to **SS-26** resonated as singlets at 3-4 ppm. The  $^{13}\text{C}$  spectra and IR spectra exhibited similar characteristic peaks as observed in the AP series of indolyl oxoacetamides. In addition, for the  $^{13}\text{C}$  spectra of the N-prenyl substituted analogues, the terminal methyl carbons of the prenyl moiety were observed around 18 and 25 ppm, while the - $\text{CH}_2$  carbon attached to the nitrogen of the indole resonated at 45 ppm. Similarly, for the N-geranyl substituted analogues, the three methyl carbons as well as the carbons of the - $\text{CH}_2\text{-CH}_2\text{-}$  linker in the geranyl moiety resonated in between 16-40 ppm, while the - $\text{CH}_2$  carbon attached to the nitrogen of the indole resonated at 45 ppm.



**Scheme 8.1.** Reagents and conditions: (i) Ethyl bromide/Benzyl chloride/Prenyl bromide/Geranyl bromide, KOH, DMF, RT, 12-16 h; (ii)  $(\text{COCl})_2$ , THF,  $0^\circ\text{C}$ , 30-180 min; (iii)  $\text{Ar-NH}_2$ , TEA, THF, RT, 2 h.



**2-(1-(3-methylbut-2-en-1-yl)-1H-indol-3-yl)-2-oxo-N-(3,4,5-trimethoxyphenyl)acetamide (SS-1)**

Yield 74%; Creamy yellow solid; m.p: 172-174°C; <sup>1</sup>H NMR (400 MHz, DMSO-*d*<sub>6</sub>) δ 10.57 (s, 1H), 8.89 (s, 1H), 8.36-8.28 (m, 1H), 7.64-7.55 (m, 1H), 7.39-7.30 (m, 4H), 5.43-5.35 (m, 1H), 4.98 (d, *J* = 7.0 Hz, 2H), 3.78 (s, 6H), 3.66 (s, 3H), 1.86 (s, 3H), 1.74 (s, 3H); <sup>13</sup>C NMR (100 MHz, DMSO-*d*<sub>6</sub>) δ 181.4, 162.1, 153.1, 141.2, 137.4, 136.6, 134.6, 134.5, 127.5, 124.1, 123.6, 122.0, 119.6, 111.9, 111.3, 98.4, 60.6, 56.2, 45.1, 25.8, 18.4; IR (KBr, ν, cm<sup>-1</sup>) 3752, 2922, 2355, 2318, 2016, 1751, 1686, 1518, 1377, 1256, 1128, 1057, 829, 789, 683; HRMS (ESI<sup>+</sup>) calculated for C<sub>24</sub>H<sub>27</sub>N<sub>2</sub>O<sub>5</sub> [M+H<sup>+</sup>], 423.1842; Found 423.1876.

**(E)-2-(1-(3,7-dimethylocta-2,6-dien-1-yl)-1H-indol-3-yl)-2-oxo-N-(3,4,5-trimethoxyphenyl)acetamide (SS-2)**

Yield 80%; Cream yellow solid; m.p: 86-88°C; <sup>1</sup>H NMR (400 MHz, DMSO-*d*<sub>6</sub>) δ 10.57 (s, 1H), 8.90 (s, 1H), 8.37-8.28 (m, 1H), 7.62-7.53 (m, 1H), 7.39-7.30 (m, 4H), 5.37 (t, *J* = 6.8 Hz, 1H), 5.06-4.95 (m, 3H), 3.78 (s, 6H), 3.65 (s, 3H), 2.11-1.99 (m, 2H), 2.07-2.02 (m, 2H), 1.85 (s, 3H), 1.55 (s, 3H), 1.51 (s, 3H); <sup>13</sup>C NMR (100 MHz, DMSO-*d*<sub>6</sub>) δ 181.4, 162.1, 153.1, 141.2, 140.8, 136.7, 134.5, 131.5, 127.5, 124.0, 123.6, 121.9, 119.5, 111.9, 111.3, 99.9, 98.6, 98.4, 60.5, 56.2, 56.1, 45.0, 26.1, 25.8, 17.9, 16.6; IR (KBr, ν, cm<sup>-1</sup>) 3574, 3240, 2371, 2318, 1807, 1651, 1412, 1346, 1256, 1128, 1022, 845, 758, 637; HRMS (ESI<sup>+</sup>) calculated for C<sub>29</sub>H<sub>35</sub>N<sub>2</sub>O<sub>5</sub> [M+H<sup>+</sup>], 491.2468; Found 491.2492.

**2-(5-(benzyloxy)-1H-indol-3-yl)-2-oxo-N-(3,4,5-trimethoxyphenyl)acetamide (SS-3)**

Yield 73%; Light yellow solid; m.p: 205-207°C; <sup>1</sup>H NMR (400 MHz, DMSO-*d*<sub>6</sub>) δ 12.03 (s, 1H), 10.47 (s, 1H), 8.69 (s, 1H), 7.91 (d, *J* = 1.5 Hz, 1H), 7.51-7.43 (m, 2H), 7.42-7.26 (m, 4H), 7.13 (s, 2H), 6.69 (dd, *J* = 7.4, 1.5 Hz, 1H), 5.10 (s, 2H), 3.79 (s, 6H), 3.66 (s, 3H); <sup>13</sup>C NMR (100 MHz, DMSO-*d*<sub>6</sub>) δ 181.3, 161.9, 155.2, 154.1, 137.9, 136.9, 136.8, 135.8, 132.6, 128.3, 127.9, 127.8, 127.2, 115.4, 112.0, 111.7, 105.9, 102.2, 70.2, 60.6, 56.1; IR (KBr, ν, cm<sup>-1</sup>) 3574, 3240, 2371, 2318, 1807, 1651, 1412, 1346, 1256, 1128, 1022, 845, 758, 637; HRMS (ESI<sup>+</sup>) calculated for C<sub>26</sub>H<sub>25</sub>N<sub>2</sub>O<sub>6</sub> [M+H<sup>+</sup>], 461.1707; Found 461.1692.

**2-(5-(benzyloxy)-1-ethyl-1H-indol-3-yl)-2-oxo-N-(3,4,5-trimethoxyphenyl)acetamide (SS-4)**

Yield 68%; Green solid; m.p: 201-203°C; <sup>1</sup>H NMR (400 MHz, DMSO-*d*<sub>6</sub>) δ 10.47 (s, 1H), 8.99 (s, 1H), 7.81 (d, *J* = 7.5 Hz, 1H), 7.74 (s, 1H), 7.51-7.43 (m, 2H), 7.42-7.32 (m, 2H), 7.36-7.26 (m, 1H), 7.24 (s, 2H), 6.92 (dd, *J* = 7.5, 1.5 Hz, 1H), 5.10 (s, 2H), 4.19 (q, *J* = 8.0 Hz, 2H), 3.73 (s, 3H), 3.72 (s, 6H), 1.11 (t, *J* = 8.0 Hz, 3H); <sup>13</sup>C NMR (100 MHz, DMSO-

$d_6$ )  $\delta$  181.4, 161.9, 155.2, 154.5, 136.9, 136.8, 135.8, 135.2, 134.1, 128.3, 127.9, 127.8, 127.2, 116.3, 114.0, 108.9, 106.0, 102.2, 70.2, 60.6, 56.1, 42.3, 13.9; IR (KBr,  $\nu$ ,  $\text{cm}^{-1}$ ) 3773, 3256, 2355, 2334, 1680, 1574, 1402, 1356, 1240, 1153, 1013, 795, 637, 511, 474; HRMS (ESI<sup>+</sup>) calculated for  $\text{C}_{28}\text{H}_{29}\text{N}_2\text{O}_6$  [M+H<sup>+</sup>], 489.1947; Found 489.1824.

***2-(5-(benzyloxy)-1-(3-methylbut-2-en-1-yl)-1H-indol-3-yl)-2-oxo-N-(3,4,5-trimethoxyphenyl)acetamide (SS-5)***

Yield 63%; Creamy white solid; m.p: 154-156°C; <sup>1</sup>H NMR (400 MHz,  $\text{CDCl}_3$ )  $\delta$  9.42 (s, 1H), 9.02 (s, 1H), 8.11 (d,  $J = 2.5$  Hz, 1H), 7.57-7.50 (m, 2H), 7.42 (d,  $J = 7.4$  Hz, 1H), 7.39-7.27 (m, 3H), 7.08 (dd,  $J = 8.9, 2.5$  Hz, 1H), 7.06 (s, 2H), 5.42 (t,  $J = 5.7$  Hz, 1H), 5.21 (s, 2H), 4.77 (d,  $J = 6.9$  Hz, 2H), 3.93 (s, 3H), 3.92 (s, 6H), 1.88 (s, 3H), 1.83 (s, 3H); <sup>13</sup>C NMR (100 MHz,  $\text{CDCl}_3$ )  $\delta$  179.2, 160.2, 156.4, 153.5, 140.9, 138.5, 137.2, 135.2, 133.1, 131.4, 129.0, 128.5, 127.9, 127.6, 117.9, 114.5, 111.4, 105.8, 97.5, 76.7, 70.6, 61.0, 56.1, 45.6, 25.7, 18.2; IR (KBr,  $\nu$ ,  $\text{cm}^{-1}$ ) 3277, 2922, 2851, 2374, 1838, 1595, 1341, 1240, 1043, 922, 885, 851, 511; HRMS (ESI<sup>+</sup>) calculated for  $\text{C}_{31}\text{H}_{33}\text{N}_2\text{O}_6$  [M+H<sup>+</sup>], 529.2333; Found 529.2322.

***(E)-2-(5-(benzyloxy)-1-(3,7-dimethylocta-2,6-dien-1-yl)-1H-indol-3-yl)-2-oxo-N-(3,4,5-trimethoxyphenyl)acetamide (SS-6)***

Yield 71%; Dark yellow solid; m.p: 110-112°C; <sup>1</sup>H NMR (400 MHz,  $\text{CDCl}_3$ )  $\delta$  9.41 (s, 1H), 9.04 (s, 1H), 8.11 (d,  $J = 2.5$  Hz, 1H), 7.57-7.50 (m, 2H), 7.49-7.27 (m, 4H), 7.11-7.04 (m, 1H), 7.06 (s, 2H), 5.41 (t,  $J = 7.9$  Hz, 1H), 5.21 (s, 2H), 4.80 (d,  $J = 6.8$  Hz, 2H), 3.93 (s, 6H), 3.87 (s, 3H), 2.24-2.03 (m, 4H), 1.87 (s, 3H), 1.67 (s, 3H), 1.64-1.58 (m, 4H); <sup>13</sup>C NMR (100 MHz,  $\text{CDCl}_3$ )  $\delta$  179.2, 160.1, 156.4, 153.5, 141.7, 141.0, 137.2, 135.1, 133.1, 132.1, 131.4, 129.0, 128.5, 127.9, 127.6, 123.4, 117.9, 114.5, 111.4, 105.7, 97.4, 76.7, 70.6, 61.0, 56.1, 45.6, 39.4, 26.1, 25.6, 17.7, 16.6; IR (KBr,  $\nu$ ,  $\text{cm}^{-1}$ ) 3788, 3327, 2926, 2374, 2340, 1788, 1589, 1452, 1290, 1184, 951, 901, 779, 689; HRMS (ESI<sup>+</sup>) calculated for  $\text{C}_{36}\text{H}_{41}\text{N}_2\text{O}_6$  [M+H<sup>+</sup>], 597.2959; Found 597.2945.

***2-(1-benzyl-5-(benzyloxy)-1H-indol-3-yl)-2-oxo-N-(3,4,5-trimethoxyphenyl)acetamide (SS-7)***

Yield 70%; Greenish white solid; m.p: 189-191°C; <sup>1</sup>H NMR (400 MHz,  $\text{CDCl}_3$ )  $\delta$  9.43 (s, 1H), 9.14 (s, 1H), 7.55-7.48 (m, 2H), 7.42 (tt,  $J = 6.5, 1.0$  Hz, 2H), 7.41-7.28 (m, 5H), 7.26-7.17 (m, 3H), 7.09-6.98 (m, 3H), 5.39 (s, 2H), 5.18 (s, 2H), 3.92 (s, 6H), 3.87 (s, 3H); <sup>13</sup>C NMR (100 MHz,  $\text{CDCl}_3$ )  $\delta$  179.5, 160.0, 157.3, 156.4, 153.5, 141.7, 137.1, 135.2, 133.1, 132.2, 131.4, 129.1, 128.6, 128.3, 127.9, 127.6, 126.8, 114.7, 111.8, 105.6, 97.4, 76.7, 70.5, 61.0, 56.1, 51.5; IR (KBr,  $\nu$ ,  $\text{cm}^{-1}$ ) 3736, 3630, 3312, 2359, 2303, 1842, 1611, 1589, 1489,

1449, 1377, 1128, 1113, 901, 829, 617; HRMS (ESI<sup>+</sup>) calculated for C<sub>33</sub>H<sub>31</sub>N<sub>2</sub>O<sub>6</sub> [M+H<sup>+</sup>], 551.2164; Found 551.2158.

**2-(7-(benzyloxy)-1H-indol-3-yl)-2-oxo-N-(3,4,5-trimethoxyphenyl)acetamide (SS-8)**

Yield 64%; Pale yellow solid; m.p: 201-203°C; <sup>1</sup>H NMR (400 MHz, DMSO-*d*<sub>6</sub>) δ 10.20 (s, 1H), 8.47 (s, 1H), 7.65 (s, 1H), 7.32 (s, 2H), 7.22-7.01 (m, 6H), 6.99-6.58 (m, 2H), 5.02 (s, 2H), 3.55 (s, 6H), 3.43 (s, 3H); <sup>13</sup>C NMR (100 MHz, DMSO-*d*<sub>6</sub>) δ 179.5, 160.0, 157.3, 156.4, 153.5, 141.7, 137.1, 135.2, 133.1, 131.4, 129.1, 128.3, 126.8, 114.7, 111.8, 105.6, 97.4, 70.5, 61.0, 56.1, 51.5; IR (KBr, ν, cm<sup>-1</sup>) 3654, 3154, 2465, 2245, 1817, 1654, 1555, 1345, 1289, 1159, 1113, 1022, 814, 795, 637, 512; HRMS (ESI<sup>+</sup>) calculated for C<sub>26</sub>H<sub>25</sub>N<sub>2</sub>O<sub>6</sub> [M+H<sup>+</sup>], 461.1707; Found 461.1692.

**2-(7-(benzyloxy)-1-(3-methylbut-2-en-1-yl)-1H-indol-3-yl)-2-oxo-N-(3,4,5-trimethoxyphenyl)acetamide (SS-9)**

Yield 66%; Yellow solid; m.p: 116-118°C; <sup>1</sup>H NMR (400 MHz, CDCl<sub>3</sub>) δ 9.41 (s, 1H), 8.98 (s, 1H), 8.10 (dd, *J* = 8.0, 0.9 Hz, 1H), 7.51-7.33 (m, 5H), 7.27 (t, *J* = 8.0 Hz, 1H), 7.05 (s, 2H), 6.88 (dd, *J* = 8.1, 0.9 Hz, 1H), 5.24 (s, 2H), 5.12-5.05 (m, 2H), 3.90 (s, 6H), 3.88 (s, 3H), 1.75 (t, *J* = 1.3 Hz, 3H), 1.68 (d, *J* = 8.4 Hz, 4H); <sup>13</sup>C NMR (100 MHz, CDCl<sub>3</sub>) δ 179.3, 160.2, 153.4, 146.8, 141.6, 136.7, 136.5, 135.1, 133.1, 130.5, 128.6, 128.1, 127.6, 125.9, 124.3, 120.2, 115.3, 111.6, 106.4, 97.4, 70.6, 61.0, 56.1, 48.3, 25.6, 18.0; IR (KBr, ν, cm<sup>-1</sup>) 3898, 3601, 3277, 2359, 2303, 1817, 1595, 1524, 1377, 1256, 1028, 935, 829, 704, 527; HRMS (ESI<sup>+</sup>) calculated for C<sub>31</sub>H<sub>33</sub>N<sub>2</sub>O<sub>6</sub> [M+H<sup>+</sup>], 529.2333; Found 529.2318.

**(E)-2-(7-(benzyloxy)-1-(3,7-dimethylocta-2,6-dien-1-yl)-1H-indol-3-yl)-2-oxo-N-(3,4,5-trimethoxyphenyl)acetamide (SS-10)**

Yield 62%; Greenish yellow solid; m.p: 117-119°C; <sup>1</sup>H NMR (400 MHz, CDCl<sub>3</sub>) δ 9.43 (s, 1H), 9.00 (s, 1H), 8.12 (dd, *J* = 8.0, 0.9 Hz, 1H), 7.52-7.33 (m, 5H), 7.27 (t, *J* = 8.0 Hz, 1H), 7.06 (s, 2H), 6.88 (dd, *J* = 8.0, 0.9 Hz, 1H), 5.45 (t, *J* = 6.4 Hz, 1H), 5.24 (s, 2H), 5.14-5.03 (m, 3H), 3.92 (s, 6H), 3.91 (s, 3H), 2.14-1.98 (m, 4H), 1.74-1.63 (m, 6H), 1.59 (s, 3H); <sup>13</sup>C NMR (100 MHz, CDCl<sub>3</sub>) δ 179.4, 160.1, 153.4, 146.8, 141.7, 140.0, 136.5, 135.1, 133.2, 130.5, 128.6, 127.6, 125.9, 124.3, 120.0, 115.3, 111.6, 110.0, 106.4, 97.4, 70.6, 61.0, 56.1, 48.3, 39.4, 37.3, 26.3, 25.6, 25.5, 17.7, 16.5; IR (KBr, ν, cm<sup>-1</sup>) 3682, 3312, 2355, 2340, 1788, 1595, 1489, 1396, 1362, 1256, 1169, 1007, 901, 633, 527; HRMS (ESI<sup>+</sup>) calculated for C<sub>36</sub>H<sub>41</sub>N<sub>2</sub>O<sub>6</sub> [M+H<sup>+</sup>], 597.2959; Found 597.2949.

***(E)-2-(6-(benzyloxy)-1-(3,7-dimethylocta-2,6-dien-1-yl)-1H-indol-3-yl)-2-oxo-N-(3,4,5-trimethoxyphenyl)acetamide (SS-11)***

Yield 79%; Off white solid; m.p: 122-124°C; <sup>1</sup>H NMR (400 MHz, CDCl<sub>3</sub>) δ 9.62 (s, 1H), 9.23 (s, 1H), 8.59 (d, *J* = 8.7 Hz, 1H), 7.77-7.55 (m, 5H), 7.36 (dd, *J* = 8.7, 2.2 Hz, 1H), 7.29 (s, 2H), 7.25-7.16 (m, 1H), 5.63 (t, *J* = 5.4 Hz, 1H), 5.40 (s, 2H), 5.38-5.28 (m, 1H), 4.59 (d, *J* = 6.8 Hz, 2H), 3.92 (s, 6H), 3.89 (s, 3H), 2.41-2.28 (m, 4H), 2.08 (s, 3H), 1.90 (s, 3H), 1.83 (m, 3H); <sup>13</sup>C NMR (100 MHz, CDCl<sub>3</sub>) δ 174.5, 155.3, 151.8, 148.7, 137.0, 136.0, 132.6, 128.4, 127.4, 123.9, 123.3, 122.7, 118.6, 117.3, 113.0, 108.2, 106.9, 92.5, 91.3, 72.6, 72.2, 71.9, 65.8, 56.2, 51.4, 40.6, 34.7, 21.4, 20.9, 13.0, 11.9; IR (KBr, ν, cm<sup>-1</sup>) 3338, 3133, 2960, 1943, 1733, 1558, 1540, 1185, 1170, 1156, 1054, 1015, 868, 816, 695, 634; HRMS (ESI<sup>+</sup>) calculated for C<sub>36</sub>H<sub>41</sub>N<sub>2</sub>O<sub>6</sub> [M+H<sup>+</sup>], 597.2959; Found 597.2936.

***(E)-2-(4-(benzyloxy)-1-(3,7-dimethylocta-2,6-dien-1-yl)-1H-indol-3-yl)-2-oxo-N-(3,4,5-trimethoxyphenyl)acetamide (SS-12)***

Yield 69%; Light yellow solid; m.p: 82-85°C; <sup>1</sup>H NMR (400 MHz, CDCl<sub>3</sub>) δ 9.61 (s, 1H), 9.10 (s, 1H), 7.92-7.84 (m, 2H), 7.70-7.61 (m, 2H), 7.59-7.46 (m, 2H), 7.30 (s, 2H), 7.28 (dd, *J* = 8.2, 0.7 Hz, 1H), 7.08 (dd, *J* = 8.0, 0.7 Hz, 1H), 5.66 (t, *J* = 5.5 Hz, 1H), 5.59 (s, 2H), 5.48-5.12 (m, 1H), 3.84 (s, 6H), 3.88 (s, 3H), 3.84-3.44 (m, 5H), 2.76 (s, 3H), 2.67 (s, 3H), 2.61-2.42 (m, 4H); <sup>13</sup>C NMR (100 MHz, CDCl<sub>3</sub>) δ 174.2, 155.7, 149.0, 148.6, 136.8, 135.5, 134.2, 132.7, 130.2, 128.6, 127.3, 123.6, 120.2, 118.7, 113.2, 112.5, 107.5, 101.7, 99.2, 92.5, 72.6, 71.9, 66.0, 56.2, 51.4, 40.7, 34.7, 21.4, 20.9, 12.9, 11.9; IR (KBr, ν, cm<sup>-1</sup>) 3565, 3502, 2324, 1942, 1868, 1843, 1669, 1340, 1203, 1124, 995, 906, 755, 695, 625; HRMS (ESI<sup>+</sup>) calculated for C<sub>36</sub>H<sub>41</sub>N<sub>2</sub>O<sub>6</sub> [M+H<sup>+</sup>], 597.2959; Found 597.2942.

***2-(1H-indol-3-yl)-2-oxo-N-(3,4,5-trimethoxybenzyl)acetamide (SS-13)***

Yield 81%; Brownish white solid; m.p: 239-241°C; <sup>1</sup>H NMR (400 MHz, DMSO-*d*<sub>6</sub>) δ 12.25 (s, 1H), 9.23 (t, *J* = 6.4 Hz, 1H), 8.75 (s, 1H), 8.29-8.20 (m, 1H), 7.59-7.50 (m, 1H), 7.33-7.22 (m, 2H), 6.68 (s, 2H), 4.38 (d, *J* = 6.3 Hz, 2H), 3.76 (s, 6H), 3.64 (s, 3H); <sup>13</sup>C NMR (100 MHz, DMSO-*d*<sub>6</sub>) δ 182.7, 164.2, 153.2, 138.8, 136.9, 136.7, 135.0, 126.6, 123.9, 123.0, 121.7, 113.0, 112.6, 105.2, 60.4, 56.2, 42.7; IR (KBr, ν, cm<sup>-1</sup>) 3736, 2835, 2355, 2318, 2122, 1751, 1595, 1449, 1362, 1256, 1134, 988, 739, 689, 511; HRMS (ESI<sup>+</sup>) calculated for C<sub>20</sub>H<sub>21</sub>N<sub>2</sub>O<sub>5</sub> [M+H<sup>+</sup>], 369.1372; Found 369.3792.

***2-(1-ethyl-1H-indol-3-yl)-2-oxo-N-(3,4,5-trimethoxybenzyl)acetamide (SS-14)***

Yield 77%; Brownish white solid; m.p: 145-147°C; <sup>1</sup>H NMR (400 MHz, DMSO-*d*<sub>6</sub>) δ 9.24 (t, *J* = 6.3 Hz, 1H), 8.84 (s, 1H), 8.27 (dd, *J* = 6.5, 1.9 Hz, 1H), 7.66 (dd, *J* = 6.6, 1.5 Hz,

1H), 7.39-7.26 (m, 2H), 6.68 (s, 2H), 4.41-4.28 (m, 4H), 3.76 (s, 6H), 3.64 (s, 3H), 1.41 (t,  $J = 7.2$  Hz, 3H);  $^{13}\text{C}$  NMR (100 MHz, DMSO- $d_6$ )  $\delta$  182.1, 164.0, 153.2, 140.7, 136.9, 136.4, 135.0, 127.3, 123.9, 123.4, 122.0, 111.7, 111.5, 105.2, 60.4, 56.2, 42.7, 41.8, 15.5; IR (KBr,  $\nu$ ,  $\text{cm}^{-1}$ ) 3723, 3601, 2901, 2355, 2318, 2106, 1717, 1589, 1396, 1240, 1184, 1128, 1007, 810, 689; HRMS (ESI $^+$ ) calculated for  $\text{C}_{22}\text{H}_{25}\text{N}_2\text{O}_5$  [ $\text{M}+\text{H}^+$ ], 397.1685; Found 397.3430.

***2-(1-(3-methylbut-2-en-1-yl)-1H-indol-3-yl)-2-oxo-N-(3,4,5-trimethoxybenzyl)acetamide (SS-15)***

Yield 79%; White solid; m.p: 179-181°C;  $^1\text{H}$  NMR (400 MHz, DMSO- $d_6$ )  $\delta$  9.25 (t,  $J = 6.3$  Hz, 1H), 8.80 (s, 1H), 8.32-8.24 (m, 1H), 7.62-7.53 (m, 1H), 7.32 (ddd,  $J = 6.5, 4.0, 1.7$  Hz, 2H), 6.67 (s, 2H), 5.38 (t,  $J = 7.0$  Hz, 1H), 4.93 (d,  $J = 7.0$  Hz, 2H), 4.36 (d,  $J = 6.3$  Hz, 2H), 3.76 (s, 6H), 3.64 (s, 3H), 1.84 (s, 3H), 1.74 (s, 3H);  $^{13}\text{C}$  NMR (100 MHz, DMSO- $d_6$ )  $\delta$  182.0, 164.0, 153.2, 140.8, 137.7, 136.8, 136.6, 135.0, 127.3, 123.9, 123.4, 122.0, 119.4, 111.7, 111.6, 105.1, 60.4, 56.2, 44.9, 42.7, 25.8, 18.4; IR (KBr,  $\nu$ ,  $\text{cm}^{-1}$ ) 3773, 3474, 2922, 2355, 2318, 2127, 1680, 1412, 1256, 1165, 1134, 1007, 810, 689; HRMS (ESI $^+$ ) calculated for  $\text{C}_{25}\text{H}_{29}\text{N}_2\text{O}_5$  [ $\text{M}+\text{H}^+$ ], 437.1998; Found 437.4182.

***(E)-2-(1-(3,7-dimethylocta-2,6-dien-1-yl)-1H-indol-3-yl)-2-oxo-N-(3,4,5-trimethoxybenzyl)acetamide (SS-16)***

Yield 72%; Yellowish white solid; m.p: 72-74°C;  $^1\text{H}$  NMR (400 MHz, DMSO- $d_6$ )  $\delta$  9.26 (t,  $J = 6.3$  Hz, 1H), 8.81 (s, 1H), 8.32-8.24 (m, 1H), 7.62-7.53 (m, 1H), 7.36-7.31 (m, 2H), 6.66 (s, 2H), 5.06-4.95 (m, 3H), 4.36 (d,  $J = 6.3$  Hz, 2H), 3.78 (s, 6H), 3.65 (s, 3H), 2.11-1.99 (m, 2H), 2.06-2.01 (m, 3H), 1.87 (s, 3H), 1.56 (s, 3H), 1.52 (s, 3H);  $^{13}\text{C}$  NMR (100 MHz, DMSO- $d_6$ )  $\delta$  182.0, 163.9, 153.2, 140.9, 140.9, 136.8, 136.6, 135.0, 131.5, 127.4, 124.0, 123.9, 123.4, 121.9, 119.4, 111.8, 111.6, 105.1, 60.4, 56.2, 44.9, 42.7, 26.1, 25.8, 17.9, 16.6; IR (KBr,  $\nu$ ,  $\text{cm}^{-1}$ ) 3736, 3331, 2851, 2318, 1751, 1611, 1504, 1472, 1377, 1234, 1134, 922, 814, 633; HRMS (ESI $^+$ ) calculated for  $\text{C}_{30}\text{H}_{37}\text{N}_2\text{O}_5$  [ $\text{M}+\text{H}^+$ ], 505.2624; Found 505.5174.

***2-(1-benzyl-1H-indol-3-yl)-2-oxo-N-(3,4,5-trimethoxybenzyl)acetamide (SS-17)***

Yield 73%; Yellowish white solid; m.p: 167-169°C;  $^1\text{H}$  NMR (400 MHz, DMSO- $d_6$ )  $\delta$  9.27 (t,  $J = 6.3$  Hz, 1H), 8.99 (s, 1H), 8.33-8.24 (m, 1H), 7.65-7.56 (m, 1H), 7.39-7.24 (m, 7H), 6.68 (s, 2H), 5.60 (s, 2H), 4.38 (d,  $J = 6.3$  Hz, 2H), 3.76 (s, 6H), 3.64 (s, 3H);  $^{13}\text{C}$  NMR (100 MHz, DMSO- $d_6$ )  $\delta$  182.3, 163.9, 153.2, 141.6, 137.1, 136.9, 136.7, 135.7, 135.0, 129.2, 128.2, 127.8, 127.3, 124.1, 123.4, 122.0, 112.0, 105.2, 60.4, 56.2, 50.2, 42.7; IR (KBr,  $\nu$ ,  $\text{cm}^{-1}$ ) 3736, 3418, 2953, 2374, 2318, 1857, 1792, 1464, 1306, 1128, 1043, 814, 795, 474; HRMS (ESI $^+$ ) calculated for  $\text{C}_{27}\text{H}_{27}\text{N}_2\text{O}_5$  [ $\text{M}+\text{H}^+$ ], 459.1842; Found 459.3230.

**2-(5-(benzyloxy)-1H-indol-3-yl)-2-oxo-N-(3,4,5-trimethoxybenzyl)acetamide (SS-18)**

Yield 71%; Cream white solid; m.p: 199-201°C; <sup>1</sup>H NMR (400 MHz, DMSO-*d*<sub>6</sub>) δ 12.03 (s, 1H), 10.08 (s, 1H), 8.69 (s, 1H), 7.88 (d, *J* = 1.5 Hz, 1H), 7.51-7.43 (m, 2H), 7.42-7.26 (m, 4H), 6.69 (dd, *J* = 7.4, 1.5 Hz, 1H), 6.55 (d, *J* = 1.1 Hz, 2H), 5.10 (d, *J* = 1.1 Hz, 2H), 4.46 (d, *J* = 1.1 Hz, 2H), 3.73 (s, 3H), 3.70 (s, 6H); <sup>13</sup>C NMR (100 MHz, DMSO-*d*<sub>6</sub>) δ 182.9, 167.1, 154.1, 153.4, 137.9, 136.9, 136.4, 132.9, 132.6, 128.3, 127.9, 127.8, 127.2, 115.4, 112.0, 111.7, 106.1, 105.9, 70.2, 60.6, 56.1, 43.6; IR (KBr, ν, cm<sup>-1</sup>) 3788, 3262, 2374, 2284, 1823, 1574, 1570, 1346, 1290, 1184, 1113, 1022, 814, 810, 637, 511; HRMS (ESI<sup>+</sup>) calculated for C<sub>27</sub>H<sub>27</sub>N<sub>2</sub>O<sub>6</sub> [M+H<sup>+</sup>], 475.1864; Found 475.1853.

**2-(5-(benzyloxy)-1-ethyl-1H-indol-3-yl)-2-oxo-N-(3,4,5-trimethoxybenzyl)acetamide (SS-19)**

Yield 78%; Bright yellow solid; m.p: 123-125°C; <sup>1</sup>H NMR (400 MHz, CDCl<sub>3</sub>) δ 9.43 (s, 1H), 9.07 (s, 1H), 8.11 (d, *J* = 2.5 Hz, 1H), 7.57-7.50 (m, 2H), 7.48-7.29 (m, 4H), 7.09 (dd, *J* = 8.9, 2.5 Hz, 1H), 7.07 (s, 2H), 5.21 (s, 2H), 4.41-4.26 (m, 4H), 3.93 (s, 6H), 3.87 (s, 3H), 1.59 (t, *J* = 7.3 Hz, 3H); <sup>13</sup>C NMR (100 MHz, CDCl<sub>3</sub>) δ 179.2, 160.2, 156.4, 153.4, 140.5, 137.1, 135.0, 133.1, 131.1, 128.9, 128.6, 127.9, 127.6, 114.5, 111.5, 111.0, 105.7, 97.2, 70.5, 61.0, 56.1, 42.4, 29.7, 15.1; IR (KBr, ν, cm<sup>-1</sup>) 3362, 2334, 2106, 1717, 1661, 1570, 1545, 1412, 1341, 1256, 1134, 972, 739, 689, 527; HRMS (ESI<sup>+</sup>) calculated for C<sub>29</sub>H<sub>31</sub>N<sub>2</sub>O<sub>6</sub> [M+H<sup>+</sup>], 503.2177; Found 503.2175.

**2-(5-(benzyloxy)-1-(3-methylbut-2-en-1-yl)-1H-indol-3-yl)-2-oxo-N-(3,4,5-trimethoxybenzyl)acetamide (SS-20)**

Yield 69%; Creamy white solid; m.p: 151-153°C; <sup>1</sup>H NMR (400 MHz, CDCl<sub>3</sub>) δ 8.89 (s, 1H), 7.74-7.64 (m, 2H), 7.45-7.26 (m, 5H), 7.23 (s, 1H), 6.89 (dd, *J* = 7.5, 1.6 Hz, 1H), 6.77 (d, *J* = 1.2 Hz, 2H), 5.33 (tt, *J* = 6.2, 1.1 Hz, 1H), 5.08 (s, 2H), 4.56-4.43 (m, 4H), 3.84 (s, 6H), 3.83 (s, 3H), 1.83-1.77 (m, 6H); <sup>13</sup>C NMR (100 MHz, CDCl<sub>3</sub>) δ 183.0, 167.1, 154.7, 153.4, 136.9, 136.7, 136.4, 135.2, 134.6, 132.9, 128.3, 127.9, 127.8, 127.0, 119.4, 115.7, 113.9, 108.2, 106.1, 105.8, 70.2, 60.6, 56.1, 43.6, 43.5, 25.7, 18.1; IR (KBr, ν, cm<sup>-1</sup>) 3686, 3291, 2355, 2303, 1751, 1611, 1468, 1362, 1150, 1043, 972, 885, 814, 773, 676; HRMS (ESI<sup>+</sup>) calculated for C<sub>32</sub>H<sub>35</sub>N<sub>2</sub>O<sub>6</sub> [M+H<sup>+</sup>], 543.2491; Found 543.2477.

**(E)-2-(5-(benzyloxy)-1-(3,7-dimethylocta-2,6-dien-1-yl)-1H-indol-3-yl)-2-oxo-N-(3,4,5-trimethoxybenzyl)acetamide (SS-21)**

Yield 65%; Green solid; m.p: 133-135°C; <sup>1</sup>H NMR (400 MHz, CDCl<sub>3</sub>) δ 9.00 (s, 1H), 8.07 (t, *J* = 2.5 Hz, 1H), 7.89 (d, *J* = 7.1 Hz, 1H), 7.55-7.48 (m, 2H), 7.48-7.25 (m, 5H), 7.06 (dt, *J* = 8.9, 2.5 Hz, 1H), 6.58 (d, *J* = 2.3 Hz, 2H), 5.41 (t, *J* = 7.0 Hz, 1H), 5.18 (s, 2H), 5.11-

5.03 (m, 1H), 4.78 (d,  $J = 6.7$  Hz, 2H), 4.52 (d,  $J = 2.4$  Hz, 2H), 3.89 (s, 6H), 3.87 (s, 3H), 2.12 (s, 2H), 2.17-2.04 (m, 2H), 1.74-1.58 (m, 8H);  $^{13}\text{C}$  NMR (100 MHz,  $\text{CDCl}_3$ )  $\delta$  179.4, 162.6, 156.3, 153.5, 141.7, 140.9, 137.4, 137.2, 133.1, 132.1, 131.4, 128.9, 128.5, 127.9, 127.6, 123.4, 117.9, 114.4, 111.7, 111.3, 105.6, 104.7, 70.5, 60.8, 56.1, 45.5, 43.6, 39.4, 26.1, 25.6, 17.7, 16.6; IR (KBr,  $\nu$ ,  $\text{cm}^{-1}$ ) 3277, 2355, 2318, 2091, 1751, 1701, 1595, 1468, 1377, 1043, 880, 704, 496; HRMS (ESI<sup>+</sup>) calculated for  $\text{C}_{37}\text{H}_{43}\text{N}_2\text{O}_6$  [ $\text{M}+\text{H}^+$ ], 611.3116; Found 611.3104.

***2-(1-benzyl-5-(benzyloxy)-1H-indol-3-yl)-2-oxo-N-(3,4,5-trimethoxybenzyl)acetamide (SS-22)***

Yield 72%; Yellowish white solid; m.p: 128-130°C;  $^1\text{H}$  NMR (400 MHz,  $\text{CDCl}_3$ )  $\delta$  9.08 (s, 1H), 8.07 (d,  $J = 2.5$  Hz, 1H), 7.88 (t,  $J = 6.1$  Hz, 1H), 7.54-7.46 (m, 2H), 7.46-7.26 (m, 6H), 7.26-7.17 (m, 3H), 7.00 (dd,  $J = 8.9, 2.5$  Hz, 1H), 6.58 (s, 2H), 5.37 (s, 2H), 5.17 (s, 2H), 4.52 (d,  $J = 6.1$  Hz, 2H), 3.88 (s, 6H), 3.86 (s, 3H);  $^{13}\text{C}$  NMR (100 MHz,  $\text{CDCl}_3$ )  $\delta$  179.7, 162.4, 156.3, 153.5, 141.6, 137.4, 135.3, 133.1, 131.4, 129.0, 128.8, 128.3, 127.9, 127.0, 114.6, 112.11, 111.6, 105.5, 104.6, 77.7, 77.0, 76.7, 70.5, 60.9, 56.1, 51.5, 43.7; IR (KBr,  $\nu$ ,  $\text{cm}^{-1}$ ) 3858, 3524, 3256, 2390, 2303, 2072, 1838, 1680, 1504, 1412, 1206, 1134, 1007, 826, 773; HRMS (ESI<sup>+</sup>) calculated for  $\text{C}_{34}\text{H}_{33}\text{N}_2\text{O}_6$  [ $\text{M}+\text{H}^+$ ], 565.2333; Found 565.2315.

***2-(7-(benzyloxy)-1H-indol-3-yl)-2-oxo-N-(3,4,5-trimethoxybenzyl)acetamide (SS-23)***

Yield 71%; Off white solid; m.p: 201-203°C;  $^1\text{H}$  NMR (400 MHz,  $\text{DMSO}-d_6$ )  $\delta$  12.45 (s, 1H), 9.24 (t,  $J = 6.3$  Hz, 1H), 8.60 (d,  $J = 3.1$  Hz, 1H), 7.87-7.80 (m, 1H), 7.62-7.55 (m, 2H), 7.47-7.31 (m, 3H), 7.18 (t,  $J = 7.9$  Hz, 1H), 6.97 (dd,  $J = 7.9, 0.8$  Hz, 1H), 6.67 (s, 2H), 5.30 (s, 2H), 4.37 (d,  $J = 6.3$  Hz, 2H), 3.76 (s, 6H), 3.64 (s, 3H);  $^{13}\text{C}$  NMR (100 MHz,  $\text{DMSO}-d_6$ )  $\delta$  182.7, 164.1, 153.2, 145.8, 137.0, 136.9, 135.0, 128.8, 126.8, 123.9, 114.4, 113.2, 106.1, 105.2, 69.9, 67.4, 60.5, 56.8, 42.7, 39.7, 39.5, 25.5; IR (KBr,  $\nu$ ,  $\text{cm}^{-1}$ ) 3788, 3262, 2374, 2284, 1823, 1574, 1570, 1346, 1290, 1184, 1113, 1022, 814, 810, 637, 511; HRMS (ESI<sup>+</sup>) calculated for  $\text{C}_{27}\text{H}_{27}\text{N}_2\text{O}_6$  [ $\text{M}+\text{H}^+$ ], 475.1864; Found 475.1853.

***2-(7-(benzyloxy)-1-(3-methylbut-2-en-1-yl)-1H-indol-3-yl)-2-oxo-N-(3,4,5-trimethoxybenzyl)acetamide (SS-24)***

Yield 61%; Creamy white solid; m.p: 150-153°C;  $^1\text{H}$  NMR (400 MHz,  $\text{CDCl}_3$ )  $\delta$  8.95 (s, 1H), 8.07 (dd,  $J = 8.0, 0.9$  Hz, 1H), 7.93 (t,  $J = 6.1$  Hz, 1H), 7.51-7.32 (m, 5H), 7.24 (t,  $J = 8.0$  Hz, 1H), 6.86 (dd,  $J = 7.9, 0.9$  Hz, 1H), 6.57 (s, 2H), 5.54-5.34 (m, 1H), 5.23 (s, 2H), 5.11-5.04 (m, 2H), 4.52 (d,  $J = 6.1$  Hz, 2H), 3.87 (s, 6H), 3.86 (s, 3H), 1.78-1.63 (m, 6H);  $^{13}\text{C}$  NMR (100 MHz,  $\text{CDCl}_3$ )  $\delta$  179.5, 162.2, 153.4, 146.7, 141.5, 137.3, 136.8, 133.2, 130.4, 128.6, 128.1, 127.6, 125.9, 124.2, 120.1, 115.2, 111.9, 106.3, 104.6, 70.6, 60.8, 56.1, 48.2,

43.6, 29.7, 25.6, 18.0; IR (KBr,  $\nu$ ,  $\text{cm}^{-1}$ ) 3686, 3291, 2355, 2303, 1751, 1611, 1468, 1362, 1150, 1043, 972, 885, 814, 773, 676; HRMS (ESI<sup>+</sup>) calculated for  $\text{C}_{32}\text{H}_{35}\text{N}_2\text{O}_6$  [ $\text{M}+\text{H}^+$ ], 543.2491; Found 543.2482.

***(E)-2-(7-(benzyloxy)-1-(3,7-dimethylocta-2,6-dien-1-yl)-1H-indol-3-yl)-2-oxo-N-(3,4,5-trimethoxybenzyl)acetamide (SS-25)***

Yield 60%; Off white solid; m.p: 98-100°C; <sup>1</sup>H NMR (400 MHz,  $\text{CDCl}_3$ )  $\delta$  8.96 (s, 1H), 8.07 (dd,  $J = 8.0, 0.9$  Hz, 1H), 7.89 (t,  $J = 6.1$  Hz, 1H), 7.51-7.32 (m, 5H), 7.24 (t,  $J = 8.0$  Hz, 1H), 6.86 (dd,  $J = 8.0, 0.9$  Hz, 1H), 6.57 (s, 2H), 5.49-5.39 (m, 1H), 5.24 (s, 2H), 5.12-5.06 (m, 3H), 4.51 (d,  $J = 6.1$  Hz, 2H), 3.88 (s, 6H), 3.86 (s, 3H), 2.11-1.97 (m, 4H), 1.76-1.55 (m, 9H); <sup>13</sup>C NMR (100 MHz,  $\text{CDCl}_3$ )  $\delta$  179.5, 162.5, 153.5, 146.7, 141.7, 140.0, 137.4, 133.1, 131.8, 130.4, 128.6, 127.6, 125.9, 124.1, 120.0, 115.3, 111.9, 106.3, 104.7, 77.3, 76.7, 70.6, 60.8, 56.1, 48.2, 43.6, 39.4, 29.7, 26.3, 25.6, 17.7, 16.4; IR (KBr,  $\nu$ ,  $\text{cm}^{-1}$ ) 3757, 3312, 2845, 2371, 2334, 1788, 1595, 1312, 1234, 1134, 1057, 991, 866, 789, 683; HRMS (ESI<sup>+</sup>) calculated for  $\text{C}_{37}\text{H}_{43}\text{N}_2\text{O}_6$  [ $\text{M}+\text{H}^+$ ], 611.3116; Found 611.3108.

***(E)-2-(6-(benzyloxy)-1-(3,7-dimethylocta-2,6-dien-1-yl)-1H-indol-3-yl)-2-oxo-N-(3,4,5-trimethoxybenzyl)acetamide (SS-26)***

Yield 71%; Off white solid; m.p: 122-124°C; <sup>1</sup>H NMR (400 MHz,  $\text{CDCl}_3$ )  $\delta$  9.21 (s, 1H), 8.56 (d,  $J = 8.7$  Hz, 1H), 8.13 (t,  $J = 6.0$  Hz, 1H), 7.77-7.58 (m, 5H), 7.34 (dd,  $J = 8.7, 2.2$  Hz, 1H), 7.19 (d,  $J = 2.2$  Hz, 1H), 6.82 (s, 2H), 5.64 (t,  $J = 5.4$  Hz, 1H), 5.41 (s, 2H), 5.32 (t,  $J = 4.9$  Hz, 1H), 4.98 (d,  $J = 6.8$  Hz, 2H), 4.76 (d,  $J = 6.1$  Hz, 2H), 3.88 (s, 6H), 3.86 (s, 3H), 2.42-2.27 (m, 4H), 2.09 (s, 3H), 1.99-1.82 (m, 6H); <sup>13</sup>C NMR (100 MHz,  $\text{CDCl}_3$ )  $\delta$  174.7, 157.7, 151.8, 148.7, 136.9, 135.9, 132.6, 132.1, 128.4, 127.3, 123.8, 123.3, 122.7, 118.6, 117.2, 113.0, 108.1, 107.2, 99.9, 91.2, 72.6, 71.7, 65.8, 56.1, 51.4, 40.5, 38.8, 34.7, 21.4, 20.9, 13.0, 11.9; IR (KBr,  $\nu$ ,  $\text{cm}^{-1}$ ) 3701, 3202, 2745, 2145, 2334, 1723, 1595, 1345, 1234, 1125, 1057, 958, 806, 759, 615; HRMS (ESI<sup>+</sup>) calculated for  $\text{C}_{37}\text{H}_{43}\text{N}_2\text{O}_6$  [ $\text{M}+\text{H}^+$ ], 611.3116; Found 611.3105.

***2-(1H-indol-3-yl)-2-oxo-N-(2-(1H-indol-3-yl)ethyl)acetamide (SS-27)***

Yield 87%; Creamy white solid; m.p: 221-223°C; <sup>1</sup>H NMR (400 MHz,  $\text{DMSO}-d_6$ )  $\delta$  12.22 (s, 1H), 10.86 (s, 1H), 8.86 (t,  $J = 6.0$  Hz, 1H), 8.79 (s, 1H), 8.25 (dt,  $J = 8.1, 2.8$  Hz, 1H), 7.62 (d,  $J = 7.8$  Hz, 1H), 7.55 (dt,  $J = 8.0, 2.9$  Hz, 1H), 7.36 (d,  $J = 8.1$  Hz, 1H), 7.33-7.19 (m, 3H), 7.09 (t,  $J = 7.5$  Hz, 1H), 7.00 (t,  $J = 7.4$  Hz, 1H), 3.57-3.50 (m, 2H), 2.97 (t,  $J = 7.6$  Hz, 2H); <sup>13</sup>C NMR (100 MHz,  $\text{DMSO}-d_6$ )  $\delta$  182.6, 163.9, 139.0, 136.7, 127.6, 126.7, 123.8, 123.1, 122.9, 121.7, 118.7, 113.0, 112.6, 112.0, 111.8, 39.8, 39.7, 39.5, 39.3, 25.3; IR (KBr,



$\nu$ ,  $\text{cm}^{-1}$ ) 3611, 2922, 2355, 2324, 1792, 1412, 1327, 1256, 1128, 1007, 826, 810, 673; HRMS (ESI<sup>+</sup>) calculated for  $\text{C}_{20}\text{H}_{18}\text{N}_3\text{O}_2$  [ $\text{M}+\text{H}^+$ ], 332.1321; Found 332.1286.

***2-(1-ethyl-1H-indol-3-yl)-2-oxo-N-(2-(1H-indol-3-yl)ethyl)acetamide (SS-28)***

Yield 80%; Creamy white solid; m.p: 168-170°C; <sup>1</sup>H NMR (400 MHz, DMSO-*d*<sub>6</sub>)  $\delta$  10.86 (s, 1H), 8.86 (t, *J* = 6.0 Hz, 1H), 8.82 (s, 1H), 8.32-8.21 (m, 1H), 7.70-7.58 (m, 2H), 7.39-7.26 (m, 3H), 7.21 (d, *J* = 2.3 Hz, 1H), 7.08 (ddd, *J* = 8.1, 6.9, 1.2 Hz, 1H), 7.00 (ddd, *J* = 8.0, 7.0, 1.1 Hz, 1H), 4.35 (q, *J* = 7.3 Hz, 2H), 3.58-3.47 (m, 2H), 2.96 (t, *J* = 7.5 Hz, 2H), 1.41 (t, *J* = 7.2 Hz, 3H); <sup>13</sup>C NMR (100 MHz, DMSO-*d*<sub>6</sub>)  $\delta$  182.2, 163.9, 140.8, 136.7, 136.4, 127.6, 127.3, 123.9, 123.3, 123.1, 122.0, 121.4, 118.7, 118.7, 112.0, 111.8, 111.6, 111.5, 41.8, 39.8, 25.3, 15.6; IR (KBr,  $\nu$ ,  $\text{cm}^{-1}$ ) 3611, 2922, 2355, 2324, 1792, 1412, 1327, 1256, 1128, 1007, 826, 810, 673; HRMS (ESI<sup>+</sup>) calculated for  $\text{C}_{22}\text{H}_{22}\text{N}_3\text{O}_2$  [ $\text{M}+\text{H}^+$ ], 360.1634; Found 360.3286.

***2-(1-(3-methylbut-2-en-1-yl)-1H-indol-3-yl)-2-oxo-N-(2-(1H-indol-3-yl)ethyl)acetamide (SS-29)***

Yield 83%; Light brown solid; m.p: 187-189°C; <sup>1</sup>H NMR (400 MHz, DMSO-*d*<sub>6</sub>)  $\delta$  10.73 (s, 1H), 8.89 (t, *J* = 6.1 Hz, 1H), 8.76 (s, 1H), 8.32-8.21 (m, 1H), 7.72 (dd, *J* = 7.4, 1.5 Hz, 1H), 7.53 (dd, *J* = 7.4, 1.5 Hz, 1H), 7.31-7.22 (m, 3H), 7.21 (d, *J* = 2.3 Hz, 1H), 7.08 (ddd, *J* = 8.1, 6.9, 1.2 Hz, 1H), 7.00 (ddd, *J* = 8.0, 7.0, 1.1 Hz, 1H), 5.37-5.29 (m, 1H), 4.93 (d, *J* = 7.0 Hz, 2H), 3.58-3.47 (m, 2H), 2.96 (t, *J* = 7.5 Hz, 2H), 1.84 (s, 3H), 1.74 (s, 3H); <sup>13</sup>C NMR (100 MHz, DMSO-*d*<sub>6</sub>)  $\delta$  182.0, 163.7, 160.4, 140.9, 137.6, 136.7, 136.6, 127.6, 127.6, 127.4, 123.9, 123.3, 123.1, 123.0, 122.0, 121.4, 119.5, 118.7, 112.0, 44.9, 39.7, 25.8, 25.3, 25.2, 18.4; IR (KBr,  $\nu$ ,  $\text{cm}^{-1}$ ) 3595, 3299, 2355, 2318, 1611, 1499, 1381, 1256, 1128, 972, 814, 773, 689, 530; HRMS (ESI<sup>+</sup>) calculated for  $\text{C}_{25}\text{H}_{26}\text{N}_3\text{O}_2$  [ $\text{M}+\text{H}^+$ ], 400.1947; Found 400.4830.

***(E)-2-(1-(3,7-dimethylocta-2,6-dien-1-yl)-1H-indol-3-yl)-2-oxo-N-(2-(1H-indol-3-yl)ethyl)acetamide (SS-30)***

Yield 69%; Light brown solid; m.p: 93-95°C; <sup>1</sup>H NMR (400 MHz, DMSO-*d*<sub>6</sub>)  $\delta$  10.87 (s, 1H), 8.86 (t, *J* = 6.0 Hz, 1H), 8.82 (s, 1H), 8.31-8.22 (m, 1H), 7.61 (d, *J* = 7.9 Hz, 1H), 7.58-7.53 (m, 1H), 7.39-7.25 (m, 3H), 7.20 (d, *J* = 2.3 Hz, 1H), 7.12-7.02 (m, 1H), 6.99 (td, *J* = 7.5, 7.0, 1.1 Hz, 1H), 5.36 (t, *J* = 6.6 Hz, 1H), 5.07-4.98 (m, 1H), 4.94 (d, *J* = 7.0 Hz, 2H), 3.51 (dt, *J* = 8.1, 6.4 Hz, 2H), 2.95 (t, *J* = 7.6 Hz, 2H), 2.11-2.01 (m, 4H), 1.84 (s, 3H), 1.56 (s, 3H), 1.52 (s, 3H); <sup>13</sup>C NMR (100 MHz, DMSO-*d*<sub>6</sub>)  $\delta$  182.0, 163.7, 141.0, 140.8, 136.7, 136.6, 131.5, 127.6, 127.4, 125.3, 124.0, 123.8, 123.3, 123.1, 122.0, 121.4, 119.4, 118.7, 112.0, 111.8, 111.7, 111.6, 44.9, 34.8, 30.8, 26.7, 25.8, 25.3, 18.0, 16.6; IR (KBr,  $\nu$ ,  $\text{cm}^{-1}$ )

3630, 3296, 2866, 2355, 2303, 1802, 1696, 1362, 1256, 1128, 1007, 951, 814, 779, 673; HRMS (ESI<sup>+</sup>) calculated for C<sub>30</sub>H<sub>34</sub>N<sub>3</sub>O<sub>2</sub> [M+H<sup>+</sup>], 468.2573; Found 468.5262.

**2-(1-benzyl-1H-indol-3-yl)-2-oxo-N-(2-(1H-indol-3-yl)ethyl)acetamide (SS-31)**

Yield 76%; Brown solid; m.p: 187-189°C; <sup>1</sup>H NMR (400 MHz, DMSO-*d*<sub>6</sub>) δ 10.73 (s, 1H), 9.07 (s, 1H), 8.89 (s, 1H), 8.69 (dd, *J* = 7.4, 1.4 Hz, 1H), 7.62 (dd, *J* = 7.5, 1.5 Hz, 1H), 7.53 (dd, *J* = 7.3, 1.5 Hz, 1H), 7.38-7.23 (m, 7H), 7.16 (s, 1H), 7.06 (m, 2H), 7.02-6.94 (m, 1H), 5.56 (s, 2H), 3.49 (t, *J* = 5.4 Hz, 2H), 2.81 (t, *J* = 5.4 Hz, 2H); <sup>13</sup>C NMR (100 MHz, DMSO-*d*<sub>6</sub>) δ 183.0, 165.7, 137.2, 136.5, 135.0, 134.6, 129.5, 128.0, 127.6, 126.7, 123.9, 122.6, 122.2, 122.1, 121.2, 119.4, 118.7, 115.9, 112.5, 111.4, 110.8, 51.5, 40.4, 26.0; IR (KBr, ν, cm<sup>-1</sup>) 3611, 2922, 2355, 2324, 1792, 1412, 1327, 1256, 1128, 1007, 826, 810, 673; HRMS (ESI<sup>+</sup>) calculated for C<sub>27</sub>H<sub>24</sub>N<sub>3</sub>O<sub>2</sub> [M+H<sup>+</sup>], 422.1790; Found 422.1683.

**2-(5-(benzyloxy)-1H-indol-3-yl)-2-oxo-N-(2-(1H-indol-3-yl)ethyl)acetamide (SS-32)**

Yield 68%; Light brown solid; m.p: 223-225°C; <sup>1</sup>H NMR (400 MHz, DMSO-*d*<sub>6</sub>) δ 12.03 (s, 1H), 10.73 (s, 1H), 8.89 (s, 1H), 8.69 (s, 1H), 7.89 (d, *J* = 1.4 Hz, 1H), 7.57-7.43 (m, 3H), 7.42-7.26 (m, 5H), 7.16 (s, 1H), 7.06 (td, *J* = 7.4, 1.5 Hz, 1H), 6.98 (td, *J* = 7.4, 1.5 Hz, 1H), 6.69 (dd, *J* = 7.4, 1.5 Hz, 1H), 5.10 (s, 1H), 5.10 (d, *J* = 2.3 Hz, 1H), 3.49 (t, *J* = 7.7 Hz, 2H), 2.81 (t, *J* = 7.7 Hz, 2H); <sup>13</sup>C NMR (100 MHz, DMSO-*d*<sub>6</sub>) δ 182.9, 165.7, 154.1, 137.9, 136.9, 136.5, 132.6, 128.3, 127.9, 127.8, 127.6, 127.2, 122.6, 121.2, 119.4, 118.7, 115.4, 112.5, 112.0, 111.7, 111.4, 105.9, 70.2, 40.4, 26.0; IR (KBr, ν, cm<sup>-1</sup>) 3752, 3262, 2340, 2122, 1788, 1582 1412, 1331, 1256, 1113, 991, 916, 851, 617; HRMS (ESI<sup>+</sup>) calculated for C<sub>27</sub>H<sub>24</sub>N<sub>3</sub>O<sub>3</sub> [M+H<sup>+</sup>], 438.1812; Found 438.1797.

**2-(5-(benzyloxy)-1-ethyl-1H-indol-3-yl)-2-oxo-N-(2-(1H-indol-3-yl)ethyl)acetamide (SS-33)**

Yield 73%; Creamy white solid; m.p: 173-175°C; <sup>1</sup>H NMR (400 MHz, CDCl<sub>3</sub>) δ 9.02 (s, 1H), 8.13-8.03 (m, 2H), 7.72-7.65 (m, 2H), 7.55-7.48 (m, 2H), 7.47-7.38 (m, 1H), 7.42 (s, 1H), 7.43-7.31 (m, 2H), 7.34-7.02 (m, 5H), 5.17 (s, 2H), 4.23 (q, *J* = 7.3 Hz, 2H), 3.75 (q, *J* = 6.7 Hz, 2H), 3.15-3.07 (m, 2H), 1.57 (t, *J* = 7.3 Hz, 3H); <sup>13</sup>C NMR (100 MHz, CDCl<sub>3</sub>) δ 180.1, 162.6, 156.2, 141.6, 137.1, 136.4, 135.3, 131.4, 129.0, 128.5, 128.3, 127.9, 127.7, 127.1, 122.2, 119.5, 118.7, 114.6, 112.7, 112.1, 111.5, 111.2, 105.4, 70.5, 51.7, 39.3, 25.3; IR (KBr, ν, cm<sup>-1</sup>) 3773, 3262, 2371, 2349, 2106, 1823, 1574, 1402, 1256, 1007, 935, 810, 739, 673; HRMS (ESI<sup>+</sup>) calculated for C<sub>29</sub>H<sub>28</sub>N<sub>3</sub>O<sub>3</sub> [M+H<sup>+</sup>], 466.2125; Found 466.2114.

***2-(5-(benzyloxy)-1-(3-methylbut-2-en-1-yl)-1H-indol-3-yl)-2-oxo-N-(2-(1H-indol-3-yl)ethyl)acetamide (SS-34)***

Yield 70%; Yellowish brown solid; m.p: 116-118°C; <sup>1</sup>H NMR (400 MHz, CDCl<sub>3</sub>) δ 8.98 (s, 1H), 8.11 (s, 1H), 8.06 (d, *J* = 2.5 Hz, 1H), 7.72-7.64 (m, 2H), 7.55-7.47 (m, 2H), 7.47-7.09 (m, 8H), 7.05 (dd, *J* = 8.8, 2.5 Hz, 1H), 5.42 (t, *J* = 6.9 Hz, 1H), 5.16 (s, 2H), 4.74 (d, *J* = 6.9 Hz, 2H), 3.75 (q, *J* = 6.7 Hz, 2H), 3.15-3.07 (m, 2H), 1.89-1.76 (m, 6H); <sup>13</sup>C NMR (100 MHz, CDCl<sub>3</sub>) δ 179.8, 162.7, 156.2, 140.8, 138.4, 137.2, 136.4, 131.4, 128.9, 128.5, 127.8, 127.6, 127.1, 122.2, 122.1, 119.5, 118.7, 118.0, 114.3, 112.7, 111.7, 111.2, 111.1, 105.6, 70.5, 45.3, 39.3, 25.7, 25.3, 18.2; IR (KBr, ν, cm<sup>-1</sup>) 3611, 2816, 2355, 2318, 2072, 1823, 1580, 1508, 1381, 1312, 1128, 972, 829, 689; HRMS (ESI<sup>+</sup>) calculated for C<sub>32</sub>H<sub>32</sub>N<sub>3</sub>O<sub>3</sub> [M+H<sup>+</sup>], 506.2438; Found 506.2430.

***(E)-2-(5-(benzyloxy)-1-(3,7-dimethylocta-2,6-dien-1-yl)-1H-indol-3-yl)-2-oxo-N-(2-(1H-indol-3-yl)ethyl)acetamide (SS-35)***

Yield 55%; Light yellow solid; m.p: 147-149°C; <sup>1</sup>H NMR (400 MHz, CDCl<sub>3</sub>) δ 8.99 (s, 1H), 8.13-8.03 (m, 2H), 7.68 (d, *J* = 7.4 Hz, 2H), 7.55-7.47 (m, 2H), 7.47-7.10 (m, 8H), 7.04 (dd, *J* = 8.9, 2.5 Hz, 1H), 5.45-5.36 (m, 1H), 5.17 (s, 2H), 5.12-5.03 (m, 2H), 4.77 (d, *J* = 6.8 Hz, 2H), 3.75 (q, *J* = 6.7 Hz, 2H), 3.11 (t, *J* = 6.9 Hz, 2H), 2.17-2.07 (m, 2H), 2.12 (s, 3H), 1.86 (s, 3H), 1.76-1.58 (m, 4H); <sup>13</sup>C NMR (100 MHz, CDCl<sub>3</sub>) δ 179.8, 162.7, 156.2, 141.6, 140.9, 137.2, 136.4, 132.0, 131.4, 128.9, 128.5, 127.8, 127.6, 127.1, 123.4, 122.2, 122.0, 119.5, 118.7, 118.05, 114.3, 112.7, 111.7, 111.2, 105.6, 70.6, 45.5, 39.4, 39.3, 26.1, 25.6, 25.3, 17.7, 16.6; IR (KBr, ν, cm<sup>-1</sup>) 3256, 2305, 2295, 2091, 1751, 1681, 1595, 1568, 1377, 1053, 865, 725, 489; HRMS (ESI<sup>+</sup>) calculated for C<sub>37</sub>H<sub>40</sub>N<sub>3</sub>O<sub>3</sub> [M+H<sup>+</sup>], 574.3064; Found 574.3054.

***2-(1-benzyl-5-(benzyloxy)-1H-indol-3-yl)-2-oxo-N-(2-(1H-indol-3-yl)ethyl)acetamide (SS-36)***

Yield 76%; Creamy white solid; m.p: 173-175°C; <sup>1</sup>H NMR (400 MHz, CDCl<sub>3</sub>) δ 9.08 (s, 1H), 8.12-8.03 (m, 2H), 7.68 (ddd, *J* = 7.4, 5.0, 3.2 Hz, 2H), 7.53-7.46 (m, 2H), 7.46-7.27 (m, 7H), 7.29-7.17 (m, 4H), 7.21-7.10 (m, 2H), 5.36 (s, 2H), 5.15 (s, 2H), 3.75 (q, *J* = 6.7 Hz, 2H), 3.15-3.07 (m, 2H); <sup>13</sup>C NMR (100 MHz, CDCl<sub>3</sub>) δ 179.7, 162.7, 156.2, 140.4, 137.2, 136.4, 131.1, 128.8, 128.5, 127.9, 127.7, 127.1, 122.2, 122.1, 119.5, 118.7, 114.4, 112.7, 111.7, 111.2, 110.9, 105.5, 76.7, 70.5, 42.2, 39.3, 25.3, 15.1; IR (KBr, ν, cm<sup>-1</sup>) 3736, 2801, 2517, 2374, 2340, 1873, 1751, 1574, 1346, 1022, 866, 829, 667, 617; HRMS (ESI<sup>+</sup>) calculated for C<sub>34</sub>H<sub>30</sub>N<sub>3</sub>O<sub>3</sub> [M+H<sup>+</sup>], 528.2282; Found 528.2270.

**2-(7-(benzyloxy)-1H-indol-3-yl)-2-oxo-N-(2-(1H-indol-3-yl)ethyl)acetamide (SS-37)**

Yield 68%; Light brown solid; m.p: 223-225°C; <sup>1</sup>H NMR (400 MHz, DMSO-*d*<sub>6</sub>) δ 12.40 (s, 1H), 10.84 (s, 1H), 8.84 (t, *J* = 6.0 Hz, 1H), 8.66 (d, *J* = 1.3 Hz, 1H), 7.83 (d, *J* = 8.0 Hz, 1H), 7.60 (dd, *J* = 9.5, 7.6 Hz, 3H), 7.48-7.31 (m, 4H), 7.25-6.93 (m, 5H), 5.31 (s, 2H), 3.53 (q, *J* = 7.0 Hz, 2H), 2.96 (t, *J* = 7.6 Hz, 2H); <sup>13</sup>C NMR (100 MHz, DMSO-*d*<sub>6</sub>) δ 182.5, 163.8, 145.9, 138.1, 137.4, 136.7, 128.9, 128.5, 128.3, 128.2, 127.6, 126.8, 123.8, 123.1, 121.4, 118.78, 118.7, 114.5, 11.16, 112.0, 111.8, 106.0, 69.9, 25.3; IR (KBr, ν, cm<sup>-1</sup>) 3752, 3262, 2340, 2122, 1788, 1582 1412, 1331, 1256, 1113, 991, 916, 851, 617; HRMS (ESI<sup>+</sup>) calculated for C<sub>27</sub>H<sub>24</sub>N<sub>3</sub>O<sub>3</sub> [M+H<sup>+</sup>], 438.1812; Found 438.1797.

**2-(7-(benzyloxy)-1-(3-methylbut-2-en-1-yl)-1H-indol-3-yl)-2-oxo-N-(2-(1H-indol-3-yl)ethyl)acetamide (SS-38)**

Yield 65%; Yellow solid; m.p: 151-153°C; <sup>1</sup>H NMR (400 MHz, CDCl<sub>3</sub>) δ 9.20 (s, 1H), 8.49 (s, 1H), 8.32 (dd, *J* = 8.0, 0.9 Hz, 1H), 7.94 (t, *J* = 7.8 Hz, 2H), 7.77-7.58 (m, 5H), 7.56-7.37 (m, 3H), 7.34 (d, *J* = 2.3 Hz, 1H), 7.14-7.07 (m, 1H), 5.70 (t, *J* = 6.5 Hz, 1H), 5.48 (s, 2H), 5.31 (d, *J* = 6.8 Hz, 2H), 4.00 (qd, *J* = 6.9, 3.9 Hz, 3H), 3.35 (t, *J* = 6.9 Hz, 2H), 1.99 (s, 3H), 1.91 (s, 3H), 1.53 (t, *J* = 7.0 Hz, 2H); <sup>13</sup>C NMR (100 MHz, CDCl<sub>3</sub>) δ 175.1, 158.0, 142.0, 136.8, 132.01, 125.7, 123.9, 123.4, 122.8, 122.4, 121.2, 119.3, 117.4, 115.4, 114.7, 113.9, 110.5, 107.8, 107.2, 106.5, 101.5, 72.6, 72.3, 65.8, 53.7, 43.4, 34.6, 20.8, 13.7, 13.3; IR (KBr, ν, cm<sup>-1</sup>) 3701, 3277, 2355, 2106, 1802, 1574, 1412, 1342, 1256, 1113, 922, 901, 866, 779, 633, 567; HRMS (ESI<sup>+</sup>) calculated for C<sub>32</sub>H<sub>32</sub>N<sub>3</sub>O<sub>3</sub> [M+H<sup>+</sup>], 506.2438; Found 506.2424.

**(E)-2-(7-(benzyloxy)-1-(3,7-dimethylocta-2,6-dien-1-yl)-1H-indol-3-yl)-2-oxo-N-(2-(1H-indol-3-yl)ethyl)acetamide (SS-39)**

Yield 64%; Light yellow solid; m.p: 99-101°C; <sup>1</sup>H NMR (400 MHz, CDCl<sub>3</sub>) δ 8.95 (s, 1H), 8.13 (s, 1H), 8.06 (dd, *J* = 8.0, 0.9 Hz, 1H), 7.72-7.64 (m, 2H), 7.52-7.33 (m, 6H), 7.30-7.20 (m, 2H), 7.24-7.12 (m, 2H), 7.11 (d, *J* = 2.3 Hz, 1H), 6.86 (dd, *J* = 8.0, 0.9 Hz, 1H), 5.44 (tq, *J* = 6.5, 1.3 Hz, 1H), 5.23 (s, 2H), 5.11-5.02 (m, 3H), 3.74 (q, *J* = 6.8 Hz, 2H), 3.14-3.06 (m, 2H), 2.09-2.04 (m, 5H), 1.78-1.63 (m, 4H), 1.59 (s, 3H); <sup>13</sup>C NMR (100 MHz, CDCl<sub>3</sub>) δ 179.9, 162.7, 146.7, 141.7, 139.9, 136.5, 136.4, 131.8, 130.4, 128.6, 128.1, 127.6, 127.1, 125.9, 124.0, 123.7, 122.2, 122.1, 120.1, 119.5, 118.7, 115.3, 112.7, 111.9, 111.2, 106.2, 70.6, 48.2, 39.4, 39.36 29.7, 26.3, 25.6, 25.3, 18.4, 17.7, 16.4; IR (KBr, ν, cm<sup>-1</sup>) 3682, 3284, 2359, 2334, 1767, 1595, 1483, 1341, 1290, 1219, 1113, 1022, 882, 880, 527, 113; HRMS (ESI<sup>+</sup>) calculated for C<sub>37</sub>H<sub>40</sub>N<sub>3</sub>O<sub>3</sub> [M+H<sup>+</sup>], 574.3064; Found 574.3054.

***(E)-2-(6-(benzyloxy)-1-(3,7-dimethylocta-2,6-dien-1-yl)-1H-indol-3-yl)-2-oxo-N-(2-(1H-indol-3-yl)ethyl)acetamide (SS-40)***

Yield 69%; Creamy yellow solid; m.p: 148-150°C; <sup>1</sup>H NMR (400 MHz, CDCl<sub>3</sub>) δ 9.19 (s, 1H), 8.54 (d, *J* = 8.7 Hz, 1H), 7.96-7.87 (m, 2H), 7.77-7.70 (m, 2H), 7.74-7.58 (m, 4H), 7.56-7.29 (m, 6H), 7.17 (d, *J* = 2.2 Hz, 1H), 5.67-5.58 (m, 1H), 5.40 (s, 2H), 5.33 (dtd, *J* = 6.3, 4.9, 4.3, 2.5 Hz, 1H), 5.01 (q, *J* = 6.7 Hz, 2H), 4.69-4.61 (m, 2H), 3.59-3.21 (m, 4H), 2.91 (d, *J* = 1.4 Hz, 3H), 2.01-1.18 (m, 7H); <sup>13</sup>C NMR (100 MHz, CDCl<sub>3</sub>) δ 175.1, 157.9, 151.7, 136.8, 135.9, 132.5, 131.6, 127.3, 123.8, 123.2, 122.7, 118.6, 117.5, 114.7, 113.9, 113.1, 107.9, 107.2, 106.5, 91.2, 72.6, 72.4, 72.2, 71.9, 65.8, 40.5, 34.6, 34.5, 21.4, 20.9, 20.5, 13.0, 11.9; IR (KBr, ν, cm<sup>-1</sup>) 3773, 3277, 2916, 2355, 2156, 1661, 1412, 1341, 1119, 1007, 922, 866, 795, 667, 515; HRMS (ESI<sup>+</sup>) calculated for C<sub>37</sub>H<sub>40</sub>N<sub>3</sub>O<sub>3</sub> [M+H<sup>+</sup>], 574.3064; Found 574.3054.

***(E)-2-(4-(benzyloxy)-1-(3,7-dimethylocta-2,6-dien-1-yl)-1H-indol-3-yl)-2-oxo-N-(2-(1H-indol-3-yl)ethyl)acetamide (SS-41)***

Yield 75%; Creamy yellow solid; m.p: 151-153°C; <sup>1</sup>H NMR (400 MHz, CDCl<sub>3</sub>) δ 8.86 (s, 1H), 7.82 (s, 1H), 7.53 (dd, *J* = 7.4, 1.4 Hz, 1H), 7.45-7.26 (m, 8H), 7.24-7.12 (m, 4H), 7.07-6.93 (m, 2H), 5.09 (d, *J* = 12.0 Hz, 3H), 4.56-4.48 (m, 2H), 3.38 (t, *J* = 5.0 Hz, 2H), 2.81 (t, *J* = 5.0 Hz, 2H), 2.04 (d, *J* = 2.0 Hz, 4H), 1.82 (d, *J* = 1.2 Hz, 3H), 1.61 (s, 3H), 1.55 (s, 3H); <sup>13</sup>C NMR (100 MHz, CDCl<sub>3</sub>) δ 174.5, 158.4, 149.0, 136.6, 135.6, 134.2, 132.8, 131.6, 127.3, 123.6, 122.5, 119.9, 118.7, 117.4, 114.6, 113.9, 113.3, 112.5, 107.9, 106.5, 101.7, 99.2, 72.6, 72.3, 71.9, 66.1, 46.17, 40.7, 34.2, 34.6, 21.5, 20.9, 20.5, 13.0, 11.8; IR (KBr, ν, cm<sup>-1</sup>) 3658, 3261, 2916, 2856, 1762, 1633, 1568, 1488, 1443, 1381, 1261, 1159, 1027, 727, 685; HRMS (ESI<sup>+</sup>) calculated for C<sub>37</sub>H<sub>40</sub>N<sub>3</sub>O<sub>3</sub> [M+H<sup>+</sup>], 574.3064; Found 574.3054.

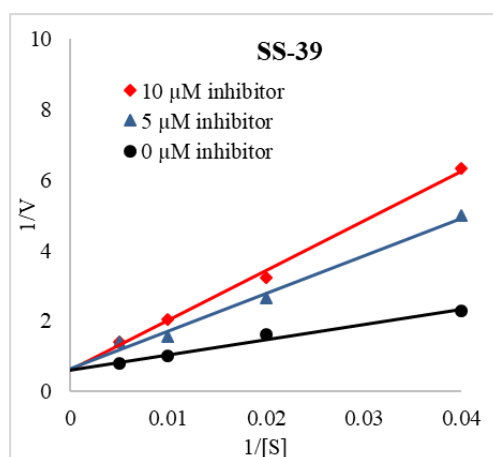
**8.3 | PL inhibition assay**

The procedure for PL inhibition assay and kinetics was performed as per the protocol detailed in chapter 4. Stock solutions of the synthesized analogues **SS-1** to **SS-41** were prepared in DMSO at linear concentrations ranging from 1.56 - 2000 µg/mL. As seen in Table 8.1, **SS-2**, the N-geranyl counterpart of **AP-21**, exhibited a comparatively greater potency over **AP-37** and **AP-21**, with an IC<sub>50</sub> value of 3.99 µM. **SS-1**, with the N-prenyl substitution, however, exhibited comparatively lower potential (IC<sub>50</sub> = 5.48 µM). Further, various benzyloxy indole analogues with different N-substitutions (**SS-3** to **SS-12**) were also evaluated. The most potent activity was found with **SS-11**, followed by **SS-10** and **SS-7**, with IC<sub>50</sub> values of 2.61, 2.84 and 3.1 µM, respectively. Of these, **SS-11** and **SS-10** possessed N-geranyl substitution in common and varied in the position of the benzyloxy substitution

at C<sub>6</sub> and C<sub>7</sub>, respectively. Conversely, the N-geranyl substituted 5-benzyloxy indolyl oxoacetamide analogue (**SS-6**) exhibited lower potential (IC<sub>50</sub> = 3.89 μM) compared to **SS-11** and **SS-10**. Further, the 4-benzyloxy-N-geranyl analogue (**SS-12**), did not exhibit potent PL inhibition (IC<sub>50</sub> - 7.91 μM).

Considering the potential role of -CH<sub>2</sub>- linker at the arylamide substitution, we intended to understand the effect of a trimethoxybenzyl in place of trimethoxyphenyl substitution (as seen with **SS-13** to **SS-26**). As summarized in Table 8.1, all these analogues exhibited potent inhibition with an exception for **SS-13** and **SS-14** that exhibited activity in the range of 15 - 25 μM. Further, these analogues exhibited a better PL inhibitory potential in comparison to their trimethoxyphenyl counterparts with an exception for 5-benzyloxy indole analogues (**SS-18** to **SS-22**) that exhibited a lower or equipotent activity. These facts supported the requirement of a linker between the amide -NH and the aryl substitution. Further, literature reports suggest that the presence of heteroaryl groups can result in better π-cation interaction in comparison to the simple aryl groups [1]. Inspired by the bis-indole nucleus in conophylline, the trimethoxybenzyl substitution was replaced with a 2-(1H-indol-3-yl)ethyl moiety to obtain analogues **SS-27** to **SS-41**. These analogues exhibited activity pattern similar to the other two series, while exhibiting better inhibition profiles. Analogue **SS-39** with N-geranyl substitution on the 7-benzyloxy indole nucleus exhibited the most potent activity in the series with IC<sub>50</sub> value of 1.68 μM comparable to that of the standard drug, orlistat (IC<sub>50</sub> = 0.99 μM).

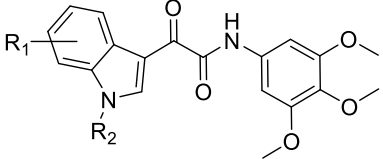
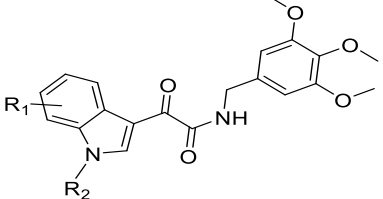
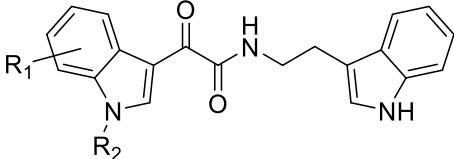
Enzyme kinetics of **SS-39** indicated a reversible competitive inhibition with K<sub>m</sub> values of 70.11, 162.09 and 232.90 μM at inhibitor concentrations of 0, 5 and 10 μM, respectively, while the V<sub>max</sub> was calculated as 1.598 μM/min (Fig. 8.4). Further, **SS-39** exhibited a K<sub>i</sub> value of 0.98 μM, comparable to the standard drug, orlistat (K<sub>i</sub> = 0.56 μM).



**Fig. 8.4.** Lineweaver-Burk plot for **SS-39** representing reversible competitive inhibition

## Chapter 8

**Table 8.1.** *In vitro* PL inhibitory activities of indolyl oxoacetamide analogues SS-1 to SS-41

											
#	R <sub>1</sub>	R <sub>2</sub>	IC <sub>50</sub> (μM)*	#	R <sub>1</sub>	R <sub>2</sub>	IC <sub>50</sub> (μM)*	#	R <sub>1</sub>	R <sub>2</sub>	IC <sub>50</sub> (μM)*
@AP-6	H	H	17.28 ± 0.49	SS-13	H	H	24.58 ± 1.62	SS-27	H	H	19.98 ± 1.92
@AP-30	H	Ethyl	17.24 ± 1.82	SS-14	H	Ethyl	18.42 ± 1.36	SS-28	H	Ethyl	16.04 ± 0.96
SS-1	H	Prenyl	5.48 ± 0.17	SS-15	H	Prenyl	4.15 ± 0.48	SS-29	H	Prenyl	3.72 ± 0.42
SS-2	H	Geranyl	3.99 ± 0.14	SS-16	H	Geranyl	3.26 ± 0.38	SS-30	H	Geranyl	2.95 ± 0.38
@AP-21	H	Benzyl	4.92 ± 0.29	SS-17	H	Benzyl	4.26 ± 0.52	SS-31	H	Benzyl	3.86 ± 0.49
SS-3	5-benzyloxy	H	5.62 ± 0.68	SS-18	5-benzyloxy	H	5.86 ± 1.26	SS-32	5-benzyloxy	H	5.17 ± 1.12
SS-4	5-benzyloxy	Ethyl	4.66 ± 0.30	SS-19	5-benzyloxy	Ethyl	5.35 ± 0.72	SS-33	5-benzyloxy	Ethyl	4.16 ± 0.47
SS-5	5-benzyloxy	Prenyl	3.94 ± 0.32	SS-20	5-benzyloxy	Prenyl	4.95 ± 0.68	SS-34	5-benzyloxy	Prenyl	4.73 ± 0.86
SS-6	5-benzyloxy	Geranyl	3.89 ± 0.27	SS-21	5-benzyloxy	Geranyl	5.22 ± 0.77	SS-35	5-benzyloxy	Geranyl	4.44 ± 0.64
SS-7	5-benzyloxy	Benzyl	3.1 ± 0.23	SS-22	5-benzyloxy	Benzyl	4.65 ± 0.73	SS-36	5-benzyloxy	Benzyl	3.37 ± 0.36
SS-8	7-benzyloxy	H	5.78 ± 0.49	SS-23	7-benzyloxy	H	5.50 ± 0.91	SS-37	7-benzyloxy	H	3.64 ± 0.57
SS-9	7-benzyloxy	Prenyl	4.14 ± 0.38	SS-24	7-benzyloxy	Prenyl	2.89 ± 0.52	SS-38	7-benzyloxy	Prenyl	2.50 ± 0.42
SS-10	7-benzyloxy	Geranyl	2.84 ± 0.29	SS-25	7-benzyloxy	Geranyl	2.34 ± 0.46	<b>SS-39</b>	<b>7-benzyloxy</b>	<b>Geranyl</b>	<b>1.68 ± 0.28</b>
SS-11	6-benzyloxy	Geranyl	2.61 ± 0.24	SS-26	6-benzyloxy	Geranyl	3.03 ± 0.72	SS-40	6-benzyloxy	Geranyl	2.24 ± 0.41
SS-12	4-benzyloxy	Geranyl	7.91 ± 0.96	<b>Orlistat</b>	-	-	0.99 ± 0.11	SS-41	4-benzyloxy	Geranyl	7.73 ± 1.47

\*All the experiments were performed in triplicate and the values are represented as mean ± SEM; @analogues taken from previous series for comparison

## 8.4 | Structure activity relationship

A general representation of the SAR of the indolyl oxoacetamide analogues **SS-1** to **SS-41** is provided in Fig. 8.5, and can be attributed to the substitutions at  $R_1$ ,  $R_2$  and Ar. At  $R_1$ , the 7-benzyloxy and 6-benzyloxy substituted indolyl oxoacetamides exhibited greater potency over the 5-benzyloxy counterpart, while the 4-benzyloxy indolyl oxoacetamides exhibited comparatively poor inhibition. On the other hand, geranyl substitution at  $R_2$  favoured better potency, followed by the prenyl and benzyl substitutions, while ethyl and unsubstituted analogues exhibited significantly lower potency. This phenomenon, however, was not observed with 5-benzyloxy analogues, wherein the N-benzyl substitution resulted in better potency, while the ethyl, prenyl and geranyl substitutions resulted in comparably lower activity. For the substitution at Ar, the 2-(indol-3-yl)ethyl moiety resulted in a better potency over the trimethoxybenzyl substitution followed by the trimethoxyphenyl substitution. Nevertheless, the PL inhibitory activities of the respective counterparts were not found to be significantly different. Further, this relation was not observed with the 5-benzyloxy analogues, wherein the trimethoxybenzyl moiety resulted in lower potency over the other two substitutions.

7-benzyloxy  $\geq$  6-benzyloxy  $>$  5-benzyloxy  $>$  4-benzyloxy

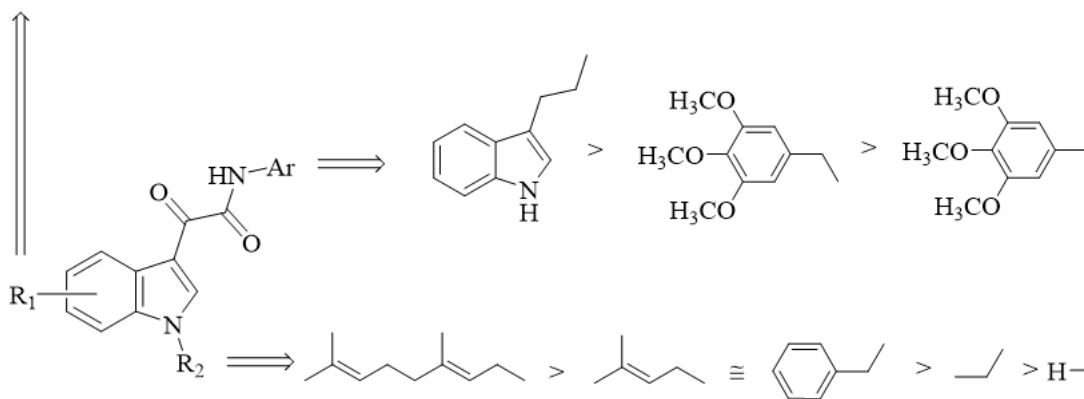


**Fig. 8.5.** Structure-activity relationship for indolyl oxoacetamide analogues **SS-1** to **SS-41**

## 8.5 | Molecular modelling studies

The indolyl oxoacetamide analogues **SS-1** to **SS-41** were subjected to molecular docking studies on human PL (PDB ID: 1LPB), and the results are summarised in Table 8.2. The MolDock scores of the analogues were in significant correlation with their PL inhibitory activity and the most potent analogues, **SS-39** and **SS-40** exhibited a potential MolDock score of -186.456 and -180.375 kcal/mol, respectively. The most common H-bond interactions were found with Phe 77 and His 151, while  $\pi$ - $\pi$  stackings were majorly found with Phe 77, Tyr 114 and Phe 215. Further, the N-geranyl substitution resulted in dense  $\pi$ -



## Chapter 8

---

alkyl interactions with the amino acids of the lid domain that were not seen with the other substitutions (Table 8.2). The docking poses of various benzyloxy substituted N-geranyl analogues (**SS-35**, **SS-39**, **SS-40** and **SS-41**) are represented in Fig. 8.6, which clearly indicated that the 6- and 7-benzyloxy substitutions favoured the binding conformation in the active site, while a high degree of steric hinderance was seen with the 4-benzyloxy analogue resulting in greater distance of 5.46 Å between reactive carbonyl and Ser 152. This distance, however, was reduced to 4.92 Å for **SS-35** due to less steric hinderance posed by the 5-benzyloxy substitution. Similar observation was found with the other N-geranyl substituted benzyloxy analogues, **SS-6**, **SS-10**, **SS-11**, **SS-12**, **SS-21**, **SS-25** and **SS-26**. This analysis clearly explained the poor inhibition exhibited by the 4-benzyloxy analogues in comparison to its other benzyloxy counterparts.

## Chapter 8

**Table 8.2.** MolDock scores and interaction summary of indolyl oxoacetamide analogues **SS-1** to **SS-41** with the active site of PL

#	*MolDock score	H-Bond	$\pi$ - $\pi$ stacking	$\pi$ -cation	$\pi$ -alkyl
SS-1	-130.409	Phe 77, Leu 153	Phe 77	-	Phe 77, Ile 78, Ala 178, Pro 180, Phe 215, Ala 260, Leu 264
SS-2	-156.058	Gly 76, Phe 77, His 151	Phe 77	Asp 79, His 263, Arg 256	Phe 77, Ile 78, Leu 153, Ala 178, Pro 180, Phe 215
SS-3	-146.067	Leu 153, Phe 215	Phe 77, Phe 215	His 263, Arg 256	Ala 178, Pro 180
SS-4	-144.509	Phe 77	Phe 77, Phe 215	His 263, Arg 256	Ala 178, Pro 180, Ala 259
SS-5	-158.197	His 151, Ser 152, His 263	Phe 77, Phe 215	His 263, Arg 256	Ile 208, Leu 213, Phe 215
SS-6	-171.507	Ser 152	Phe 77, Phe 215	His 263	Ile 78, Pro 180, Cys 181, Phe 215, Arg 256, Ala 259, Ala 260
SS-7	-160.351	Gly 76, Phe 77, His 151	Phe 77, Tyr 114, Phe 215	His 263, Arg 256	Ile 78, Ala 178, Pro 180, Ala 260
SS-8	-149.745	Gly 76, Phe 77, His 151, Arg 256	Tyr 114, Phe 215	His 263, Arg 256	Ile 78, Asp 79, Pro 180, Ala 260
SS-9	-159.382	Phe 77, His 151, Arg 256	Tyr 114, Phe 215	His 263, Arg 256	Ile 78, Leu 213, Ala 259, Leu 264
SS-10	-158.501	Phe 77	Phe 77, Tyr 114, Phe 215	Asp 79, Arg 256	Ile 78, Leu 153, Ala 178, Pro 180, Phe 215, Ala 259, Ala 260
SS-11	-162.254	Phe 77, Tyr 114, Leu 153	Phe 215	His 263, Arg 256	Phe 77, Tyr 114, Ala 178, Ile 209, Leu 213
SS-12	-153.515	Phe 77	Tyr 114, Phe 215	Arg 256	Pro 180, Ala 259, Ala 260
SS-13	-128.723	Phe 77, His 263	Phe 77, Phe 215	Arg 256	Ile 78, Ala 178
SS-14	-136.352	Phe 77, Leu 153, Arg 256, His 263	Phe 77, Phe 215	His 263, Arg 256	Ile 78, Ala 178, Ala 260, Leu 264
SS-15	-154.514	Phe 77, His 263	Phe 77, Phe 215	Arg 256	Ile 78, Ala 178, Phe 215, Ala 260, His 263
SS-16	-153.101	Phe 77, Arg 256, His 263	Tyr 114, Phe 215	Arg 256	Phe 77, Ile 78, Ala 178, Pro 180, Ile 209, Leu 213
SS-17	-135.654	Gly 76, Phe 77, His 151, Leu 153, Arg 256	Phe 77, Tyr 114, Phe 215	His 263, Arg 256	Ala 178, Ala 260, Leu 264
SS-18	-134.01	Phe 77, Leu 153, Phe 215,	Phe 77, Tyr 114, Phe 215	His 263	Pro 180, Ala 260
SS-19	-135.564	Tyr 114	Phe 77, Tyr 114, Phe 215	His 263	Phe 77, Ile 78, Pro 180

## Chapter 8

SS-20	-155.29	Arg 256	Phe 77	His 263	His 151, Ala 178, Pro 180, Ala 259, Ala 260
SS-21	-158.488	Arg 256	Phe 77, Tyr 114, Phe 215	His 151, His 263	Ala 178, Pro 180, Ala 259
SS-22	-156.326	Phe 77, Leu 153	Phe 77, Tyr 114, Phe 215	His 263	Ala 260, Leu 264
SS-23	-142.633	Gly 76, Phe 77, His 151, Arg 256	Tyr 114	His 263	Leu 153, Ala 178, Pro 180, Ala 259, Ala 260, Leu 264
SS-24	-153.547	Ser 152, His 263	Phe 77, Phe 215	Arg 256	Ile 78, Leu 153, Tyr 114, Ala 178, Pro 180, Ala 260
SS-25	-184.728	Arg 256		Asp 79, Arg 256	Phe 77, Ile 78, Ala 178, Pro 180, Ala 259, Ala 260
SS-26	-165.908	Gly 76, Phe 77, His 151, Ser 152, Arg 256	Phe77, Tyr 114, Phe 215	Arg 256	Pro 180, Ile 209, Leu 213, Phe 215, Leu 264
SS-27	-138.285	Phe 77, Phe 215	Phe 215	Arg 256	Ala 178, Pro 180, Arg 256, Ala 259, Ala 260, Leu264
SS-28	-133.292	Phe 77, His 151, Leu 153, Arg 256, His 263	Phe 77	Arg 256	Ile 78, Ala 178, Phe 215, Arg 256, Ala 259, Ala 260
SS-29	-148.187	Gly 76, Phe 77, His 151, Leu 153	Phe 77	His 263	Ile 78, Ala 178, Ala 259, Ala 260, Leu264
SS-30	-157.894	Phe 77, Ser 152	Tyr 114, His 263	Asp 79, Arg 256	Ile 78, Pro 180, Leu 213, Phe 215, Ala 259, Leu 264
SS-31	-152.087	Phe 77, His 151, Leu 153, Arg 256, His 263	Phe 77	Arg 256, His 263	Ile 78, Ala 178, Ala 259, Ala 260, Leu264
SS-32	-154.359	Phe 215, His 263	Tyr 114, His 263, Phe 215	Arg 256	Ala 178, Pro 180, Ala 259, Ala 260, Arg 256
SS-33	-164.456	Gly 76, Phe 77, His 151	Phe 215	Arg 256, His 263	Ile 78, Tyr 114, Leu 153, Ala 260
SS-34	-159.698	His 151, Ser 152, His 263	Phe 77	Arg 256	Ile 78, Tyr 114, Ala 178, Pro 180, Ile 209, Phe 215
SS-35	-169.096	Phe 77, Tyr 114, Ser 152, His 263	Phe 77, Phe 215	Arg 256	Ile 78, Pro180, Ile 209, Ala 260, Leu 264
SS-36	-155.245	His 151	Phe77, Phe 215, Trp 252	Arg 256, His 263	Pro 180, Arg 256, Ala 259
SS-37	-151.593	Phe 77, His 151, Ser 152, His 263	Tyr 114, Phe 215	His 263	Leu 153, Ala 178, Pro 180, Ile 209, Ala 259, Ala 260
SS-38	-170.222	Phe 77, Arg 256	Phe 77, Tyr 114	Arg 256, His 263	Ile 78, Ala 178, Pro 180, Ala 259, Ala 260
<b>SS-39</b>	<b>-186.456</b>	<b>Phe 77, Arg 256, His 263</b>	<b>Tyr 114, Phe 215</b>	<b>Arg 256</b>	<b>Phe 77, Ile 78, Ala 178, Pro 180, Ile 209, Leu 213, Phe 215, Ala 259, Ala 260, Leu 264</b>
SS-40	-180.375	Ser 152	Phe 77, Tyr 114, Phe 215	His 263	Phe 77, Ile 78, Ala 178, Pro 180, Ile 209, Leu 213, Ala 259, Ala 260, Leu 264
SS-41	-158.398	Arg 256	Phe 215	Arg 256	Ile 78, Leu 153, Leu 213, Ala 259, Ala 260, Leu264

\* MolDock scores are represented in kcal/mol.

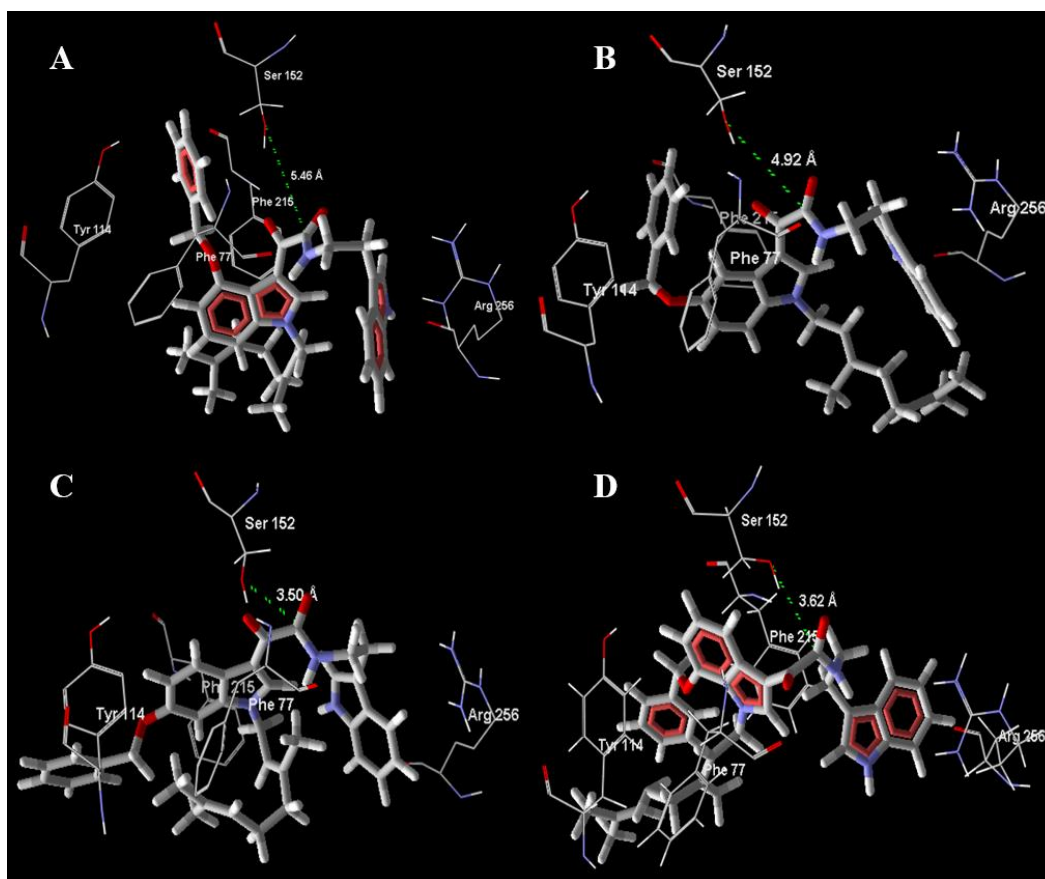


**Fig. 8.6.** 2D docking poses of **SS-41** (A), **SS-35** (B), **SS-40** (C) and **SS-39** (D) highlighting the distance of the reactive carbonyl from Ser 152

On the other hand, the 5-benzyloxy analogues with varying N-substitutions exhibited a different PL inhibitory pattern in comparison to the other benzyloxy analogues. As summarised in SAR, the N-geranyl substitutions resulted in better inhibition, followed by prenyl and benzyl, while the ethyl and unsubstituted analogues resulted in comparatively poor PL inhibition. This observation, however, was not found with the 5-benzyloxy analogues wherein N-geranyl substitution reduced the PL inhibitory activity. Hence, the docking poses of the various N-substituted 5-benzyloxy analogues were analysed. As represented in Fig. 8.7, the presence of ethyl (**SS-33**) and benzyl (**SS-36**) substitutions resulted in the 5-benzyloxy moiety to exist outwards from the active site, favouring a better interaction distance between the reactive carbonyl group and Ser 152. Further, the prenyl substituted analogue (**SS-34**) exhibited a similar conformation, however, this distance has increased to 5.04 Å. On the contrary, the N-geranyl substitution resulted in an inward existence of the 5-benzyloxy moiety, owing to the higher affinity of the former towards the lid domain, eventually resulting in greater steric hinderance due to the benzyloxy moiety.

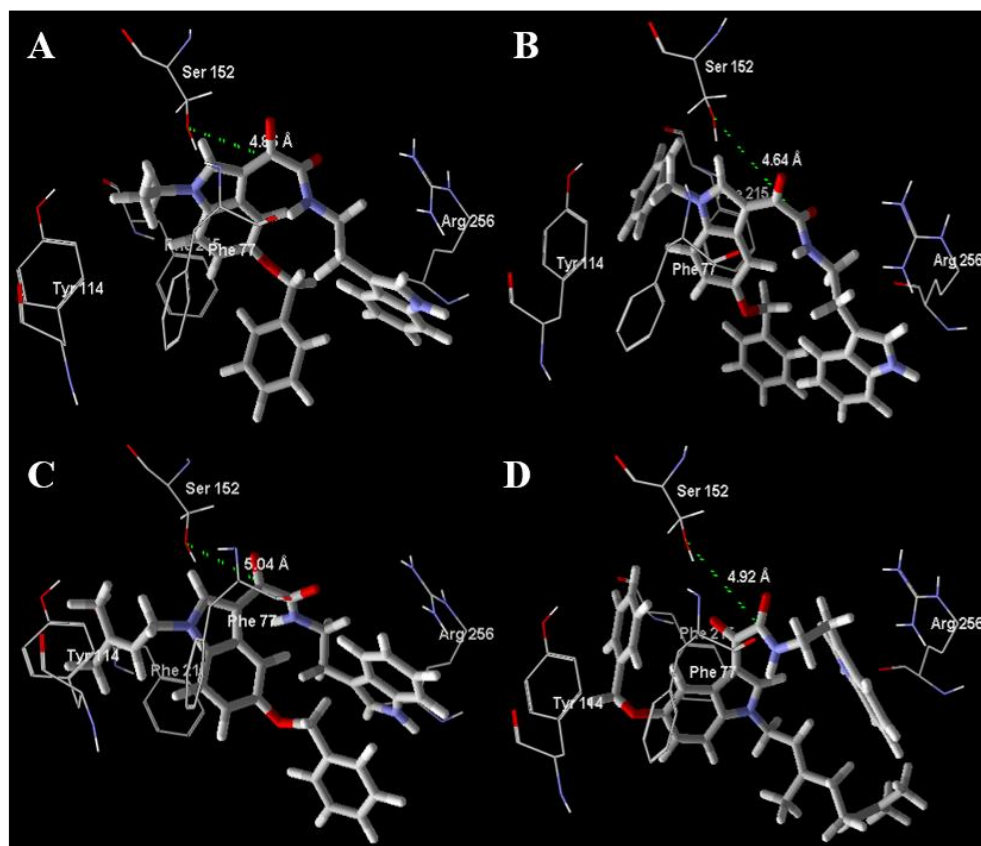


**Fig. 8.7.** 2D docking poses of **SS-33** (A), **SS-36** (B), **SS-34** (C) and **SS-35** (D) highlighting the distance of the reactive carbonyl from Ser152

A 10 ns MD simulation has been performed for the most potent analogue, **SS-39** in complex with PL and the ligand RMSD is represented in Fig. 8.8. Analogue **SS-39** exhibited stable binding conformation throughout the run and deviated by 1 Å after 9 ns.

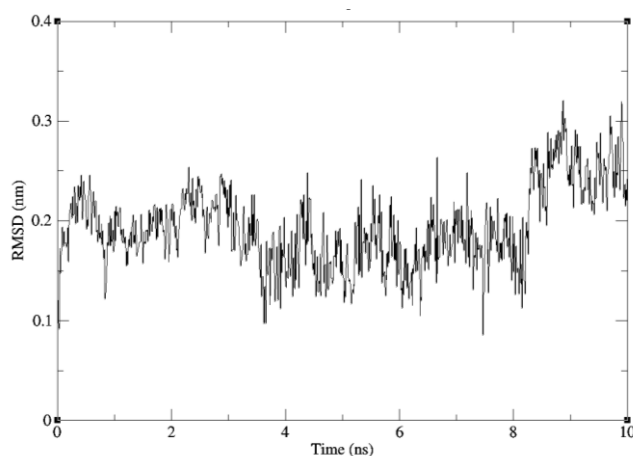


**Fig. 8.8.** RMSD of **SS-39** retrieved through 10 ns MD trajectory

A summary of the various interactions exhibited by **SS-39** with the active site during the MD simulation is detailed under Table 8.3. **SS-39** exhibited stable H-bond interaction

## Chapter 8

and  $\pi$ -cation interaction with Phe 77, Tyr 114, Phe 215 and Arg 256 respectively, throughout the run. Further, a greater intensity of  $\pi$ - $\pi$  stackings were observed with **SS-39** in comparison to **AP-37**. In addition, **SS-39** exhibited stable hydrophobic interactions with various amino acids of the lid domain.

**Table 8.3.** Interaction chart of **SS-39** with PL at different time frames during MD simulation

Time Frame (ns)	$\pi$ - $\pi$ stacking	$\pi$ -cation interactions	$\pi$ -alkyl
0	Phe 77, Tyr 114, Phe 215	Arg 256	Phe 77, Ile 78, Ala 178, Ile 209, Ala 259
1	Phe 77, Tyr 114, Phe 215	-	Phe 77, Ile 78, Ala 178, Ile 209, Arg 256, Ala 259
2	Phe 77, Tyr 114, Phe 215	-	Phe 77, Ile 78, Ala 178, Ile 209, Ala 259, Ala 260
3	Phe 77, Phe 215	-	Phe 77, Ile 78, Ala 178, Ala 259, Ala 260
4	Phe 77, Tyr 114, Phe 215	Arg 256	Phe 77, Ile 78, Ala 178, Pro 180, Leu 213, Arg 256, Ala 259
5	Tyr 114	Arg 256	Phe 77, Ile 78, Leu 213
6	Tyr 114	Arg 256	Phe 77, Leu 213, Arg 256
7	Phe 77, Tyr 114, Phe 215, His 263	Arg 256	Phe 77, Ile 78, Pro 180, Ile 209, Arg 256
8	Tyr 114, Phe 215	Arg 256	Phe 77, Ile 78, Arg 256, Ala 259
9	Phe 77, Phe 215	Arg 256	Phe 77, Ile 78, Arg 256, Ala 259
10	Phe 77, Phe 215, His 263	-	Phe 77, Ile 78, Ile 209, Leu 213, Arg 256, Ala 259

In conclusion, a series of 41 indolyl oxoacetamide analogues have been synthesized and screened *in vitro* to determine their PL inhibition activity. Analogue **SS-39** exhibited a potent PL inhibitory activity of 1.68  $\mu$ M, comparable to the standard drug, orlistat ( $IC_{50}$  = 0.99  $\mu$ M). Apart from, 10 other analogues, (**SS-7**, **SS-10**, **SS-11**, **SS-16**, **SS-24**, **SS-25**, **SS-26**, **SS-30**, **SS-38** and **SS-40**) exhibited better potential in comparison to the NP lead, conophylline ( $IC_{50}$  = 3.31  $\mu$ M).

### References

- [1] Q.S. Du, J.Z. Meng, S.M. Liao, R.B. Huang, Energies and physicochemical properties of cation- $\pi$  interactions in biological structures, *J. Mol. Graph. Model.* 34 (2012) 38–45.

### 9 | ADMET Prediction and *In Vivo* Experiments

#### 9.1 | Rationale

The results from the previous chapters 6-8 have identified conophylline inspired carbazolyl and indolyl oxoacetamide analogues to exhibit potential PL inhibitory activity. Nevertheless, the *in vivo* efficacy of a given drug candidate is predominantly affected, not only by its *in vitro* profile, but also the various pharmacokinetic parameters and the toxicity properties that decide the fate of the drug candidate [1]. For instance, over 50% of the drug failures at various stages of clinical trials have been attributed to their unacceptable Absorption, Distribution, Metabolism, Excretion and Toxicity (ADMET) properties [2]. These properties can be evaluated by a wide range of medium to high throughput *in vitro* assays. However, these assays are time consuming and expensive. Recent years has observed the development of *in silico* ADMET prediction which is based on various data modelling methods, wherein they predict these properties using the input from high quality experimental data [3].

Considering the above facts, the present chapter is focussed towards understanding the ADMET parameters of the most potential analogues from the previous chapters, that in turn would identify the best candidate to proceed for the *in vivo* experiments.

#### 9.2 | Materials and methods

##### 9.2.1 / ADMET prediction

A total of 11 analogues were considered for the ADMET prediction and included the most potential analogues from the DK series (**DK-5**, **DK-6** and **DK-16**), AP series (**AP-21** and **AP-37**) and SS series (**SS-25**, **SS-38**, **SS-40** and **SS-40**) alongside conophylline (NP Lead) and orlistat (standard). For the DK, AP and SS series, analogues with IC<sub>50</sub> less than 10 µM, 5 µM and 2.5 µM, respectively were selected. Various online tools and freeware including SwissADME, admetSAR, ProTox-II and ToxTree v.3.1.0 were used to determine the ADMET [4–7].

##### 9.2.2 / *In vivo* experiments

###### 9.2.2.1 / Animals and diets

Male Swiss albino mice (15–20 g) were purchased from the Central Animal House of Birla Institute of Technology and Science, Pilani (BITS Pilani), Pilani Campus (India) (Registration number: 417/PO/ReBi/2001/CPCSEA). The mice were housed in polyacrylic cages and maintained under standard husbandry conditions (room temperature 22 ± 1°C and

relative humidity of 60%) with 12h light/dark cycle. The animals were fed with either normal pellet diet (NPD) or High Fat Diet (HFD) and filtered water *ad libitum*. The high-fat diet used for the study is summarized in Table 9.1, and contained 20% protein, 45% lipids and 35% carbohydrates by weight [8].

**Table 9.1.** Composition of the HFD used in the *in vivo* experiments

Ingredients	g/kg	Ingredients	g/kg
Lard	350	Cellulose	50
Casein	200	NaCl	30
Starch	100	Soybean oil	32
Corn starch	80	Cholic acid	2
Sucrose	90	L-Cysteine	3
Vitamin mix	60	DL-Methionine	3

### 9.2.2.2 / *Experimental protocol*

Animals were treated according to the guidelines of the Committee for the Purpose of Control and Supervision on Experiments on Animals and all the experimental procedures on animals were in compliance with the Institutional Animal Ethics Committee of BITS Pilani (protocol No: IAEC/RES/20/06/Rev-2/24/20). Briefly, the protocol was divided in to two parts; i) Oral Triglyceride Tolerance Test, ii) HFD fed mice model (4-week treatment study).

#### *Oral Triglyceride Tolerance Test (OTTT)*

The OTTT was conducted as per the previously reported literature to examine the effect of **SS-39** on the intestinal absorption of triglycerides as well as to calculate its dose for the long term treatment study [9]. The mice were divided into six groups (n = 4) and subjected to an overnight fast, before starting the experiment. The mice were then orally administered with (1) olive oil as a positive control, (2) filtered water as a negative control, (3) olive oil plus orlistat (10 mg/kg) as reference control (4) olive oil plus **SS-39** (low dose - 5 mg/kg), (5) olive oil plus **SS-39** (medium dose - 10 mg/kg) and (6) olive oil plus **SS-39** (high dose - 20 mg/kg). The amount of olive oil administered per animal was fixed to 5 mL/kg. Blood samples were collected at 0, 1.5, 3, 4.5, and 6 h after administration of olive oil, and triglyceride contents were detected using commercially available kits (Spinreact S.A.U, Spain).

#### *High fat Diet fed mice model*

The effect of **SS-39** on fat accumulation was examined by administering the drug to HFD fed mice over a period of 4 weeks [10]. Prior to the treatment, all the animals under



## Chapter 9

HFD groups were adapted to the high fat diet for a period of 2 weeks. After the adaptation period, the animals were divided into five groups as summarized in Table 9.2. For the treatment groups, orlistat or **SS-39** were dissolved in 3 %v/v Tween-80 solution and administered to the animals with an oral gavage.

**Table 9.2.** Summary of various groups and drugs administered during the 4-week treatment study

Group No.	Group Name	Drug and Dose
I	NPD	3% v/v Tween-80
II	HFD (Control)	3% v/v Tween-80
III	HFD plus Orlistat (reference)	Orlistat (10 mg/kg)
IV	HFD plus <b>SS-39</b> (Low dose)	<b>SS-39</b> (10 mg/kg)
V	HFD plus <b>SS-39</b> (High dose)	<b>SS-39</b> (20 mg/kg)

The body weights of the animals were recorded weekly and were subjected to an overnight fast at the end of every week, followed by the collection of blood samples using the retro-orbital puncture. The blood samples were then centrifuged (1500 g) to obtain the serum. Various biochemical parameters including glucose, triglycerides, cholesterol and high-density lipoproteins-cholesterol (HDL) were estimated from the serum using commercially available diagnostic kits (Spinreact S.A.U., Spain and Accurex Biomedical Pvt. Ltd., India). The low density lipoprotein-cholesterol (LDL) was calculated using the formula reported in the literature [11].

$$\text{LDL} = [(\text{Serum cholesterol} - \text{HDL}) * 0.9] - [\text{Serum triglycerides} * 0.1] \text{ ----- Formula 9.1}$$

### *Quantification of faecal triglycerides*

Since the inhibition of PL is characterized by the excretion of faeces rich in triglycerides, the faeces of the mice were collected daily during the long-term treatment period, and triglycerides were quantified at the end of every week. The procedure for quantification of faecal triglycerides was performed as per the literature report with minor modifications [9]. Briefly, 1 g of faeces was taken in a separatory funnel and subjected to vigorous shaking in 0.15 M NaCl. To this suspension, chloroform : methanol (4:1 v/v) was added and the shaking was continued. The mixture was allowed to separate and the lower organic phase was then collected, filtered and dried *in vacuo*. The obtained triglycerides were then dissolved in 1 mL ethanol, and the quantity of triglycerides were estimated using commercial kit (Spinreact S.A.U., Spain).

### *Statistical analysis*

All the data were represented as mean  $\pm$  SEM, and the differences were analysed using one-way analysis of variance (ANOVA) followed by post-hoc analysis of Tukey's multiple comparison test to determine significant differences between the groups. Statistical calculation was performed using GraphPad Prism (v 5.0). A level of  $p < 0.05$  was considered to be statistically significant.

### **9.3 | Results and Discussion**

#### **9.3.1 | ADMET prediction**

A total of 11 analogues were considered for the ADMET prediction and the results are summarised in Table 9.3. All the analogues in DK and AP series, as well as conophylline were found to possess a high GI absorption. On the contrary, a majority of the analogues in the SS series (except **SS-38**) possessed low GI absorption similar to the standard drug, orlistat. Further, all the analogues did not possess good blood-brain barrier (BBB) permeability and were found to be good substrates for the CYP3A4 enzyme. The toxicity property was assessed based on three parameters; oral toxicity, carcinogenicity and hepatotoxicity. Orlistat and conophylline possessed moderate oral toxicity (as seen with their low LD<sub>50</sub> of 1300 and 1000 mg/kg, respectively), and were also found to be genotoxic. In addition, orlistat was found to be positive for hepatotoxicity, which is in accordance to the reported literature. The analogues from DK series also possessed genotoxicity and hepatotoxicity. In particular, the most potent analogue from this series, **DK-5**, possessed significant oral toxicity (LD<sub>50</sub> - 1470 mg/kg). Similar results were observed with the AP series, wherein all the analogues possessed significant oral toxicity. However, these analogues were devoid of carcinogenicity or hepatotoxicity. For the SS series, **SS-25** and **SS-39** did not possess oral toxicity. Further, all the analogues in this series were devoid of carcinogenicity and hepatotoxicity. The above analysis clearly indicated analogue **SS-39** to be suitable for further *in vivo* experiments, based on its *in vitro* potential as well as supportive ADMET properties.

## Chapter 9

**Table 9.3.** Summary of ADMET parameters predicted for the potent analogues from each series along with conophylline and orlistat

Series	Molecule	Absorption	Distribution		Metabolism						Toxicity			
					Substrate	Inhibitor					Oral toxicity	Carcinogenicity		Liver toxicity
		GI absorption	BBB permeant	Pgp substrate	CYP 3A4	CYP1 A2	CYP 2C19	CYP 2C9	CYP 2D6	CYP 3A4	*LD <sub>50</sub>	Genotoxic	Non genotoxic	
<b>NP Lead</b>	Conophylline	High	No	Yes	Yes	No	No	No	No	No	1000	Yes	No	No
<b>I</b>	<b>DK-5</b>	<b>High</b>	<b>No</b>	<b>No</b>	<b>Yes</b>	<b>No</b>	<b>Yes</b>	<b>Yes</b>	<b>No</b>	<b>Yes</b>	<b>1470</b>	<b>Yes</b>	<b>Yes</b>	<b>Yes</b>
	DK-6	High	No	No	Yes	No	Yes	Yes	Yes	Yes	5000	Yes	Yes	Yes
	DK-16	High	No	No	Yes	Yes	Yes	Yes	Yes	Yes	5000	Yes	No	Yes
<b>II</b>	AP-21	High	No	No	Yes	No	Yes	Yes	Yes	Yes	380	No	No	No
	<b>AP-37</b>	<b>High</b>	<b>No</b>	<b>No</b>	<b>Yes</b>	<b>No</b>	<b>Yes</b>	<b>Yes</b>	<b>Yes</b>	<b>Yes</b>	<b>78</b>	<b>No</b>	<b>No</b>	<b>No</b>
<b>III</b>	SS-25	Low	No	Yes	Yes	Yes	No	No	Yes	No	5000	No	No	No
	SS-38	High	No	No	Yes	Yes	Yes	Yes	Yes	Yes	1250	No	No	No
	<b>SS-39</b>	<b>Low</b>	<b>No</b>	<b>Yes</b>	<b>Yes</b>	<b>Yes</b>	<b>No</b>	<b>No</b>	<b>Yes</b>	<b>Yes</b>	<b>5000</b>	<b>No</b>	<b>No</b>	<b>No</b>
	SS-40	Low	No	Yes	Yes	Yes	No	No	Yes	Yes	1000	No	No	No
<b>Reference</b>	<b>Orlistat</b>	<b>Low</b>	<b>No</b>	<b>Yes</b>	<b>Yes</b>	<b>No</b>	<b>No</b>	<b>Yes</b>	<b>No</b>	<b>No</b>	<b>1300</b>	<b>Yes</b>	<b>No</b>	<b>Yes</b>

\*Predicted value represented as mg/kg; Most potent analogue from each series and orlistat highlighted in grey and bold

9.3.2 / *In vivo experiments*9.3.2.1 / *Oral Triglyceride Tolerance Test (OTTT)*

The serum triglyceride levels determined during various time points of OTTT is represented in Fig. 9.1. The triglyceride levels increased drastically in the positive control group followed by the low dose group of **SS-39** (group 1 and 4, respectively) at 1.5 h. On the contrary, administration of medium and high dose of **SS-39** (group 5 and 6, respectively) did not result in significant increase in the triglyceride levels. Moreover, the triglyceride levels in these groups were not significantly ( $p < 0.05$ ) different from the orlistat group (group 3), calculated at similar time point. These results clearly indicated that **SS-39** at 10 and 20 mg/kg dose exhibited profiles comparable to the standard drug orlistat.

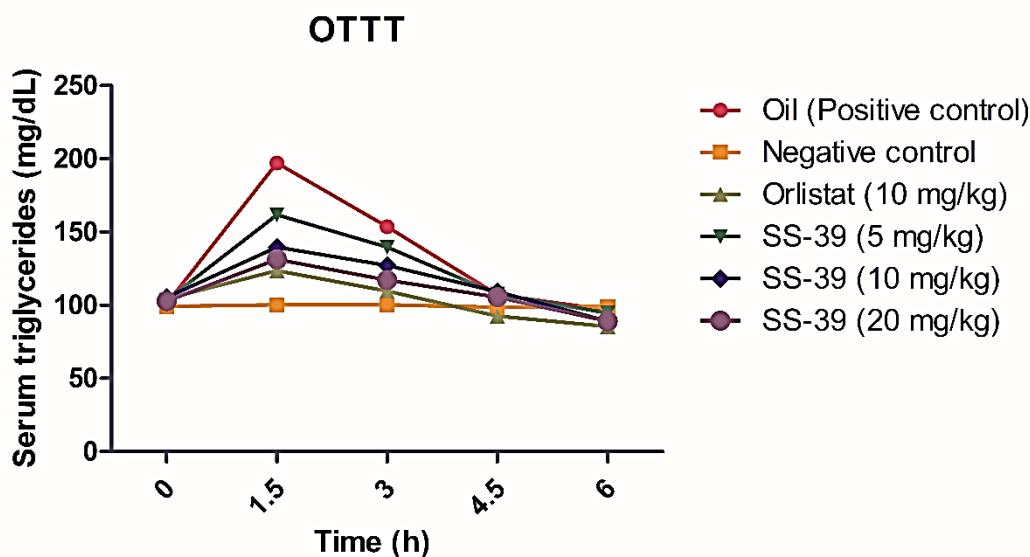


**Fig. 9.1.** Graphical representation of results from the OTTT summarising the serum triglyceride levels at various time points ( $n = 4$ ;  $p < 0.05$ )

9.3.2.2 / *4-week treatment protocol*

The results from the OTTT highlighted **SS-39** to exhibit significant reduction in triglyceride absorption at 10 and 20 mg/kg dose. Consequently, these two doses of **SS-39** were selected for the long-term treatment study, while orlistat (10 mg/kg) was used as reference control. The body weights of the animals in various groups were determined at the end of every week and are represented in Fig. 9.2A. The weights of the HFD group animals has significantly increased to 40g by the end of 4<sup>th</sup> week. However, a significant reduction was observed in the treatment groups, wherein the **SS-39** (20 mg/kg) administered group exhibited similar results in comparison to the orlistat treated group.

## Chapter 9

Various biochemical parameters were also assessed during the treatment period and are summarized in Fig. 9.2 and 9.3. For the serum glucose, the HFD control group exhibited significant variation compared to the NPD group. Further, the glucose levels were significantly reduced in the orlistat treated group after the treatment period. However, the **SS-39** treated groups did not exhibit significant reduction in the serum glucose in comparison to the HFD control (Fig. 9.2B). Similarly, the HFD control group exhibited significant variation with reference to the triglycerides, cholesterol, HDL and LDL, while orlistat group exhibited no significant difference from NPD group after the treatment period. Further, the **SS-39** at 20 mg/kg dose exhibited results comparable to the orlistat, with an exception for the LDL. The low dose group of **SS-39** (10 mg/kg), however, exhibited significant difference in comparison to the reference group (Fig. 9.3).

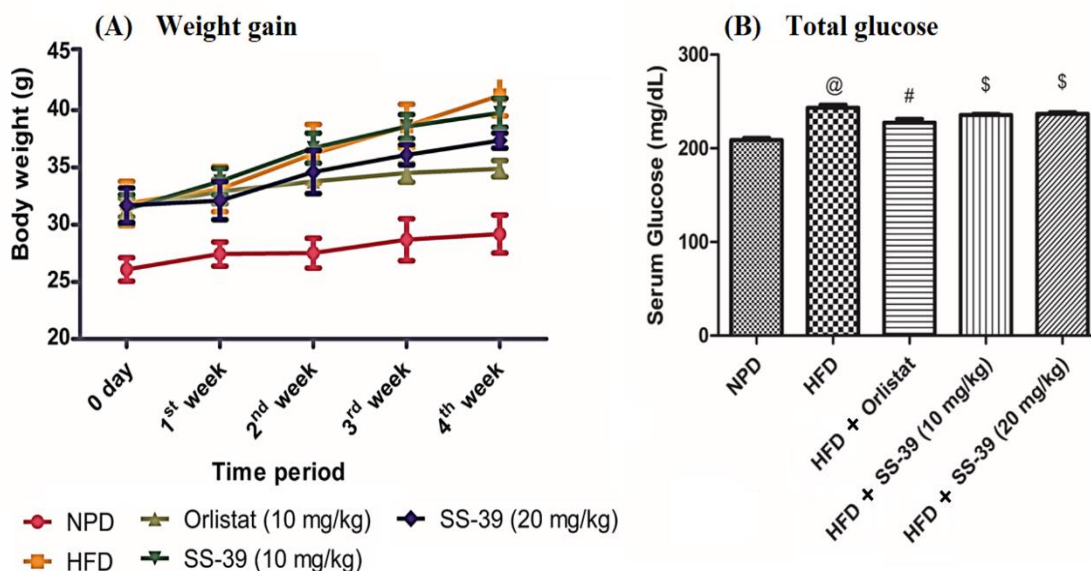


**Fig. 9.2.** (A) Increment in body weights of various groups during the four-week treatment protocol; (B) Serum glucose levels determined from various groups at the end of the four-week treatment period. (All values are represented as mean  $\pm$  SEM; <sup>@</sup> $p < 0.001$  Vs. NPD; <sup>#</sup> $p < 0.01$  Vs. HFD; <sup>\$</sup>ns Vs. HFD).

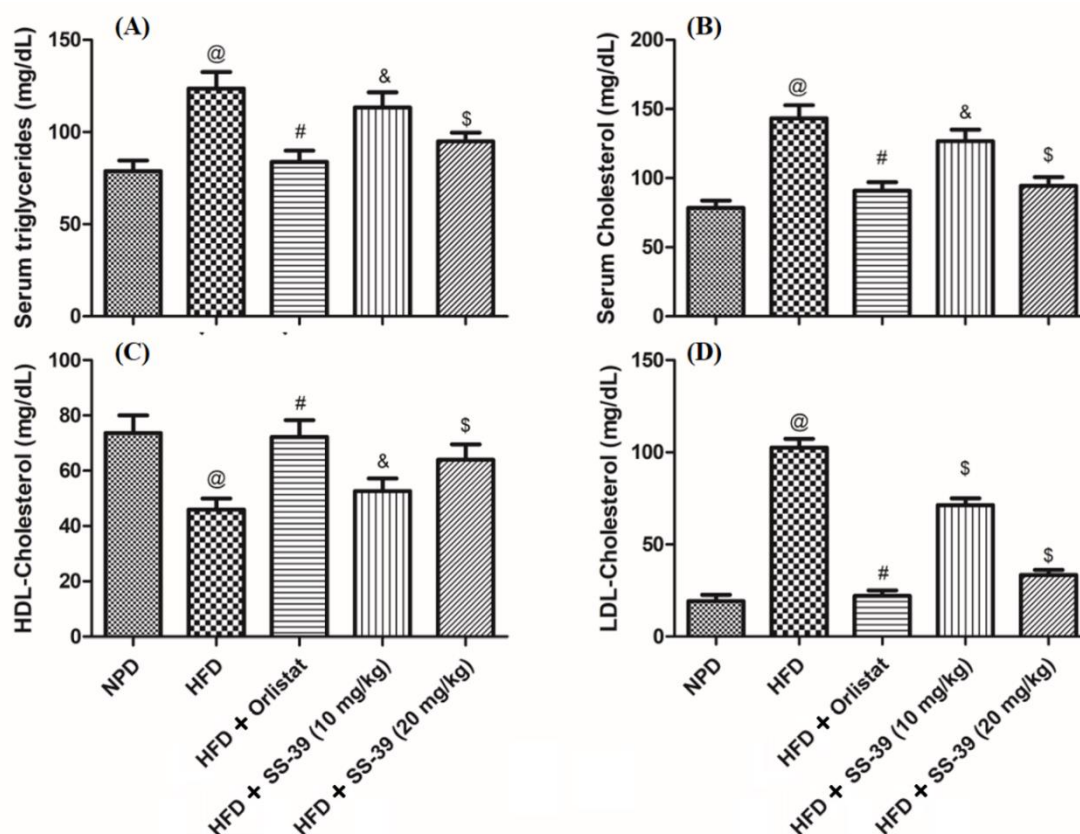


**Fig. 9.3.** (A) Serum triglyceride and (B) Serum total cholesterol (@ $p < 0.001$  Vs. NPD; #ns Vs. NPD; & $p < 0.001$  Vs. HFD + Orlistat; \$ns Vs. HFD + Orlistat) (C) Serum HDL-cholesterol (@ $p < 0.001$  Vs. NPD; #ns Vs. NPD; \$ $p < 0.001$  Vs. HFD + Orlistat; \$ $p < 0.05$  Vs. HFD + Orlistat) (D) Serum LDL-cholesterol (@ $p < 0.001$  Vs. NPD; #ns Vs. NPD; \$ $p < 0.001$  Vs. HFD + Orlistat). All the biochemical parameters were determined after the 4-week treatment period and the values are represented as mean  $\pm$  SEM).

### 9.3.2.3 / Quantification of faecal triglycerides

The results from OTTT indicated that **SS-39** inhibited intestinal absorption of triglycerides similar to orlistat. Further, **SS-39** at 20 mg/kg exhibited similar activity compared to orlistat (10 mg/kg), in various biochemical parameters during the four-week treatment study. In order to understand, if **SS-39** has exhibited its antiobesity action through the inhibition of PL, the triglyceride levels were quantified from the faecal samples

As represented in Fig. 9.4, the faecal triglyceride levels were significantly higher in the HFD control compared to the NPD group. Further, these levels increased significantly with the administration of either orlistat (10 mg/kg) or **SS-39** (20 mg/kg). Moreover, the triglyceride levels in these two groups did not exhibit any significant difference. However,

**SS-39** at low dose (10 mg/kg) was not effective, as it did not exhibit significant difference from the HFD control.

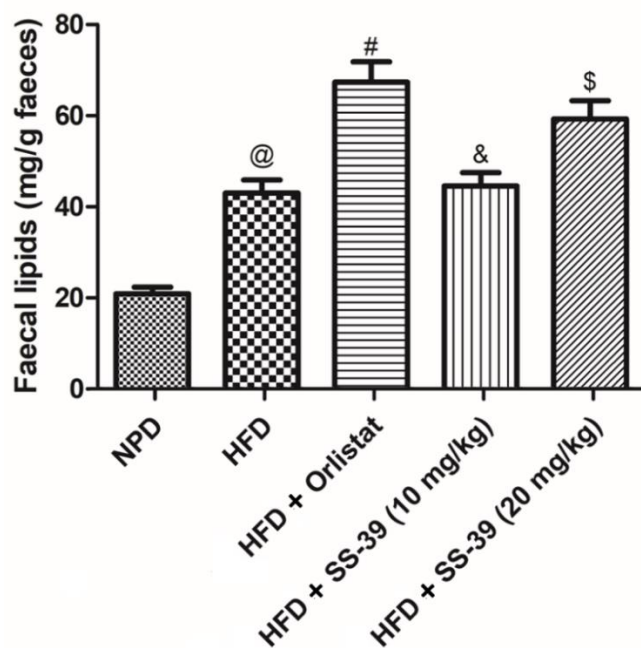


**Fig. 9.4.** Faecal triglyceride levels determined from various groups. (All the values are represented as mean  $\pm$  SEM calculated from four readings, corresponding to four weeks.  $p < 0.001$  Vs. NPD; # $p < 0.001$  Vs. NPD; & $ns$  Vs. HFD; \$ $ns$  Vs. HFD + Orlistat).

In summary, the ADMET prediction highlighted **SS-39** as a suitable candidate for *in vivo* experiments. **SS-39** was found to possess low GI absorption similar to the standard, orlistat. Further, it was devoid of any form of toxicity in contrary to orlistat. For the *in vivo* experiments, two studies were conducted, namely OTTT and 4-week treatment study. **SS-39** at 20 mg/kg dose exhibited similar pharmacological efficacy in comparison to the standard drug, orlistat (10 mg/kg). Further, the quantification of faecal triglycerides clearly indicated that **SS-39** acted through PL inhibition.

### References

- [1] G. Moroy, V.Y. Martiny, P. Vayer, B.O. Villoutreix, M.A. Miteva, Toward *in silico* structure-based ADMET prediction in drug discovery, *Drug Discov. Today*. 17 (2012) 44–55.
- [2] F. Cheng, W. Li, G. Liu, Y. Tang, *In silico* ADMET prediction: Recent advances, current challenges and future trends, *Curr. Top. Med. Chem.* 13 (2013) 1273–1289.
- [3] S.R. Kazmi, R. Jun, M.S. Yu, C. Jung, D. Na, *In silico* approaches and tools for the prediction of drug metabolism and fate: A review, *Comput. Biol. Med.* (2019) 54–64.
- [4] F. Cheng, W. Li, Y. Zhou, J. Shen, Z. Wu, G. Liu, P.W. Lee, Y. Tang, admetSAR: A comprehensive source and free tool for assessment of chemical ADMET properties, (2012) 3099–3105.
- [5] H. Yang, C. Lou, L. Sun, J. Li, Y. Cai, Z. Wang, W. Li, G. Liu, Y. Tang, admetSAR 2.0: Web-service for prediction and optimization of chemical ADMET properties, *Bioinformatics*. 35 (2018) 1067–1069.
- [6] P. Banerjee, A.O. Eckert, A.K. Schrey, R. Preissner, ProTox-II: A webserver for the prediction of toxicity of chemicals, *Nucleic Acids Res.* 46 (2018) W257–W263.
- [7] A. Daina, O. Michielin, V. Zoete, SwissADME: A free web tool to evaluate pharmacokinetics, drug-likeness and medicinal chemistry friendliness of small molecules, *Sci. Rep.* 7 (2017) 42717.
- [8] D. Shi, C. Chen, S. Zhao, F. Ge, D. Liu, H. Song, Walnut polyphenols inhibit pancreatic lipase activity *in vitro* and have hypolipidemic effect on high-fat diet-induced obese mice, *J. Food Nutr. Res.* 2 (2014) 757–763.
- [9] T.Y. Chen, M.M.C. Wang, S.K. Hsieh, M.H. Hsieh, W.Y. Chen, J.T.C. Tzen, Pancreatic lipase inhibition of strictinin isolated from Pu'er tea (*Camellia sinensis*) and its anti-obesity effects in C57BL6 mice, *J. Funct. Foods*. 48 (2018) 1–8.
- [10] G. Avci, I. Küçükkurt, E. Küpeli Akkol, E. Yesilada, Effects of escin mixture from the seeds of *Aesculus hippocastanum* on obesity in mice fed a high fat diet, *Pharm. Biol.* 48 (2010) 247–252.
- [11] Y. Chen, X. Zhang, B. Pan, X. Jin, H. Yao, B. Chen, Y. Zou, J. Ge, H. Chen, A modified formula for calculating low-density lipoprotein cholesterol values, *Lipids Health Dis.* 9 (2010) 52.



### 10 | Conclusion and Future Perspectives

#### 10.1 | General conclusion

Recent decades have seen drastic changes in the global food system and eating habits, that has resulted in a rapid upsurge in energy consumption transforming obesity into a global epidemic. Moreover, the severe comorbid factors associated with chronic obesity, has placed the global obese population under a greater risk of mortality. Orlistat, a potent pancreatic lipase inhibitor, have been used clinically over the past two decades in successful treatment of obesity. However, a long-term exposure to this drug resulted in severe adverse events including hepatotoxicity and acute pancreatitis, highlighting the urge to develop safer and effective anti-obesity drugs.

Natural products as a vast reservoir of biologically active chemical entities, represent an effective source in the treatment of various diseases and disorders, while maintaining tolerable side effects. Henceforth, the thesis work initiated with a detailed literature search to identify structural features of natural products and synthetic scaffolds, that resulted in potential PL inhibition. A set of 20 Indian medicinal plants/parts were selected and screened for their PL inhibitory potential. The study highlighted the methanol extract of *Tabernaemontana divaricata* leaves as a source of potential PL inhibitory leads. Further experiments that involved bioassay guided fractionation resulted in the isolation and identification of conophylline as a potent PL inhibitory lead (with an  $IC_{50}$  of 3.31  $\mu$ M). The structural features of conophylline were further established by performing *in-silico* molecular docking and molecular dynamics studies. In addition, HPTLC method development, validation and quantification of conophylline in *T. divaricata* samples obtained from various seasons and different extraction methods was also performed. Nevertheless, conophylline possessed lower potential in comparison to orlistat ( $IC_{50} = 0.99$   $\mu$ M).

Hence, molecular modelling and bioassay guided lead optimization was performed that resulted in various carbazolyl and indolyl oxoacetamide analogues. Analogue **SS-39** exhibited a potent activity with an  $IC_{50}$  of 1.68  $\mu$ M comparable to orlistat. Apart from various other indolyl oxoacetamides also exhibited potent PL inhibitory activity ( $IC_{50} < 5$   $\mu$ M). The potent PL inhibition exhibited by various indolyl oxoacetamides has inspired to further understand their *in vivo* efficacy. Prior to the *in vivo* studies, the most potent analogues from various series of carbazolyl and indolyl oxoacetamides were evaluated for their ADMET properties using various *in silico* tools, that helped to decide the suitable candidate for animal

experiments. The prediction highlighted **SS-39** to possess low GI absorption similar to orlistat and was devoid of any form of toxicity in contrary to orlistat. Hence **SS-39** was selected for the *in vivo* experiments and two studies were conducted, namely OTTT and 4-week treatment study (using HFD fed mice model). **SS-39** at 20 mg/kg exhibited a similar anti-obesity efficacy in comparison to the standard drug, orlistat (10 mg/kg). Further, the quantification of faecal triglycerides clearly indicated that **SS-39** acted through PL inhibition.

In conclusion, the thesis work resulted in a potent indolyl oxoacetamide analogue, **SS-39** identified through molecular modelling and bioassay guided structural modifications to conophylline (Fig. 10.1), wherein the anti-obesity efficacy of this analogue was significantly similar to the standard, orlistat. Further, **SS-39** did not possess any toxicity in contrary to orlistat, as observed with preliminary ADMET prediction.

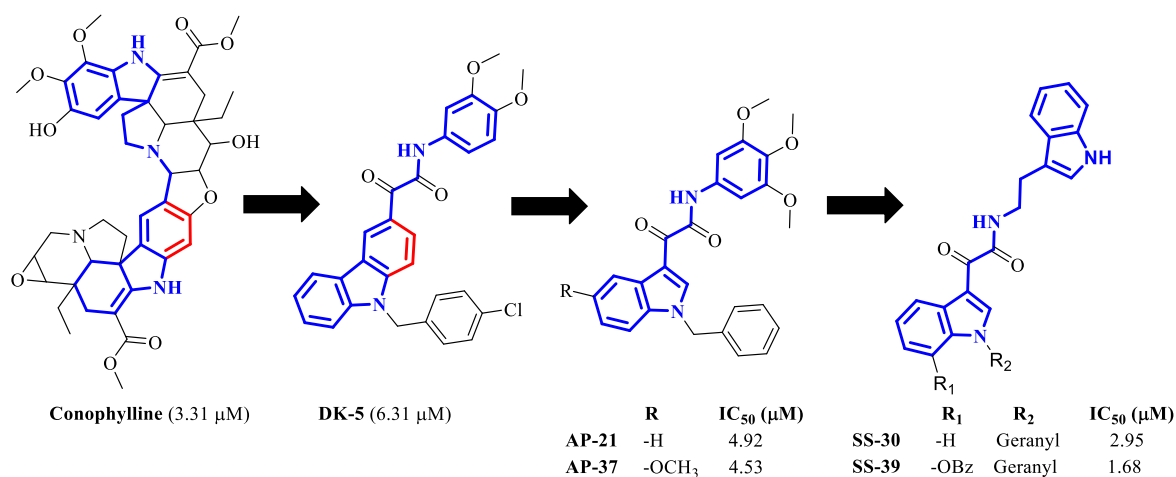


**Fig. 10.1.** Schematic flow representing the structural modifications of conophylline to identify potent PL inhibitory bis(indolyl)oxoacetamide analogues

## 10.2 | Specific conclusions

### 10.2.1 | Chapter 1

- The prevalence of global obesity has tripled since 1975, with 650 million obese adults worldwide as per recent WHO statistics accounting to 13% of global population
- PL inhibition is considered among safe and effective strategies for the obesity treatment, due to the fact that the target is peripheral; the inhibitor does not require any systemic absorption and the inhibition would specifically prevent fat absorption
- Orlistat, a potent PL inhibitor is among the widely prescribed drugs for long term treatment of obesity, however, recent decades have seen considerable reports on severe adverse effects due to chronic administration of orlistat that included

hepatotoxicity and acute pancreatitis highlighting the urge to develop safer and effective anti-obesity drugs

### 10.2.2 / Chapter 2

- A detailed literature search on various natural and synthetic scaffolds reported for PL inhibition was performed to identify structural features required for potent PL inhibition
- At least 750 natural products and 300 synthetic analogues have been evaluated for PL inhibition
- These analogues exhibited enormous chemical diversity, but a majority did not possess potential PL inhibitory activity comparable to that of orlistat
- A negligible expanse of research used the advantage of *in silico* techniques in understanding the molecular interactions with the active site
- The literature search highlighted two structural features for potential PL inhibition, namely
  - a) large molecular volume that can be able to interact with the active site as well as the hydrophobic lid domain
  - b) presence of an ester or ester mimicking group with a reactive carbonyl functionality that would interact with Ser152 of the active site

### 10.2.3 / Chapter 3

- The aim and the objectives were detailed considering the potential gaps in the existing research

### 10.2.4 / Chapter 4

- The general procedures for **i)** plant material collection, processing and extraction; **ii)** PL inhibition assay; **iii)** molecular docking and molecular dynamics were provided in detail

### 10.2.5 / Chapter 5

- Preliminary screening of 120 plant extracts from 20 Indian medicinal plants/parts was performed that highlighted *T. divaricata* leaves as a source of potential leads
- Conophylline was identified as a potential natural product lead for PL inhibition, with an IC<sub>50</sub> of 3.31 μM
- Molecular modelling studies validated the requirement of dimeric scaffolds with large molecular volume
- First ever HPTLC method was developed and validated for estimation of conophylline

- Extractive yield of conophylline was maximum during August month when subjected to ultrasonic extraction

### 10.2.6 / Chapter 6

- A total of 24 carbazolyl oxoacetamide analogues were synthesised and evaluated for PL inhibition assay
- **DK-5** was the most potent analogue from this series with  $IC_{50}$  of 6.31  $\mu$ M
- Presence of *N*-benzyl substitution on carbazole and ring activating groups on aryl extension of the amide resulted in enhanced PL inhibition
- Three structural requirements were identified in this chapter that can enhance the PL inhibitory potential of any ligand;
  - i) interaction distance between the reactive carbonyl functionality and Ser152;
  - ii) requirement of dense hydrophobic moieties and
  - iii)  $\pi$ -cation interaction with Arg 256

### 10.2.7 / Chapter 7

- A total of 39 indolyl oxoacetamide analogues were synthesised, evaluated for PL inhibition assay
- **AP-37** and **AP-21** from this series exhibited potential activity with  $IC_{50}$  of 4.53 and 4.92  $\mu$ M
- A similar SAR was observed as with the carbazolyl oxoacetamides. In addition, the presence of a methylene bridge between the aryl extension and the amide nitrogen resulted in enhanced activity
- The role of interaction distance the reactive carbonyl functionality and Ser152, and  $\pi$ -cation interaction with Arg 256 has been validated in this chapter

### 10.2.8 / Chapter 8

- A total of 41 indolyl oxoacetamides analogues were synthesised, evaluated for PL inhibition assay
- A potent PL inhibition with  $IC_{50}$  of 1.68  $\mu$ M was achieved with **SS-39** comparable to the standard drug, orlistat ( $IC_{50} = 0.99 \mu$ M)
- Presence of heteroaryl extension on the amide linked through two carbon chain resulted in enhanced activity
- The study highlighted the  $C_6$  and  $C_7$  positions of the indolyl oxoacetamides to be favourable for the substitution of aromatic rings, that resulted in potent PL inhibitory activity when combined with *N*-geranyl substitution on the indole

### 10.2.9 | Chapter 9

- ADMET prediction highlighted **SS-39** as a suitable candidate for *in vivo* experiments
- **SS-39** at 20 mg/kg dose exhibited comparable anti-obesity efficacy compared to orlistat (10 mg/kg)
- The quantification of faecal triglycerides clearly indicated that **SS-39** acted through PL inhibition

### 10.3 | Future scope and limitations

The present thesis resulted in the identification of three structural features that resulted in potent PL inhibition. These features included i) dense hydrophobic moieties; ii) an  $\alpha$ -ketoamide and iii) a heteroaromatic aryl extension for Arg 256 interaction. The most analogue, **SS-39**, exhibited an  $IC_{50}$  of 1.68  $\mu$ M comparable to orlistat. The potency of these analogues can be further improved through various structural modifications. For example, the replacement of the  $\alpha$ -ketoamide with an  $\alpha$ -ketoester may enhance the reactivity of the carbonyl functionality by 2-3 folds. Similarly, analogues with dual ester or ester mimicking groups can enhance the binding time of the ligands in the active site. Other possibilities include C-alkylation and arylation in contrary to the O- and N-alkylation and arylation used in the present thesis, that can improve hydrophobic interactions with the lid domain by eliminating the negative charge due to lone pair of electrons on O and N. Finally, use of heterocycles with ring activating groups that can enhance  $\pi$ -cation interaction with Arg 256, or substitutions that can interact with Arg 256 through H-bonds might result in analogues with sub nanomolar potency.

Few limitations were identified in the present thesis. First, a preliminary ADMET prediction highlighted the analogue **SS-39** to be non-toxic in contrary to orlistat. Nevertheless, further high throughput assays and *in vivo* experiments of this molecule might be required to validate its non-toxicity. Second,  $\alpha$ -ketoamides might be prone to partial degradation in the presence of various protein digesting enzymes of the stomach as well as the highly acidic environment. Hence, the stability of the  $\alpha$ -ketoamide in the gastric environment needs to be understood and necessary chemical or pharmaceutical modifications might result in improved efficacy of this analogue. In addition, the GI absorption of this drug and further metabolism can be evaluated experimentally through pharmacokinetic studies. Further, the effect of **SS-39** on PL in combination with orlistat can be evaluated through synergy experiments, which might result in significant dose reduction of these analogues with an improved efficacy.

## **Publications**

---

### **From Thesis:**

- **SNC Sridhar**, S Mutya, AT Paul (2017). Bis-indole alkaloids from *Tabernaemontana divaricata* as potent pancreatic lipase inhibitors: Molecular modelling studies and Experimental validation. *Medicinal Chemistry Research* 26 (6), 1268–1278.
- **SNC Sridhar**, P Sengupta, AT Paul (2018). Development and validation of a new HPTLC method for quantification of conophylline in *Tabernaemontana divaricata* samples obtained from different seasons and extraction techniques: Insights into variation of pancreatic lipase inhibitory activity. *Industrial Crops and Products* 111, 462-470.
- **SNC Sridhar**, G Ginson, POV Reddy, MP Tantak, D Kumar, AT Paul (2017). Synthesis, evaluation and molecular modelling studies of 2-(carbazol-3-yl)-2-oxoacetamide analogues as a new class of potential pancreatic lipase inhibitors. *Bioorganic & Medicinal Chemistry* 25 (2), 609-620.
- **SNC Sridhar**, S Palawat, AT Paul (2019). Design, synthesis, biological evaluation and molecular modelling studies of indole glyoxylamides as a new class of potential pancreatic lipase inhibitors. *Bioorganic Chemistry* 85, 373-381.
- Patent application (under communication)

### **Other publications:**

- **SNC Sridhar**, S Kumari, AT Paul (2014). Diabetic complications: A natural product perspective. *Pharmaceutical Crops* 5 (1), 39-60.
- **SNC Sridhar**, D Bhurta, D Kantiwal, G Ginson, V Monga, AT Paul (2017). Design, synthesis, biological evaluation and molecular modelling studies of novel diaryl substituted pyrazolyl thiazolidinediones as potent pancreatic lipase inhibitors. *Bioorganic & Medicinal Chemistry Letters* 27 (16), 3749-3754.
- M Katoch, AT Paul, G Singh, **SNC Sridhar** (2017). Fungal endophytes associated with *Viola odorata* Linn. as bioresource for pancreatic lipase inhibitors. *BMC Complementary and Alternative Medicine* 17 (1), 385.

### **Book Chapter**

---

- **SNC Sridhar**, G Ginson, A Verma, AT Paul (2019). Chapter 6: Natural Products-Based Pancreatic Lipase Inhibitors for Obesity Treatment in Book titled “*Natural Bioactive compounds: Production and Applications: Volume 1*”. Editors: MS Akhtar, MK Swamy and UR Sinniah. Published by Springer Singapore (doi: 10.1007/978-981-13-7154-7).

## Conferences

---

- Poster presentation on “**Computational Approaches for Exploring the Natural Product Based Pancreatic Lipase Inhibitors**” in International Symposium, “Natural Products and Drug discovery: Future Perspectives”, organized by University of Innsbruck, at Vienna University of Technology, Vienna, Austria during November 2014
- Oral presentation on “**Synthesis, Evaluation and Molecular Modelling Studies of 2-(Carbazol-3-yl)-2-oxoacetamide Analogues as a New Class of Potential Pancreatic Lipase Inhibitors**” in 24<sup>th</sup> ISCB International Conference (ISCBC-2018), organized by Indian Society of Chemists and Biologists at Manipal University Jaipur, during January 2018
- Oral presentation on “**Conophylline - A Potent Pancreatic Lipase Inhibitor from *Tabernaemontana divaricata*: Molecular Modelling, *In Vitro* Studies and Analytical Method Development**” in the International Conference “Challenges for Global Competitiveness of AYUSH and Natural Products”, organized by Delhi Pharmaceutical Sciences and Research University (New Delhi), during February 2018
- Poster presentation on “**Conophylline, A Potential Natural Product Lead for Pancreatic Lipase Inhibition: *In silico*, *Synthesis* and *In vitro* studies**” at 1<sup>st</sup> National Biomedical Research Competition, organized by Society of Young Biomedical Scientists, at AIIMS Rishikesh during November 2018
- Oral presentation on “**Identification of Natural Product Leads for Pancreatic Lipase Inhibition: Insights and Case Studies**” at 1<sup>st</sup> National Biomedical Research Competition, organized by Society of Young Biomedical Scientists, at AIIMS Rishikesh during November 2018

**BRIEF BIOGRAPHY OF THE CANDIDATE**

S N C Sridhar was born in Khammam, Telangana, India. He pursued his Bachelor's degree (B. Pharmacy) from G. Pulla Reddy College of Pharmacy (affiliated to Osmania University, Hyderabad, Telangana) and Master's degree (M.S. Pharm.) in Medicinal Chemistry from the National Institute of Pharmaceutical Education and Research (NIPER, S.A.S. Nagar, Punjab) during 2006-10 and 2010-12, respectively. He pursued his Master's thesis under the guidance of Prof. Prasad V. Bharatam on the topic "Molecular Docking and Synthesis of Novel PPAR $\gamma$  Ligands". In July 2012, he joined Lalitha College of Pharmacy (Hyderabad, Telangana) as an Assistant Professor and continued till May 2013. During this period, he qualified the APSET-2012 (equivalent to CSIR-NET lectureship). In August 2013, he joined Department of Pharmacy, BITS Pilani (Pilani Campus) as a Ph.D. scholar under the supervision of Dr. Paul Atish Tulshiram in the area of anti-obesity natural products. Mr. S N C Sridhar has authored 06 research publications and 01 review article in international peer reviewed journals along with 01 book chapter (invited). A part of his Ph.D. thesis is under communication for patent application. He has presented his work in several international and national conferences. He has many awards to his credit, including the DBT-CTEP Travel Grant, Novartis BioCamp winning team member, CSIR-SRF, Dr. Shyambalaji Achuthan award for excellence in Pharmacology and a 2<sup>nd</sup> prize in oral presentation.

**BRIEF BIOGRAPHY OF THE SUPERVISOR**

Dr. Paul Atish Tulshiram is currently the Assistant Professor & Head of Department of Pharmacy. He completed his Bachelors in Pharmacy from University of Pune (Maharashtra). He pursued M.S. (Pharmaceutical Sciences) and Ph.D. in Natural Products from National Institute of Pharmaceutical Education and Research (NIPER, S.A.S Nagar, Punjab). After completion of his doctorate, he joined the research group of Prof. Ikhlas Khan as Postdoctoral Research Associate at the National Center for Natural Product Research (University of Mississippi, USA). His current research interest is identification of pancreatic lipase inhibitory natural products and synthesis of their inspired analogues for obesity management. He has 03 research grants from agencies such as DST-SERB, DST (SEED), DBT etc. and has completed 02 projects. He has published more than 15 research articles in reputed international journals and has also contributed 24 official monographs on polyherbal formulations in The *Ayurvedic* Pharmacopoeia of India. Currently he is supervising 5 Ph.D. students. He is a reviewer for various journals of reputed publishers such as Bentham, Elsevier, ACS etc. and also for funding agencies such as DST-SERB, South African Medical Research Council etc.